



The synthesis and biological activity of cyclometalated gold^{III} complexes

Morwen Ruth Maddern Williams

PhD Thesis

School of Chemistry

University of East Anglia, Norwich

April 2018

Supervised by Professor Manfred Bochmann and Professor Mark Searcey

© This copy of the thesis has been supplied on condition that anyone who consults it is understood to recognise that its copyright rests with the author and that use of any information derived therefrom must be in accordance with current UK Copyright Law. In addition, any quotation or extract must include full attribution.

Statement of original work

The work described in this thesis has been conducted by the author and is, to the best of my knowledge, original. Where other peoples' work has been referred to, this has been cited.

Morwen Ruth Maddern Williams

Abstract

The discovery of cisplatin revolutionised the treatment of cancer and opened the door to investigations into the discovery and use of other metallodrugs as chemotherapeutic agents. Both gold^I and gold^{III} complexes have demonstrated promising anticancer properties both *in vitro* and *in vivo*.

The following work will focus on the synthesis and anticancer activity of cyclometalated gold^{III} complexes with both tridentate (C[^]N[^]P[^]C) pincer ligands and bidentate (C[^]N) cyclometalated ligands to improve their physiological stability. Biologically relevant ligands were then incorporated into the complexes via the free coordination sites. These were selected to enhance the cytotoxicity of the complexes towards human cancer cell lines as well as improving the selectivity towards cancer cell lines over healthy cells.

Chapter 1 explores the use of gold^{III} compounds as anticancer agents and their typical cellular and molecular targets. Chapter 2 introduces the synthesis and anticancer activity of the first (C[^]N[^]P[^]C)Au^{III} complexes of acyclic carbene ligands, decorated with amine and amino ester functional groups. Chapter 3 introduces the synthesis and anticancer properties of cyclometalated gold^{III} complexes with acridine-decorated functional groups, chosen to promote DNA binding. Chapter 4 discusses the synthesis and biological activity of cyclometalated gold^{III} complexes with dithiocarbamate ligands.

The complexes were all tested for their anticancer activity *in vitro* towards a panel of human cancer cell lines, including some cell lines that typically show a reduced sensitivity towards cisplatin. Investigations into the possible mechanism of action of these complexes were also undertaken, including DNA binding assays, GSH reactivity and the production of ROS.

Acknowledgements

I would like to thank my two supervisors, Professor Manfred Bochmann and Professor Mark Searcey, for their help and guidance throughout my time at UEA, and EPSRC for funding this work. I would also like to thank the Bochmann research group for providing a fun working environment and most particularly Dr Benoît Bertrand for his support and encouragement. I would also like to express my gratitude to Professor Maria O'Connell for the use of her cell biology lab. Finally, I would like to thank my parents and my twin sister for their help and encouraging words when things got tough!

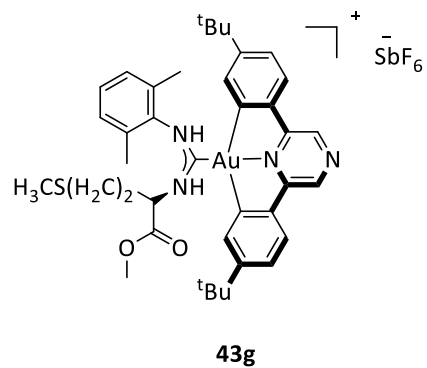
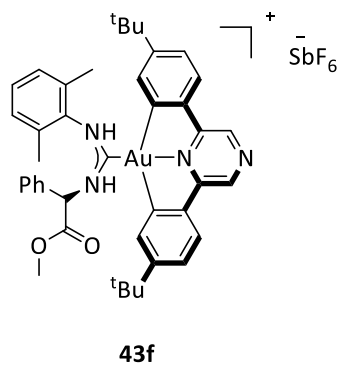
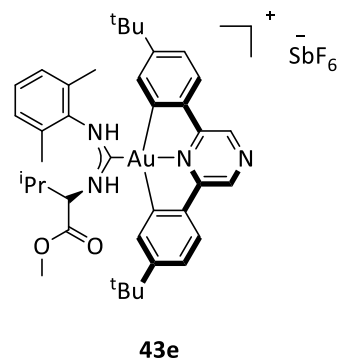
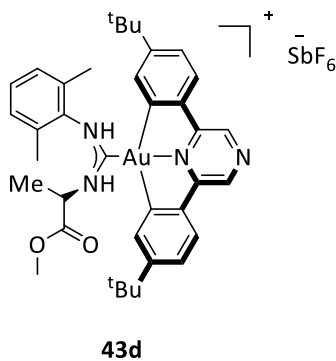
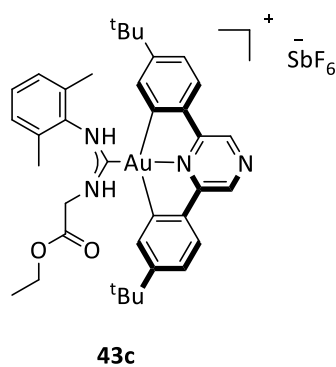
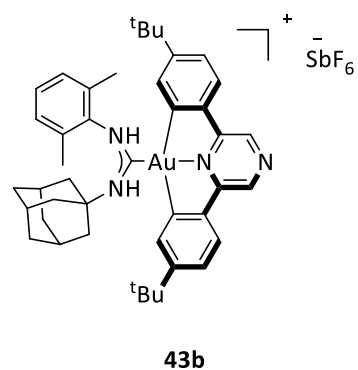
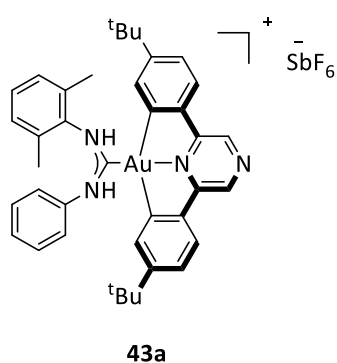
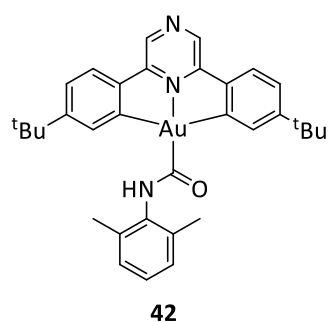
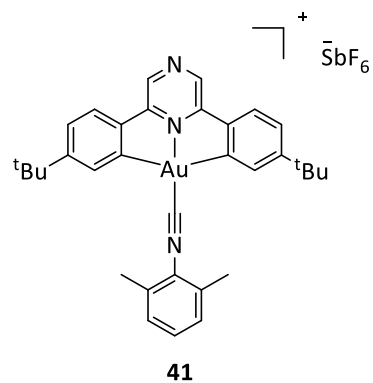
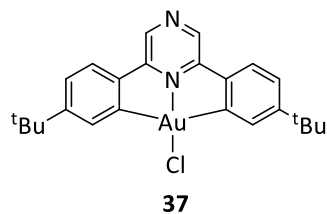
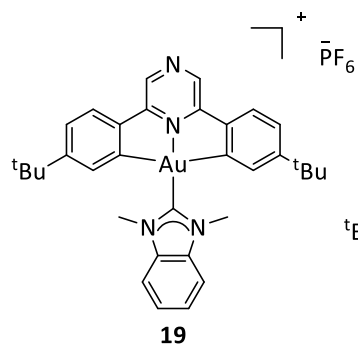
Abbreviations

>	less than	EC ₅₀	the concentration of a drug that gives the half-maximal response
<	more than		
°	degrees	ESDT	ethylsarcosine dithiocarbamate
°C	degrees Celsius		
Å	angstrom	Et	ethyl
ACC	acyclic carbene	<i>Et al.</i>	et alia
Ala	alanine	en	ethylenediamine
Anal.	analytically	ER	endoplasmic reticulum
Arg	arginine	FRET	fluorescence resonance energy transfer
Asn	asparagine	g	grams
Asp	aspartic acid	Gln	glutamine
bipy	bipyridyl	Glu	glutamic acid
bipy ^{dmb}	6-(1,1-dimethyl-benzyl)-2,2'-bipyridine	Gly	glycine
BCA	bicinchoninic acid	GSSG	oxidised glutathione
Calcd.	calculated	GR	glutathione reductase
CDI	carbonyldiimidazole	GSH	glutathione
Cys	cysteine	h	hours
d	doublet	His	histidine
damp	dimethylamino methyl phenyl	IC ₅₀	the concentration of a drug that causes a 50% reduction in cell viability
DCFDA	2',7'-dichlorofluorescein diacetate	ICP-MS	inductively coupled plasma mass-spectrometry
DMDT	dimethyl-dithiocarbamate	Ile	isoleucine
DMEM	Dulbecco's Modified Eagle's Medium	ⁱ Pr	<i>iso</i> -Propyl
DMSO	dimethylsulfoxide	IR	infra-red
DTC	dithiocarbamate	<i>J</i>	Coupling constant
		K	Kelvin

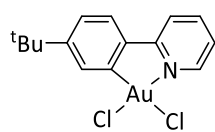
Leu	leucine	s	singlet
Lys	lysine	SD	standard deviation
M	molar	Sec	selenocysteine
m	multiplet	Ser	serine
mM	millimolar	t	triplet
Me	methyl	Thr	threonine
Met	methionine	Tyr	tyrosine
min	minutes	^t Bu	<i>tert</i> -butyl
MHz	megahertz	THF	tetrahydrofuran
MTS	3-(4,5-dimethylthiazol-2-yl)5-(3-carboxymethoxyphenyl)-2-(4-sulfophenyl)-2H-tetrazolium	Tol	tolyl
		TrxR	thioredoxin reductase
		UV-Vis	ultraviolet-visible
ⁿ Bu	<i>n</i> -Butyl	Val	valine
NAC	N-acetyl cysteine	Xy	xylyl
NHC	N-heterocyclic carbene		
nM	nanomolar		
NMR	nuclear magnetic resonance		
OTf	triflate anion		
PARP	poly-(ADP-ribose)-polymerase		
PBS	phosphate buffered saline		
Phe	phenylalanine		
ppm	parts per million		
Pro	proline		
py	pyridine		
rt	room temperature		
ROS	reactive oxygen species		
RPMI	Roswell Park Memorial Institute		

Structures

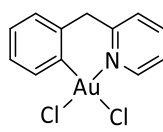
Chapter 2



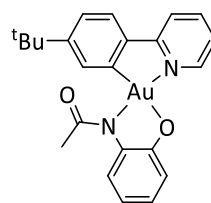
Chapter 3



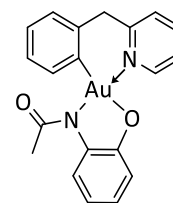
49



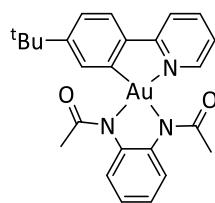
50



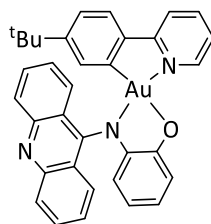
51



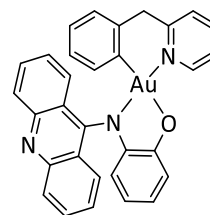
52



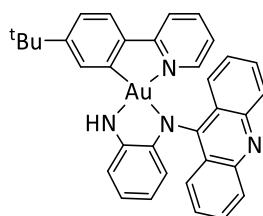
53



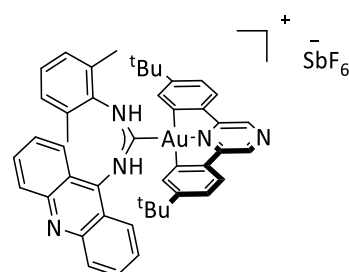
54



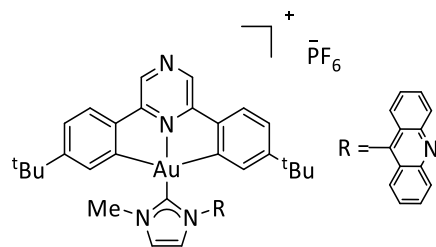
55



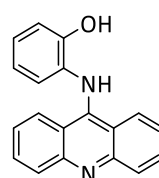
56



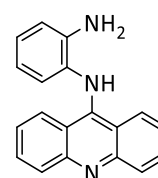
57



58

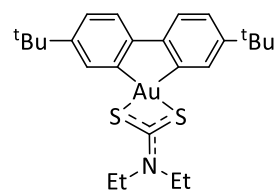
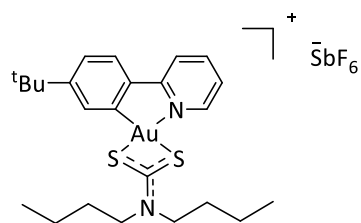
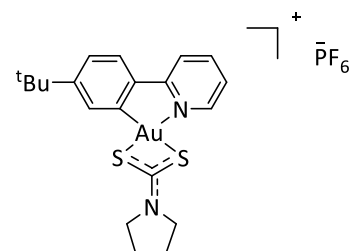
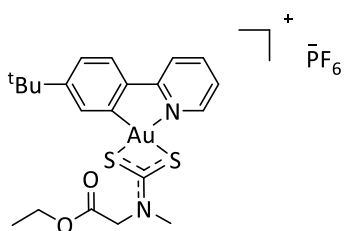
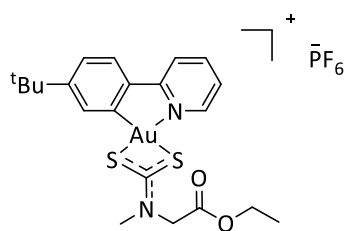
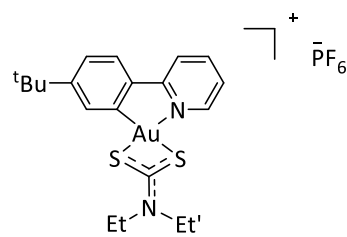
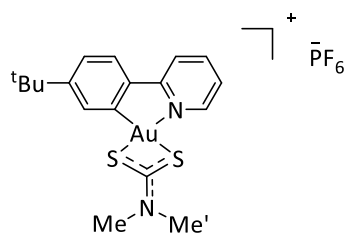


L1



L2

Chapter 4



Contents

Statement of original work	i
Abstract	ii
Acknowledgements	iii
Abbreviations	iv
Structures	vi
Chapter 1 Gold^{III} compounds as anticancer agents and their cellular and molecular targets	1
1.1 Gold ^{III} complexes for chemotherapeutic purposes	2
1.2 Cellular and molecular targets of gold ^{III} complexes	19
1.3 Conclusion	26
Chapter 2 The synthesis and anticancer activity of (C^NP^z^C)Au^{III} complexes of acyclic carbene ligands decorated with amino esters	29
2.1 Abstract	30
2.2 Introduction	30
2.3 Results and Discussion	37
2.4 Conclusion	50
2.5 Experimental	51
Chapter 3 The synthesis and anticancer activity of cyclometalated gold^{III} complexes with acridine decorated functional groups	71
3.1 Abstract	72
3.2 Introduction	72
3.3 Results and Discussion	77
3.4 Conclusion	94
3.5 Experimental	95
Chapter 4 The synthesis and anticancer activity of cyclometalated gold^{III} dithiocarbamate complexes	114
4.1 Abstract	115
4.2 Introduction	115
4.3 Results and Discussion	119
4.4 Conclusion	132
4.5 Experimental	133
References	147

Chapter 1

Gold^{III} compounds as anticancer agents and their cellular and molecular targets.

1.1 Part 1 – gold^{III} complexes for chemotherapeutic purposes

1.11 Introduction

The discovery of the anticancer drug *cis*-diamminedichloroplatinum^{II} or cisplatin in the 1960s marked the start of a new era in the discovery and use of metallodrugs.¹ Cisplatin and its clinically approved derivatives, carboplatin and oxaliplatin (Figure 1), are highly effective chemotherapeutic agents and they are widely used for the treatment of various types of cancer, in particular head and neck, testicular and ovarian cancers.² However, despite the clinical success of these drugs, platinum based metallodrugs do not specifically target the cancer cells but also affect other rapidly dividing cells such as those found in the bone marrow and in the gastrointestinal tract and this causes severe side effects which can limit the administrable dose to patients.³ Other drawbacks include acquired or intrinsic drug resistance as well as a limited spectrum of action.⁴ All of these factors have increased the interest into the development of other metallodrugs. Both gold^I and gold^{III} complexes have demonstrated promising anticancer properties.⁵⁻⁸

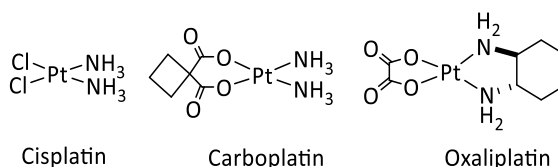


Figure 1 – structures of the three clinically available platinum based chemotherapeutics; cisplatin, carboplatin and oxaliplatin.²

The application of gold in medicine dates far back into history, perhaps as early as 2500 BC.⁹ However, perhaps the most notable find was the discovery that gold^I thiolates could be used to reduce joint pain which led to initial investigations into the use of gold complexes for the treatment of rheumatoid arthritis.¹⁰ In the 1970s Sutton *et al.* developed an orally active thioglucose gold^I phosphine complex, auranofin (Figure 2), which was approved for clinical use for the treatment of rheumatoid arthritis in the 1980s.¹¹ During this time, auranofin was also shown to possess anticancer properties both *in vitro* and *in vivo* and this was the start of the development of other gold^I complexes for anticancer applications.¹²

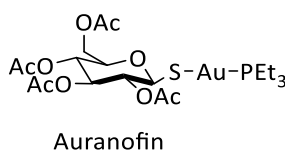


Figure 2 – structure of auranofin.¹¹

Gold^{III} complexes were initially investigated as potential anticancer agents because, being isoelectronic and isostructural to platinum^{II}, they were thought to be able to mimic the activity of cisplatin in a biological system. However, gold^{III} complexes are frequently unstable under physiological conditions as they are easily reduced to gold^I and elemental gold. Their physiological stability can be improved by finetuning the ligand environment around the gold^{III} centre and a diverse range of different complexes have been shown to have both *in vitro* and *in vivo* anticancer activity.⁵⁻⁸

1.12 Gold^{III} complexes with N-donor ligands

There are numerous examples of multidentate N-donor ligand complexes showing *in vitro* anticancer activity.¹³⁻¹⁵ Isab *et al.* synthesised tetracoordinate gold^{III} complexes of ethylenediamine and N-substituted ethylenediamine, [Au(en)₂Cl]₃, **1** (Figure 3) and tested their cytotoxicity *in vitro* on human gastric carcinoma (SGC-7901) and prostate cancer (PC-3) cell lines. The complexes exhibited a concentration dependent cytotoxic effect on both cell lines and were thought to act by interrupting the mitotic cycle and inducing both apoptosis and necrosis.¹³

Examples of cytotoxic bipyridyl gold^{III} complexes are also known. [Au(bipy)(OH)₂PF₆], **2** (Figure 3) synthesised by Marcon *et al.* displayed high cytotoxicity towards both cisplatin sensitive and cisplatin resistant human ovarian carcinoma cells (A2780 S/R) with IC₅₀ values, (the concentration of a drug that causes a 50% reduction in cell viability), falling in the low micromolar range.¹⁴

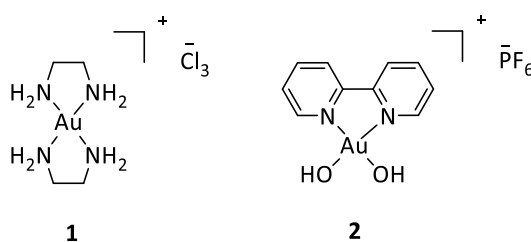


Figure 3 – cytotoxic gold^{III} complexes of ethylenediamine and bipyridyl.^{13, 14}

Similar bipyridyl derivatives, synthesised by Amani *et al.* with 4,4'-dimethyl-2,2'-bipyridine ligands, **3** (Figure 4) were tested on three human cancer cell lines; skin carcinoma (A431), cervical carcinoma (HeLa) and colon carcinoma (HT-29) in comparison to both cisplatin and its derivative carboplatin. All the gold derivatives were more cytotoxic than carboplatin against all three cell lines and also showed higher cytotoxicity than cisplatin against the HeLa

cells.¹⁵ Although the mechanism of action of these gold^{III} bipyridyl derivatives was not determined, the complexes showed weak and reversible interactions with calf thymus DNA, which suggests that DNA is not the primary target of these complexes.¹⁴

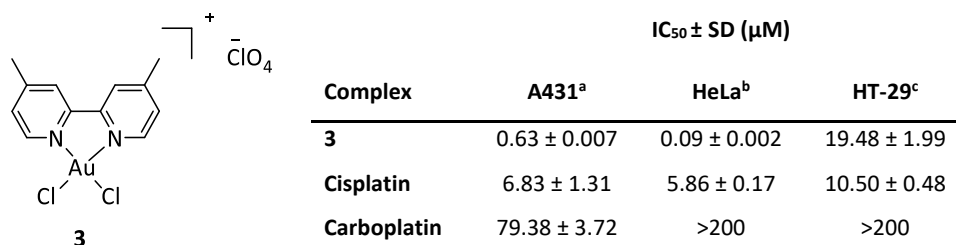


Figure 4 – structure of the bipyridyl gold^{III} derivative, **3** and its anticancer activity towards three human cancer cell lines in comparison to platinum based chemotherapeutic agents; ^a Skin carcinoma, ^b Cervical carcinoma, ^d Colon carcinoma. Data taken from ref¹⁵.

Gold^{III} complexes of 1,4,7-triazacyclononane, **4** (Figure 5) synthesised by Shi *et al.* showed greater cytotoxicity than cisplatin against both human lung carcinoma (A549) and human colon carcinoma (HCT-116) cancer cells, possibly acting by inducing conformational changes to DNA by non-covalent interactions.¹⁶ DNA binding was also a mechanism of action for tridentate terpyridine derivatives, **5** (Figure 5) synthesised by the same group and these complexes were shown to target intracellular DNA *in vitro*. Once again, promising cytotoxicities were observed although it should be noted that they were comparable to those of the free terpyridine ligands.¹⁷ Other tridentate (N[^]N[^]N) aminoquinoline derivatives, **6** synthesised by Yang *et al.* showed significant cytotoxicities against a panel of human cancer cell lines including A549, with three times the activity of cisplatin against this cell line. The complexes could replace ethidium bromide from an EB-DNA system. Ethidium bromide is a DNA intercalating agent, commonly used as a nucleic acid stain or fluorescent tag. This suggested that the complexes were acting as DNA intercalating agents.¹⁸

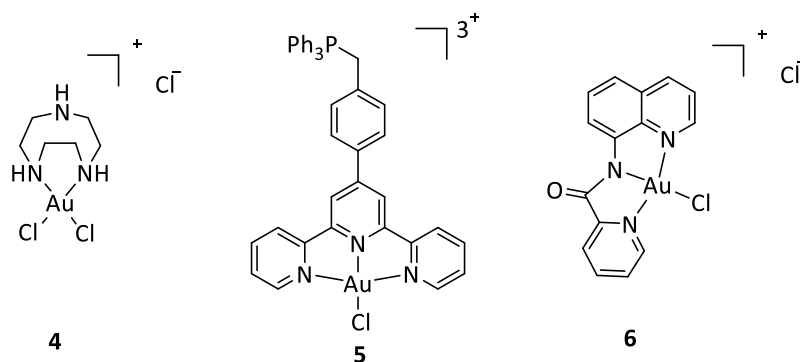


Figure 5 – Cytotoxic triazacyclononane, terpyridine and aminoquinoline gold^{III} complexes.¹⁶⁻¹⁸

The cytotoxic activities of the dinuclear, gold^{III} oxo-bridged complex, **7** (Figure 6) synthesised by Gabbiani *et al.* was initially assayed against both cisplatin sensitive and cisplatin resistant ovarian cancer (A2780 S/R) and displayed promising results with IC₅₀ values of 1.8 and 4.8 μM for A2780 S/R respectively. The complex was further tested on a panel of 36 cancer cell lines and again showed promising results although it was also noted that the cytotoxicity profile of the complex differed from that of cisplatin, implying that their respective modes of action were different and that DNA was not the primary target. Further work determined that the mechanism of action was likely to involve a variety of protein targets including the enzyme Thioredoxin reductase (TrxR).¹⁹

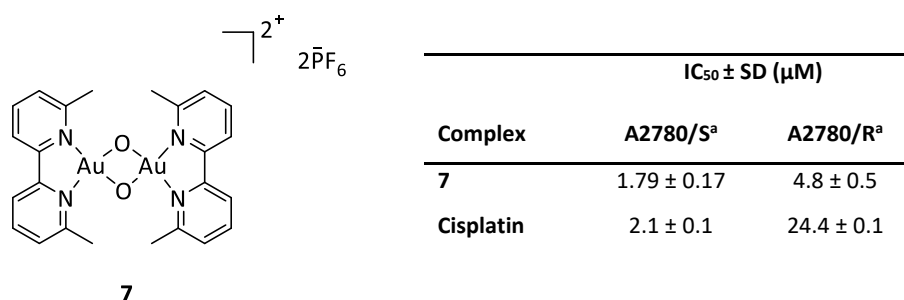


Figure 6 – structure of the dinuclear gold^{III} oxo-bridged complex, **7** and its anticancer activity towards A2780 cells in comparison to cisplatin; ^a Ovarian cancer. Data taken from ref¹⁹.

1.13 Cyclometalated gold^{III} complexes

The physiological stability of a gold^{III} centre can be improved by introducing either a bidentate, (C[^]N) or tridentate, (C[^]N[^]C), (C[^]N[^]N) or (N[^]C[^]N) cyclometalating ligand. Both neutral and cationic (C[^]N)AuL₂ complexes have shown promising anticancer activity.^{20, 21} Derivatives of Au(damp)Cl₂, **8** (Figure 7), (damp = 2-((dimethylamino)methyl)phenyl), were originally synthesised by Parish *et al.* and were assessed for their ability to inhibit tumour cell growth. Au(damp)Cl₂ had a similar toxicity profile to cisplatin against a panel of human cancer cell lines *in vitro*, as well as showing promising *in vivo* activity against solid breast cancer xenografts (ZR-75-1) in a nude mice model.²⁰ These complexes have since been shown to act as potent TrxR inhibitors.²²

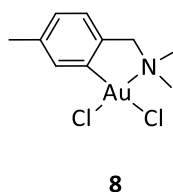


Figure 7 – Au(damp)Cl₂.²⁰

There are also numerous examples of cytotoxic gold^{III} complexes with 2-phenylpyridine cyclometalating ligands, and a general formula of Au(C[^]N)X₂; **9-11**.^{21, 23-25} Derivatives synthesised by Fan *et al.* (Figure **8**) bearing either carboxylate, **9a** or isothiocyanate, **9b** ligands were tested for their cytotoxicity *in vitro* against human leukaemia (MOLT-4) and mouse tumour (C2C12) cell lines and showed high cytotoxicity towards both cell lines with IC₅₀ values in the low micromolar range.^{21, 23}

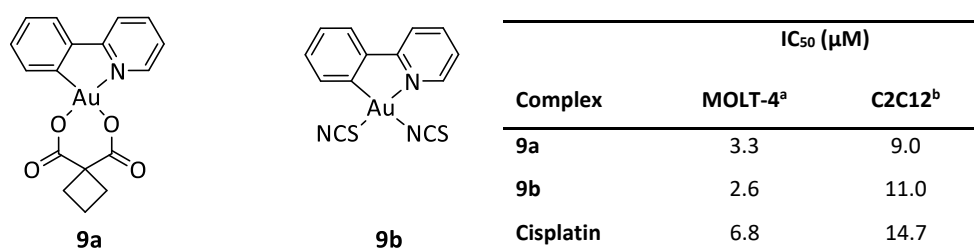


Figure **8** – structures of **9a** and **9b** and their anticancer activity towards human and mouse cancer cell lines in comparison to cisplatin; ^a Human leukaemia, ^b Mouse tumour. Data taken from ref^{21, 23}.

A cationic water soluble gold^{III} complex, [Au(butyl-C[^]N)biguanidine]Cl, **10** (Figure **9**) synthesised by Zhang *et al.* combined the lipophilic, cyclometalated (C[^]N) ligand and the hydrophilic, H-bonding NH₂ groups of the biguanidine ligand. The complex was tested on a panel of human cancer cell lines and also on normal lung fibroblast cells (CCD-19-Lu) for comparison and showed high cytotoxicities towards the cancer cell lines, with IC₅₀ values in the low micromolar ranges and, more importantly, a lower cytotoxicity towards the healthy CCD-19-Lu cells. The complex was also found to induce stress to the endoplasmic reticulum in HeLa cells, possibly by upregulating certain ER-stress markers such as CHOP and HSP70 and causing partial S-phase cell cycle arrest and subsequently cell death.²⁴

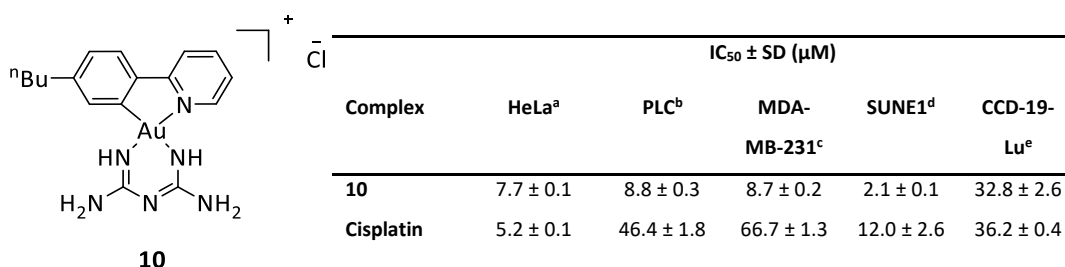


Figure **9** – structure of complex **10** and its anticancer activity towards human cell lines in comparison to cisplatin; ^a Cervical epithelial carcinoma, ^b Hepatocellular carcinoma, ^c Breast carcinoma, ^d Nasopharyngeal carcinoma, ^e Normal lung fibroblasts. Data taken from ref²⁴.

Rubbiani *et al.* synthesised a series of both neutral and cationic 2-phenylpyridine gold^{III} 2,4,6-tris(trifluoromethyl)phenyl complexes, **11** (Figure 10) as prospective anticancer agents. The complexes were assessed for their cytotoxicity against cervical cancer (HeLa) cells and noncancerous, human lung fibroblast cells (MRC-5) for comparison. For complex **11**, a low EC₅₀, (the concentration of a drug that gives the half-maximal response), of 0.42 μM was observed for the HeLa as well as an interesting selectivity profile for the cancer cells over the noncancerous MRC-5 cells; (EC_{50MRC-5}/EC_{50HeLa} = 6.43).²⁵

A series of neutral cyclometalated (C^N)Au(N^N) chelated complexes, **12** (Figure 10) were synthesised by Kilpin *et al.* and their cytotoxicities against mouse leukaemia cells (P388) were tested. Derivatives bearing electron withdrawing toluene sulfonyl groups appeared to show the highest activities; for example complex **12** had an IC₅₀ of 0.30 μM (in comparison to cisplatin with an IC₅₀ of 8.15 μM).²⁶

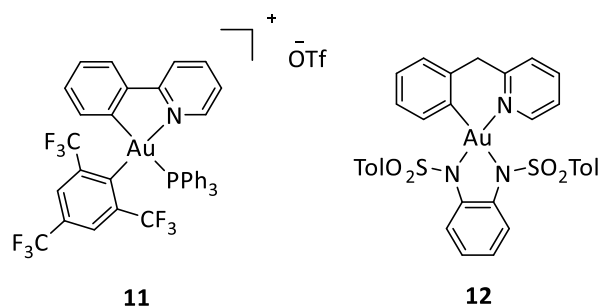


Figure 10 – structures of complexes **11** and **12**.^{25, 26}

There are also examples of gold^{III} complexes with tridentate cyclometalating ligands that show anticancer activity.²⁷⁻²⁹ The cyclometalated (N^N^C) complex, [Au(bipy^{dmb})(OH)]PF₆, **13** (Figure 11), (bipy^{dmb} = 6-(1,1-dimethyl-benzyl)-2,2'-bipyridine), was synthesised by Coronello *et al.* and tested for its cytotoxic activity against ovarian cancer (A2780 S/R). Results indicated that although the complex showed comparable cytotoxicity to cisplatin, with results for both cell lines falling between 1-7 μM, it also showed poor DNA binding abilities, suggesting that the cell death is not a consequence of direct nuclear DNA damage, as with platinum based compounds.²⁷ Further research established that **13** was a potent and highly selective inhibitor of the enzyme TrxR.³⁰

A dinuclear oxo-bridged gold^{III} complex, **14** (Figure 11) synthesised by Gabbiani *et al.* used the same (N^N^C) skeleton, (bipy^{dmb}). In comparison to its mononuclear precursor, the oxo-bridged derivative showed only moderate cytotoxicity towards a panel of twelve human cancer cell lines with mean IC₅₀ values rising to around 20 μM.²⁸

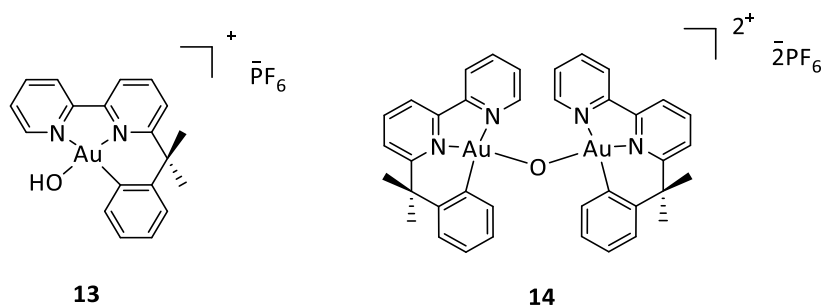


Figure 11 – the mononuclear (C^N^C) complex, **13** and its dinuclear oxo-bridged variant, **14**.²⁷

28

The cationic $[(C^N^C)Au^{III}py]CF_3SO_3$ derivative, **15** (Figure 12) was synthesised by Zhang *et al.* and combined the hydrophilic, H-bonding biguanidine motif, seen with complex **10** and the (C^N^C) pincer scaffold. The complex was found to self-assemble into supramolecular polymers in acetonitrile. These polymers were found to be stable towards glutathione, (GSH) a common drug deactivating peptide found inside cells, and displayed sustained cytotoxicity towards melanoma cells (B16) as well as selective cytotoxicity towards this cell line over noncancerous lung fibroblast cells (CCD-19-Lu).²⁹

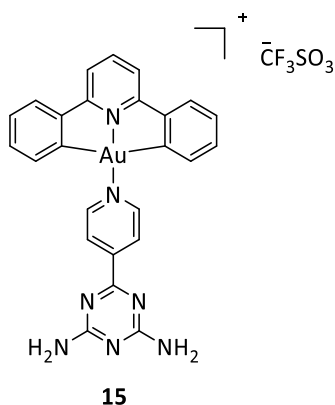


Figure 12 – structure of **15**.²⁹

Li *et al.* also used the 2,6-diphenylpyridine (C^N^C) skeleton to synthesise a series of complexes with highly cytotoxic phosphine ligands, **16a** as well as a series of dinuclear derivatives where the gold^{III} centres were joined by bridging (1,2-bis(diphenylphosphino)(CH₂)_n) ligands with the hydrocarbon linker of varying size, **16b** ($n = 1-6$) (Figure 13). The cytotoxicity of the complexes was tested towards several human cancer cell lines including nasopharyngeal carcinoma (SUNE1 and CNE1), hepatocellular carcinoma, (HEPG2) and cervical epithelial carcinoma (HeLa). While complex **16a** displayed only moderate cytotoxicity in comparison to cisplatin, the dinuclear derivatives, **16b** showed

significantly increased activities with IC_{50} values falling to nM concentrations. However, it must be noted that these cytotoxic values also correlate to those of the metal-free phosphine ligands which were equally cytotoxic. Interestingly, a slight trend towards increasing cytotoxicity with the increasing length of the hydrocarbon linker was also observed, with IC_{50} values falling as low as 0.043 μ M for the propane derivative. This could be due to the increase in lipophilicity of the complex and therefore an easier transition through the cell membrane. This trend ceased once the linker became longer than propane and the cytotoxicities of the butane, pentane and hexane derivatives were all significantly lower, possibly because the complex became too big to easily cross the cell membrane. The phosphine derivatives showed no significant DNA binding nor any ability to induce cell cycle arrest.³¹

The same group also showed that a derivative of **16b** (n=3) also showed significant *in vivo* anticancer activity when assessed on human liver hepatoma xenographs (PLC) in a nude mice model with a tumour reduction of 77%, (in comparison to cisplatin with a tumour reduction of 28%), and no obvious side effects. The complex was also shown to be a potent inhibitor of TrxR with an IC_{50} of 2.7 nM and was thought to induce apoptosis by the induction of ER stress.³²

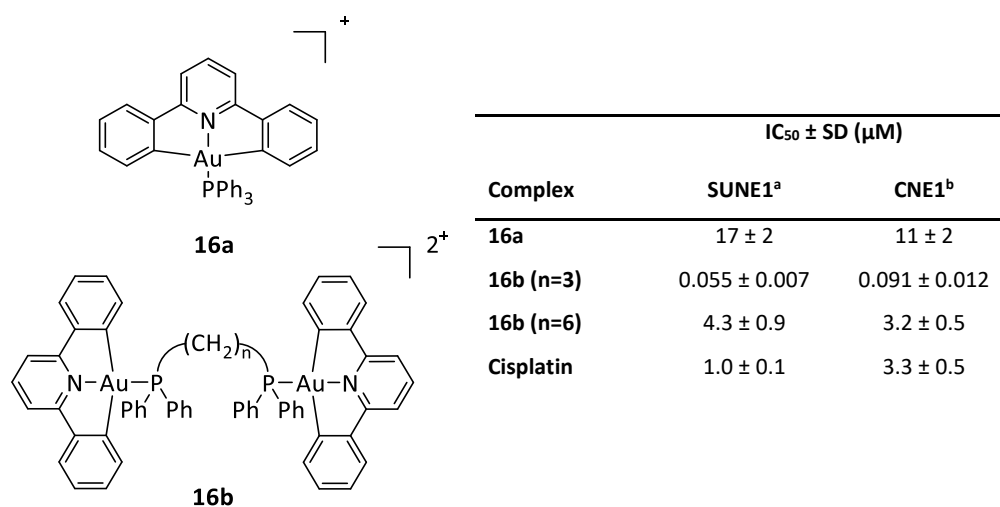
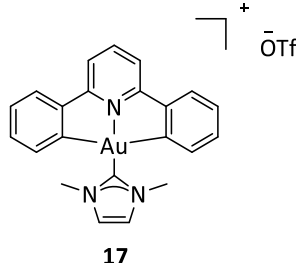


Figure 13 – cyclometalated gold^{III} phosphine pincer complex, **16a** and its dinuclear derivative, **16b** and their anticancer activity towards human cell lines in comparison to cisplatin; ^a Nasopharyngeal carcinoma (cisplatin sensitive), ^b Nasopharyngeal carcinoma (cisplatin resistant). Data taken from ref³¹.

1.14 Gold^{III} N-heterocyclic carbene complexes

There are many examples of both cationic and neutral cytotoxic gold^I complexes bearing N-heterocyclic carbene (NHC) ligands.³³⁻³⁶ Several examples of gold^{III}(NHC) complexes with biological activity also exist.^{37, 38} Yan *et al.* synthesised a cyclometalated [Au(C[^]N[^]C)(NHC)]OTf complex, **17** (Figure 14) which displayed significant *in vitro* cytotoxicity across a panel of human cancer cell lines with IC₅₀ values between 0.17 and 1.2 μM as well as reduced cytotoxicity for normal lung fibroblast cells (CCD-19-Lu) (IC₅₀ of 25 μM). The *in vivo* cytotoxicity was also examined in a nude mice model where it reduced tumour growth by up to 47% in comparison to the control with no apparent toxicity induced side effects including death or weight loss.³⁷

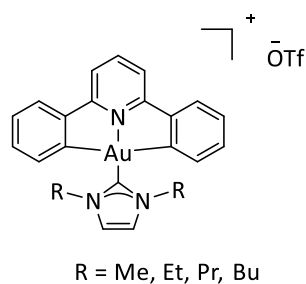


17

Complex	IC ₅₀ ± SD (μM)			
	HepG2 ^a	SUNE1 ^b	NCI-H460 ^c	CCD-19-Lu ^d
17	0.37 ± 0.03	0.25 ± 0.02	0.17 ± 0.05	25 ± 3.8
Cisplatin	10.5 ± 0.5	4.9 ± 0.8	3.5 ± 1.0	51 ± 7

Figure 14 – gold^{III} NHC derivative, **17** and its anticancer activity towards human cell lines in comparison to cisplatin; ^a Hepatocellular carcinoma, ^b Non-small cell lung carcinoma, ^c Nasopharyngeal carcinoma, ^d Normal lung fibroblasts. Data taken from ref³⁷.

Fung *et al.* also used the same [Au(C[^]N[^]C)(NHC)]OTf scaffold to synthesise a series of complexes by increasing the length of the N-hydrocarbon chain; methyl, ethyl, propyl and butyl, **18** (Figure 15). The increased length of the alkyl chain and therefore the increase in the lipophilicity of the complex resulted in enhanced cytotoxicity towards HeLa, HCT-116 and NCI-H460 cell lines, with a gradual decrease in the IC₅₀ from 2.04 μM to 0.36 μM (and thus a gradual increase in cytotoxicity) from the N-methyl to the N-butyl derivatives towards the HeLa cells. The butyl derivative also showed potent selectivity for cancer cells over healthy human hepatocyte cells (MIHA) with more than 30-fold lower cytotoxicity towards the healthy cells. An *in vivo* nude mice model against HeLa xenografts demonstrated a 71% reduction in tumour size after treatment with 3 mg kg⁻¹ of the complex as well as a 53% reduction when NCI-H460 xenografts were treated with the same dosage. Derivatives bearing photoaffinity probes were also synthesised and used to identify a number of intracellular proteins as the molecular targets of these compounds, including HSP60, vimentin, nucleophosmin and YB-1.³⁸

**18**

Complex	IC ₅₀ ± SD (μM)			
	HeLa ^a	HCT-116 ^b	NC1-H460 ^c	MIHA ^d
18 (R=Me)	2.0 ± 0.2	4.4 ± 1.5	2.4 ± 0.3	42.8 ± 12.3
18 (R=Bu)	0.4 ± 0.1	0.2 ± 0.1	0.2 ± 0.1	11.8 ± 3.2
Cisplatin	15.3 ± 1.1	11.8 ± 2.8	54.9 ± 3.6	95.2 ± 2.2

Figure 15 – derivatives of **18** and their anticancer activity towards human cell lines in comparison to cisplatin; ^a Cervical carcinoma, ^b Colon cancer, ^c Lung cancer, ^d Normal hepatocyte. Data taken from ref³⁸.

A similar pyrazine-based (C[^]N[^]P^z[^]C) pincer ligand was used by Bertrand *et al.* along with a benzimidazole-based NHC ligand, **19** (Figure 16). This derivative showed excellent *in vitro* cytotoxicity with IC₅₀ values in the micromolar and sub-micromolar range against MCF-7 and HL60 and A549 cells, although it showed poor selectivity for cancer cells over healthy MRC-5 cells.³⁹

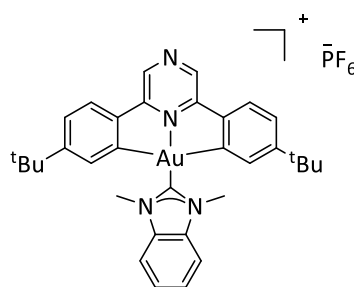
**19**

Figure 16 – structure of benzimidazole-based gold^{III} NHC complex, **19**.³⁹

Another example of a cytotoxic gold^{III}NHC complex, synthesised by Zou *et al.* used a tridentate (N[^]N[^]N) pincer ligand to stabilise the gold^{III} centre, making a series of [Au(N[^]N[^]N)(NHC)]OTf complexes, **20** (Figure 17) (n = 3,7,9 and 15). The complex bearing the longest hydrocarbon chain, n = 15, displayed the most promising cytotoxicity against HeLa cells, (IC₅₀ of 1.4 μM) and also significantly increased cellular uptake. An *in vivo* study in nude mice, bearing HeLa xenografts showed tumour inhibition of up to 70% after eleven days with no observable toxicity induced side effects. The complexes were also shown to act as TrxR inhibitors.⁴⁰

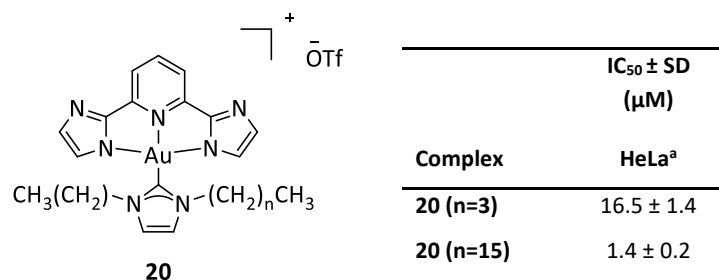


Figure 17 – derivatives of **20** and their anticancer activity towards human cervical cancer cells; ^a Cervical carcinoma. Data taken from ref⁴⁰.

Rana *et al.* synthesised a novel [Au(NHC)₂Cl₂]⁺PF₆⁻ complex, **21** (Figure 18) and tested its cytotoxicity against HCT-116, HepG2, A549 and MCF-7 human cancer cell lines where it displayed a higher cytotoxicity than cisplatin across all four cell lines.⁴¹ Another gold^{III} hetero bis-carbene dichloro complex, published by Sivaram *et al.*, **22** (Figure 18) also displayed prominent cytotoxicity against non-small cell lung cancer cells (NCI-H1666) with a low IC₅₀ value of 0.2 μM, (IC₅₀ of cisplatin = 2.5 μM).⁴²

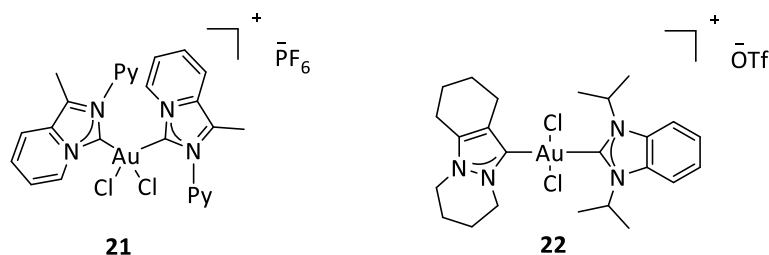


Figure 18 – examples of [Au^{III}(NHC)₂Cl₂]⁺ complexes with biological activity.^{41, 42}

1.15 Gold^{III} dithiocarbamate

Gold^{III} dithiocarbamate derivatives, with the general structure AuX₂(DTC) have also shown cytotoxic activity.^{43, 44} Two of the most widely studied are AuX₂(DMDT), **23a** and AuX₂(ESDT), **23b** (Figure 19) (DTC = dithiocarbamate, DMDT = N,N-dimethyldithiocarbamate and ESDT = ethylsarcosinedithiocarbamate). Both the dichloro and dibromo derivatives have been studied. These complexes have shown both *in vitro* and *in vivo* cytotoxicity towards cancer cells, as well as significant inhibition of TrxR and the induction of reactive oxygen species (ROS).^{43, 44}

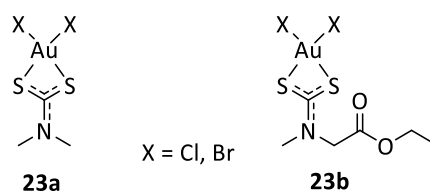


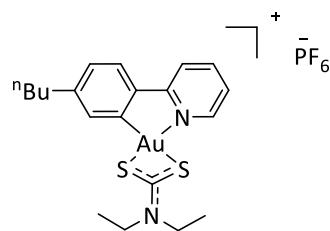
Figure 19 – structures of gold^{III} dithiocarbamate derivatives **23a** and **23b**.^{43, 44}

Another gold^{III} dithiocarbamate derivative with cytotoxic potential is complex **24**, [Au(Et₂DTC)₂]Cl (Figure 20) synthesised by Altaf *et al.* The complex displayed *in vitro* cytotoxicity towards A2780 S/R and MCF-7 cells, (EC₅₀ of 6.3, 29.8 and 3.9 μM respectively), as well as showing some selectivity towards cancer cells over healthy MRC-5 cells, (EC₅₀ of 19.7 μM).⁴⁵

Complex	EC ₅₀ ± SD (μM)			
	A2780/S ^a	A2780/R ^a	MCF-7 ^b	MRC-5 ^c
24	6.3 ± 2.1	29.8 ± 5.8	3.9 ± 2.3	19.7 ± 6.4
Cisplatin	10.0 ± 1.6	21.0 ± 2.1	>50	>50

Figure 20 – gold^{III} DTC derivative, **24** and its anticancer activity towards human cell lines in comparison to cisplatin; ^a Ovarian cancer, ^b Breast carcinoma, ^c Normal lung fibroblasts. Data taken from ref⁴⁵.

There are few examples of cyclometalated gold^{III} dithiocarbamate complexes. Zhang *et al.* synthesised a series of [(C[^]N)Au^{III}(R₂NCS₂)]PF₆ complexes, **25** (Figure 21) and demonstrated that they could act as potent deubiquitinase inhibitors. The *in vitro* cytotoxicities of the [(C[^]N)Au^{III}(DTC)]PF₆ complexes were also tested on several cancer cell lines and also a non-tumorigenic immortalized liver cell line (MIHA) for comparison. The complexes all showed significantly higher cytotoxicities than cisplatin with IC₅₀ values ranging from 0.07 to 6.30 μM, (in comparison to cisplatin; IC₅₀ values of 11.6 to 59.0 μM). Complexes containing a diethyldithiocarbamate ligand also displayed specificity towards the MCF-7 breast cancer cells with more than 80-fold higher activity towards this cell line in comparison to the MIHA cells.⁴⁶



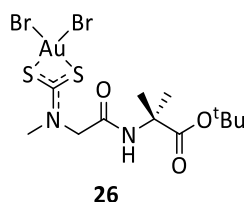
25

Complex	IC ₅₀ ± SD (μM)					
	MCF-7 ^a	MDA-MB-231 ^b	HeLa ^c	B16 ^d	NC1-H460 ^e	MIHA ^f
25	0.09 ± 0.05	0.20 ± 0.03	0.50 ± 0.14	0.37 ± 0.01	1.3 ± 0.4	1.2 ± 0.4
Cisplatin	30 ± 6	60 ± 2	12 ± 2	33 ± 3	59 ± 11	55 ± 0.6

Figure 21 – cyclometalated gold^{III} dithiocarbamate derivative, **25** and its anticancer properties in comparison to cisplatin; ^{a/b} Breast carcinoma, ^c Cervical carcinoma, ^d Melanoma, ^e Lung carcinoma, ^f Non-tumorigenic immortalised liver cells. Data taken from ref ⁴⁶.

1.16 Gold^{III} dithiocarbamate oligopeptide complexes

Dithiocarbamate ligands can also be used to functionalise gold^{III} centres with cancer targeting oligopeptides that act as carrier mediated delivery systems and exploit the peptide transporters that are upregulated in certain cancer cell lines. Nardon *et al.* synthesised one derivative, complex **26** (Figure 22), and demonstrated both its *in vitro* and *in vivo* anticancer activity on MDA-MB-231 breast cancer cells.⁴⁷



26

Figure 22 – gold^{III} dithiocarbamate oligopeptide complex.

1.17 Other gold^{III} sulfur complexes

There are also examples of other gold^{III} sulfur complexes that show cytotoxic activity towards cancer cell lines.^{23, 48} Fan *et al.* synthesised a series of cyclometalated 2-phenylpyridine gold^{III} complexes and attached both monodentate (SCN⁻), **27a** and bidentate (thiolactic acid), **27b** ligands (Figure 23). *In vitro* cytotoxicity studies against MOLT-4 and C2C12 showed comparable results to cisplatin with IC₅₀ values of under 4.0 μM for the leukaemic cell line, (in comparison to cisplatin with an IC₅₀ of 6.8 μM).²³

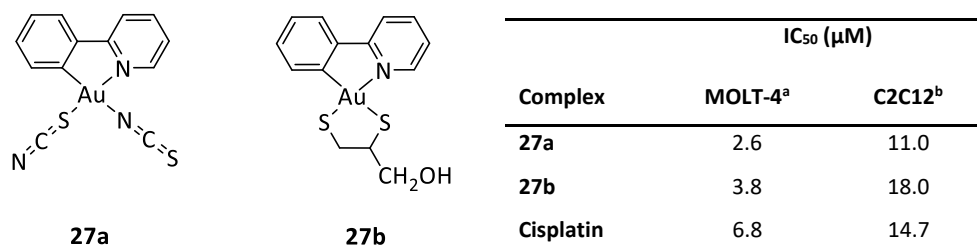


Figure 23 – structures of **27a** and **27b** and their anticancer activity towards human and mouse cancer cell lines in comparison to cisplatin; ^a Human leukaemia, ^b Mouse tumour. Data taken from ref²³.

The same group also synthesised a cyclometalated gold^{III} thiosalicylate complex, **28** (Figure 24) which demonstrated high cytotoxicity against P388 leukaemia cells with an IC₅₀ of 2.5 μM.⁴⁸

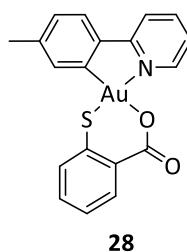
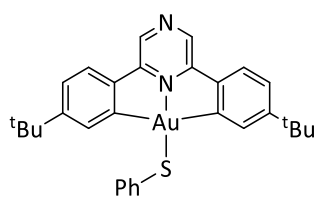
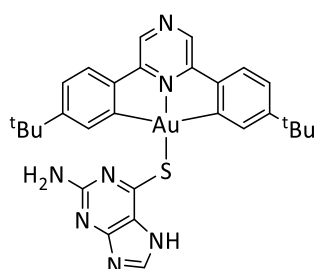


Figure 24 – structure of the gold^{III} thiosalicylate derivative, **28**.⁴⁸

Bertrand *et al.* synthesised neutral derivatives with thiophenol, **29a** and thioguanine, **29b** ligands based on the cyclometalated (C[^]N[^]^C) pyrazine pincer system (Figure 25). Whereas the thiophenol derivative showed no *in vitro* cytotoxicity, the thioguanine complex was toxic at sub-micromolar levels towards leukaemia (HL60) and breast cancer (MCF-7) cells, (IC₅₀ of 0.9 and 0.4 μM respectively) whereas the cytotoxicity towards human lung cancer (A549) cells was considerably lower (IC₅₀ of 29.0 μM). In this particular case, the cytotoxic properties of **29b** were attributed to the thioguanine ligand, a clinically used anticancer drug, rather to the (C[^]N[^]^C)Au^{III}S scaffold.³⁹

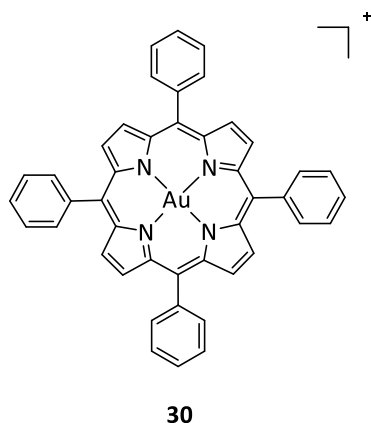
**29a****29b**

Complex	IC ₅₀ ± SD (μM)		
	HL60 ^a	MCF-7 ^b	A549 ^c
29b	0.90 ± 0.22	0.78 ± 0.11	29.0 ± 1.8
Cisplatin	3.7 ± 0.3	21.2 ± 3.9	33.7 ± 3.7

Figure 25 – structures of **29a** and **29b** and the cytotoxicity of **29b** towards human cancer cell lines in comparison to cisplatin; ^a Leukaemia, ^b Breast carcinoma, ^c Lung carcinoma. Data taken from ref³⁹.

1.18 Gold^{III} porphyrin complexes

Experiments conducted by Che *et al.* showed that gold^{III} tetraarylporphyrins, like complex **30** (Figure 26) showed high activity across a panel of human cancer cell lines including some drug resistant variants; the multi-drug resistant human oral carcinoma (KB-V1) and also cisplatin-resistant human nasopharyngeal carcinoma (CNE1). IC₅₀ values were between 0.11-0.73 μM across the board, indicating that no cross resistance was occurring and suggesting that the complex was inducing cytotoxicity via different mechanisms to cisplatin.⁴⁹

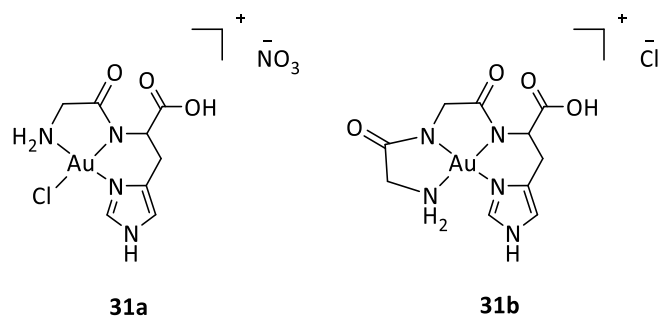


Complex	IC ₅₀ ± SD (μM)			
	KB-3-1 ^a	KB-V1 ^b	SUNE1 ^c	CNE1 ^d
30	0.20 ± 0.03	0.11 ± 0.02	0.11 ± 0.02	0.17 ± 0.02
Cisplatin	13.2 ± 1.24	12.6 ± 0.78	12.6 ± 0.92	40.8 ± 2.17

Figure 26 – gold^{III} porphyrin complex, **30** and its cytotoxicity towards human cancer cell lines; ^a Oral epidermoid carcinoma, ^b Oral epidermoid carcinoma (multi drug resistant), ^c Nasopharyngeal carcinoma, ^d Nasopharyngeal carcinoma (cisplatin resistant). Data taken from ref⁴⁹.

1.19 Gold^{III} amino acid and peptide conjugates

One example of a gold^{III} oligopeptide complex has already been discussed, (**26**)⁴⁷ but other gold^{III} amino acid and peptide conjugated complexes have also been investigated for their chemotherapeutic potential.⁵⁰⁻⁵² Two such derivatives are the complexes with *L*-Histidine containing peptides synthesised by Glisic *et al.*; a tridentate Gly-*L*-His dipeptide derivative, [Au(Gly-*L*-His)Cl]NO₃, **31a** and a tetradentate Gly-Gly-*L*-His tripeptide derivative, [Au(Gly-Gly-*L*-His)Cl], **31b** (Figure 27). The cytotoxic activity of both complexes was strongly cell line dependent. For example, while **31b** was highly cytotoxic towards cervical cancer (HeLa) and promyelocytic leukaemia (HL60); (IC₅₀ values of 0.005 and 2.98 μM respectively), **31a** showed only moderate activity; (IC₅₀ values of 15.9 and 11.9 μM). However, against breast cancer (MCF-7) and colon cancer (HT-29) it was **31a** which showed the better activity; (19.7 and 14.7 μM) while **31b** was nontoxic, (>100 μM). Remarkably, both derivatives also showed significantly reduced activity towards healthy lung fibroblast cells (MRC-5) with IC₅₀ values of more than 100 μM.⁵⁰



Complex	IC ₅₀ ± SD (μM)				
	HeLa ^a	HL60 ^b	MCF-7 ^c	HT-29 ^d	MRC-5 ^e
31a	15.90 ± 1.69	11.93 ± 1.02	19.68 ± 0.23	14.70 ± 1.36	>100
31b	0.0045 ± 0.0002	2.98 ± 0.12	>100	>100	>100
Cisplatin	2.02 ± 0.12	10.31 ± 2.54	1.56 ± 0.26	18.6 ± 2.32	0.48 ± 0.02

Figure 27 – gold^{III} complexes with L-Histidine containing peptide, **31a** and **31b** and their cytotoxic activity towards human cancer cell lines in comparison to cisplatin; ^a Cervical carcinoma, ^b Promyelocytic leukaemia, ^c Breast carcinoma, ^d Colon carcinoma, ^e Normal lung fibroblasts. Data taken from ref⁵⁰.

Lemke *et al.* synthesised a phenylalanine-NHC gold^{III} conjugate, **32** (see Figure 28) although the complex showed relatively poor activity towards both HeLa and HT-29 cells with IC₅₀ values of between 40 and 100 μM.⁵¹ Other trihalide derivatives **33**, reported by Ortego *et al.* conjugated amino ester derivatives, (*L*-AlaOMe, *L*-ValOMe and *L*-PheOMe), to a gold^{III} centre via a pyridine nitrogen. These also showed reduced cytotoxicity towards a panel of human cancer cell lines with IC₅₀ values of above 50 μM.⁵²

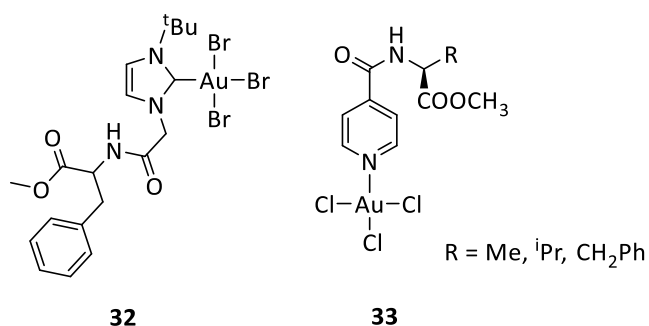


Figure 28 – examples of other gold^{III} amino acid conjugates.^{51, 52}

1.2 Part 2 – cellular and molecular targets of gold^{III} complexes

1.2.1 DNA binding

Due to the high levels of structural and electronic similarity between gold^{III} and platinum^{II} complexes, (d^8 , square planar), initial mechanistic studies focused on DNA and RNA as the primary molecular target for gold^{III} complexes as these are the major targets for platinum based chemotherapeutic agents like cisplatin.⁵³ However, mechanistically, platinum^{II} and gold^{III} appear to be rather different and although there are examples of gold^{III} complexes targeting both double-stranded DNA and higher order DNA structures like G-quadruplexes, these structures are clearly not the primary molecular target.^{39, 49}

The cytotoxic effects of cisplatin mainly result from its interaction with DNA. Cisplatin forms covalent adducts between purine DNA base pairs, usually between two guanines or one guanine and one adenine, and this causes the formation of adducts and the distortion of the DNA helix which inhibits DNA replication and transcription processes (Figure 29).⁵³

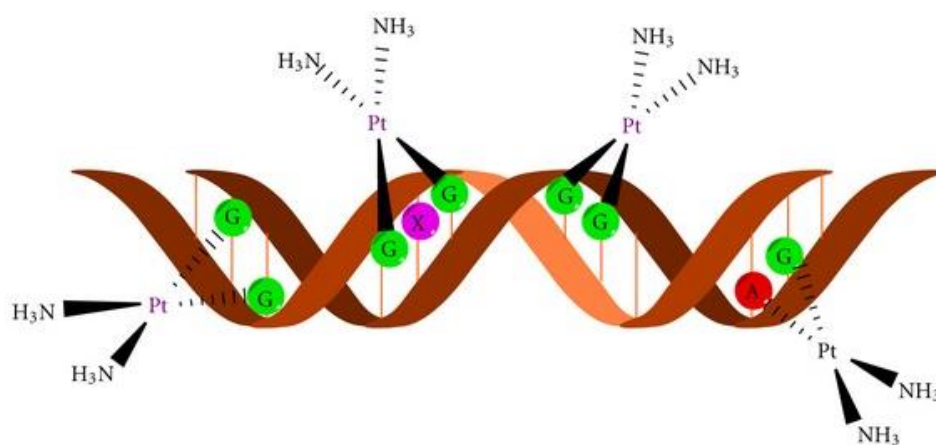


Figure 29 – mechanism of cisplatin. Image taken from *Bioinorganic Chemistry and Applications*, 2012, ref⁵⁴.

Porphyrin gold^{III} complexes like derivative **30** (Figure 26) are also able to interact strongly with DNA, causing DNA fragmentation, although these interactions are different from those of cisplatin and are non-covalent and reversible.^{49, 55} The mechanism of this complex is clearly non-specific as numerous other molecular targets have also been confirmed for porphyrin gold^{III} complexes.⁵⁶⁻⁵⁸

Similarly triazacyclononane gold^{III} derivatives like derivative **4** (Figure 5) can induce non-covalent conformational changes to DNA.¹⁶ Further studies on dithiocarbamate complexes, **23a/b** (Figure 19) by Ronconi *et al.* showed that the complexes are able to produce complex-

DNA adducts, resulting in the inhibition of DNA synthesis and consequently cell death. More importantly, it was also shown there was no cross resistance with cisplatin, suggesting that the DNA lesions induced by the dithiocarbamate derivatives are repaired less effectively than those induced by cisplatin. However, in spite of the complexes showing affinity towards DNA, the adducts formed were less stable than those induced by the reference drug cisplatin, once again suggesting that the interaction with the DNA double helix was weak and reversible in nature.⁵⁹

DNA intercalation is another reversible mode of DNA-ligand binding which consists of the direct insertion of planar aromatic moieties in between the base pairs of DNA which causes unwinding to the double helix. Terpyridine gold^{III}, **5** and aminoquinoline gold^{III}, **6** derivatives (Figure 5) can bind to intracellular DNA by intercalation of the planar gold^{III} coordination plane between the DNA base pairs although it has not been determined whether or not this interaction is responsible for the cytotoxicities of the complexes.^{17, 18} Cyclometalated gold^{III} NHC complexes, **18** (Figure 15) can also bind to double stranded DNA by intercalation, causing inhibition of the enzyme topoisomerase (TopoI) and the induction of apoptosis.³⁷ TopoI is an enzyme that unwinds chromosomal DNA and is an important target for anti-cancer agents.⁶⁰

1.22 *G-quadruplex and i-motif stabilisation*

G-quadruplexes are emerging as promising targets for the development of novel anticancer agents. These are four-stranded DNA structures that form in guanine-rich DNA sequences and are found both in the telomers and in the over-expressed gene promoter regions of cancer genes (Figure 30).^{61, 62} I-motifs are higher-order DNA structures that are formed in sequences rich in cytosine via hydrogen bonding between the hemiprotonated pairs of cytosines (Figure 30).⁶³ Stabilisation of i-motif structures has been shown to have an effect on telomerase activity and oncogene expression and therefore compounds that stabilise these structures have potential as anticancer drugs.⁶⁴

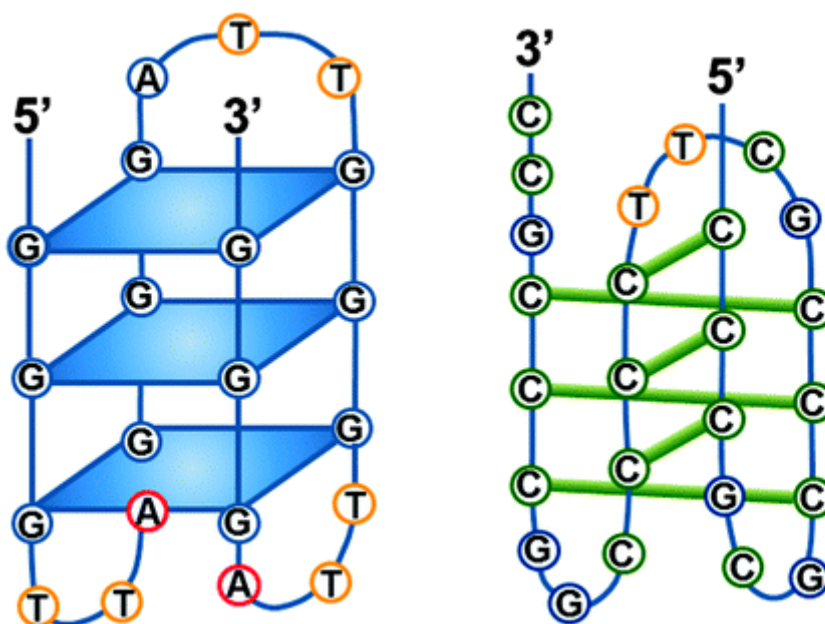


Figure 30 – structure of G-quadruplex (left) and i-Motif (right) structures. Image adapted from *Chemistry Society Reviews*, 2014, ref⁶⁵.

There are several recent examples of gold^{III} complexes that target these structures. For example, Gratteri *et al.* showed that dioxobridged gold^{III} complexes like derivative **7** (Figure 6) and cyclometalated oxo compounds like **13** and **14** (Figure 11) all showed high levels of binding to human G-quadruplexes whereas double stranded DNA was not affected at all.⁶⁶ Recently Bertrand *et al.* also showed that a gold^{III} benzimidazole-based NHC complex, **19** (Figure 16) could selectively stabilise both G-quadruplex and i-motif structures over double stranded DNA.³⁹

1.23 Inhibition of the proteasome

Another emerging target for gold complexes is the ubiquitin proteasome. The proteasome is an important regulator of cellular growth and apoptosis and specific proteasome inhibitors can act as novel anticancer agents.⁶⁷ Milacic *et al.* showed that the dithiocarbamate derivative **23a**, (Figure 19) was able to suppress tumour growth by the direct inhibition of the chymotrypsin-like activity both in purified rabbit 20S proteasome and also in the 26S proteasome of intact MDA-MB-231 breast cancer cells.⁶⁸ Tomasello *et al.* showed similar results for **23b** in intact MCF-7 cells.⁶⁹ The proteasome has also been identified as a major target of gold^{III} dithiocarbamate peptide conjugates, **26** (Figure 22) both in purified human

20S proteasome and also in intact MDA-MB-231 cell extracts as well as in an *in vivo* nude mice model.⁴⁷

Other cyclometalated gold^{III} dithiocarbamate derivatives, like derivative **25** (Figure **21**), have shown potent deubiquitinase inhibition properties.⁴⁶ These are protease enzymes that regulate the ubiquitin system by specifically hydrolysing peptide bonds between ubiquitin and its conjugated proteins. The regulation of the ubiquitin cycle is important for many cellular processes in cancer cells including DNA repair, the cell cycle and some signalling pathways and therefore deubiquitinase inhibitors are emerging as promising targets for new anticancer agents.⁷⁰

1.24 *Inhibition of thioredoxin reductase (TrxR)*

Thioredoxin reductase, (TrxR) catalyses the NADPH-dependent reduction of thioredoxin disulphide and other oxidised cell constituents. TrxR contributes to the redox homeostasis in cells thus helping to prevent oxidative stress which can result in DNA damage. Reduced thioredoxin acts as a growth factor in cancer tumours and consequently the overexpression of this enzyme has been observed in many cancer cell lines and high intracellular levels have also been associated with cellular resistance to platinum-based drugs.⁷¹

The enzyme has a high degree of sequence homology to the antioxidant enzyme glutathione reductase, (GR) but contains an essential selenocysteine, (SeCys) residue in the active site, (Figure **31**), which is not present in GR. This SeCys residue is a major target of gold-containing complexes; for example, the anti-rheumatic drug auranofin (Figure **2**) is a potent and specific TrxR inhibitor.^{71, 72} Due to the high selectivity of gold compounds for selenocysteines, the inhibition of TrxR tends to be highly selective and the inhibition of GR requires significantly higher drug concentrations.⁷³

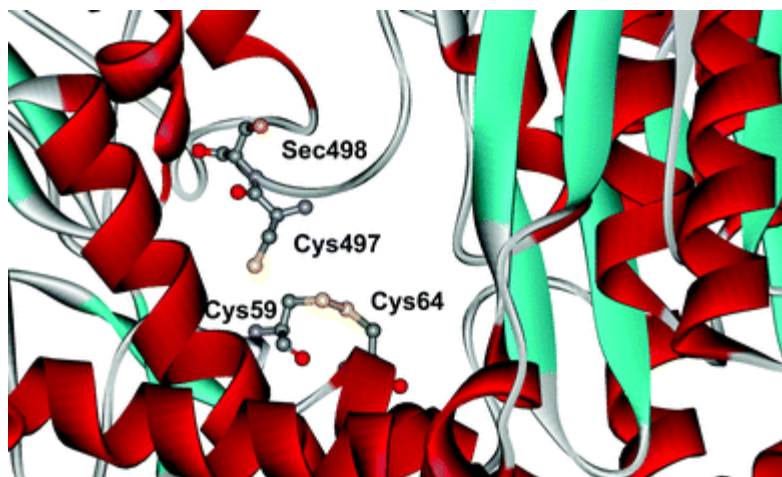


Figure 31 – catalytic site of TrxR. Image adapted from Dalton Transactions, 2011, ref⁷⁴.

There are numerous examples of both gold^I and gold^{III} complexes that show high levels of TrxR inhibition.^{44, 75, 76} For example, enzyme inhibition studies on cyclometalated gold^{III} 2,4,6-tris(trifluoromethyl)phenyl complexes, **11a-11d** (Figure 32) showed that the complexes were acting as TrxR inhibitors with up to 49-fold selectivity towards this enzyme over glutathione reductase (GR).²⁵ As both of these enzymes are two of the main components of the cellular antioxidant mechanism, the inhibition of these enzymes can cause a strong cellular response in the form of reactive oxygen species (ROS).^{71, 77, 78} The complexes were also shown to induce a strong increase in intracellular ROS levels in a concentration-dependent manner, further confirming their ability to inhibit TrxR.²⁵

11a, PPh₃
11b, OH₂
11c,
11d,

Complex	IC ₅₀ (μM)		
	TrxR ^a	GR ^b	Selectivity (IC _{50TrxR} /IC _{50GR})
11a	2.0	12.3	6.2
11b	1.0	>50	>49.0
11c	6.3	>50	>7.9
11d	1.1	36.4	32.8
Auranofin	0.009	15	1666

Figure 32 – the inhibition of TrxR and GR by gold^{III} derivatives **11a-11d** in comparison to auranofin. Data taken from ref²⁵.

1.25 Induction of apoptosis

The induction of apoptosis, (the process of programmed cell death), is a highly complex process which involves an energy-dependent cascade of molecular events which includes the permeabilization of the outer membrane of the mitochondria and the initiation of both caspase-dependent and caspase-independent cell death.⁷⁹

Park *et al.* demonstrated that treatment of HL60 leukaemia cells with auranofin induced apoptosis in both a concentration and time dependent manner, causing the generation of ROS. This, in turn, caused the subsequent activation of p38 mitogen-activated protein kinase, (p38 MAPK) leading to the activation of initiator caspases to stimulate further apoptotic events including the activation of caspase-3, PARP degradation, DNA fragmentation and finally cell death.⁸⁰

Further work on gold^{III} porphyrin complexes, **30** (Figure **26**) also showed the induction of apoptosis related to the production of ROS in human nasopharyngeal carcinoma cell lines. Treatment with the gold^{III} complex caused a depletion of the mitochondrial transmembrane potential, ($\Delta\psi_m$) which led to cytochrome *c* release, nucleus translocation of apoptosis inducing factor and the generation of ROS. Similarly to the studies on auranofin, conducted by Park *et al.*, treatment with the gold^{III} porphyrin complex also led to the subsequent activation of p38 MAPK and led to further apoptotic events.⁵⁶

1.26 Glutathione and other protein targets

Glutathione (GSH) is a tripeptide formed by glutamic acid, cysteine and glycine (Figure **33**) that reaches millimolar concentration inside cells. It plays an important role in many cellular processes including the maintenance of the intracellular redox homeostasis by the scavenging of ROS. An increased intracellular concentration of GSH in cancer cells contributes towards the extravascular growth of metastatic cells as well as being a major contributing factor towards drug resistance by deactivation.^{81, 82}

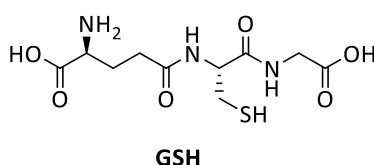


Figure **33** – structure of the GSH tripeptide.⁸²

There are many examples of GSH deactivating gold^{III} complexes. Further work by Gabbiani *et al.* on the dinuclear, gold^{III} oxo-bridged complex, **7** (Figure 6) showed a rapid reduction by GSH, which suggested that within the cellular environment the complex is reduced to a gold^I active species.^{19, 28} The gold dithiocarbamate complex, derivative **24** (Figure 20) also reacted with reduced glutathione and *L*-cysteine in a time dependent manner by the substitution of one diethyldithiocarbamate ligand for one cysteine molecule.⁴⁵

Stability in the presence of reduced glutathione can improve the cytotoxic potential of gold^{III} complexes. In comparison to the dinuclear (N[^]N) chelate complex, **7** (Figure 6), discussed earlier, the cyclometalated (N[^]N[^]C) complex, **14** (Figure 11) showed significantly increased stability under physiological conditions and was not reduced in the presence of GSH. Upon reaction with two model proteins; hen egg white lysozyme, (HEWL) and horse heart cytochrome *c*, (cyt *c*) the complex formed a monometallic adduct with the gold centre remaining in the +3 oxidation state and maintaining the (N[^]N[^]C) ligand, thus implying that the reaction of the complex with proteins facilitates the cleavage of the oxygen bridge and the conversion of the bimetallic species to the monometallic equivalent.^{19, 28}

Complex **19** (Figure 16) was also stable in the presence of GSH, showing no reduction to gold⁰ or gold^I. Results also suggested that the complex inhibited MDM2-p53 protein-protein interactions, another emerging target for anticancer agents (Figure 34).³⁹ MDM2 inhibits the p53 tumour suppressor and overexpression of this enzyme is associated with many different cancers thus making the disruption of MDM2-p53 protein-protein interactions a promising target for selective anticancer cytotoxicity.⁸³

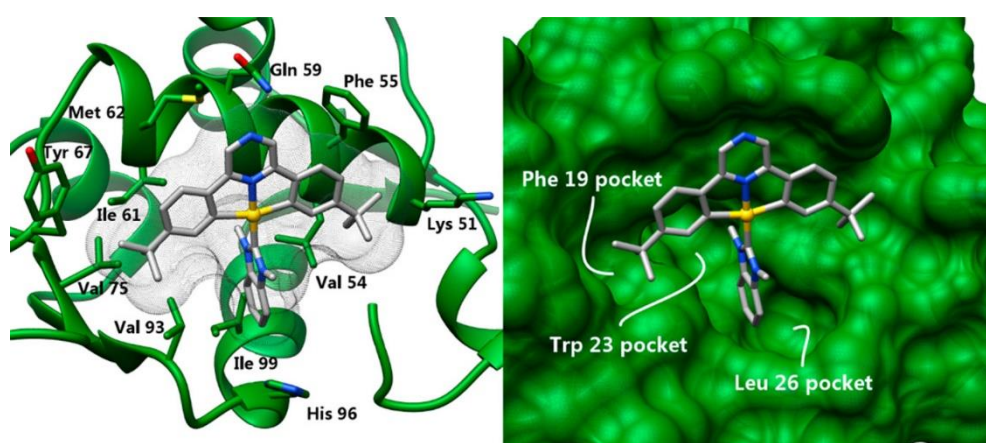


Figure 34 – representation of the cyclometalated gold^{III} benzimidazole-based derivative, complex **19** docked in MDM2. Image taken from *Inorganic Chemistry*, 2017, ref³⁹.

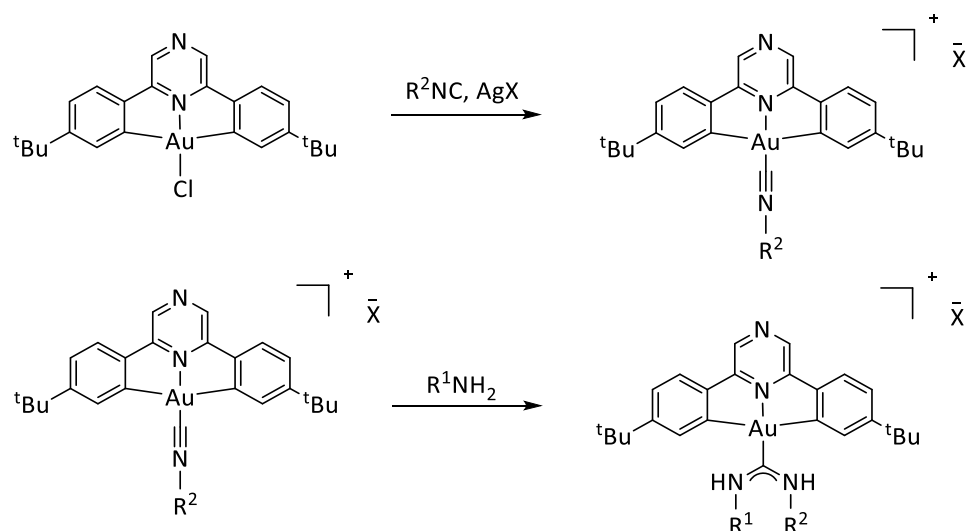
Gold^{III} tetraarylporphyrins, like complex **30** (Figure **26**) are also highly stable under physiological conditions and are not reduced in the presence of glutathione, making them promising as potential chemotherapeutic agents. Biochemical and cellular experiments also identified heat-shock protein 60, Hsp60, to be an important molecular target of the complex.⁸⁴ Hsp60 is an essential chaperone for mitochondrial protein transport and folding and plays an important role in the regulation of apoptosis as well as in the regulation of tumours. It is also upregulated in some human cancers.⁸⁵

1.3 Conclusion

Gold^{III} complexes are undeniably an emerging class of potential chemotherapeutic agents. In recent years, numerous and structurally diverse gold^{III} complexes have been synthesised and characterised as prospective anticancer agents and have shown potent cytotoxicity both *in vitro* and *in vivo* towards human cancer cells. Certainly, the majority of the complexes discussed here appear to show comparable or higher cytotoxicity than the clinically available drug cisplatin, which again highlights their chemotherapeutic potential. However, although biochemical experiments have successfully identified a large variety of molecular targets for these complexes, more extensive studies are required to fully determine the mechanism of action of cytotoxic gold^{III} complexes *in vivo*. Until the full picture is determined, it will be impossible to know the full potential of gold^{III} complexes as prospective anticancer drugs.

The following work will focus on the synthesis and anticancer activity of cyclometalated gold^{III} complexes with both tridentate (C[^]N[^]^C) pincer ligands and bidentate (C[^]N) cyclometalated ligands to improve their physiological stability. Biologically relevant ligands, selected to enhance the cytotoxicity of the complexes towards cancer cell lines, were then incorporated into the complexes via the free coordination sites.

Chapter **2** introduces the synthesis and anticancer activity of the first (C[^]N[^]^C)Au^{III} complexes of acyclic carbene ligands, decorated with amine and amino ester functional groups. The synthesis started with the formation of the cationic gold-isocyanide complex and the subsequent nucleophilic attack by an amine, as depicted in Scheme **1**.



Scheme 1 – the synthetic pathway to the acyclic carbene complexes introduced in Chapter 2.

Chapter 3 introduces the synthesis and anticancer properties of cyclometalated gold^{III} complexes with acridine-decorated functional groups, chosen to promote DNA binding and thus increase the cytotoxicity of the complexes. These complexes included a series of neutral mono-cyclometalated (C[^]N)-(N[^]X)Au^{III} complexes with both simple and acridine-decorated (N[^]O) and (N[^]N) chelating ligands, and two cationic bis-cyclometalated (C[^]N[^]z[^]C)Au^{III} complexes where the acridine moiety was connected to an acyclic diamino carbene ligand or to an N-heterocyclic carbene ligand, (Figure 35).

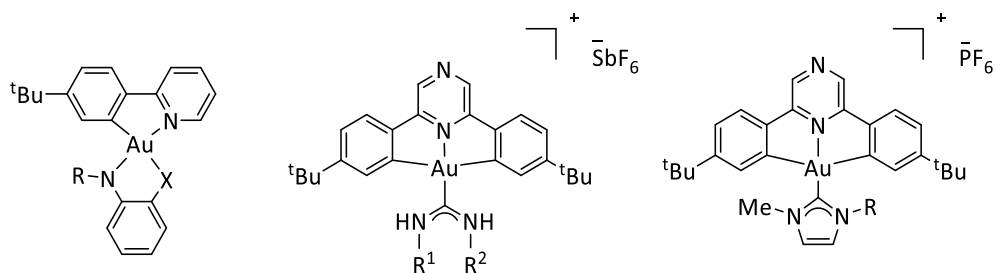
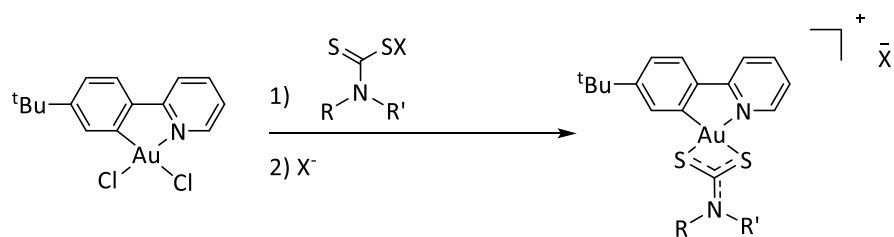


Figure 35 – mono-cyclometalated (C[^]N)-(N[^]X)Au^{III} complexes and cationic bis-cyclometalated (C[^]N[^]z[^]C)Au^{III} complexes with acridine decorated ACC and NHC ligands discussed in Chapter 3.

Chapter 4 discusses the synthesis and biological activity of cyclometalated gold^{III} complexes with dithiocarbamate ligands, synthesised by the reaction of the cyclometalated gold^{III} dichloride precursor with the respective dithiocarbamate ligand, followed by an anion exchange reaction to give the cationic cyclometalated gold^{III} dithiocarbamate complex, (Scheme 2).



Scheme 2 – the synthesis of the cyclometalated gold^{III} dithiocarbamate complexes, discussed in Chapter 4.

The complexes were all tested for their anticancer activity *in vitro* towards a panel of human cancer cell lines in comparison to the clinically available drug cisplatin. Investigations into the possible mechanism of action of these complexes were also undertaken, including cell uptake studies, DNA binding assays, GSH reactivity, reactivity towards other representative biomolecules and the production of ROS.

Chapter 2

The synthesis and anticancer activity of (C^{N^pz}C)Au^{III} complexes of acyclic carbene ligands decorated with amino esters.

Based on: (C^{N^pz}C)Au^{III} complexes of acyclic carbene ligands: synthesis and anticancer properties. *Dalton Trans.*, 2017, **46**, 13397-13408.⁸⁶

2.1 Abstract

A series of novel cationic gold^{III} pincer complexes containing a cyclometalated pyrazine based ($C^AN^{Pz^A}C$) pincer ligand and acyclic diamino carbene ancillary ligands were synthesised and characterised as prospective anticancer agents. The two-step synthesis included the formation of a cationic ($C^AN^{Pz^A}C$)Au^{III} isocyanide complex, (**41**) followed by a nucleophilic attack onto the highly electrophilic isocyanide carbon by a broad range of nucleophiles including water, (**42**) amines (**43a** and **43b**) and amino ester derivatives (**43c-43g**). This allowed the synthesis of a library of [($C^AN^{Pz^A}C$)Au(ACC)]SbF₆ complexes with aniline, (**43a**) adamantyl amine, (**43b**) as well as five amino ester derivatives, (**43c-43g**). The complexes were tested with a preliminary cytotoxicity assay against human adenoma-type lung cancer cells (A549) and the four most promising, (**43b-43d** and **43g**) were then further tested on a panel of human cancer cell lines and also healthy lung fibroblast cells (MRC-5) for comparison. The four selected complexes showed promising cytotoxicity results in comparison to cisplatin as well as an improved selectivity for MCF-7 breast adenocarcinoma cells over healthy lung fibroblast cells.

2.2 Introduction

As discussed previously (Section 1.13) cyclometalating ligands are frequently used to stabilise a gold^{III} centre towards reduction under physiological conditions and thus enhance the cytotoxic potential of prospective anticancer agents. Both bidentate (C^AN) and tridentate (C^AN^AN) or (C^AN^AC) ligands can be used for this purpose.^{25, 27, 31, 39} These complexes tolerate a broad range of ancillary ligands such as N-heterocyclic carbene (NHC); **17**,³⁷ N-donor; **15**,²⁹ phosphine; **11**,²⁵ and sulfur-based ligands; **29a**,³⁹ which enables the optimization of the biological properties of these complexes (Figure 36).

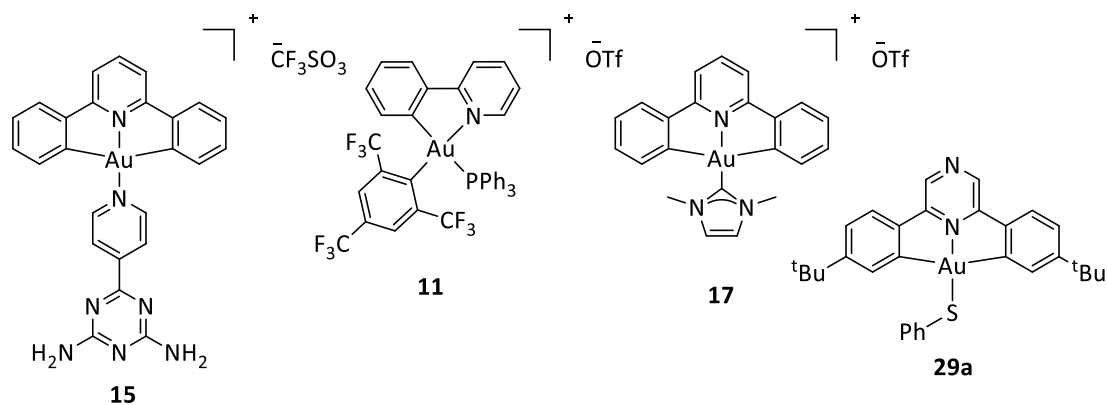
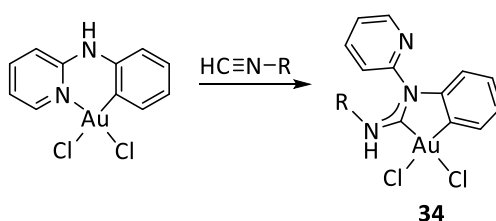


Figure 36 – examples of cyclometalated gold^{III} complexes with cytotoxic properties.^{25, 29, 37, 39}

In the 1970s, Parks *et al.* and Minghetti *et al.* reported the synthesis of the first gold^{III} acyclic carbene complexes, prepared by the reaction of isocyanides and amines with AuCl₄. These were shown to behave as oxidising agents.^{87, 88} Further early work on gold^{III} open-carbene systems by Usón *et al.* also described the synthesis of mononuclear, mono-carbene gold^{III} complexes, synthesised by the reaction of primary or secondary amines with gold^{III} isocyanide complexes to produce the corresponding acyclic carbene complex.⁸⁹ More recently Crespo *et al.* synthesised acyclic carbene complexes, **34** by the insertion of an isocyanide into a gold-nitrogen bond, (Scheme 3).⁹⁰



*Scheme 3 – the insertion of an isocyanide into a gold-nitrogen bond to produce an acyclic carbene.*⁹⁰

The same group demonstrated the biological activity of several acyclic carbene complexes towards three human cancer cell lines; T-cell leukaemia (Jurkat), pancreatic cancer (MiaPaca2) and lung cancer (A549), (Figure 37). Derivatives **35a** and **35b** displayed a higher cytotoxicity than cisplatin towards all three cell lines (IC₅₀ values of between 0.8 – 25 μM in comparison to cisplatin 11 – >100 μM). The derivatives also appeared to show some selectivity towards certain cell lines. While derivative **35a** was highly cytotoxic towards the MiaPaca2 cell line (IC₅₀ value of 1.7 μM), it was poorly cytotoxic towards the A549 cells (IC₅₀ of 17.5 μM). In comparison, derivative **35b** showed an increased cytotoxicity towards A549 over MiaPaca2 cells, (IC₅₀ values of 1.5 vs 25 μM respectively).⁹¹

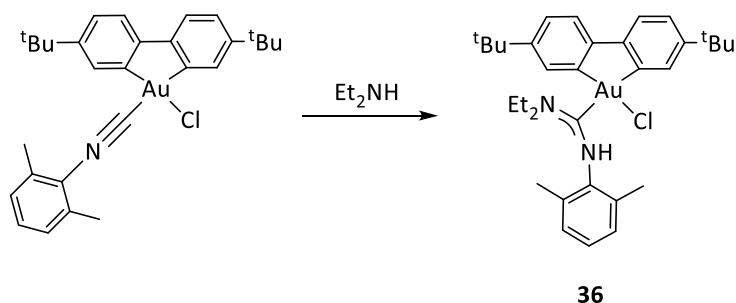
Complex 35a: A gold(III) center coordinated to two pentafluorophenyl (C₆F₅) ligands, a bidentate ligand with a pyridine ring and a secondary amine, and an acyclic carbene ring. The acyclic carbene ring is substituted with a naphthalene group.

Complex 35b: A gold(III) center coordinated to two pentafluorophenyl (C₆F₅) ligands, a bidentate ligand with a pyridine ring and a secondary amine, and an acyclic carbene ring. The acyclic carbene ring is substituted with a phenyl group.

Complex	IC ₅₀ ± SD (μM)		
	Jurkat ^a	MiaPaca2 ^b	A549 ^c
35a	0.8 ± 0.7	1.7 ± 0.8	17.5 ± 1.7
35b	1.26 ± 0.6	25	1.52 ± 0.8
Cisplatin	10.8 ± 1.2	114.2 ± 9.1	76.5 ± 7.4

Figure 37 – biologically active acyclic carbene derivatives 35a and 35b and their cytotoxicity towards human cancer cell lines in comparison to cisplatin; ^a T-cell leukaemia, ^b Pancreatic cancer, ^c Lung cancer. Data taken from ref⁹¹.

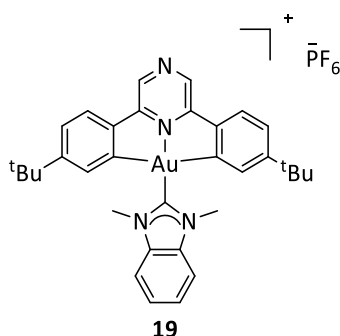
The nucleophilic attack of an amine onto a gold-isocyanide complex is another method that can be used for the synthesis of acyclic carbene complexes (Scheme 4). David *et al.* used this method to synthesise the (C[^]C) cyclometalated gold^{III} N-acyclic carbene complex, AuCl(^tBu₂Bip)-[C(NEt₂)(NHXY)], **36**.⁹²



*Scheme 4 – the nucleophilic attack of an amine onto a gold- isocyanide complex to produce an acyclic carbene, 36.*⁹²

Gold^{III} acyclic carbene complexes were therefore chosen as the proposed synthetic target as they presented a simple way to functionalise gold^{III} complexes with bio-active functional groups. These functional groups could be fine-tuned to enhance the anticancer activity and improve the selectivity of the complex towards cancer cells over healthy cells.

As described in Section 1.14, the pyrazine-based gold^{III} pincer complex with a benzimidazole-based ligand, [(C[^]N^{p2}^C)Au(NHC)]⁺, **19** (Figure 38), showed promising cytotoxicity towards human leukaemia (HL60), breast (MCF-7), and lung (A549) cancer cells. However, it also displayed rather poor selectivity towards healthy lung fibroblast cells (MRC-5) which suggested that the selectivity of the complex needed to be improved. The [(C[^]N^{p2}^C)Au(NHC)]⁺ complexes were also very stable under physiological conditions and were tolerant to increased levels of glutathione (GSH).³⁹ As discussed previously in Section 1.26, an increased intracellular concentration of GSH is often associated to high levels of cellular growth in cancer as well as being a major contributing factor towards drug resistance by deactivation.^{81, 82}



Complex	IC ₅₀ ± SD (μM)			
	HL60 ^a	MCF-7 ^b	A549 ^c	MRC-5 ^d
19	0.31 ± 0.15	0.56 ± 0.02	7.8 ± 1.3	1.4 ± 0.4
Cisplatin	3.7 ± 0.25	21.2 ± 3.9	33.7 ± 3.7	10.7 ± 3.0

Figure 38 – Structure of the benzimidazole-based NHC complex, **19** and its cytotoxicity towards human cell lines in comparison to cisplatin; ^a Leukaemia, ^b Breast carcinoma. ^c Lung carcinoma, ^d Normal lung fibroblasts. Data taken from ref³⁹.

Some of the limitations of platinum based chemotherapeutics were outlined in Section 1.11. These include a limited spectrum of action, drug resistance and severe side effects.^{3, 4} Improving the selectivity of potential new chemotherapeutic agents for cancer cells over healthy cells helps to avoid the side effects that limit the effectiveness of platinum based anticancer agents.⁵

Recently, the coupling of organometallics to peptides has been shown to increase their selectivity for cancer cells.^{93, 94} This concept has been applied predominantly to gold^I complexes using mono- or polypeptide vectors.⁹⁵ Several examples of gold^{III} complexes conjugated to amino acid and peptide derivatives have already been discussed in Section 1.19. These have also shown an increased selectivity towards cancer cells over healthy cells. For example, Glisic *et al.* synthesised two gold^{III} complexes with *L*-Histidine containing peptides (Figure 39); a tridentate Gly-*L*-His dipeptide derivative, [Au(Gly-*L*-His)Cl]NO₃, **31a** and a tetradentate Gly-Gly-*L*-His tripeptide derivative, [Au(Gly-Gly-*L*-His)Cl], **31b**. The cytotoxic activity of both complexes was assessed towards cancer cell lines as well as healthy MRC-5 cells and although their activity was strongly cell line dependent, both complexes were nontoxic towards the healthy cells with IC₅₀ values of more than 100 μM.⁵⁰

Amino acid and peptide derivatives have also been conjugated to gold^{III} centres using other methods. As mentioned previously, Lemke *et al.* synthesised a phenylalanine-NHC gold^{III} conjugate; **32**,⁵¹ and Ortego *et al.* conjugated amino ester derivatives to a gold^{III} centre via a pyridine nitrogen; **33** (Figure 39).⁵² Other authors have used dithiocarbamate ligands to conjugate cancer targeting oligopeptides to gold^{III} centres (Section 1.16). One dipeptide derivative [AuBr₂(DTC-Sar-AA-O^tBu)], **26** synthesised by Nardon *et al.* showed high levels of

cytotoxicity towards MDA-MB-231, breast cancer cells both *in vitro* and in an *in vivo* nude mice model (Figure 39).⁴⁷

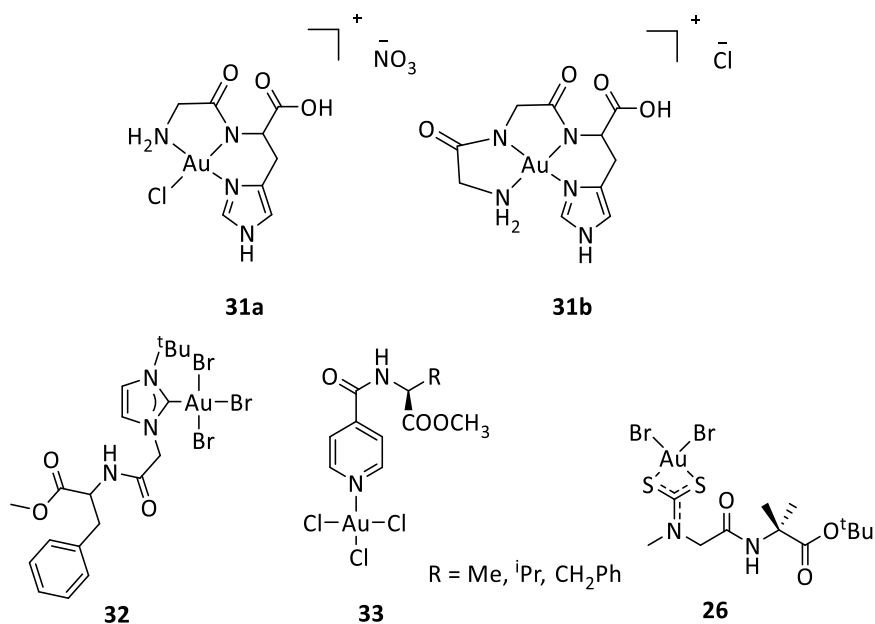
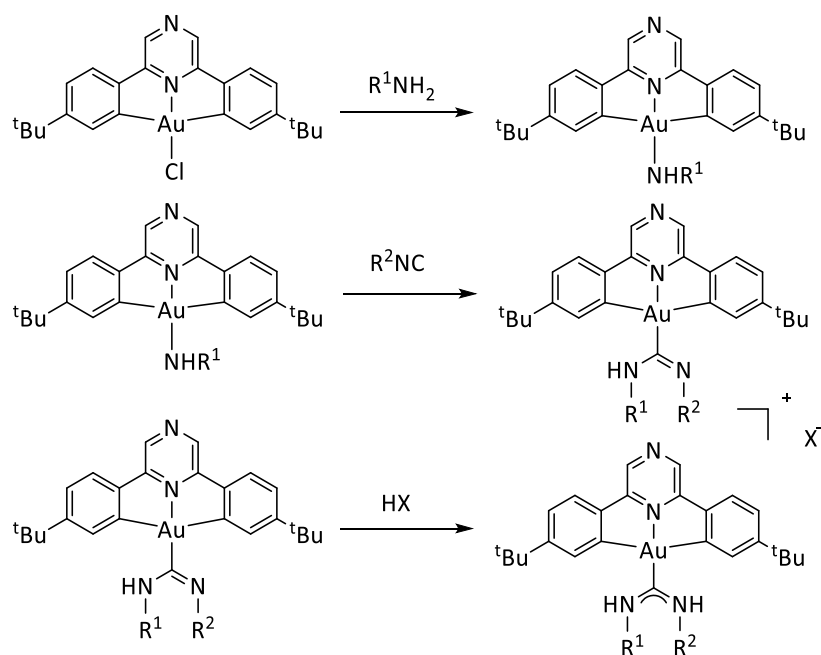


Figure 39 – Structures of previously reported gold^{III} derivatives with amino acid and peptide conjugates.^{47, 50-52}

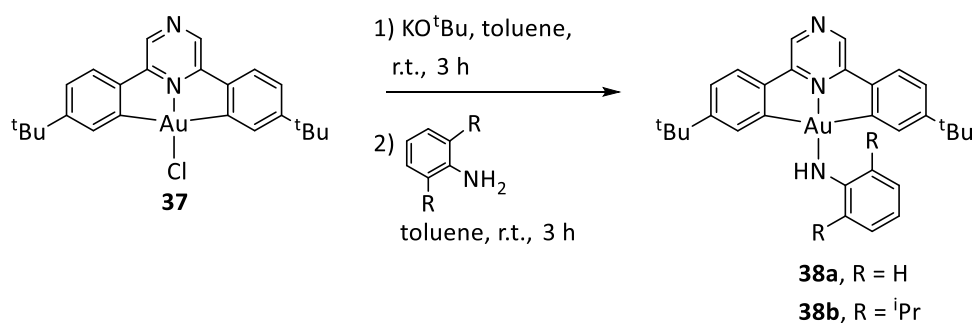
Discussed above are several examples of gold^{III} complexes conjugated to amino acid derivatives but there are no examples of cyclometalated complexes. We therefore decided to explore the synthesis and anticancer activity of cyclometalated ($\text{C}^{\wedge}\text{N}^{\text{P}2}\text{C}$) gold^{III} acyclic carbene complexes bearing amino ester substituents.

The first synthetic pathway to the cyclometalated acyclic carbene complexes was initially explored by our group using a three-step synthesis; the formation of the gold^{III} amino complex, followed by an insertion of an isocyanide into the Au-N bond to afford the corresponding insertion product, and protonation to form the acyclic carbene, (Scheme 5).



Scheme 5 – the first synthetic pathway to the gold^{III} acyclic carbene complex.

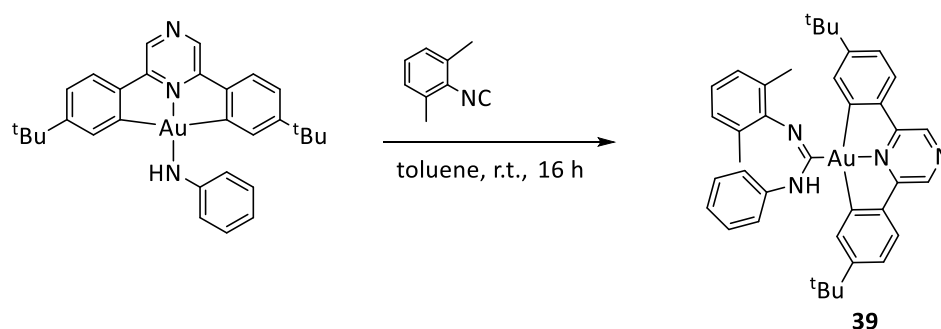
This was initially explored using aniline and 2,6-diisopropylaniline, using a method previously reported by our group for other N-based ligands.⁹⁶ Complexes **38a** and **38b** were obtained after activation of the $(C^{\wedge}N^{p^z} \wedge C)Au-Cl$, **37** with *tert*-butoxide in toluene at room temperature, followed by the addition of the aniline derivative, as depicted in Scheme 6.



Scheme 6 – synthesis of $(C^{\wedge}N^{p^z} \wedge C)Au$ aniline complexes.

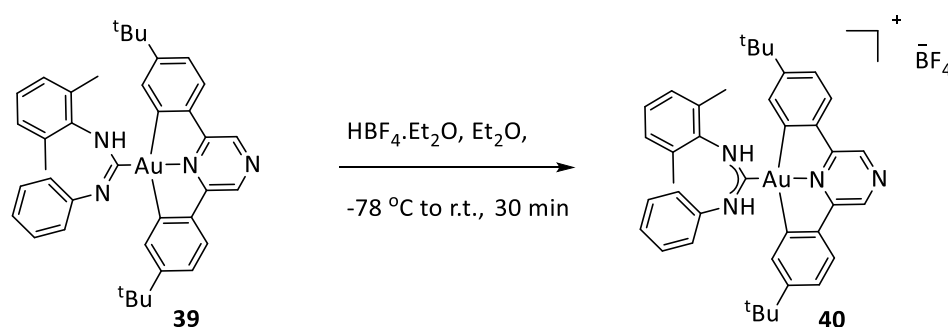
Complex **38a** was then reacted successfully with 2,6-dimethylphenylisocyanide in toluene, at room temperature overnight to afford the corresponding insertion product, complex **39** (Scheme 7). The reaction was also attempted with **38b** but the sterically hindered 2,6-diisopropylaniline ligand did not react and the starting material was isolated again. In an attempt to vary the isocyanide, an insertion into the Au-N bond of **38a** was also attempted with both *tert*-butyl isocyanide and cyclohexyl isocyanide. Both reactions were unsuccessful; whereas *tert*-butyl isocyanide inserted successfully, the product would subsequently

rearrange to produce the corresponding cyanide complex. This was also previously observed during other reactions using the pyridine based pincer ligand undertaken by our group.⁹⁷ Cyclohexyl isocyanide also reacted but formed a mixture of products that could not be purified.



Scheme 7 – synthesis of the insertion product from the corresponding aniline complex.

The protonation of complex **39** with $\text{HBF}_4 \cdot \text{OEt}_2$ produced the air-stable gold^{III} acyclic diamino carbene, complex **40** (Scheme **8**).



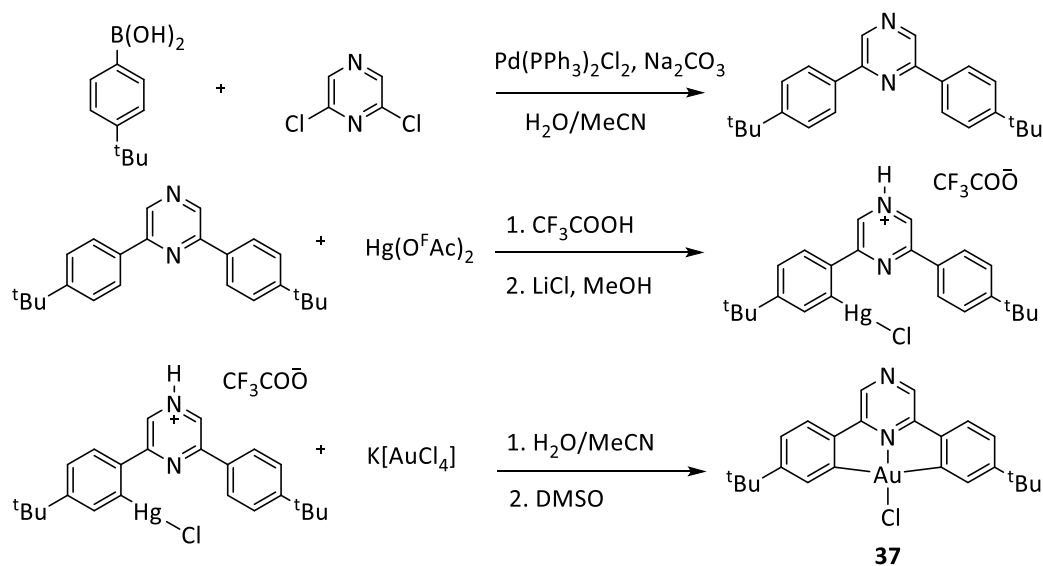
Scheme 8 – protonation of complex 39 to produce the acyclic carbene complex, 40.

The first synthetic pathway offered a successful route to the gold^{III} acyclic diamino carbene complexes but offered little versatility as neither the amine nor the isocyanide functional groups could be easily changed and consequently biologically relevant functionality could not be introduced into the system. We therefore developed the second synthetic pathway with the aim to incorporate a wider range of primary amines and amino esters to the $(\text{C}^{\wedge}\text{N}^{\text{Pz}}\wedge\text{C})\text{Au}^{\text{III}}$ backbone. This allowed the synthesis of a library of $[(\text{C}^{\wedge}\text{N}^{\text{Pz}}\wedge\text{C})\text{Au}(\text{ACC})]\text{SbF}_6$ complexes which were subsequently screened for their cytotoxicity against human lung cancer cells (A549). The four most promising were then further tested against a panel of human cancer cell lines including lung adenocarcinoma (A549), leukaemia (HL60), colon cancer (HCT-116), breast cancer (MCF-7 and MDA-MB-231) as well as healthy fibroblasts (MRC-5) for comparison.

2.3 Results and Discussion

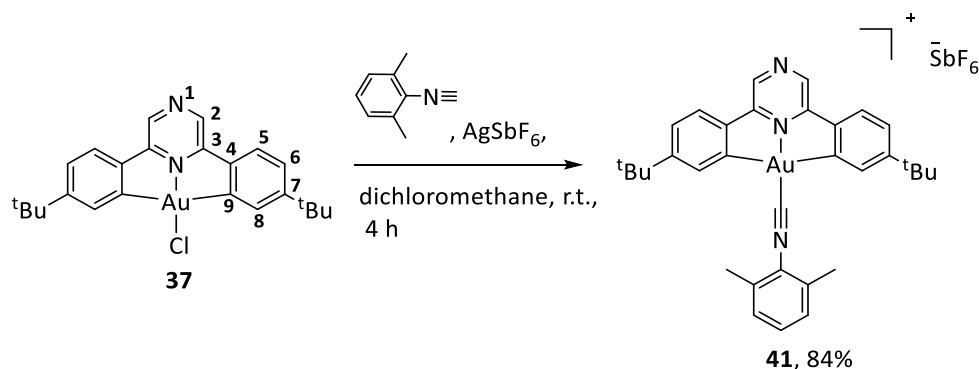
2.3.1 Synthesis and structural characterisation

The cyclometalated ($C^{\wedge}N^{pz^{\wedge}}C$)AuCl starting material, **37** was synthesised using previous methods; via a Suzuki cross-coupling reaction to generate the ($HC^{\wedge}N^{pz^{\wedge}}CH$) ligand and a mercuriation reaction, followed by a transmetalation to obtain the cyclometalated product, as depicted in Scheme 9.⁹⁶



Scheme 9 – synthesis of ($C^{\wedge}N^{pz^{\wedge}}C$)Au^{III}Cl, **37**.⁹⁶

Following reported procedures,⁸⁷⁻⁸⁹ the ($C^{\wedge}N^{pz^{\wedge}}C$)Au^{III} isocyanide complex was chosen as the starting point for this pathway because the isocyanide triple bond could be attacked by a wide range of primary amine nucleophiles. 2,6-dimethylphenyl isocyanide was chosen because it would not rearrange to form the corresponding cyanide complex. Complex **41** was synthesised in high yield, (84%) under strictly inert conditions (Scheme 10) and its formation was confirmed by both NMR and IR spectroscopy as well as elemental analysis. An upfield shift of the signal for H² from 8.71 to 8.93 ppm in the ¹H NMR and the appearance of a C≡N vibration at 2267 cm⁻¹ in the IR spectrum also confirmed the presence of the coordinated isocyanide.



Scheme 10 – synthesis of complex 41.

Slow diffusion of petroleum ether through a saturated solution of dichloromethane under a nitrogen atmosphere gave crystals of complex **41** as long orange needles. These were characterised in the solid state by single crystal X-ray diffraction by Dr Julio Fernandez-Cestau (Figure **40**).

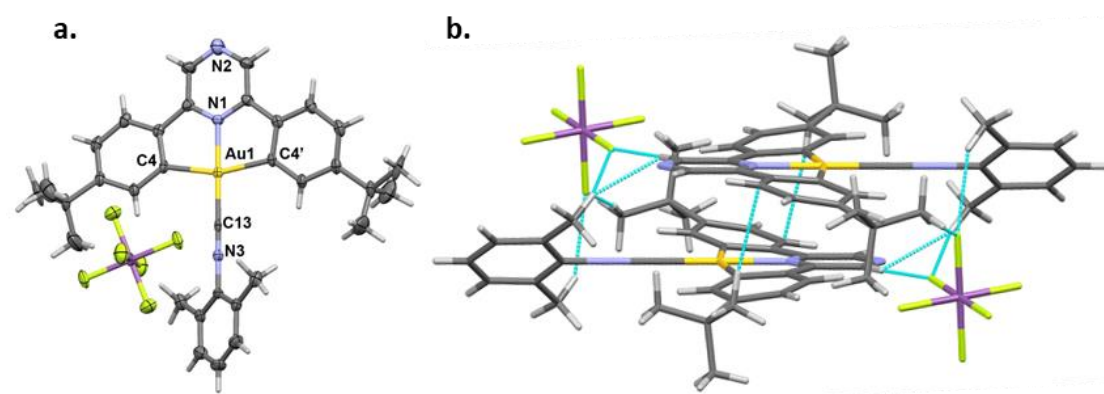
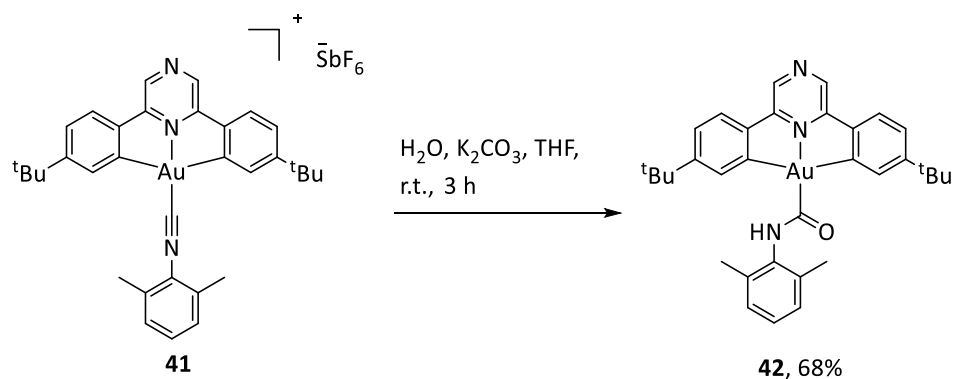


Figure 40 – a. Crystal structure of complex 41. Ellipsoids set at 50% probability. Selected bond distances (Å) and angles (°): Au1-N1 1.975(4), Au1-C4 2.113(4), Au1-C13 1.992(6), C13-N3 1.124(7), C4-Au1-N3 80.31(11), C4-Au1-C13 99.69(11), Au1-C13-N3 180. b. Crystal packing of complex 41.

The crystals display the expected slightly distorted square planar structure to the gold^{III} centre that is usually observed due to the accommodation of the (C^NN^{DZ}C) pincer ligand. Crystal packing showed the presence of dimers, stabilised by of $\pi \cdots \pi$ and F \cdots H interactions.

Complex **41** was very hydrolytically sensitive and reacted readily with water to form the formamide, complex **42**, as depicted in Scheme **11**. The amide bond in this structure was confirmed by the presence of both an NH vibration at 3296 cm⁻¹ and a C=O vibration at 1643

cm^{-1} in the IR spectrum and a singlet at 168.8 ppm for the C=O carbon in the $^{13}\text{C}[^1\text{H}]$ NMR spectrum.



Scheme 11 – nucleophilic attack of water to form the formamide by-product, **42**.

Slow evaporation of a saturated dichloromethane solution of **42** gave crystals suitable for X-ray diffraction. These were characterised in the solid state by single crystal X-ray diffraction by Dr Julio Fernandez-Cestau (Figure **41**).

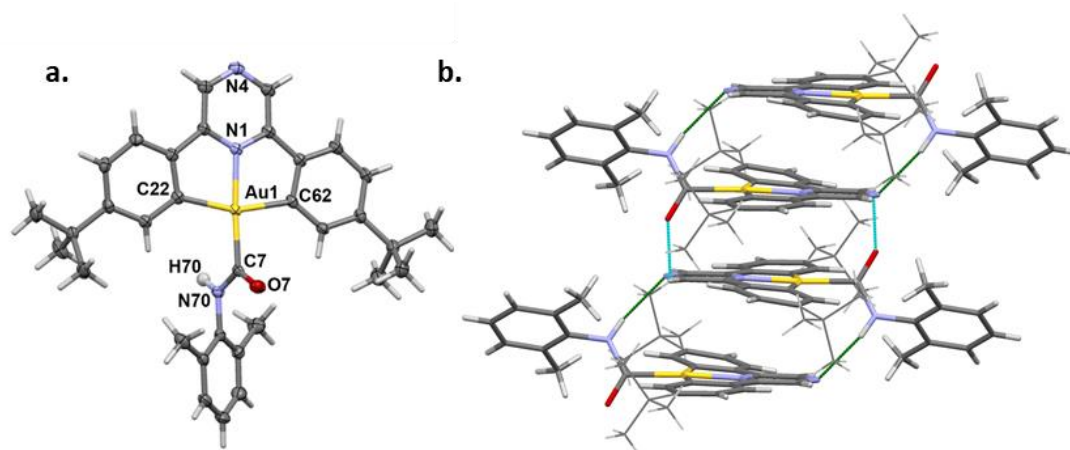
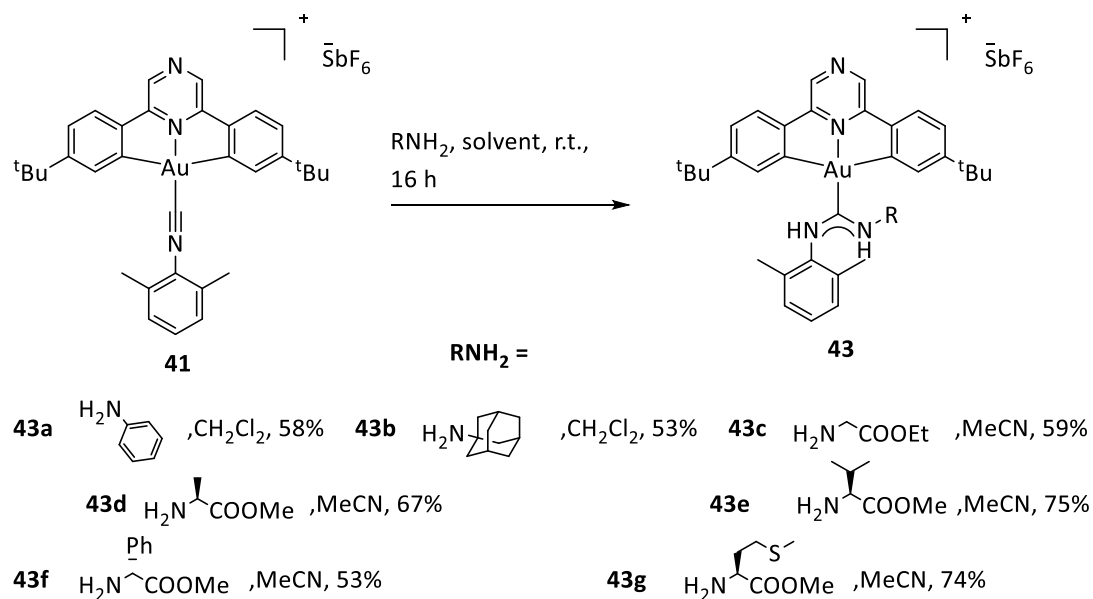


Figure 41 – **a.** Crystal structure of complex **42**. Ellipsoids set at 50% probability. Selected bond distances (\AA) and angles ($^\circ$): Au1-N1 2.0396(15), Au1-C7 2.0251(18), Au1-C22 2.0957(19), Au1-C62 2.0756(19), C7-N70 1.365(2), C7-Au1-N1 176.18(7), C7-Au1-C62 97.15(7), N1-Au1-C62 80.21(7), C7-Au1-C22 102.83(7), N1-Au1-C22 79.86(7), C62-Au1-C22 160.01(7). **b.** Crystal packing of complex **42**.

The gold^{III} centre once again displayed the typical distorted square planar geometry. The crystals formed a rod structure with the molecules packed in antiparallel columns stabilised by π - π stacking and weak intermolecular N70-H70 \cdots N4 hydrogen bonds.

The (C^NP^z^C)Au^{III} isocyanide complex, **41** was then reacted with an array of amines and amino ester substrates under strictly anhydrous conditions, at room temperature for 16 hours (Scheme **12**) to form our library of complexes.



Scheme **12** – synthesis of complexes **43a-43g**.

Complex **41** was reacted with distilled aniline strictly anhydrous conditions to produce the air-stable gold^{III} acyclic diamino carbene, complex **43a** in good yield, (58%) (Figure **42**). Two inequivalent NH peaks appeared in the ¹H spectrum at 9.68 and 9.40 ppm, and the movement of other diagnostic peaks such as the upfield shift of H² to 8.96 ppm and the downfield shift of H⁸ to form a multiplet with H⁵, all suggested carbene formation. The C=N vibration at 1586 cm⁻¹ in the IR spectrum also confirmed the successful formation of the acyclic diamino carbene complex. Elemental analysis also confirmed the predicted percentage of carbon, hydrogen and nitrogen in the expected monomeric unit of the complex.

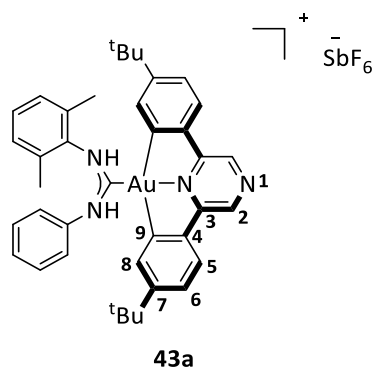


Figure **42** – structure of complex **43a**.

A reaction of complex **41** with adamantylamine lead to the isolation of **43b** in reasonable yield, (53%) (Figure **43**).

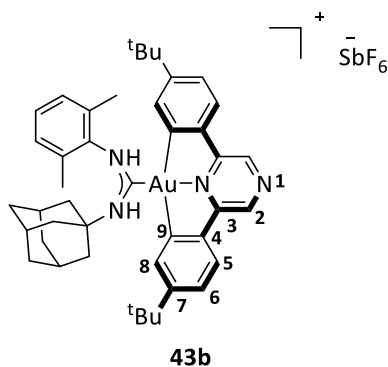


Figure **43** – structure of complex **43b**.

The formation of complex **43b** was confirmed by NMR and IR spectroscopy. Both the up-field shift to 8.92 ppm in the H^2 peak and the appearance of two broad NH singlets at 8.42 and 6.64 ppm in the ^1H NMR spectrum indicated the formation of a carbene. The IR spectrum also showed a carbene vibration at 1586 cm^{-1} and two distinct NH vibrations at 3312 cm^{-1} and 3210 cm^{-1} , giving further evidence to the differing chemical character of the aryl and alkyl amines. Light yellow square plate crystals were successfully grown by the slow evaporation of a dichloromethane/toluene (50:1) solution and characterised in the solid state by single crystal X-ray diffraction by Dr Julio Fernandez-Cestau (Figure **44**).

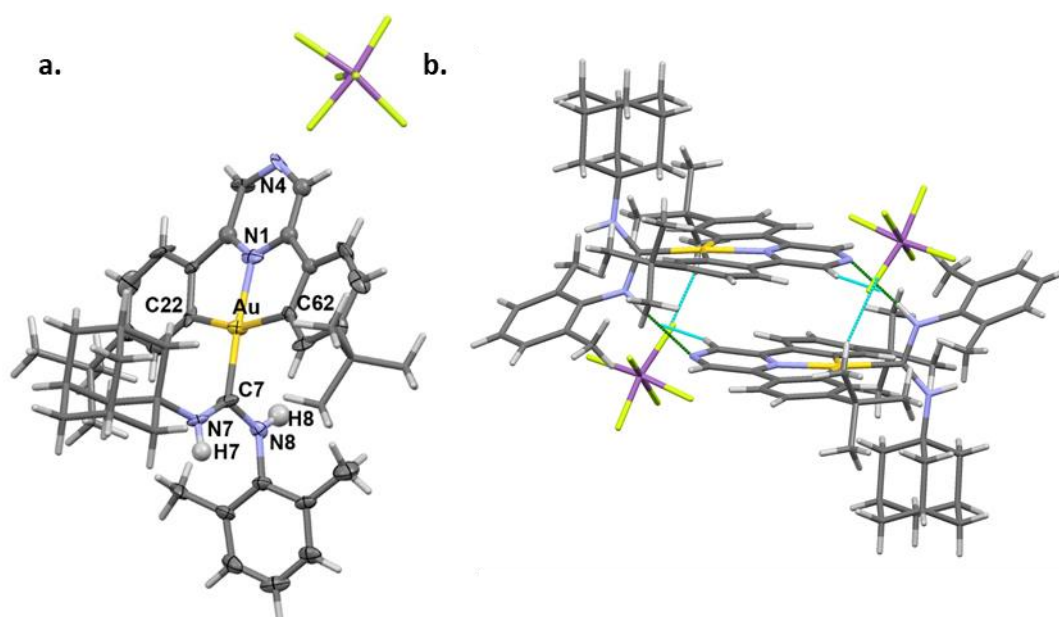


Figure 44 – **a.** Crystal structure of complex **43b**. Ellipsoids set at 50% probability. Toluene molecules are omitted for clarity. Selected bond distances (Å) and angles (°): Au-N1 2.01(1), Au-C7 2.03(1), Au-C22 2.10(1), Au-C62 2.09(1), N1-Au-C7 175.8(4), N1-Au-C22 80.4(4), N1-Au-C62 80.5(4), C22-Au-C7 101.6(5), C62-Au-C7 97.4(4), C22-Au-C62 160.9(4). **b.** Crystal packing of complex **43b**.

The expected distorted square planar geometry was observed around the gold^{III} centre and the molecules were packed in antiparallel columns stabilised by π - π stacking, weak intermolecular N8-H8 \cdots N4 hydrogen bonds and F \cdots H interactions with the SbF₆ anions.

The same synthesis pathway was then used to synthesise five acyclic diamino carbene complexes with amino ester decorated functional groups (**43c-43g**) (Figure 45). The amino esters were bought as their commercially available hydrochloride salts, (Gly-OEt.HCl, Ala-OMe.HCl, Val-OMe.HCl, PhGly-OMe.HCl, and Met-OMe.HCl), and were neutralised with K₂CO₃ before the resulting amines were reacted with complex **41** under strictly anhydrous conditions. Complexes **43c-43g** were all obtained in moderate to good yields, (59%, 67%, 75%, 53% and 74% respectively).

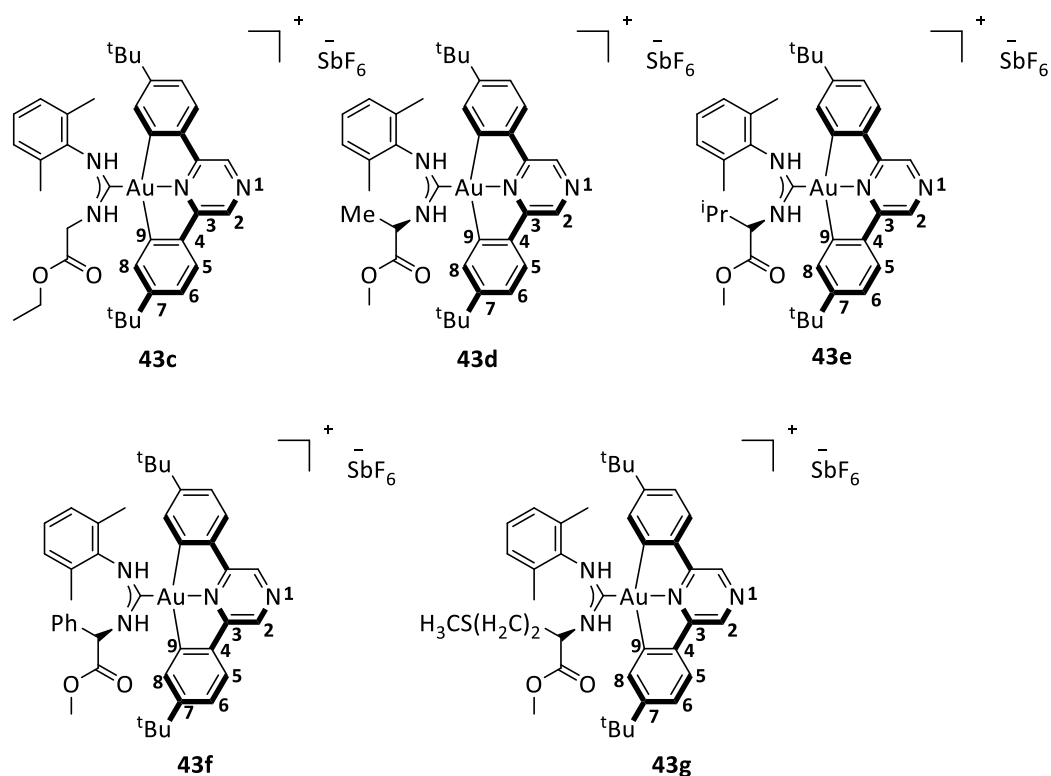


Figure 45 – structures **43c-43g**, the acyclic carbene complexes decorated with amino ester functional groups.

The formation of the carbene complexes was confirmed using both ^1H and $^{13}\text{C}[^1\text{H}]$ NMR spectroscopy as well as IR spectroscopy. For complex **43c**, which contained the non-chiral glycine ethyl ester derived acyclic carbene, both the ^1H and $^{13}\text{C}[^1\text{H}]$ NMR spectra showed equivalent signals for the ($\text{C}^{\wedge}\text{N}^{\text{Pz}}\wedge\text{C}$) pincer ligand. However, in the case of **43d-43g**, when a chiral amino ester was introduced, we saw a loss of symmetry in the ($\text{C}^{\wedge}\text{N}^{\text{Pz}}\wedge\text{C}$) pincer ligand, and many of the diagnostic peaks such as the *tert*-butyl, H^5 and H^8 were doubled. This loss of equivalency is due to the square planar geometry of the gold^{III} centre which permits the chiral alkyl side chain of the amino ester to interact with the ($\text{C}^{\wedge}\text{N}^{\text{Pz}}\wedge\text{C}$) pincer ligand. The effect is most prominent in complexes **43e** and **43f** due to the steric bulk of the isopropyl and phenyl side chains interacting to a greater extent with the pincer ligand. All the complexes also displayed a prominent carbene vibration at around 1585 cm^{-1} and a tight C=O vibration at around 1740 cm^{-1} in their IR spectra.

Suitable crystals for X-ray diffraction of the glycine amino ester derivative, **43c**, were successfully grown by the slow diffusion of petroleum ether through a saturated dichloromethane solution. These were characterised in the solid state by single crystal X-ray diffraction by Dr Julio Fernandez-Cestau (Figure 46).

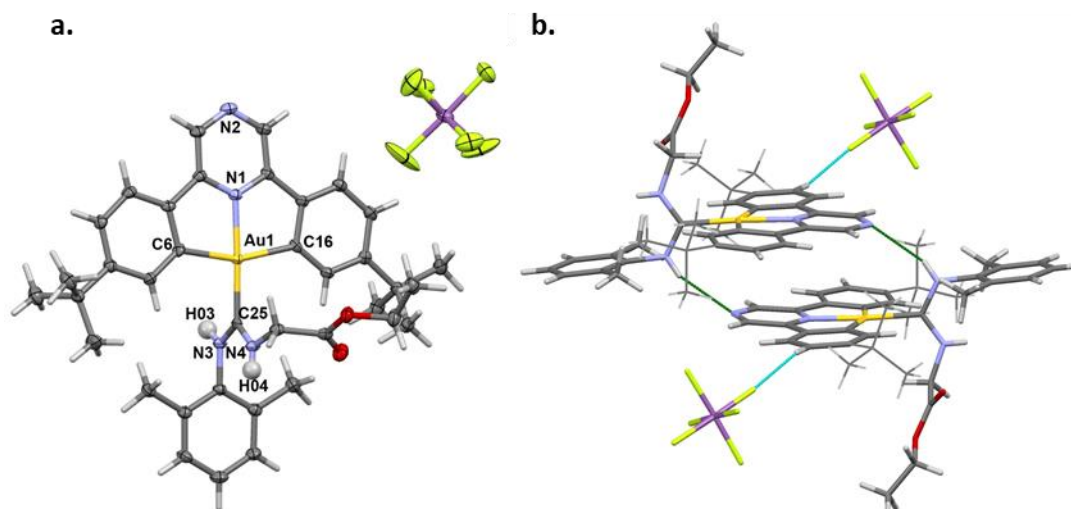


Figure 46 – **a.** Crystal structure of complex **43c**. Ellipsoids set at 50% probability. Selected bond distances (Å) and angles (°): Au1-N1 2.012(2), Au1-C25 2.010(3), Au1-C6 2.098(3), Au1-C16 2.102(3), N1-Au1-C25 177.0(1), C6-Au1-C16 160.8(1), N1-Au1-C6 80.6(1), N1-Au1-C16 80.3(1), C6-Au1-C25 98.8(1), C16-Au1-C25 100.4(4), N3-C25-N4 118.5(3). **b.** Crystal packing of complex **43c**.

Once again, the typical, slightly distorted square planar geometry around the gold^{III} centre was observed, with the crystals packed in anti-parallel columns, stabilised NH⁺⋯N^{pz} hydrogen bonds and F⋯H interactions with the SbF₆ anions.

2.32 In vitro antiproliferative activity

Although poorly soluble in aqueous medium by themselves, all the complexes appeared soluble enough in DMSO not to precipitate when diluted up to 100 μM in aqueous cell medium with 1% of DMSO. A preliminary cytotoxicity screening for all the air stable complexes was carried out on human lung adenocarcinoma cells (A549). This cell line was chosen for its ability to discriminate between structurally similar (C^{^N^{DZ}^C})Au^{III} carbene complexes.³⁹

Complexes **42** and **43a-43g**, as well as the starting gold chloride, complex **37**, were tested at concentrations of 100 μM and 10 μM in comparison to the clinically available drug cisplatin. The preliminary cytotoxicity assay for complexes **43b** and **43g** was carried out by Dr Benoît Bertrand. The inhibition of cellular proliferation was determined using an MTS assay after 72 hours of incubation. This is a colorimetric assay for the quantification of viable cells based on the reduction of MTS tetrazolium compound by viable cells to generate a coloured formazan product. The results are summarised in Figure **47**.

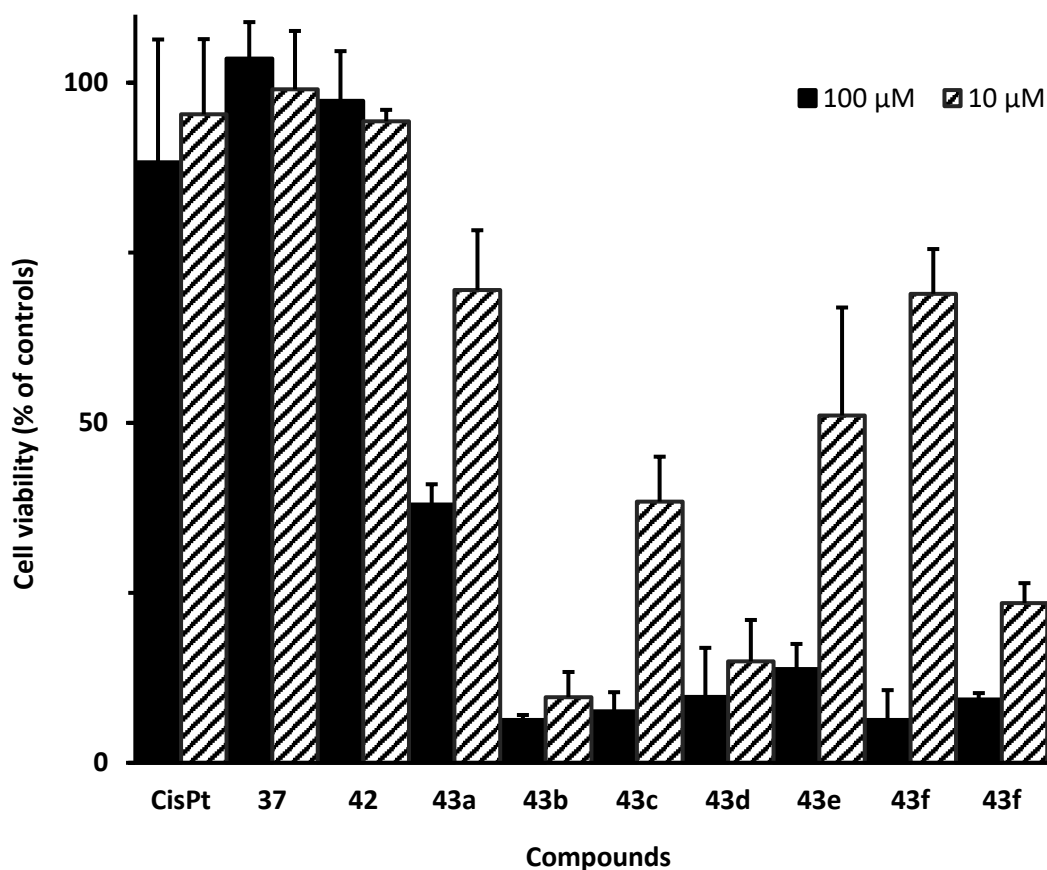


Figure 47 – Inhibition of A549 cellular proliferation by complexes **37**, **42**, and **43a-43g** in DMSO in comparison to cisplatin. Data represents the average \pm the standard deviation of three experiments.

Both of the neutral complexes; the gold chloride starting material, **37** and the formamide hydrolysis product, **42** appeared to be non-toxic at both 10 and 100 μM concentrations. This is consistent with previous cytotoxicity results obtained by our group using neutral ($\text{C}^{\wedge}\text{N}^{\wedge}\text{C}$)Au complexes with phenylacetylde and thiophenolate ligands.³⁹ It is possible that this reduced cytotoxicity is a product of reduced cellular uptake.

The acyclic diamino carbene complex with the aniline substituent, **43a** appeared poorly toxic at both concentrations, (cell viability of 38.0% at 100 μM and 69.5% at 10 μM). This is in good agreement with previous cytotoxicity data obtained by our group for the BF_4 analogue of this complex, **40** synthesised by the first synthetic pathway, discussed in Section 2.2, (cell viability of 64.6% and 69.5% for 100 μM and 10 μM respectively) (Figure 48). This indicates that the two different anions BF_4 and SbF_6 were only having a marginal effect on the toxicity of the complexes at low concentrations.

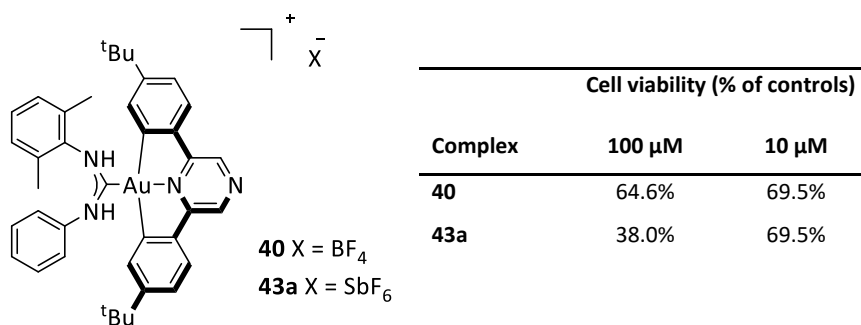


Figure 48 – structure of the aniline acyclic carbene complexes, **40** and **43a** synthesised by the first and second synthetic pathways respectively and their cytotoxicity towards A549 Lung cancer cells, portrayed as % of cell viability.

Complexes **43b-43g** all appeared to inhibit cancer cellular proliferation at 100 μM , (cell viability of 6.3%, 7.6%, 9.7%, 13.8%, 6.3% and 9.3% for complexes **43b-43g** respectively). The two complexes with the most lipophilic side chains; **43e** (isopropyl) and **43f** (phenyl) showed reduced cytotoxicity at 10 μM , (51.1% and 69.0% respectively). Only four complexes showed less than 50% cell viability at 10 μM , **43b-43d** and **43g**, (9.6%, 38.4%, 14.9%, and 23.5% for complexes **43b-43d** and **43g** respectively). These four complexes were therefore selected for further testing.

IC_{50} values for these four complexes, (the half maximal inhibitory concentration, i.e. the concentration required to inhibit 50% of cellular proliferation), were then determined on a panel of human cancer cell lines. These included solid tumour cell lines; lung adenocarcinoma cells (A549), breast adenocarcinoma (MCF-7 and MDA-MB-231) and human colon cancer (HCT-116) and suspension cells; promyelocytic leukaemia (HL60) and also healthy lung fibroblast cells (MRC-5). The results are reported in Table 1 in comparison to cisplatin and our previously reported benzimidazole-based NHC complex, **19** (Figure 49).

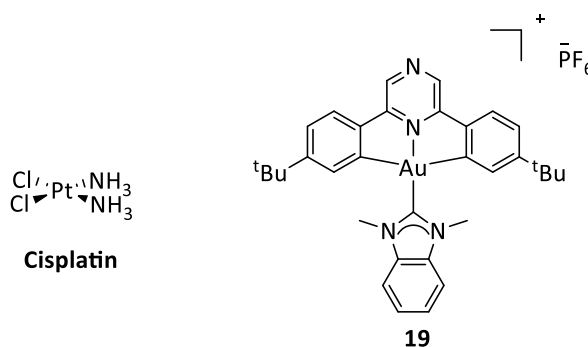


Figure 49 – structures of cisplatin and complex **19**.

Table 1 – IC_{50} values for complexes **43b-43d**, **43g** and **19** in comparison to cisplatin against different human cancer cell lines and healthy lung fibroblast cells after 72 h of incubation.

Complex	$IC_{50} \pm SD (\mu M)^a$					
	A549	MCF-7	HL60	HCT-116	MDA-MB-231	MRC-5
43b	6.1 ± 1.1	5.2 ± 0.2	0.8 ± 0.1	0.6 ± 0.1	0.3 ± 0.1	0.37 ± 0.03
43c	13.0 ± 3.6	6.4 ± 1.6	16.7 ± 2.5	8.4 ± 0.5	5.1 ± 2.0	8.8 ± 1.0
43d	7.9 ± 1.5	3.9 ± 0.6	8.1 ± 0.9	8.1 ± 0.4	4.7 ± 0.7	6.9 ± 1.1
43g	7.7 ± 1.6	3.4 ± 0.2	6.9 ± 0.6	7.3 ± 0.4	11.1 ± 2.8	6.4 ± 0.7
19	7.8 ± 1.3 ^b	0.56 ± 0.02 ^b	0.3 ± 0.1 ^b	11.2 ± 1.5	5.7 ± 0.4	1.4 ± 0.4 ^b
Cisplatin	33.7 ± 3.7 ^b	21.2 ± 3.9 ^b	3.7 ± 0.3 ^b	5.3 ± 0.2	28.4 ± 0.1	10.7 ± 3.0 ^b

^a Mean ± the standard error of at last three independent experiments. ^b Values from ref ³⁹.

All four of the selected acyclic diaminocarbene complexes were between 3-5 times more cytotoxic than cisplatin against the A549 and MCF-7 cell lines and the adamantyl derivative, **43b** was also more cytotoxic than cisplatin against the HL60, HCT-116, and MDA-MB-231 cell lines. However, all the new carbene complexes appeared slightly less active than our previously reported benzimidazole-based NHC complex, **19** against both MCF-7 and HL60 although they showed comparable cytotoxicity against A549, HCT-116 and MDA-MB-231. Even so, the low micromolar activities of these complexes against the A549, MCF-7 and MDA-MB-231 cell lines, which all show reduced sensitivity to cisplatin, make them promising for the development of new anticancer drugs.

The adamantyl derivative, **43b** was over ten times more active than **19** against HCT-116 and MDA-MB-231 cells. Among the amino ester derivatives **43c**, **43d**, and **43g**, the glycine based complex, **43c** was the least cytotoxic in the series while the alanine, **43d** and methionine, **43g** derivatives showed similar activities across the panel of cancer cell lines, (with the exception of MDA-MB-231). Complex **43b** showed the highest overall activity with IC_{50} values in the low micromolar ranges for A549 and MCF-7 cells and values of under 1 μM for HL60, MDA-MB-231 and HCT-116 cells. This complex, however, also showed very poor selectivity for the healthy MRC-5 cells.

The amino ester derivatives, (**43c**, **43d** and **43g**) appeared to have reduced activity against the healthy MRC-5 cells, particularly in comparison to our previously reported heterocyclic complex, **19**.³⁹ All of the amino-ester containing complexes also showed an improved selectivity for MCF-7 cells *versus* healthy MRC-5 fibroblasts (selectivity factor $S_{MCF-7/MRC5} = >1$) and were also significantly more selective than cisplatin ($S_{MCF-7/MRC5} = 0.5$).

2.33 Quantification of reactive oxygen species

The induction of reactive oxygen species (ROS) is a recognised mechanism of action for metal-based drugs, including Au^I-NHC complexes.⁷⁵ With this in mind, we tested the four most active acyclic diaminocarbene complexes, **43b-43d** and **43g** for the production of ROS. The amount of intracellular ROS was measured after treatment of A549 cells with 100 μ M, 50 μ M and 10 μ M concentrations of these complexes and also the less cytotoxic aniline derivative, **43a**, to act as a negative control. The results are summarised in Figure 50. None of the complexes tested appeared to increase the production of ROS and therefore this mode of action can be ruled out for these acyclic diamino carbene complexes.

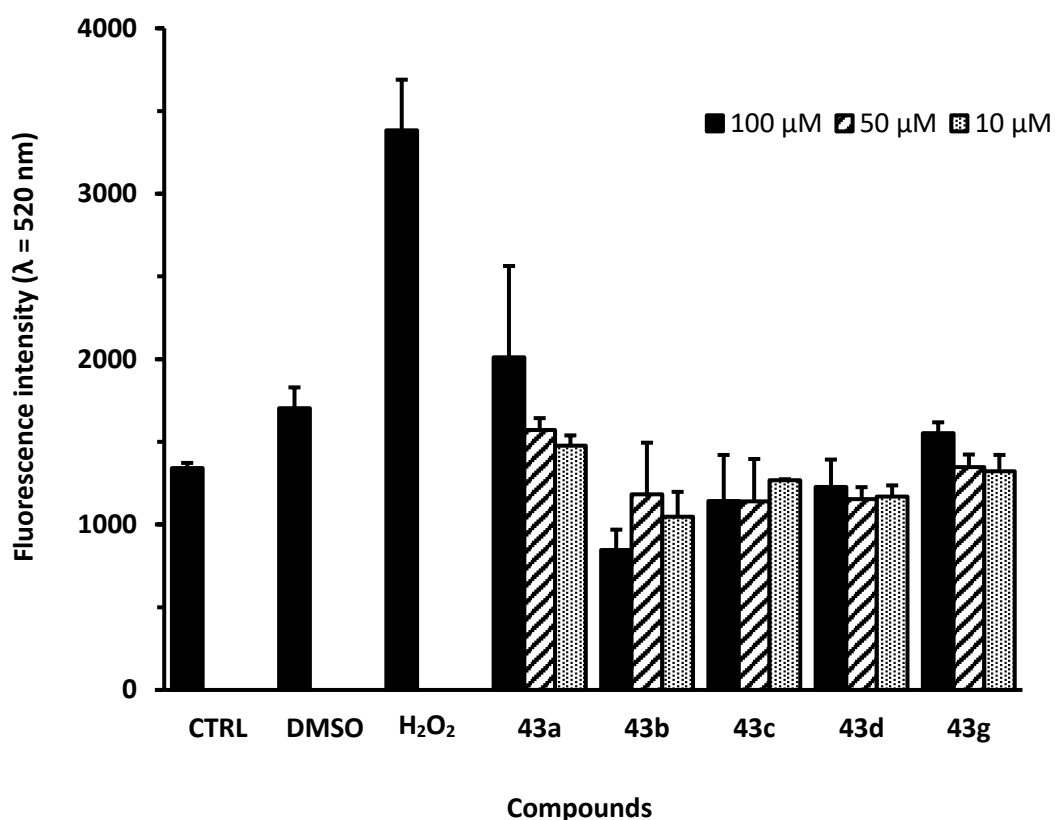


Figure 50 – ROS measurements in A549 cells after 24 h incubation with complexes **43a-43d** and **43g**.

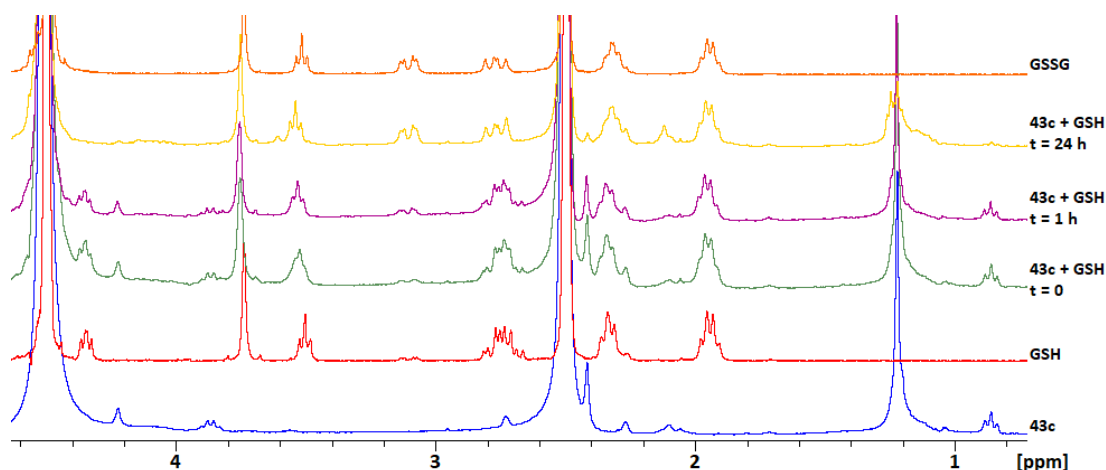


Figure 52a – ^1H NMR spectra of a 1:1 mixture of **43c** with GSH at different reaction times at room temperature, in comparison with the starting materials **43c**, GSH and GSSG ($\text{DMSO-}d_6/\text{D}_2\text{O}$ 1:1).

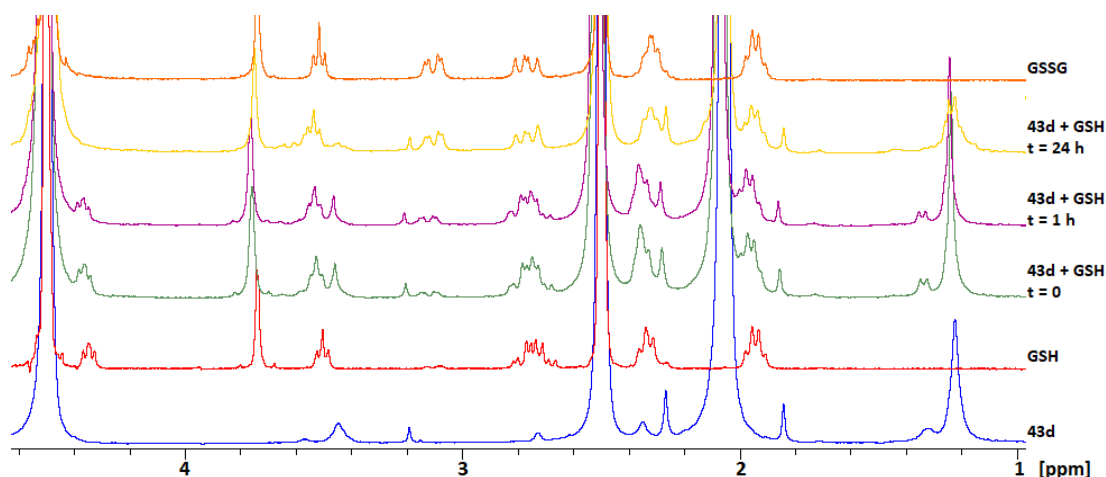


Figure 52b – ^1H NMR spectra of a 1:1 mixture of **43d** with GSH at different reaction times at room temperature, in comparison with the starting materials **43d**, GSH and GSSG ($\text{DMSO-}d_6/\text{D}_2\text{O}$ 1:1).

2.4 Conclusion

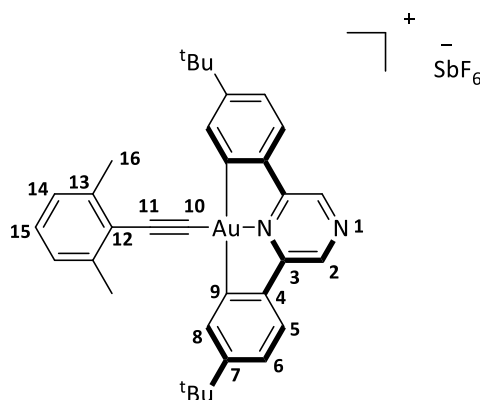
This chapter has described the synthesis and characterization of nine new pyrazine-based cyclometalated $(\text{C}^{\wedge}\text{N}^{\text{pz}}\wedge\text{C})\text{Au}^{\text{III}}$ complexes along with the first examples of cyclometalated gold^{III} complexes decorated with amino acid derivatives. The two-step synthesis started with the formation of a cationic $(\text{C}^{\wedge}\text{N}^{\text{pz}}\wedge\text{C})\text{Au}^{\text{III}}$ isocyanide complex followed by the nucleophilic attack onto the highly electrophilic isocyanide carbon by a broad range of nucleophiles, leading to the synthesis of two amine derivatives and five amino ester decorated $[(\text{C}^{\wedge}\text{N}^{\text{pz}}\wedge\text{C})\text{Au}^{\text{III}}(\text{ACC})]\text{X}$ complexes.

A preliminary cytotoxicity assay against human lung adenocarcinoma cells, (A549) showed that complexes **43b** (adamantyl), **43c** (glycine), **44d** (alanine) and **44g** (methionine) were the most promising candidates. These were further tested on a panel of human cancer cell lines and one healthy cell line for comparison. The amino ester derivatives displayed some promising selectivity profiles for MCF-7 breast cancer cells over healthy MRC-5 cells.

The antiproliferative mode of action of these complexes is unknown although certain methods can be ruled out; in this case, we established that these complexes did not increase the formation of reactive oxygen species. However, two of the amino ester derivatives, **43c** and **43d** showed reduction in the presence of GSH which could indicate that they are reduced to a gold^I active species within a cellular environment. Further work could investigate the possible modes of action of these acyclic carbene complexes and also continue to work on improving the cell selectivity.

2.5 Experimental

When required, manipulations were performed using standard Schlenk techniques under dry nitrogen or in an MBraun glove box. Nitrogen was purified by passing through columns of supported P₂O₅ with moisture indicator and activated 4 Å molecular sieves. Anhydrous solvents were freshly distilled from appropriate drying agents. ¹H and ¹³C[¹H] spectra were recorded using a Bruker Avance DPX-300 spectrometer. ¹H NMR spectra (300.13 MHz) were referenced to the residual protons of the deuterated solvent used. ¹³C[¹H] NMR spectra (75.47 MHz) were referenced internally to the D-coupled ¹³C resonances of the NMR solvent. Elemental analyses were carried out at London Metropolitan University. Complex **37** was synthesized following reported procedures.⁹⁶

2.51 Synthesis of $[(C^{\wedge}N^{\rho z^{\wedge}}C)Au(2,6\text{-dimethylphenyl isocyanide})]SbF_6$ (**41**)


A mixture of **37** (0.150 g, 0.261 mmol), 2,6-dimethylphenyl isocyanide (0.041 g, 0.313 mmol), AgSbF₆ (0.107 g, 0.313 mmol) and a few pellets of 4 Å molecular sieves were combined in a flame-dried Schlenk flask under a nitrogen atmosphere with dry dichloromethane (15 mL). The mixture was left to stir at room temperature for 4 h. A white precipitate of AgCl was removed by filtration through celite, and the filtrate collected under an N₂ atmosphere. The solvent was evaporated to a minimum and the product precipitated with an excess of light petroleum (bp. 40-60 °C). The supernatant was removed and the residue dried under vacuum to yield a yellow solid (0.198 g, 84%). Anal. Calcd. for C₃₃H₃₅AuN₃SbF₆ (906.4): C, 43.73; H, 3.89; N, 4.64. Found: C, 43.84; H, 3.69; N, 4.75. ¹H NMR (CD₂Cl₂, 300 MHz, 298 K): δ 8.93 (s, 2H, H²), 7.89 (d, ⁴J = 1.80 Hz, 2H, H⁸), 7.77 (d, ³J = 8.25 Hz, 2H, H⁵), 7.59 (t, ³J = 7.47 Hz, 1H, H¹⁵), 7.53 (dd, ³J = 8.25 Hz, ⁴J = 1.8 Hz, 2H, H⁶), 7.42 (d, ³J = 7.47 Hz, 2H, H¹⁴), 2.73 (s, 6H, H¹⁶), 1.36 (s, 18H, ^tBu). ¹³C[¹H] NMR (CD₂Cl₂, 75 MHz): δ 168.1 (s, C⁹), 159.5 (s, C⁴), 158.4 (s, C⁷), 143.8 (s, C³), 140.2 (s, C²), 137.4 (s, C¹³), 134.4 (s, C⁸), 133.6 (s, C¹⁴), 129.6 (s, C¹⁵), 127.6 (s, C⁵), 126.7 (s, C⁶), 36.2 (s, C(CH₃)₃), 31.1 (s, C(CH₃)₃), 19.4 (s, C¹⁶). IR: ν_{max} (neat)/cm⁻¹: 2957 (CH), 2267 (C≡N).

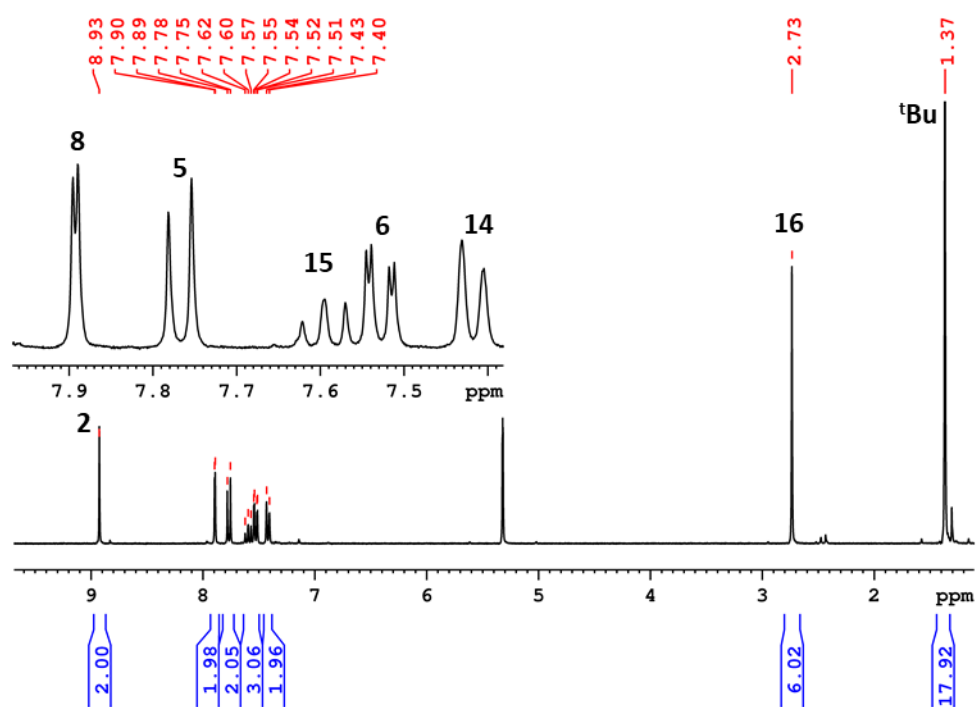


Figure 2.51a – ^1H NMR of complex **41** in CD_2Cl_2 .

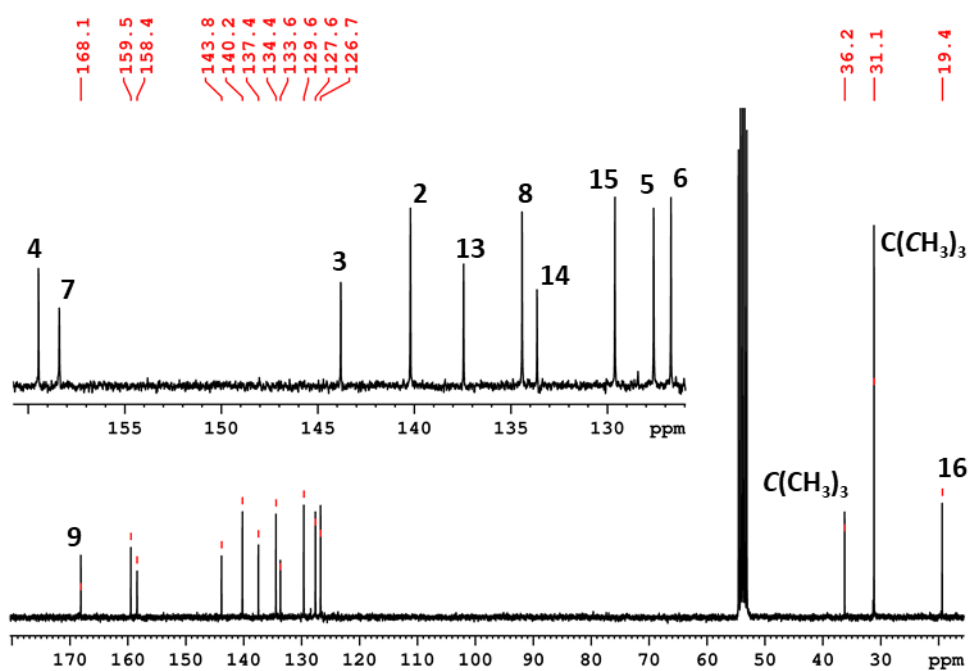
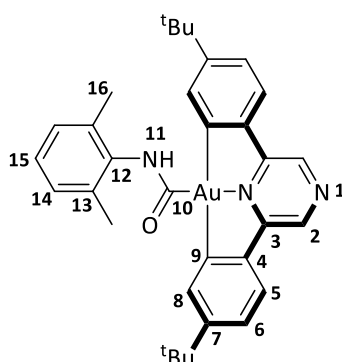


Figure 2.51b – ^{13}C NMR of complex **41** in CD_2Cl_2 .

2.52 Synthesis of $(C^{\wedge}N^{p^z^{\wedge}C})Au(2,6\text{-dimethylphenyl formamide})$ (**42**)


A mixture of **41** (0.055 g, 0.061 mmol) and K_2CO_3 (0.025 g, 0.182 mmol), dissolved in a mixture of tetrahydrofuran (5 mL) and water (2 mL), was stirred at room temperature for 3 h. The THF was removed under vacuum and water (10 mL) was added. The product was extracted using dichloromethane (3×10 mL) and the organic layer washed with water (3×10 mL) and dried with anhydrous Na_2SO_4 . The solution was evaporated and the solid residue washed twice with light petroleum (bp. 40-60 °C) and dried, to yield a bright yellow solid (0.038 g, 68%). Anal. Calcd. for $C_{33}H_{36}AuN_3O$ (687.6): C, 57.64; H, 5.28; N, 6.11. Found: C, 57.42; H, 5.18; N, 6.19. 1H NMR (CD_2Cl_2 , 300 MHz, 298 K): δ 8.80 (s, 2H, H^2), 8.00 (d, $^4J = 2.01$ Hz, 2H, H^8), 7.60 (d, $^3J = 8.16$ Hz, 2H, H^5), 7.33 (dd, $^3J = 8.16$ Hz, $^4J = 2.01$ Hz, 2H, H^6), 7.16 (s, 3H, H^{14+15}), 7.07 (s, 1H, NH), 2.50 (s, 6H, H^{16}), 1.34 (s, 18H, tBu). $^{13}C[^1H]$ NMR (CD_2Cl_2 , 75 MHz): δ 168.8 (s, C^{10}), 167.5 (s, C^9), 156.6 (s, C^7), 156.4 (s, C^4), 144.8 (s, C^3), 138.4 (s, C^2), 136.7 (s, C^{12}), 135.8 (s, C^{13}), 134.9 (s, C^8), 128.5 (s, C^{14}), 127.2 (s, C^{15}), 126.0 (s, C^5), 124.3 (s, C^6), 35.7 (s, $C(CH_3)_3$), 31.4 (s, $C(CH_3)_3$), 19.7 (s, CH_3^{16}). IR: ν_{max} (neat)/ cm^{-1} : 3296 (NH), 2962 (CH), 1643 (C=O).

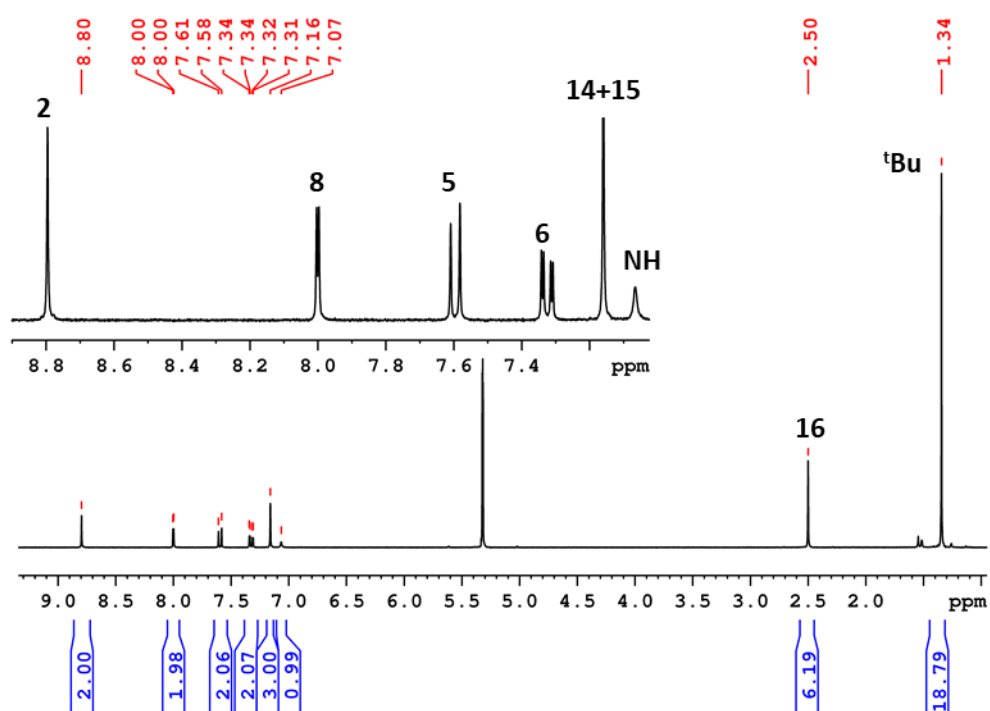


Figure 2.52a – ^1H NMR of complex **42** in CD_2Cl_2 .

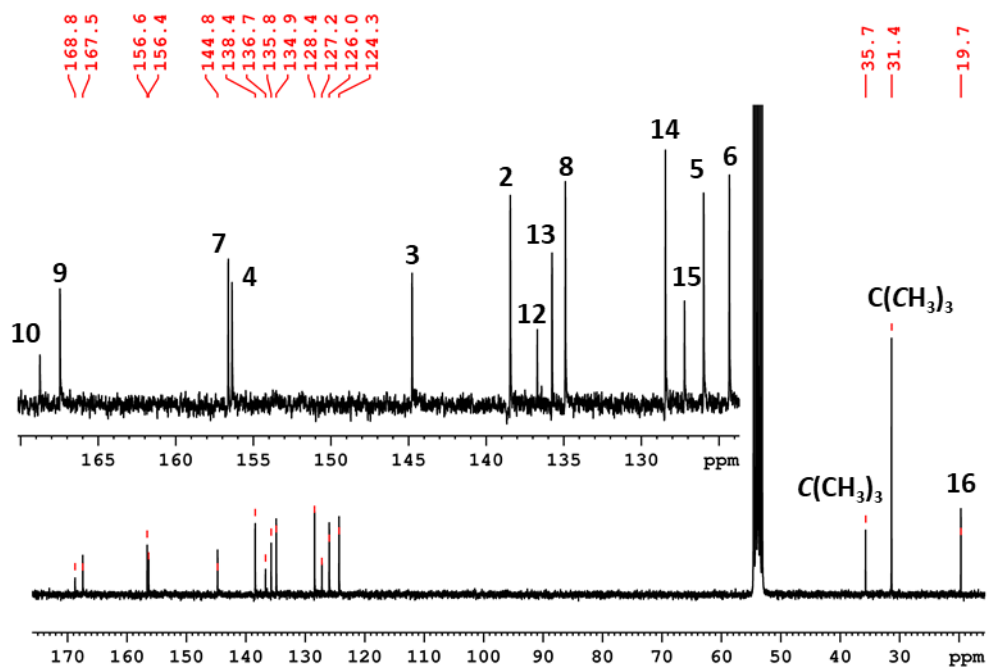


Figure 2.52b – ^{13}C NMR of complex **42** in CD_2Cl_2 .

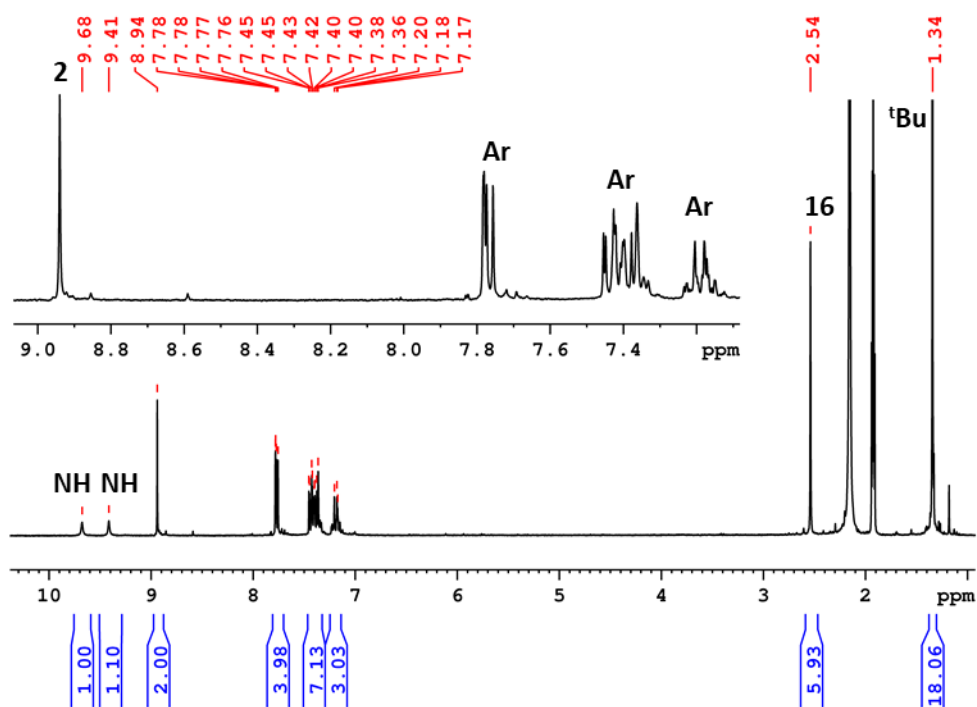


Figure 2.53a – ^1H NMR of complex **43a** in CD_3CN .

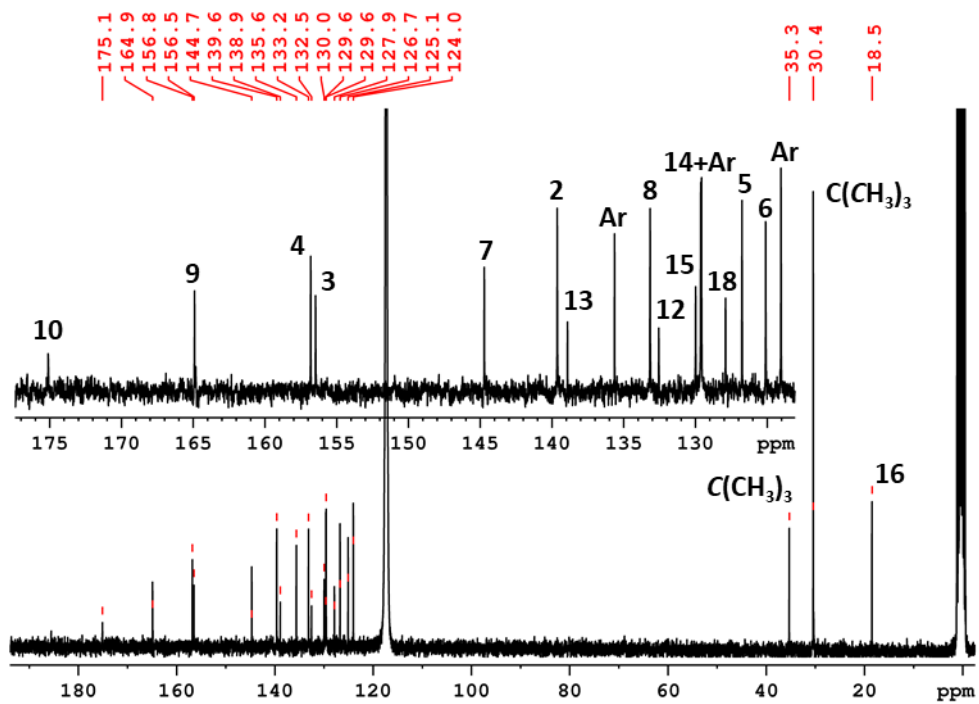
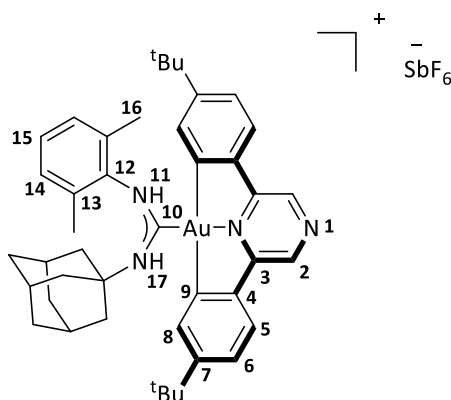


Figure 2.53b – ^{13}C NMR of complex **43a** in CD_3CN .

2.54 Synthesis of $[(C^{\wedge}N^{pz^{\wedge}}C)Au[C(NH-1-Ad)(NHC_6H_3Me_2-2,6)]]SbF_6$ (**43b**)



Complex **41** (0.050 g, 0.055 mmol) and 1-adamantylamine (0.017 g, 0.110 mmol) were combined in a flame-dried Schlenk flask, under N_2 atmosphere with molecular sieves and dry dichloromethane (5 mL). The solution was stirred at room temperature for 16 h. The product was precipitated with an excess of light petroleum (bp. 40-60 °C), filtered off and dried under vacuum to yield a bright yellow solid (0.031 g, 53%). Anal. Calcd. for $C_{43}H_{52}AuN_4SbF_6 \cdot 2H_2O$ (1093.66): C, 47.22; H, 5.16; N, 5.12. Found: C, 47.16; H, 4.71; N, 5.30. 1H NMR (CD_2Cl_2 , 300 MHz, 298 K): δ 8.92 (s, 2H, H^2), 8.42 (s, 1H, NH), 7.78 – 7.72 (m, 4H, $H^{5/8}$), 7.49 (dd, $^3J = 8.30$ Hz, $^4J = 1.8$ Hz, 2H, H^6), 7.47 – 7.36 (m, 3H, H^{14+15}), 6.64 (s, 1H, NH), 2.55 (s, 6H, H^{16}), 2.04 (s, 9H, $CH^{Ad.} + CH_2^{Ad.}$), 1.54 – 1.51 (m, 6H, $CH_2^{ad.}$), 1.36 (s, 18H, tBu). $^{13}C[^1H]$ NMR (CD_2Cl_2 , 75 MHz): δ 172.4 (s, C^{10}), 166.5 (s, C^9), 157.9 (s, C^7), 157.3 (s, C^4), 144.5 (s, C^3), 139.5 (s, C^2), 135.9 (s, C^{13}), 134.6 (s, C^8), 130.8 (s, C^{15}), 130.5 (s, C^{14}), 127.0 (s, C^5), 125.6 (s, C^6), 57.5 (s, $C^{Ad.}$), 44.6 (s, $CH_2^{Ad.}$), 36.0 (s, $C(CH_3)_3$), 35.6 (s, $C^{Ad.}$), 31.2 (s, $C(CH_3)_3$), 29.8 (s, $CH_2^{Ad.}$), 19.5 (s, C^{16}). IR: ν_{max} (neat)/ cm^{-1} : 3311 (NH), 3210 (NH), 2958 (CH), 1586 (carbene).

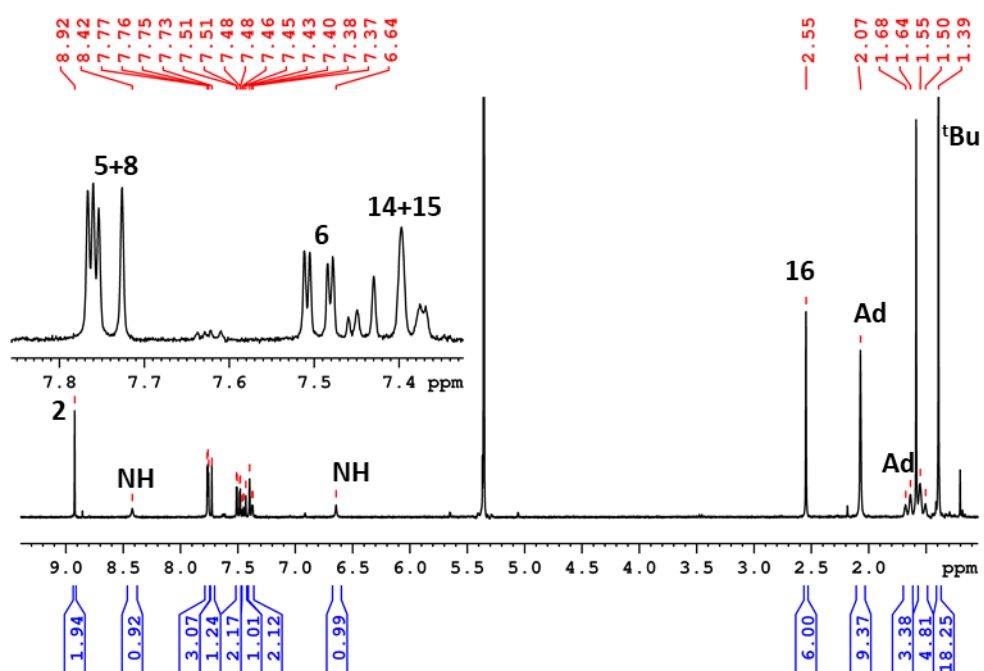


Figure 2.54a – ^1H NMR of complex **43b** in CD_2Cl_2 .

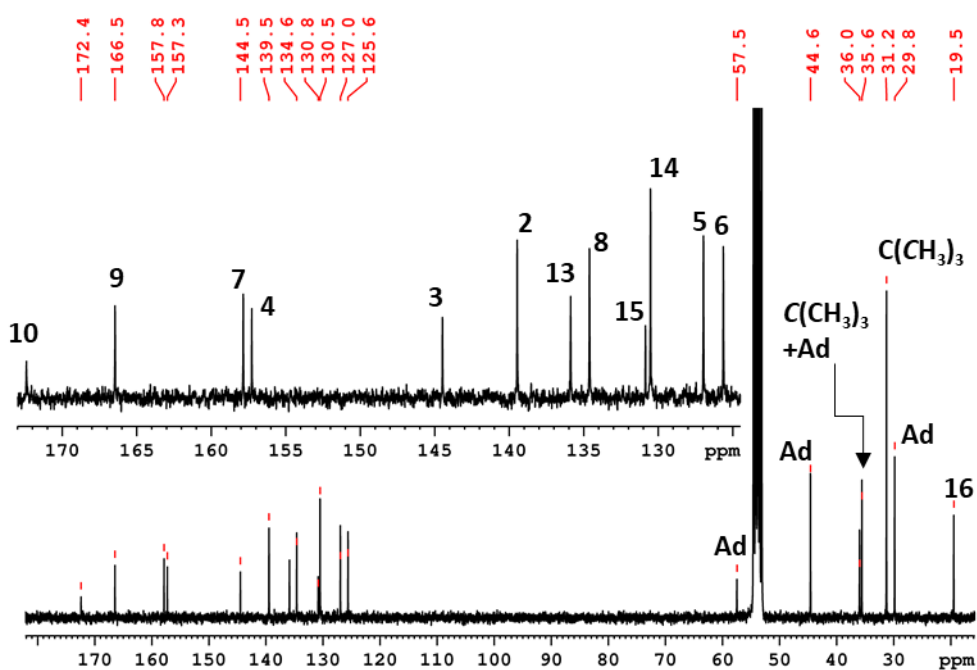
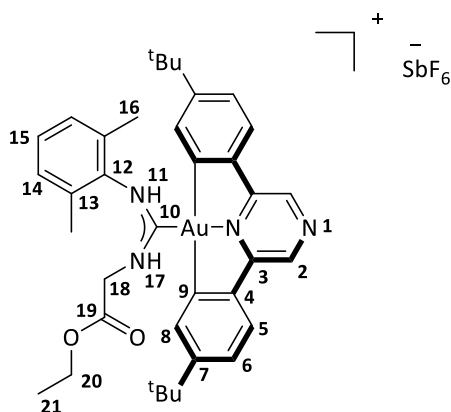


Figure 2.54b – ^{13}C [^1H] NMR of complex **43b** in CD_2Cl_2 .

2.55 Synthesis of $[(C^{\wedge}N^{pz^{\wedge}}C)Au[C(NHCH_2CO_2Et)(NHC_6H_3Me_2-2,6)]]SbF_6$ (**43c**)



Glycine ethyl ester HCl (0.020 g, 0.146 mmol) was added to a flame-dried Schlenk flask charged with K_2CO_3 (0.012 g, 0.088 mmol) and acetonitrile (10 mL). The solution was sonicated for 30 min and transferred to a separate flame-dried Schlenk flask containing **41** (0.066 g, 0.073 mmol). The reaction was then stirred for 16 h at room temperature and the precipitate removed from solution via filtration through a celite plug. Next, the solvent was removed under vacuum and the solid residue re-dissolved in dichloromethane (2 mL). The product was precipitated using a 2:1 mixture of light petroleum (bp. 40-60 °C) / diethyl ether (5 mL) and after removing the solvent, dried under vacuum to yield a bright yellow solid (0.062 g, 0.061 mmol, 59%). Calcd. for $C_{37}H_{44}AuF_6N_4O_2Sb$ (1009.5): C, 44.02; H, 4.39; N, 5.55. Found: C, 43.91; H 4.45; N 5.48. 1H NMR (CD_3CN , 300 MHz, 298 K): δ 9.66 (s, 1H, NH), 8.99 (s, 2H, H²), 7.81 (d, $^3J_{H-H} = 8.3$ Hz, 2H, H⁵), 7.70 (d, $^4J_{H-H} = 2.0$ Hz, 2H, H⁸), 7.57 (s, 1H, NH), 7.45 (dd, $^3J_{H-H} = 8.3$ Hz, $^4J_{H-H} = 2.0$ Hz, 2H, H⁶), 7.40 – 7.28 (m, 3H, H¹⁴⁺¹⁵), 4.25 (d, $^3J_{H-H} = 4.3$ Hz, 2H, H¹⁸), 3.97 (q, $^3J_{H-H} = 7.2$ Hz, 2H, H²⁰) 2.50 (s, 6H, H¹⁶), 1.33 (s, 18H, ^tBu), 1.01 (t, $^3J_{H-H} = 7.2$ Hz, 3H, H²¹). $^{13}C[^1H]$ NMR (CD_3CN , 75 MHz): δ 177.7 (s, C¹⁰), 168.2 (s, C¹⁹), 165.2 (s, C⁹), 156.8 (s, C⁴), 156.4 (s, C³), 144.9 (s, C⁷), 139.6 (s, C²), 135.8 (s, C¹³), 133.3 (s, C⁸), 132.4 (s, C¹²), 129.8 (s, C¹⁵), 129.4 (s, C¹⁴), 126.8 (s, C⁵), 125.0 (s, C⁶), 61.6 (s, C²⁰), 50.0 (s, C¹⁸), 35.3 (s, C(CH₃)₃), 30.4 (s, C(CH₃)₃), 18.3 (s, C¹⁶), 13.3 (s, C²¹). IR: ν_{max} (neat)/ cm^{-1} : 3317 (NH), 3171 (NH), 2963 (CH), 1740 (C=O), 1585 (carbene).

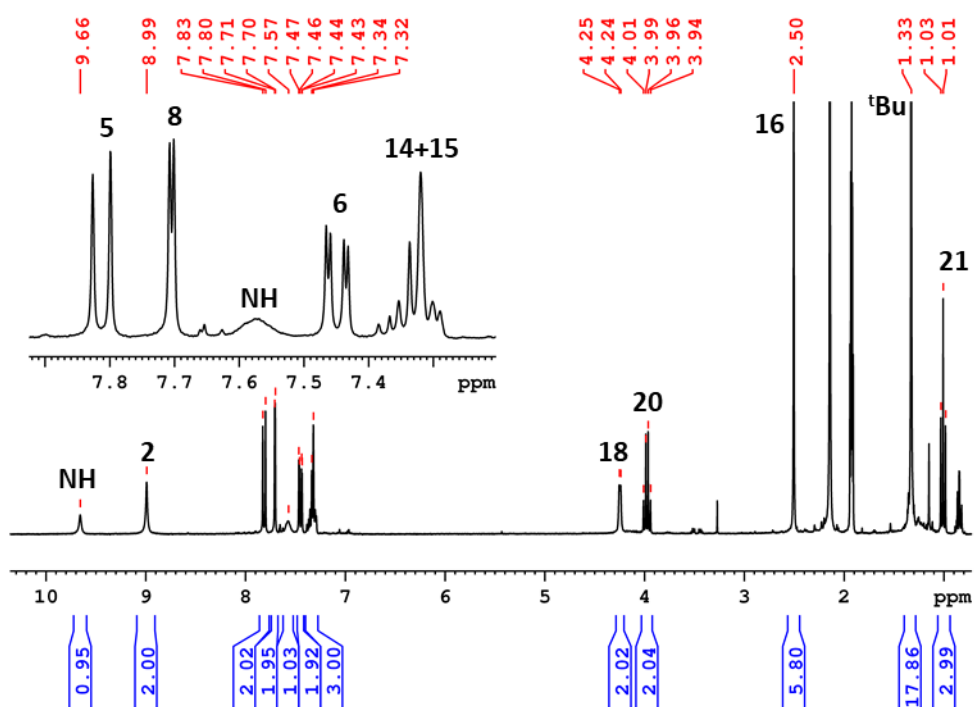


Figure 2.55a – ^1H NMR of complex **43c** in CD_3CN .

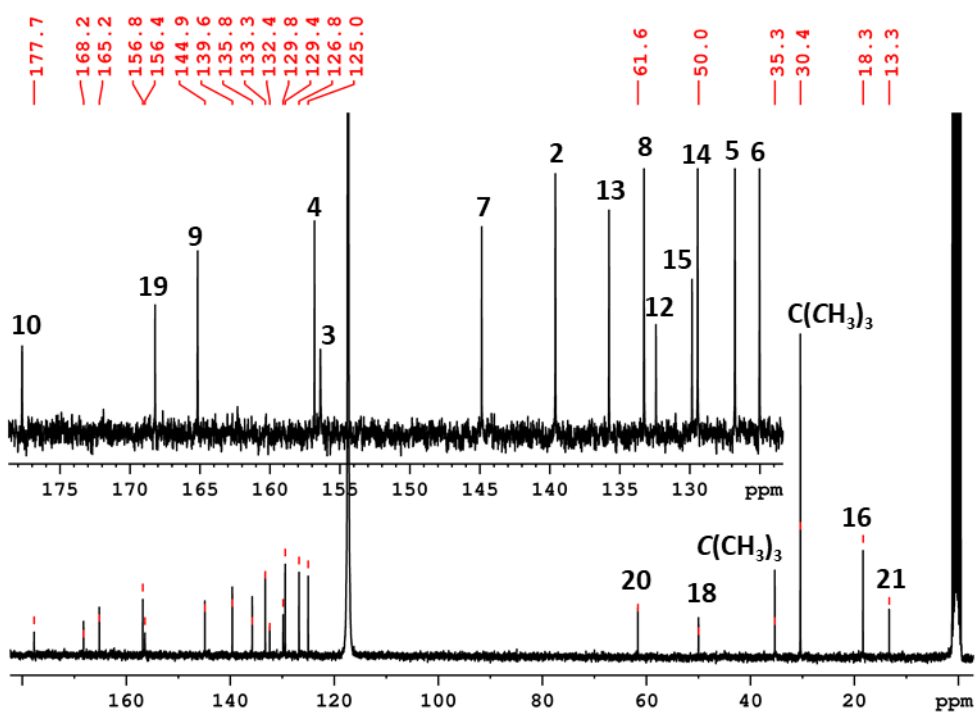
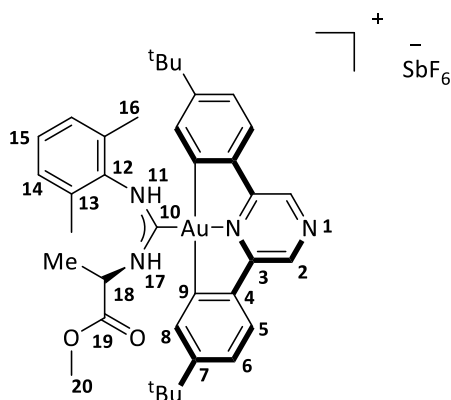


Figure 2.55b – ^{13}C NMR of complex **43c** in CD_3CN .

2.56 Synthesis of $[(C^{\wedge}N^{p\wedge}C)Au[C(NHCH(Me)CO_2Me)(NHC_6H_3Me_{2-2},6)]]SbF_6$ (**43d**)



L-alanine methyl ester HCl (0.020 g, 0.146 mmol) was added to a flame-dried Schlenk flask charged with K_2CO_3 (0.012 g, 0.088 mmol) and acetonitrile (5 mL). The solution was sonicated for 30 min and transferred to a separate flame-dried Schlenk flask containing **41** (0.066 g, 0.073 mmol). The reaction was then stirred for 16 h at room temperature and the precipitate removed from solution via filtration through a celite plug. Next, the solvent was removed under vacuum and the solid residue re-dissolved in dichloromethane (2 mL). The product was precipitated using a 2:1 mixture of light petroleum (bp. 40-60 °C) / diethyl ether (5 mL), and after removing the solvent, dried under vacuum to yield a bright yellow solid (0.070 g, 0.069 mmol, 67%). Calcd. for $C_{37}H_{44}AuF_6N_4O_2Sb$ (1009.50): C, 44.02; H, 4.39; N, 5.55. Found: C, 43.92; H 4.37; N 5.46. 1H NMR (CD_3CN , 300 MHz, 298 K): δ 9.40 (s, 1H, NH), 9.00 (s, 2H, $H^{2/2'}$), 7.85 (d, $^3J_{H-H} = 8.3$ Hz, 1H, $H^{5/5'}$), 7.81 (d, $^3J_{H-H} = 8.3$ Hz, 1H, $H^{5/5'}$), 7.74 (d, $^4J_{H-H} = 2.0$ Hz, 1H, $H^{8/8'}$), 7.70 (s, 1H, NH), 7.66 (d, $^4J_{H-H} = 2.0$ Hz, 1H, $H^{8/8'}$), 7.49 (dd, $^3J_{H-H} = 8.3$ Hz, $^4J_{H-H} = 2.0$ Hz, 1H, $H^{6/6'}$), 7.45 (dd, $^3J_{H-H} = 8.3$ Hz, $^4J_{H-H} = 2.0$ Hz, 1H, $H^{6/6'}$), 7.37-7.27 (m, 3H, $H^{14+14'+15}$), 4.86 (m, 1H, H^{18}), 3.53 (s, 3H, H^{20}), 2.58 (s, 3H, H^{16}), 2.44 (s, 3H, $H^{16'}$), 1.39 (d, $^3J_{H-H} = 7.2$ Hz, 3H, CH_3^{Ala}), 1.32 (s, 9H, tBu), 1.32 (s, 9H, tBu). ^{13}C [1H] NMR (CD_3CN , 75 MHz): δ 176.2 (s, C^{10}), 170.9 (s, C^{19}), 165.2 (s, C^9), 164.9 (s, $C^{9'}$), 157.0 (s, C^7), 156.8 (s, $C^{7'}$), 156.4 (s, C^4), 156.3 (s, $C^{4'}$), 145.0 (s, C^3), 144.9 (s, $C^{3'}$), 139.8 (s, C^2), 139.7 (s, $C^{2'}$), 135.9 (s, C^{13}), 135.7 (s, $C^{13'}$), 133.9 (s, C^8), 132.9 (s, $C^{8'}$), 132.4 (s, C^{12}), 129.9 (s, C^{15}), 129.5 (s, C^{14}), 129.4 (s, $C^{14'}$), 127.1 (s, C^5), 126.8 (s, $C^{5'}$), 125.3 (s, C^6), 125.1 (s, $C^{6'}$), 58.6 (s, C^{18}), 52.6 (s, C^{20}), 35.3 (s, $C(CH_3)_3$), 30.4 (s, $C(CH_3)_3$), 30.4 (s, $C(CH_3)_3$), 18.6 (s, H^{16}), 18.5 (s, $H^{16'}$), 17.4 (s, CH_3^{Ala}). IR: ν_{max} (neat)/ cm^{-1} : 3319 (NH), 3062 (NH), 2961 (CH), 1750 (C=O), 1582 (carbene).

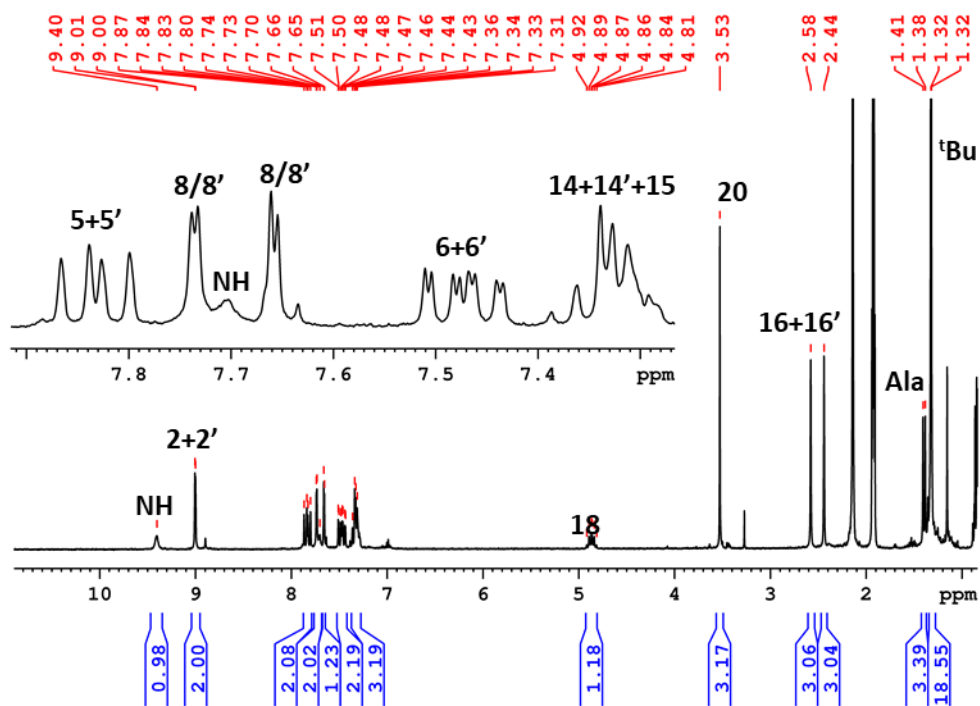


Figure 2.56a – ^1H NMR of complex **43d** in CD_3CN .

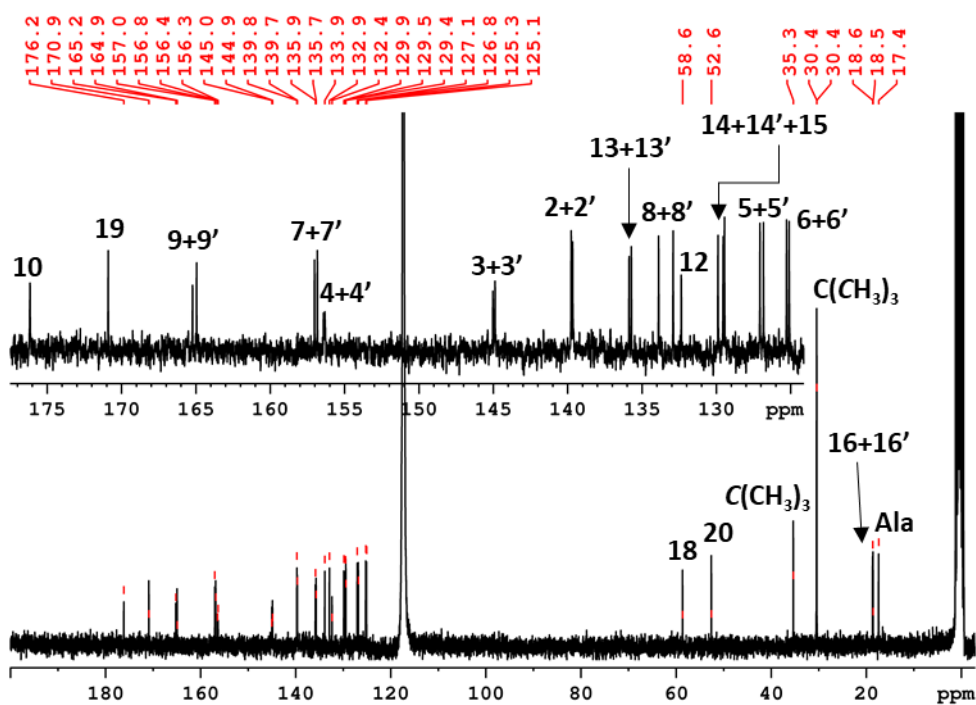
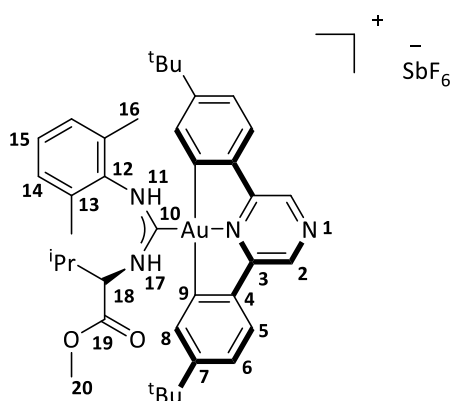


Figure 2.56b – ^{13}C [^1H] NMR of complex **43d** in CD_3CN .

2.57 Synthesis of $[(C^{\wedge}N^{Pz^{\wedge}}C)Au[C(NHCH(iPr)CO_2Me)(NHC_6H_3Me_{2-2,6})]]SbF_6$ (**43e**)



L-valine methyl ester HCl (0.029 g, 0.175 mmol) was added to a flame-dried Schlenk flask charged with K_2CO_3 (0.012 g, 0.088 mmol) and acetonitrile (5 mL). The solution was sonicated for 30 min and transferred to a separate flame-dried Schlenk flask containing **41** (0.079 g, 0.087 mmol). The mixture was stirred for 16 h at room temperature and the precipitate removed by filtration through a celite plug. Next, the solvent was removed under vacuum and the solid residue re-dissolved in dichloromethane (2 mL). The product was precipitated using a 2:1 mixture of light petroleum (bp. 40-60 °C) / diethyl ether (5 mL), and after removing the solvent, dried under vacuum to yield a bright yellow solid (0.068 g, 75%). Anal. Calcd. for $C_{39}H_{48}AuN_4O_2SbF_6$ (1037.56): C, 45.15; H, 4.66; N, 5.40. Found: C, 44.86; H, 4.52; N, 5.52. 1H NMR (CD_3CN , 300 MHz, 298 K): δ 9.50 (s, 1H, NH), 9.03 (s, 1H, H^2), 9.02 (s, 1H, $H^{2'}$), 7.89-7.82 (m, 2H, $H^{5+5'}$), 7.77 (d, $^4J = 1.9$ Hz, 1H, H^8), 7.54-7.46 (m, 4H, NH + $H^{6+6'+8'}$), 7.42-7.32 (m, 3H, $H^{14+14'+15}$), 4.50 (m, 1H, H^{18}), 3.39 (s, 3H, H^{20}), 2.56 (s, 3H, H^{16}), 2.54 (s, 3H, $H^{16'}$), 2.13 (m, 1H, $H^{Val.}$), 1.33 (s, 9H, tBu), 1.32 (s, 9H, tBu), 0.84 (d, $^3J_{H-H} = 6.9$ Hz, 6H, $CH_3^{Val.}$). $^{13}C[^1H]$ NMR (CD_3CN , 75 MHz): δ 177.7 (s, C^{10}), 171.7 (s, C^{19}), 166.5 (s, C^9), 165.6 (s, C^9'), 157.9 (s, C^7), 157.8 (s, $C^{7'}$), 157.4 (s, C^4), 157.4 (s, $C^{4'}$), 145.9 (s, C^3), 145.8 (s, $C^{3'}$), 140.7 (s, C^2), 136.7 (s, C^{13}), 136.5 (s, $C^{13'}$), 134.6 (s, C^8), 134.0 (s, $C^{8'}$), 133.0 (s, $C^{2'}$), 131.1 (s, C^{15}), 130.7 (s, C^{14}), 130.6 (s, $C^{14'}$), 127.9 (s, C^5), 127.8 (s, $C^{5'}$), 126.5 (s, C^6), 126.2 (s, $C^{6'}$), 69.4 (s, C^{18}), 53.2 (s, C^{20}), 36.3 (s, $C(CH_3)_3$), 36.3 (s, $C(CH_3)_3$), 32.2 (s, $C^{Val.}$), 31.4 (s, $C(CH_3)_3$), 31.4 (s, $C(CH_3)_3$), 19.9 (s, C^{16}), 19.7 (s, $C^{16'}$), 19.5 (s, $C^{Val.}$), 19.3 (s, $C^{Val.}$). IR: ν_{max} (neat)/ cm^{-1} : 3300 (NH), 3189 (NH), 2965 (CH), 1742 (C=O), 1582 (carbene).

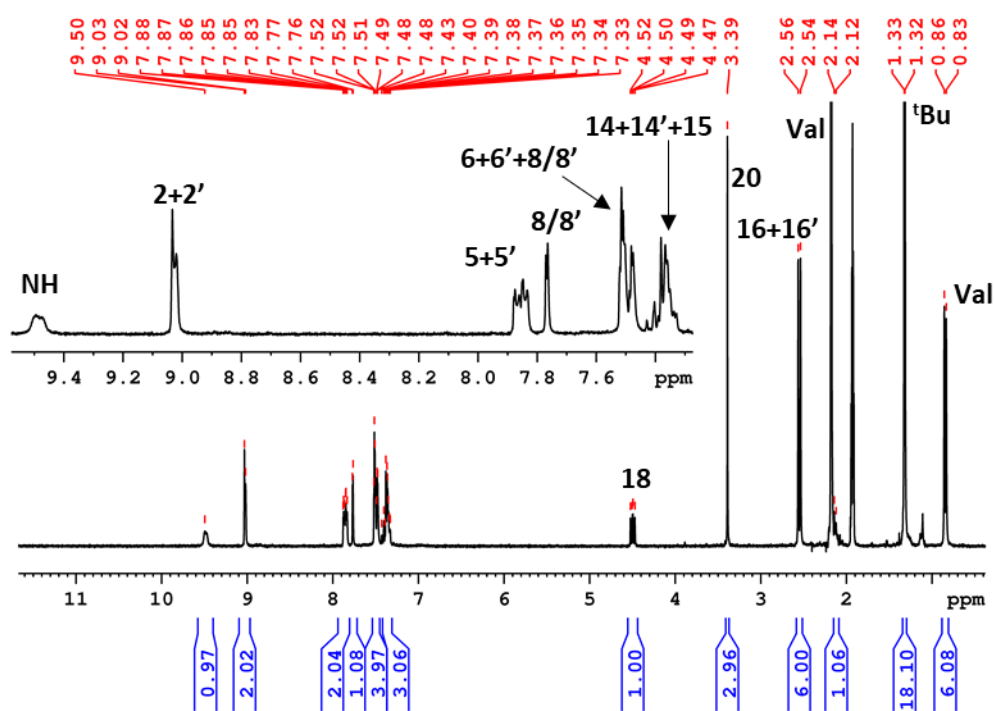


Figure 2.57a – ^1H NMR of complex **43e** in CD_3CN .

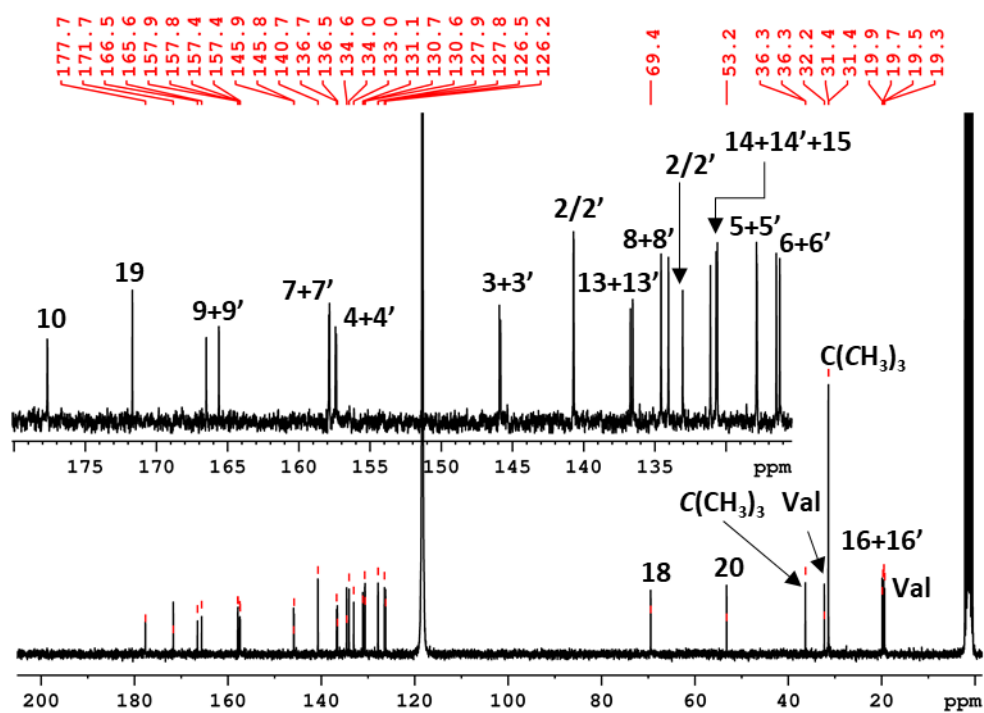
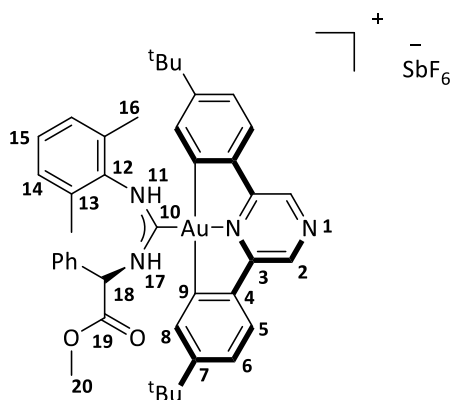


Figure 2.57b – ^{13}C NMR of complex **43e** in CD_3CN .

2.58 Synthesis of $[(C^{\wedge}N^{Pz^{\wedge}}C)Au[C(NHCH(Ph)CO_2Me)(NHC_6H_3Me_2-2,6)]]SbF_6$ (**43f**)



D-phenylglycine methyl ester HCl (0.030 g, 0.146 mmol) was added to a flame-dried Schlenk flask charged with K_2CO_3 (0.012 g, 0.087 mmol) and acetonitrile (5 mL). The solution was sonicated for 30 min and transferred to a separate flame-dried Schlenk flask containing **41** (0.066 g, 0.073 mmol). The reaction was stirred for 16 h at room temperature and the precipitate removed from solution via filtration through a celite plug. The solvent was removed under vacuum and the solid residue re-dissolved in dichloromethane (2 mL). The product was precipitated using a 2:1 mixture of light petroleum (bp. 40-60 °C) / diethyl ether (5 mL), and after removing the solvent, dried under vacuum to yield an orange solid (0.059 g, 0.055 mmol, 53%). Calcd. for $C_{42}H_{46}AuF_6N_4O_2Sb \cdot 2CH_2Cl_2$ (1241.4): C, 42.57; H, 4.06; N, 4.51. Found: C, 42.55; H 4.03; N 4.15. 1H NMR (CD_3CN , 300 MHz, 298 K): δ 9.51 (s, 1H, NH), 9.02 (s, 1H, H^2), 8.97 (s, 1H, $H^{2'}$), 8.11 (d, $^3J_{H-H} = 6.0$ Hz, 1H, NH), 7.87 (d, $^3J_{H-H} = 8.2$ Hz, 1H, H^5), 7.74 (d, $^3J_{H-H} = 8.2$ Hz, 1H, $H^{5'}$), 7.68 (d, $^4J_{H-H} = 1.6$ Hz, 1H, H^8), 7.51 (dd, $^3J_{H-H} = 8.2$ Hz, $^4J_{H-H} = 1.6$ Hz, 1H, H^6), 7.41-7.30 (m, 4H, $H^{6'+14+14'+15}$), 7.28 (d, $^4J_{H-H} = 1.6$ Hz, 1H, H^8), 7.21-7.06 (m, 5H, $H^{PhGly.}$), 5.68 (d, $^3J_{H-H} = 6.0$ Hz, 1H, H^{18}), 3.54 (s, 3H, H^{20}), 2.51 (s, 3H, H^{16}), 2.43 (s, 3H, $H^{16'}$), 1.35 (s, 9H, tBu), 1.17 (s, 9H, tBu). $^{13}C[^1H]$ NMR (CD_3CN , 75 MHz): δ 176.5 (s, C^{10}), 169.4 (s, C^{19}), 165.3 (s, C^9), 164.3 (s, $C^{9'}$), 157.1 (s, C^7), 156.5 (s, $C^{7'}$), 156.4 (s, C^4), 156.4 (s, $C^{4'}$), 145.0 (s, C^3), 144.4 (s, $C^{3'}$), 139.6 (s, C^2), 139.6 (s, $C^{2'}$), 135.7 (s, C^{13}), 135.6 (s, $C^{13'}$), 134.7 (s, C^{12}), 133.4 (s, C^8), 133.0 (s, $C^{8'}$), 132.1 (s, $C^{PhGly.}$), 130.0 (s, C^{15}), 129.6 (s, C^{14}), 129.6 (s, $C^{14'}$), 129.4 (s, $C^{PhGly.}$), 129.0 (s, $C^{PhGly.}$), 128.3, (s, $C^{PhGly.}$), 127.1 (s, C^5), 126.5 (s, $C^{5'}$), 125.3 (s, C^6), 125.0 (s, $C^{6'}$), 65.5 (s, C^{18}), 53.2 (s, C^{20}), 35.3 (s, $C(CH_3)_3$), 35.1 (s, $C(CH_3)_3$), 30.4 (s, $C(CH_3)_3$), 30.4 (s, $C(CH_3)_3$), 18.6 (s, C^{16}), 18.5 (s, $C^{16'}$). IR: ν_{max} (neat)/ cm^{-1} : 3295 (NH), 3173 (NH), 2963 (CH), 1744 (C=O), 1586 (carbene).

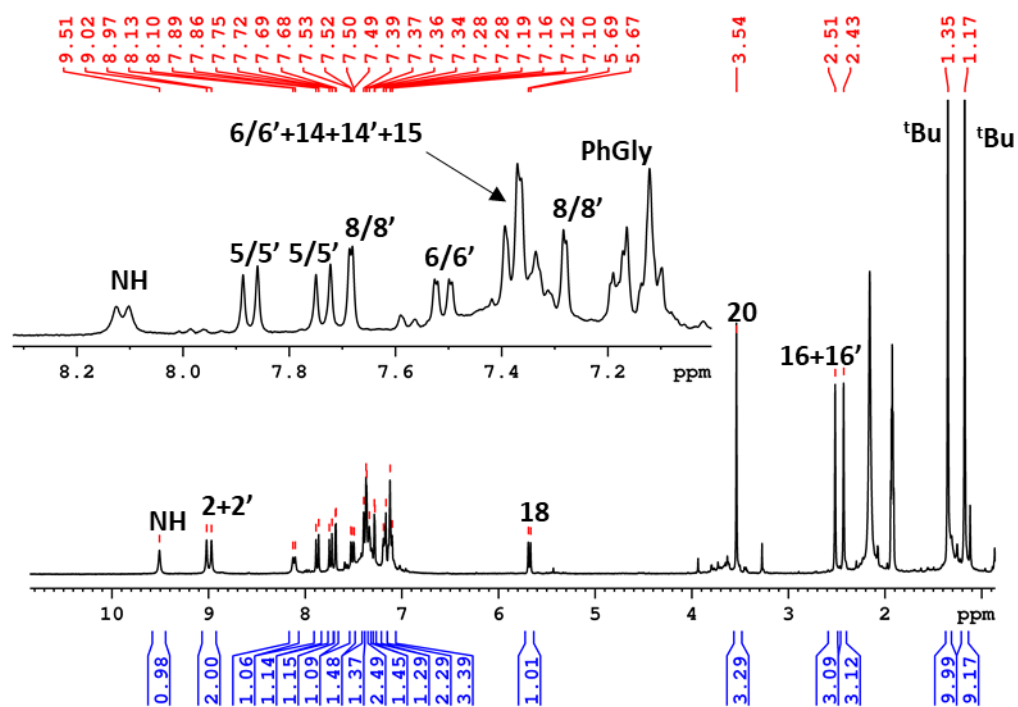


Figure 2.58a – ^1H NMR of complex **43f** in CD_3CN .

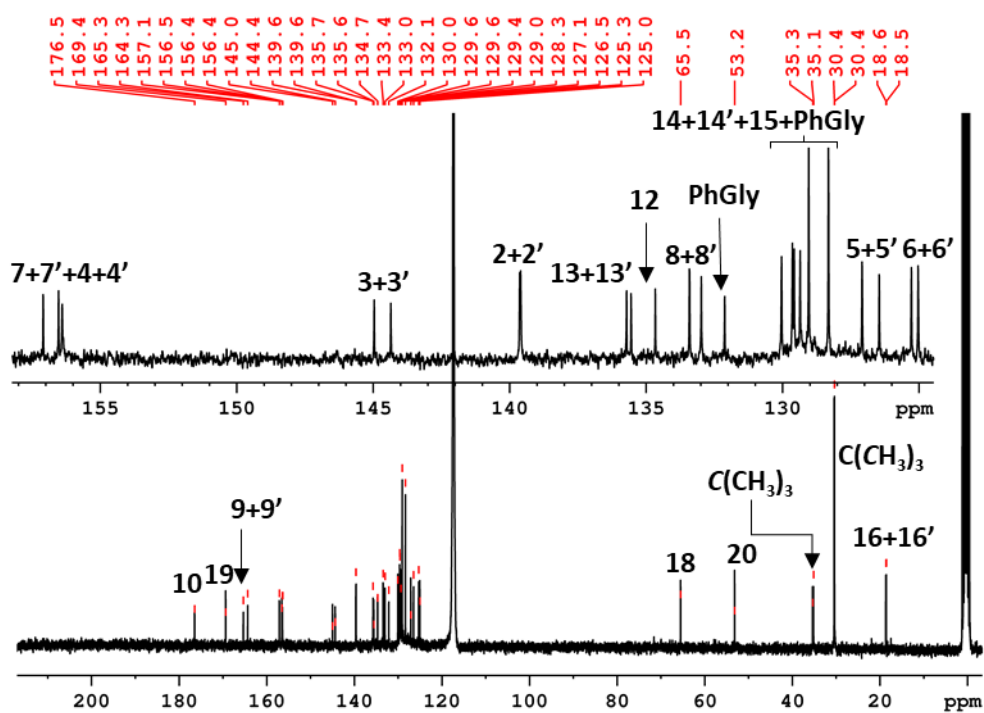
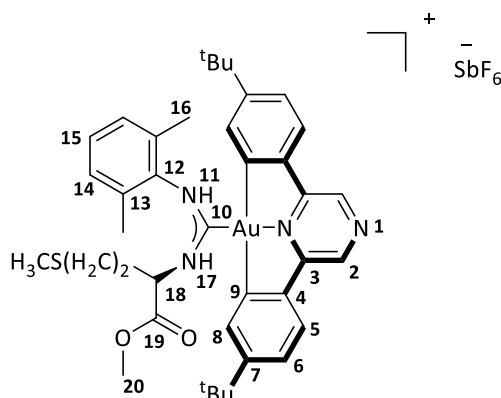


Figure 2.58b – ^{13}C [^1H] NMR of complex **43f** in CD_3CN .

2.59 Synthesis of $[(C^{\wedge}N^{Pz^{\wedge}}C)Au][C(NHCH(CH_2CH_2SMe)CO_2Me)(NHC_6H_3Me_2-2,6)]SbF_6$ (**43g**)



L-methionine methyl ester HCl (0.035 g, 0.175 mmol) was added to a flame-dried Schlenk flask charged with K_2CO_3 (0.012 g, 0.087 mmol) and acetonitrile (5 mL). The solution was sonicated for 30 min and transferred to a separate flame-dried Schlenk flask containing **41** (0.079 g, 0.087 mmol). The reaction was then stirred for 16 h at room temperature and the precipitate removed from solution via filtration through a celite plug. Next, the solvent was removed under vacuum and the solid residue re-dissolved in dichloromethane (2 mL). The product was precipitated using a 2:1 mixture of light petroleum (bp. 40-60 °C) / diethyl ether (5 mL), and after removing the solvent, dried under vacuum to yield an orange solid (0.069 g, 74%). Anal. Calcd. for $C_{39}H_{48}AuN_4O_2SSbF_6$ (1069.6): C, 43.79; H, 4.52; N, 5.24. Found: C, 43.58; H, 4.37; N, 5.08. 1H NMR (CD_2Cl_2 , 300 MHz, 298 K): δ 8.88 (s, 2H, H²), 8.71 (s, 1H, NH), 8.29 (d, $^3J_{H-H} = 9.0$ Hz, 1H, NH), 7.76 – 7.60 (m, 4H, H^{5/8}), 7.50 – 7.30 (m, 5H, H⁶⁺¹⁴⁺¹⁵), 5.00 (m, 1H, H¹⁸), 3.60 (s, 3H, H²⁰), 2.63 (s, 3H, H¹⁶), 2.52 (s, 3H, H^{16'}), 2.14 (m, 2H, H^{Met.}), 1.66 (s, 3H, H^{Met.}), 1.36 (s, 9H, ^tBu), 1.33 (s, 9H, ^tBu), 1.14 (s, 2H, H^{Met.}). $^{13}C[^1H]$ NMR (CD_2Cl_2 , 75 MHz): δ 178.2 (s, C¹⁰), 170.6 (s, C¹⁹), 165.8 (s, C⁹), 165.1 (s, C^{9'}), 158.1 (s, C⁷), 158.0 (s, C^{7'}), 157.0 (s, C⁴), 156.9 (s, C^{4'}), 144.7 (s, C³), 144.6 (s, C^{3'}), 139.5 (s, C²), 139.4 (s, C^{2'}), 136.3 (s, C¹³), 135.7 (s, C^{13'}), 133.9 (s, C⁸), 132.9 (s, C^{8'}), 131.7 (s, C¹⁵), 130.9 (s, C¹⁴), 130.5 (s, C^{14'}), 130.2 (s, C¹²), 127.3 (s, C⁵), 127.1 (s, C^{5'}), 125.9 (s, C⁶), 125.8 (s, C^{6'}), 61.5 (s, C²⁰), 36.0 (s, C¹⁸), 36.0 (s, C^{Met.}), 31.3 (s, C(CH₃)₃), 31.2 (s, C(CH₃)₃), 30.4 (s, C(CH₃)₃), 30.0 (s, C(CH₃)₃), 19.4 (s, C¹⁶), 19.2 (s, C^{16'}), 18.9 (s, C^{Met.}), 14.8 (s, C^{Met.}). IR: ν_{max} (neat)/ cm^{-1} : 3304 (NH), 3169 (NH), 2960 (CH), 1744 (C=O), 1585 (carbene).

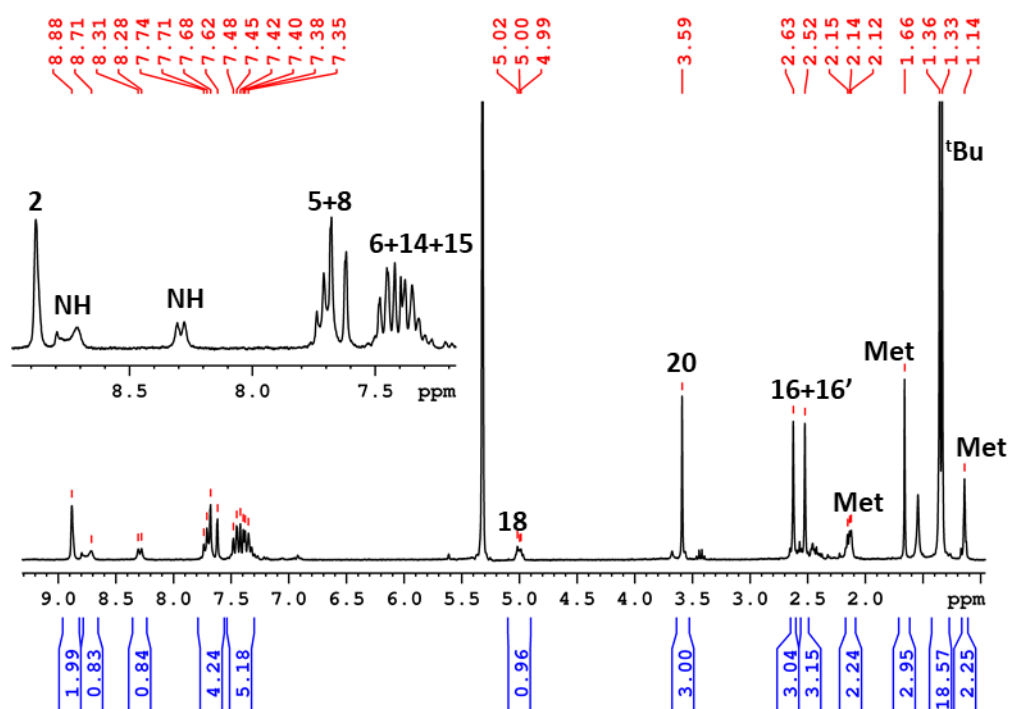


Figure 2.59a – ^1H NMR of complex **43g** in CD_2Cl_2 .

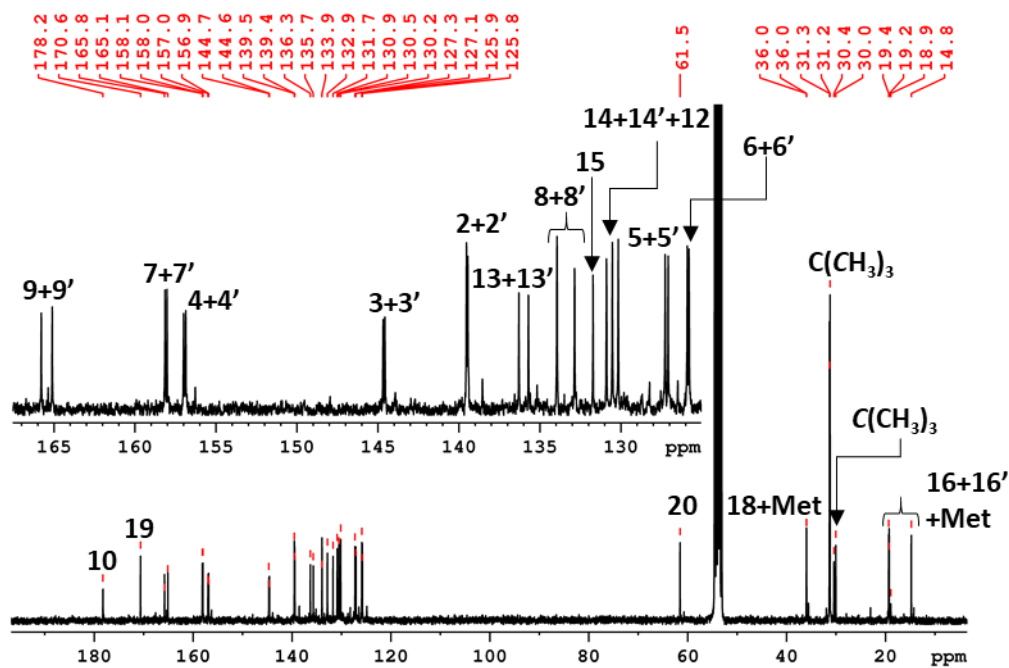


Figure 2.59b – ^{13}C [^1H] NMR of complex **43g** in CD_2Cl_2 .

2.510 *X-ray crystallography*

Crystal structures were solved by Dr Julio Fernandez-Cestau.

2.511 *Antiproliferation assay*

The human A549 and HL60 cancer cell lines (from ECACC) were cultured in RPMI 1640 medium with 10% foetal calf serum, 2 mM L-glutamine, 100 U mL⁻¹ penicillin and 100 µg mL⁻¹ streptomycin (Invitrogen). The cells were maintained under a humidified atmosphere at 37 °C and 5% CO₂. The human MCF-7, HCT116 and MDA-MB-231 cancer cell lines (from ECACC) and the healthy fibroblast MRC-5 cells were cultured in DMEM medium with 10% foetal calf serum, 2 mM L-glutamine, 100 U mL⁻¹ penicillin and 100 µg mL⁻¹ streptomycin (Invitrogen). The cells were maintained under a humidified atmosphere at 37 °C and 5% CO₂. Inhibition of cancer cell proliferation was measured by the 3-(4,5-dimethylthiazol-2-yl)5-(3-carboxymethoxyphenyl)-2-(4-sulfophenyl)-2H-tetrazolium (MTS) assay using the CellTiter 96 Aqueous One Solution Cell Proliferation Assay (Promega) and following the manufacturer's instructions. Briefly, the cells (3×10^4 per 100 µL for HL60, 8×10^3 per 100 µL for A549, MCF-7, HCT116, MDA-MB-231 and 2×10^3 per 100 µL for MRC-5) were seeded in 96-well plates and left untreated or treated with 1 µL of DMSO (vehicle control) or 1 µL of complexes diluted in DMSO at different concentrations, in triplicate for 72 h at 37 °C with 5% CO₂. Following this, MTS assay reagent was added for 4 h and absorbance measured at 490 nm using a Polarstar Optima microplate reader (BMG Labtech). IC₅₀ values were calculated using GraphPad Prism Version 5.0 software.

2.512 *ROS assay*

100 µL of A549 cells were seeded at a density of 1×10^5 cells per mL in a 96-well black plate with a transparent bottom. The cells were incubated at 37 °C for 24 h. The medium was removed and replaced with 50 µM H₂DCFDA (from Life Technologies) solution in PBS for 40 min. H₂DCFDA was removed and replaced with fresh medium. The cells were left for recovery for 20 min at 37 °C. Basal fluorescence was measured at 485/520 nm on a POLARstar Optima. The cells were incubated with 10 µM, 50 µM, or 100 µM of compounds, 1% DMSO (negative control) and 100 µM of H₂O₂ (positive control) for 24 h. Fluorescence was read at 485/520 nm. Basal fluorescence was subtracted from the fluorescence in the treated cells to calculate the amount of fluorescence caused by the compounds.

Chapter 3

The synthesis and anticancer activity of cyclometalated gold^{III} complexes with acridine decorated functional groups.

3.1 Abstract

A series of novel gold^{III} complexes containing a cyclometalating (C^N) or (C^NP^zC) ligand and an acridine functional group have been synthesised and characterised as prospective anticancer drug candidates. Two types of complexes were synthesised. Firstly, a series of neutral mono-cyclometalated (C^N)-(N^X)Au^{III} complexes with acridine-decorated (N^O) and (N^N) chelating ligands (**51-56**). Secondly, two cationic bis-cyclometalated (C^NP^zC)Au^{III} complexes where the acridine moiety was connected to an acyclic diamino carbene ligand, (**57**) or to an N-heterocyclic carbene ligand, (**58**). The complexes have been screened for their cytotoxic activity against a panel of human cancer cell lines and show greater or comparable activity to cisplatin under the conditions used in this assay. Cell uptake studies demonstrated a clear correlation between cellular uptake and the *in vitro* cytotoxicity of the complexes. DNA binding studies showed that two of the derivatives achieve high levels of DNA stabilisation suggestive of DNA intercalation.

3.2 Introduction

Chapter 1 has already discussed the anticancer activity of a diverse number of structurally different gold^{III} complexes with chemotherapeutic properties. In particular, cyclometalated gold^{III} complexes have been attracting significant interest, (Section 1.13). Both bidentate, (C^N) or tridentate, (C^NC), (C^NN) or (N^CN) cyclometalating ligands can be used to improve the physiological stability of the gold^{III} centre within the cellular environment.^{5, 6, 25, 28, 31}

Some of the first cytotoxic (C^N) cyclometalated gold^{III} derivatives were synthesised in the 1990s by Parish *et al.* These derivatives of ((dimethylamino)methyl)phenyl, **8** (Figure 53) displayed a similar cytotoxicity profile to cisplatin in both *in vitro* and *in vivo* experiments.²⁰ Numerous other cyclometalated gold^{III} complexes with a variety of different ligand systems have since been synthesised and tested for their cytotoxicity against human cancer cell lines.^{14, 37, 45, 46}

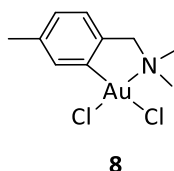


Figure 53 – Au(damp)Cl₂.²⁰

Kilpin *et al.* introduced a series of neutral cyclometalated (C[^]N)Au(N[^]N) chelated complexes containing phenylenediamine and ethylenediamine moieties, with the nitrogen atoms bearing electron withdrawing SO₂Tol and COMe moieties, **12a-12d** (Figure 54), (Tol = *p*-tolyl). The derivatives were tested for their *in vitro* cytotoxicity against mouse leukaemia cells (P388) and some showed very promising results in comparison to cisplatin. Several different (C[^]N) cyclometalating ligands were used, including the 6-membered ring, 2-benzyl pyridine cyclometalating ligand (**12a** and **12c**) and the more rigid 5-membered ring, 2-phenyl pyridine cyclometalating ligand (**12b** and **12d**). Derivatives **12a** and **12c**, containing the less rigid 6-membered ring appeared to show increased cytotoxicity towards P388 cells with IC₅₀ values falling to <1 μM.²⁶

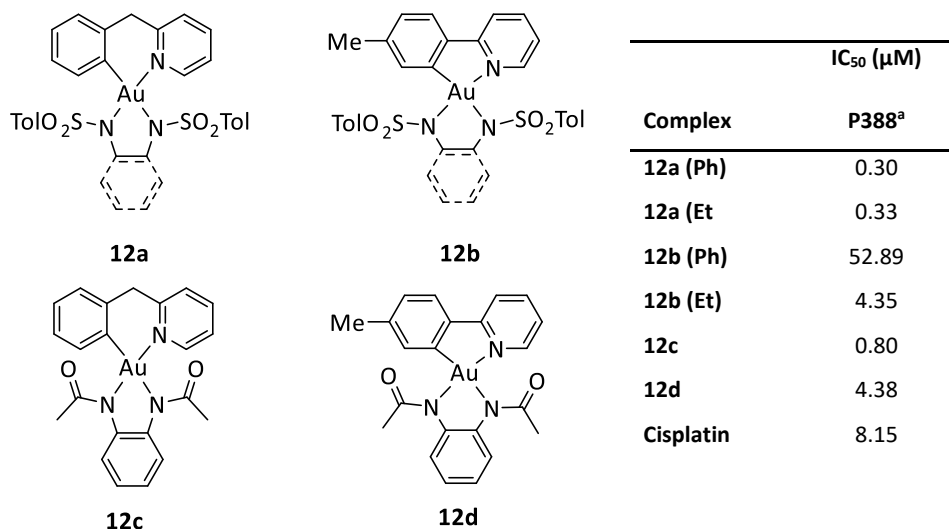


Figure 54 – structures of (C[^]N)-(N[^]N) derivatives **12a-12d** and their cytotoxicity towards cancer cells in comparison to cisplatin; ^a Mouse leukaemia. Data taken from ref²⁶.

Other (C[^]N)-(N[^]N) derivatives, by Zhang *et al.* also used the more rigid five membered ring cyclometalating (butyl-C[^]N) ligand to stabilise a cationic water soluble gold^{III} complex, [Au(butyl-C[^]N)biguanidine]Cl, **10** (Figure 55) which combined the lipophilic, cyclometalated (C[^]N) ligand and the hydrophilic, H-bonding NH₂ groups of the biguanidine ligand. The complex showed high levels of cytotoxicity towards cancer cell lines, with IC₅₀ values in the

low micromolar ranges as well as a high selectivity profile towards cancer cells over healthy CCD-19-Lu cells.²⁴

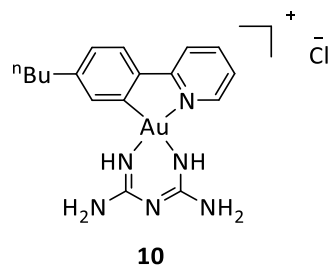


Figure 55 – structure of the cyclometalated [Au(butyl-C^N)biguanidine]Cl complex.²⁴

Goss *et al.* also reported on the reactions of cyclometalated LAu^{III}Cl₂ complexes with catechol and phenol derivatives, using both the more flexible 6-membered ring and the more rigid five-membered ring cyclometalating ligands (Figure 56). Reactions with catechol gave stable complexes containing five-membered Au-O-C-C-O rings, **44a** and **44b**. Reactions with 2-acetamidophenol also gave the corresponding (C^N)-(N^O) complexes with Au-N-C-C-O rings, **44c**. The catechol derivatives **44a** and **44b** showed the highest antitumor activity towards p388 cells with IC₅₀ values of 0.66 and 0.46 μM respectively (in comparison to cisplatin with an IC₅₀ of 8.15 μM). However, the (C^N)-(N^O) derivatives also displayed significant levels of activity in comparison to cisplatin, (IC₅₀ of 2.5 μM).⁹⁸

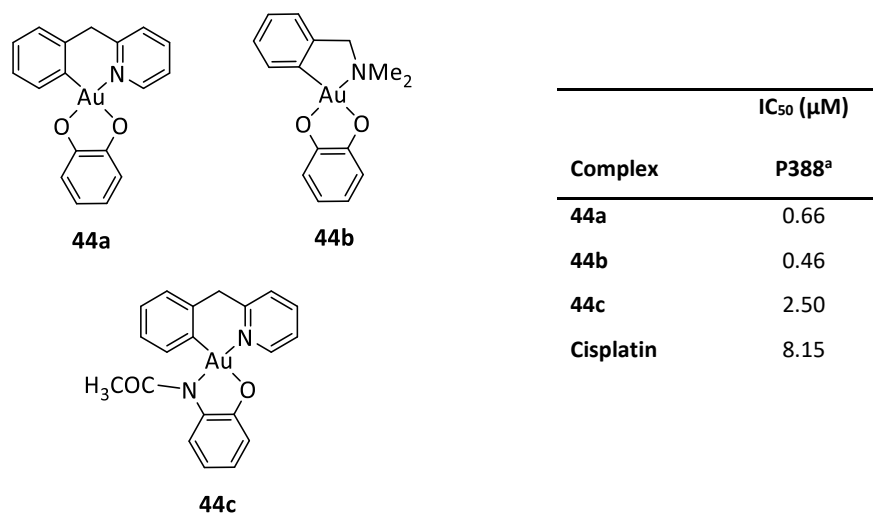


Figure 56 – structures of (C^N)-(O^O) and (C^N)-(N^N) derivatives **44a-44c** and their cytotoxicity towards cancer cells in comparison to cisplatin; ^a Mouse leukaemia. Data taken from ref⁹⁸.

Chapter 2 has described the synthesis and anticancer activity of novel cyclometalated ($C^{\wedge}N^{p2\wedge}C$) gold^{III} complexes with acyclic carbene ligands decorated with amine and amino ester derivatives, **43a-g** (Figure 57).⁸⁶ Although the antiproliferative screening of these complexes identified them as promising potential chemotherapeutic agents, they were also reduced to a gold^I species in the presence of glutathione (GSH). Section 1.26 has already discussed the overexpression of GSH by cancer cells and the role it plays in the deactivation of platinum based chemotherapeutic agents.^{81, 82} Gold^{III} N-heterocyclic carbene (NHC) complexes appear to be more stable towards reducing agents like GSH and are also highly cytotoxic towards cancer cell lines (Section 1.14). Our group recently published a paper on the synthesis and anticancer activity of a pyrazine-based ($C^{\wedge}N^{p2\wedge}C$) pincer complex with a benzimidazole-based NHC ligand, **19** (Figure 57). This derivative showed high levels of *in vitro* cytotoxicity with IC₅₀ values in the micromolar and sub-micromolar range against a panel of cancer cell lines.³⁹

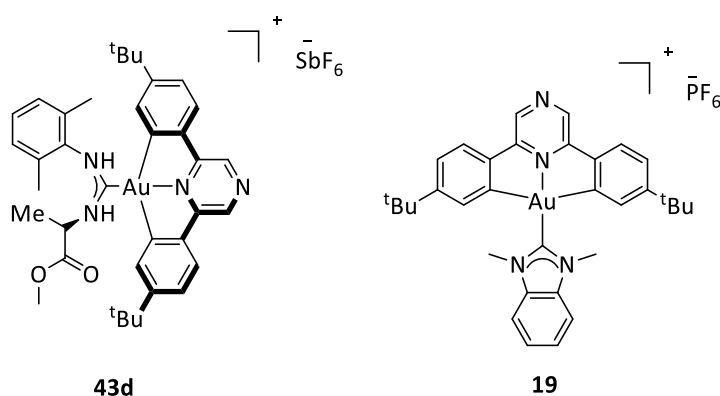


Figure 57 – examples of cytotoxic gold^{III} complexes with cyclometalating ($C^{\wedge}N^{p2\wedge}C$) ligands and acyclic/ heterocyclic carbene ligands.^{39, 86}

Section 1.21 discusses the mechanism of cisplatin; the formation of covalent adducts between purine base pairs which results in the distortion of the DNA helix and the inhibition of DNA replication and transcription processes.⁵³ In spite of the structural and electronic similarity between gold^{III} and platinum^{II} compounds, they appear to have very different molecular targets within the cell and the binding of gold^{III} complexes to DNA is often weak and reversible in nature.^{49, 59}

Acridines, however, are known to bind to DNA by intercalation; by the direct insertion of the three planar aromatic rings in between the base pairs of DNA which causes unwinding of the double helix.^{99, 100} For example, Janočková *et al.* synthesised a series of acridine analogues, **45** (Figure 58) and demonstrated their ability to inhibit cancer cell growth in acute

promyelocytic leukaemia cells (HL60); (IC_{50} of 1.6 μM). DNA binding studies towards calf thymus DNA showed a strong interaction through DNA intercalation resulting in the inhibition of certain enzymes such as topoisomerase 1 and 2.⁹⁹ These enzymes unwind chromosomal DNA and represent an important target for anti-cancer agents.⁶⁰ Howell *et al.* also studied the DNA binding and *in vitro* cytotoxicity of 9-aminoacridine carboxamides, **46** towards various types of tertiary DNA structures. The derivatives were shown to target G-quadruplex structures with some selectivity.¹⁰¹

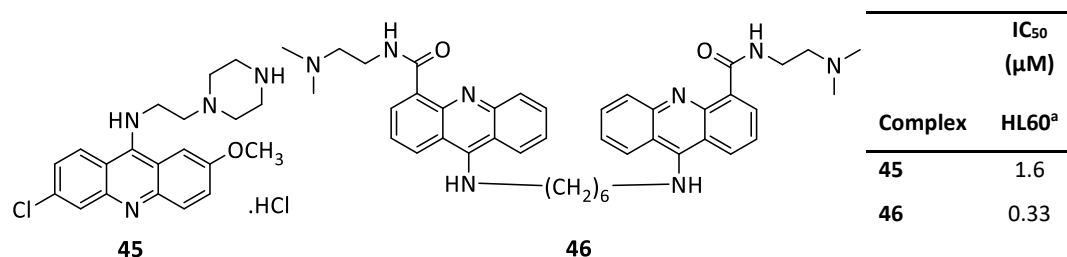


Figure 58 – two acridine derivatives with cytotoxic properties towards human cancer cells; ^a Leukaemia. Data taken from ref^{99, 101}.

There are also examples of acridine motifs being used to enhance the cytotoxicity of metal based chemotherapeutic agents.^{102, 103} Smyre *et al.* made the platinum-acridine hybrid, **47** (Figure 59) which showed extremely high levels of cytotoxicity towards non-small cell lung cancers, including in a very aggressive NCI-H460 xenograft model. The complex showed pronounced cytotoxic enhancement of 40-200 fold compared to cisplatin with IC_{50} values in the low nanomolar range. DNA binding studies showed that the compound also produced permanent DNA adducts more readily than cisplatin (half-lives of 20 min and 2 h respectively), suggesting that it was able to inhibit DNA replication to a greater extent.¹⁰²

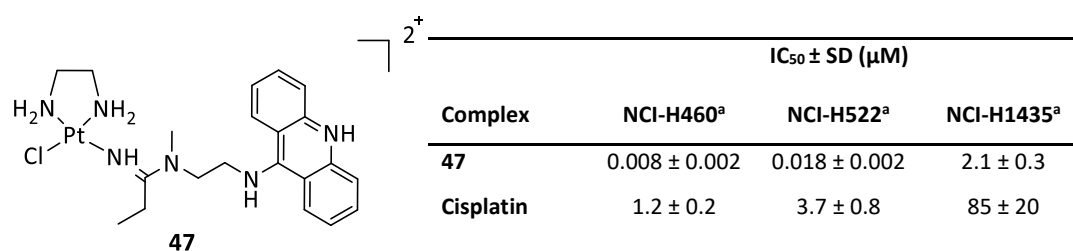


Figure 59 – structure of the platinum-acridine hybrid, **47** and its cytotoxicity towards cancer cell lines in comparison to cisplatin; ^a Non-small cell lung cancer. Data taken from ref¹⁰².

Other cytotoxic metal-acridine hybrids were synthesised by Matsheku *et al.*, this time using iron, rhodium, iridium, ruthenium and osmium. All the derivatives displayed good *in vitro* cytotoxicity towards HL60 cells although the rhodium derivative, **48** (Figure **60**) showed the highest activity as well as a good selectivity profile for this cell line over healthy skin fibroblast cells (FG0). NMR studies also suggested that DNA was the molecular target of this compound.¹⁰³

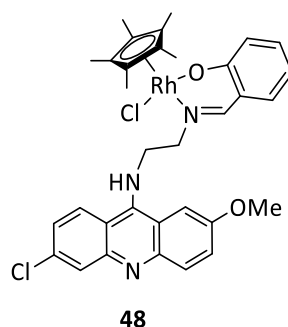


Figure **60** – the rhodium-acridine hybrid with cytotoxic properties.¹⁰³

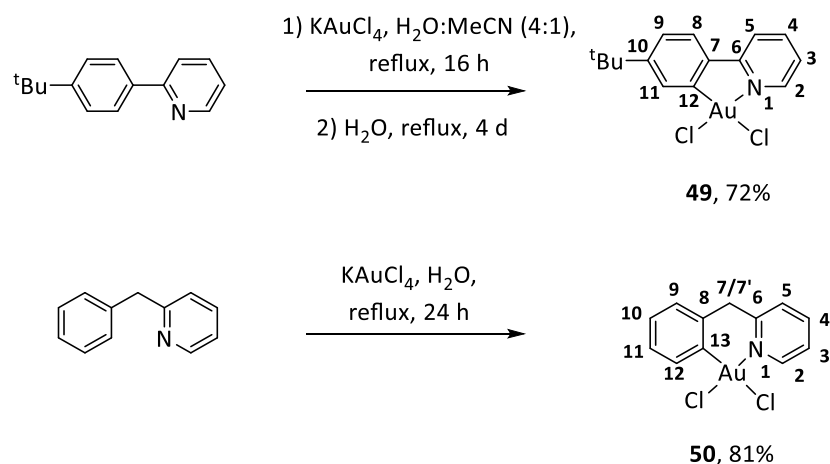
Although there are examples of cytotoxic gold^I-acridine hybrids, there do not appear to be any examples of cytotoxic gold^{III}-acridine hybrids.^{104,105} This chapter introduces the synthesis and anticancer activity of some of the first cyclometalated gold^{III} complexes with acridine decorated functional groups. Firstly, a series of neutral (C[^]N)-(N[^]O) and (C[^]N)-(N[^]N) derivatives, (**51-56**), both with and without acridine functional groups, and secondly two pincer (C[^]N^{p2}^C) complexes where the acridine functionality is joined by either an acyclic carbene (**57**) or an NHC ligand (**58**). The complexes were tested for their cytotoxicity towards three cancer cell lines; lung adenocarcinoma (A549), breast cancer (MCF-7) and leukaemia (HL60). The DNA binding abilities of the complexes towards dsDNA was also assessed using both UV-Vis spectroscopy and FRET DNA melting assays.

3.3 Results and Discussion

3.31 Synthesis and structural characterisation

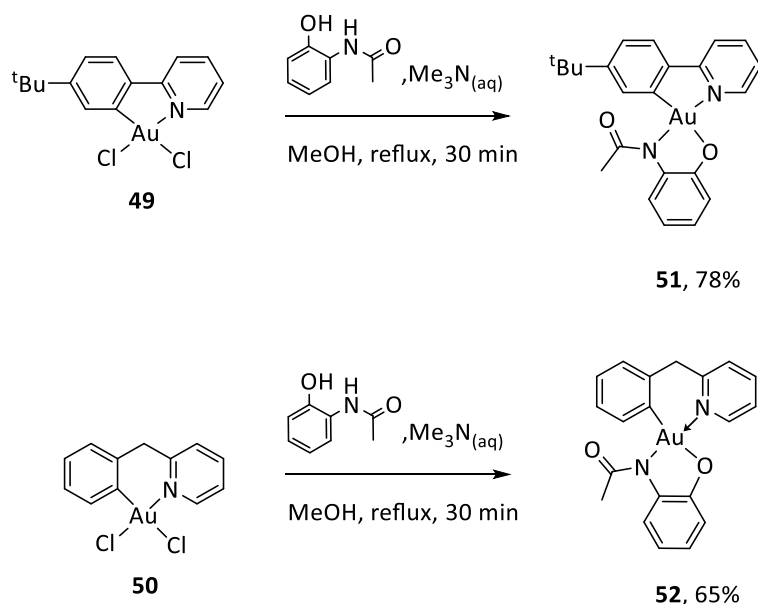
The cyclometalated 2-phenyl pyridine gold dichloride precursor was synthesised by a similar method to that described by Constable *et al.*; by refluxing potassium tetrachloroaurate with 4-*tert*-butyl-2-phenyl pyridine in a 4:1 mixture of water and acetonitrile for 16 hours to form the N-coordinated gold trichloride, followed by a further reflux in water to form the cyclometalated gold dichloride, complex **49**, in good yield (72%) as depicted in Scheme **13**.¹⁰⁶ Similarly, the 2-benzyl pyridine gold dichloride precursor, complex **50**, was synthesised in

high yield (81%) by the method described by Cinellu *et al.*; by refluxing 2-benzyl pyridine and potassium tetrachloroaurate in water (Scheme **13**).¹⁰⁷



Scheme **13** – synthesis of the two ($\text{C}^{\wedge}\text{N}$) cyclometalated gold^{III} dichloride starting materials, **49** and **50**.^{106, 107}

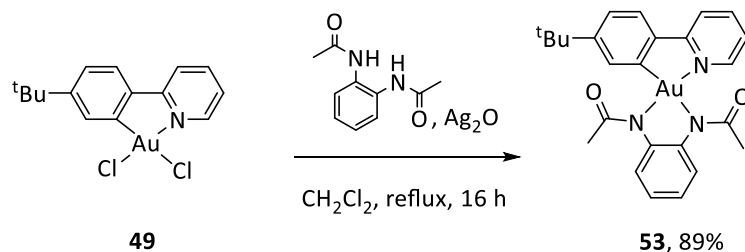
When the cycloaurated gold^{III} dichloride starting materials were reacted with 2-acetamidophenol in refluxing methanol with excess trimethylamine, the mono-cyclometalated ($\text{C}^{\wedge}\text{N}$)-($\text{N}^{\wedge}\text{O}$) complexes, **51** and **52**, were isolated in good yields, (78% and 65% respectively), by precipitation with water (Scheme **14**).



Scheme **14** – synthesis of the mono-cyclometalated ($\text{C}^{\wedge}\text{N}$)-($\text{N}^{\wedge}\text{O}$) complexes **51** and **52**.

Complex **53** was synthesised in high yield, (89%), by reacting the gold dichloride starting material with 1,2-diacetamidobenzene and silver oxide in refluxing dichloromethane

(Scheme 15). The reaction was also attempted with the 2-benzyl pyridine gold dichloride starting material, **50** but caused decomplexation to the less rigid 6-membered ring.



Scheme 15 – synthesis of the mono-cyclometalated (C^N)-(N^N) complex, **53**.

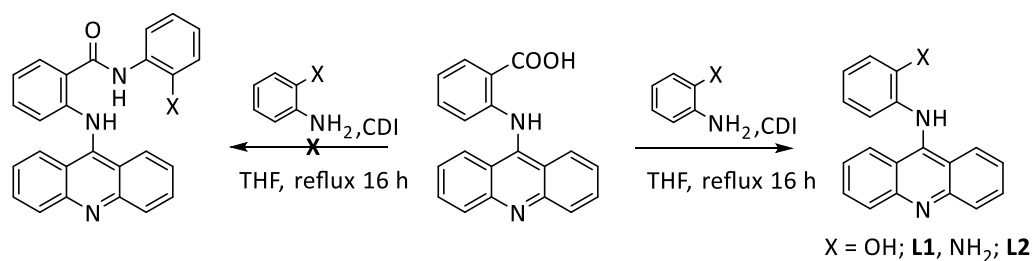
¹H and ¹³C[¹H] NMR were used to fully characterise complexes **49-53**. The purity of the complexes was also assessed by elemental analysis. Upon reaction of complex **49** with 2-acetamidophenol, the characteristic doublet observed for H² shifted downfield from 9.71 ppm to 8.97 ppm showing that the mono-cyclometalated (C^N)-(N^O) complex, **51**, had been obtained. The singularity of each of the signals in the ¹H NMR spectrum confirmed that only one isomer of complex **51** had been obtained.

A slight downfield shift of H², from 9.26 ppm to 9.24 ppm was also seen when complex **50** was reacted with 2-acetamidophenol, confirming the coordination of the pyridine ring to the gold^{III} centre. The H⁷ methylene protons for complex **52** were also seen as a singlet at 4.29 ppm, suggesting a loss of chemical inequivalence for the methylene protons and therefore the disruption of the characteristic AB system, indicating ring opening of the cyclometalating (C^N) 2-benzylpyridine ligand, possibly through loss of N-coordination. This feature was expected as this compound was previously synthesised by Goss *et al.*⁹⁸

Complex **53** was poorly soluble in the deuterated NMR solvents and therefore signals in both the ¹H and particularly the ¹³C[¹H] NMR were poorly resolved. This complex also showed a downfield shift of the H² signal to 9.30 ppm, as a poorly resolved broad singlet. Two separate signals at 2.27 and 2.15 ppm for the two methyls of the acetate groups confirmed the formation of the bis-chelated (C^N)-(N^N) complex. These signals were not observed in the ¹³C[¹H] NMR spectrum although an HMQC carbon proton correlation spectrum confirmed their presence around 25 ppm (Section 3.52).

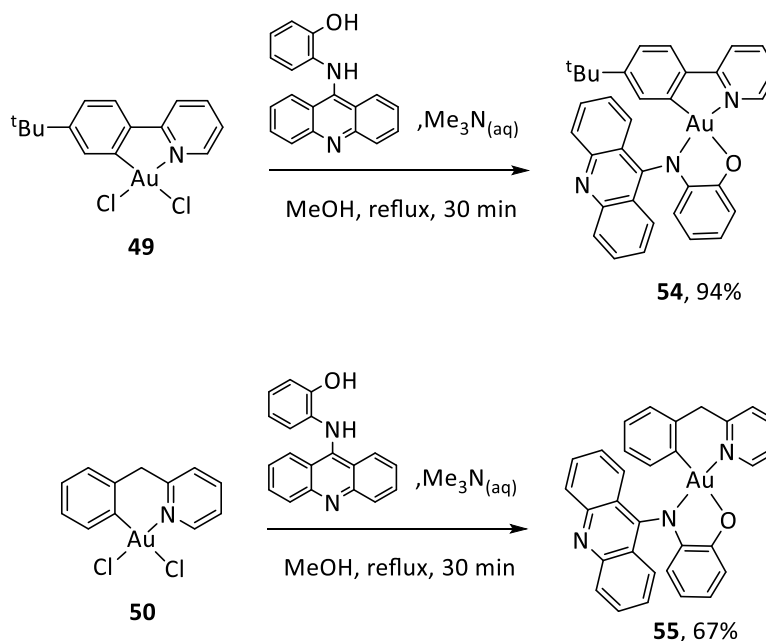
Following the success, forming (N^O) and (N^N) chelate complexes with simpler ligands, an acridine moiety was attached to 2-amino phenol by a CDI assisted coupling with 4-(acridin-9-ylamino)-benzoic acid. Instead of reacting at the carboxylic acid functional group as was

expected the compound instead reacted at the 9-amino group of the acridine moiety, joining the substituted phenol directly to the acridine by displacing the 4-aminobenzoic acid and forming **L1**. The same reaction also occurred when *o*-phenylenediamine was used, forming **L2**, as depicted in Scheme 16.



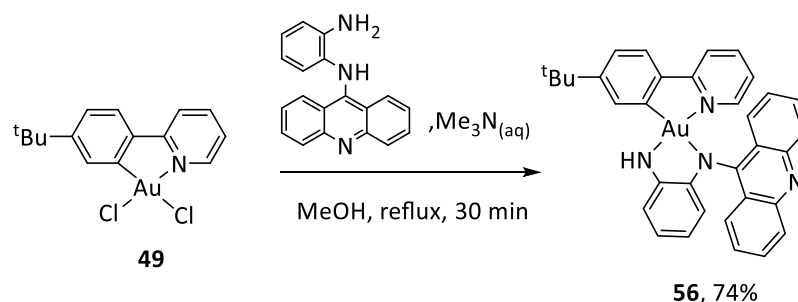
*Scheme 16 – synthesis of the substituted acridine ligands **L1** and **L2**.*

Complex **54** was obtained in high yield, (94%), by reacting one equivalent of complex **49** with **L1** in refluxing methanol with an excess of trimethylamine, followed by precipitation with water (Scheme 17). A reaction between complex **50** and **L1** under the same conditions was also successful and complex **55** was obtained in moderate yield, (67%).



*Scheme 17 – synthesis of the acridine-decorated (C^N)-(N^O) complexes, **54** and **55**.*

The corresponding (C^N)-(N^N) complex, **56** was obtained in good yield, (74%) by the reaction of complex **49** with **L2** under the same reaction conditions (Scheme 18). Once again, the reaction was also attempted with **50** but this caused ring opening to the less rigid 6-membered cyclometalating ring.



Scheme 18 – synthesis of the acridine-decorated (C^N)-(N^N) derivative, **56**

Diagnostic signals in the NMR spectra for the acridine substituted complexes, **54-56** were harder to determine due to the complexity of signals in the aromatic region. Complex **54** showed a slight downfield shift to 9.61 ppm of the H^2 signal in the 1H NMR spectrum which was seen as a doublet of doublets, due to coupling between both H^3 and H^4 . Signals for the acridine substituent were clearly seen by a doublet of doublets at 8.49 ppm and a doublet at 8.30 ppm, for H^{21+24} .

The 1H NMR spectrum of complex **55** was harder to resolve due to the steric bulk of the acridine moiety interacting with the phenyl ring of the cyclometalating (C^N) ligand, preventing free rotation and thus causing broad and poorly resolved signals. By lowering the temperature to $-10^\circ C$ it was possible to slow the movement enough to obtain a well-resolved spectrum (Figure **61**). Due to the lack of free rotation, all of the acridine protons, H^{22-25} were chemically inequivalent and seen as separate signals. Unlike complex **52**, the characteristic AB system of two doublets at 4.43 ppm and 3.91 ppm was observed for the methylene bridge indicating the chemical inequivalence of these protons, confirming that ring opening had not occurred.

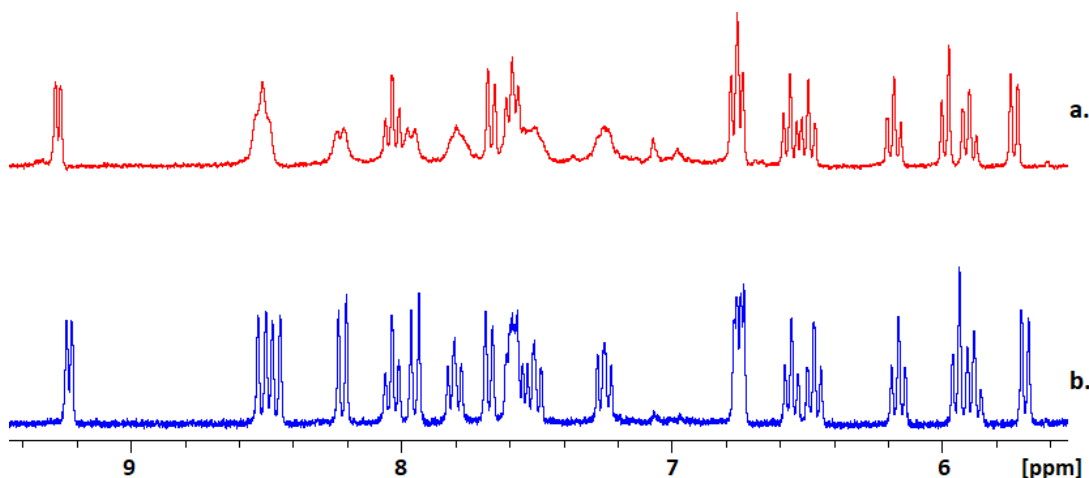


Figure 61 – **a.** aromatic region of the 1H NMR spectrum of **55** at room temperature and **b.** aromatic region of the 1H NMR spectrum of **55** at $-10^\circ C$.

Complex **56** presented further problems with a large downfield shift in the H² signal to around 7.73 ppm in the ¹H NMR spectrum, where it overlapped with other aromatic signals. For all of the three acridine-based complexes, **54-56**, only one set of signals were observed for each proton, demonstrating the formation of only one isomer in each case, as seen previously with the simpler (N[^]O) and (N[^]N) complexes, **51-53**.

Slow diffusion of light petroleum ether through a dilute dichloromethane solution of complex **54** yielded crystals suitable for X-ray diffraction. The crystals were characterised in the solid state by Dr Julio Fernandez-Cestau (Figure **62**).

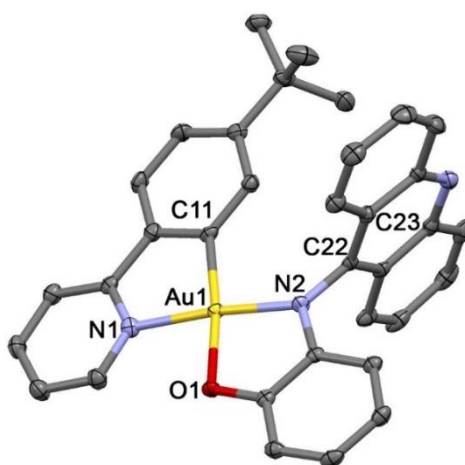


Figure **62** – crystal structure of complex **54**·CH₂Cl₂ (dichloromethane and hydrogen atoms omitted for clarity). Selected bond distances (Å) and angles (°). Au1-N1 2.028(3), Au1-C11 2.034(4), Au1-O1 2.049(3), Au1-N2 1.990(3), C11-Au1-N1 81.1(1), C11-Au1-N2 103.8(1), N2-Au1-O1 82.5(1), O1-Au1-N1 92.7(1), N1-Au1-N2 174.3(1), C11-Au1-O1 173.1(1), torsion Au1-N2-C22-C23 110.4(3).

The crystals display the typical, slightly distorted square planar geometry to the gold^{III} centre that occurs due to the accommodation of a cyclometalating ligand, with a C11-Au-N1 bond angle of 81.1°. The acridine substituted nitrogen is in *trans* position to the nitrogen of the cyclometalated ligand, as this is the most electronically favoured orientation. The most electron donating atom is in *trans* position to the carbon of the cyclometalating ligand, despite the steric hindrance of the *tert*-butyl group. The acridine moiety is twisted with a Au1-N2-C22-C23 torsion angle of 110°, presumably to avoid steric hindrance with the hydrogens of the *tert*-butyl group. As suggested by the NMR spectra, the crystal structure confirmed that only one isomer of the complex was obtained.

Crystals were also obtained of complex **56** using the same method of slow diffusion of light petroleum ether into a dilute dichloromethane solution of the complex. The crystals were characterised in the solid state by Dr Julio Fernandez-Cestau (Figure **63**).

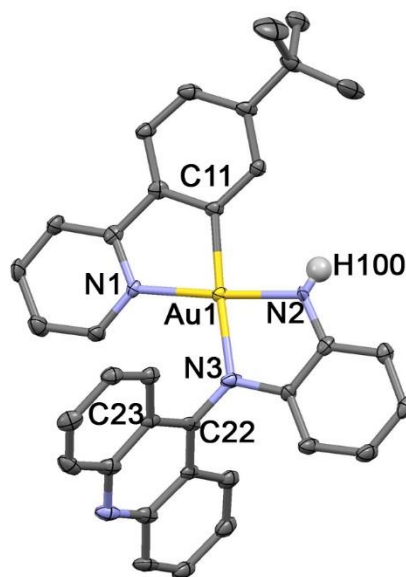
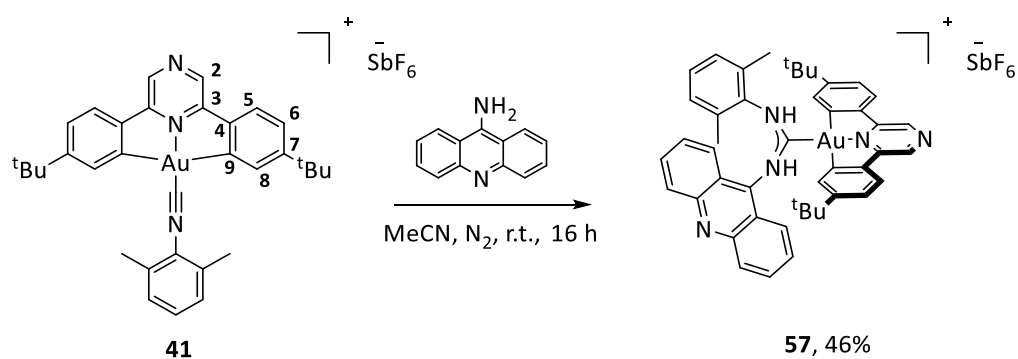


Figure **63** – crystal structure of complex **56**·CH₂Cl₂ (dichloromethane and hydrogen atoms omitted for clarity). Selected bond distances (Å) and angles (°). Au1-N1 2.063(7), Au1-C11 2.015(6), Au1-N2 1.956(8), Au1-N3 2.081(6), N1-Au1-C11 80.9(3), C11-Au1-N2 95.2(3), N2-Au1-N3 80.3(3), N3-Au1-N1 103.9(3), Au1-N2-H100 119(6), N1-Au1-N2 175.4(3), C11-Au1-N3 173.0(3), torsion Au1-N3-C22-C23 67.3(9).

Once again, the crystals display the typical, slightly distorted square planar geometry to the gold^{III} centre with a C11-Au1-N1 bond angle of 80.9° to the cyclometalating ligand. Whereas for the (N[^]O) chelate, complex **54**, the acridine substituted nitrogen is in *trans* position to the nitrogen of the cyclometalating ligand, in the case of the (N[^]N) chelate, complex **56**, the acridine substituent is instead in *trans* position to the carbon, presumably to avoid the steric hindrance of the *tert*-butyl group as both of the coordination sites of the (N[^]N) chelate are equivalent. Consequently, the torsion angle of the Au1-N3-C22-C23 is smaller (67.3°).

As described previously in Section **2.31** (Scheme **9**), the cyclometalated (C[^]N^{pz}[^]C)AuCl starting material, complex **37**, was synthesised using previous methods; via a Suzuki cross-coupling reaction to generate the HC[^]N^{pz}[^]CH ligand, an activation reaction with Hg(O₂CCF₃)₂ and a transmetalation reaction to obtain the cyclometalated product.⁹⁶ This was used as a starting material for the pincer complexes **57** and **58**.

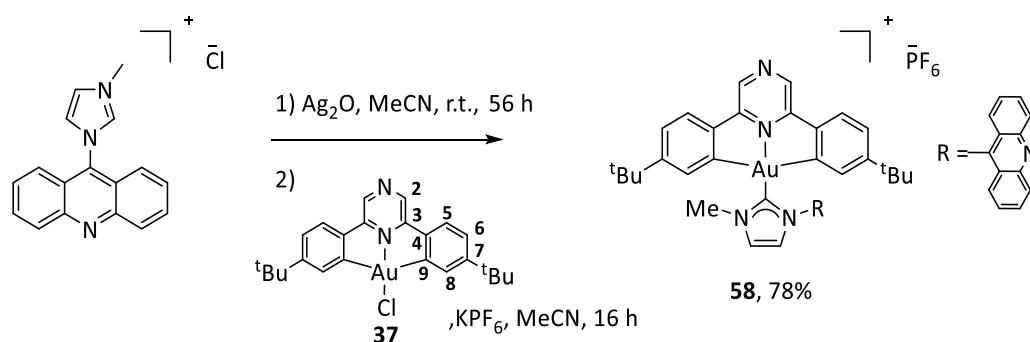
Chapter 2 describes the synthesis and anticancer activity of $(C^{\wedge}N^{p2\wedge}C)Au^{III}$ complexes with acyclic carbene ligands.⁸⁶ Complex **57**, the acridine functionalised acyclic carbene, was synthesised using the same method; via the formation of a cationic $[(C^{\wedge}N^{p2\wedge}C)Au^{III}]^+$ isocyanide complex, **41** followed by the nucleophilic attack of 9-amino acridine onto the highly electrophilic isocyanide carbon (Scheme 19). This allowed the comparison between gold^{III} complexes stabilised by a $(C^{\wedge}N)$ or a $(C^{\wedge}N^{p2\wedge}C)$ cyclometalated ligand. This complex was obtained in moderate yield, (46%), due to the presence of the formamide hydrolysis product, **42** which was formed after the reaction of the isocyanide intermediate with water.



*Scheme 19 – synthesis of the acridine functionalised $(C^{\wedge}N^{\wedge}C)Au^{III}$ open diaminocarbene, **57**.*

Upon formation of complex **57**, a broad NH singlet appears in the 1H spectrum at 10.34 ppm and the upfield H^2 shift to 9.13 ppm confirms that a reaction has occurred and suggests that the acyclic carbene has been formed. The signal for H^8 at 7.96 ppm is also in good agreement with H^8 signals observed for the acyclic carbene complexes synthesised in Chapter 2. The IR spectrum of complex **57** shows a carbene vibration at 1586 cm^{-1} and two NH vibrations at 3388 cm^{-1} and 3270 cm^{-1} , again confirming the successful formation of **57**.

Complex **58** was synthesised in high yield, (78%), by reacting an acridine functionalised imidazolium salt with silver oxide, followed by the addition of the cyclometalated $(C^{\wedge}N^{p2\wedge}C)AuCl$ starting material and potassium hexafluorophosphate, as depicted in Scheme 20. The slight downfield shift in the signal for H^2 and a larger downfield shift in H^8 from 7.88 to 7.21 ppm in the 1H NMR spectrum and also the appearance of a signal at 154.9 ppm for the Au bound NHC in the ^{13}C NMR spectrum both suggest carbene formation, as previously reported by our group for cyclometalated pyrazine-based $(C^{\wedge}N^{p2\wedge}C)$ pincer complex with a benzimidazole-based NHC ligands.³⁹



Scheme 20 – synthesis of acridine functionalised ($\text{C}^{\text{N}^{\text{pz}}\text{C}}\text{Au}^{\text{III}}$) NHC, **58**.

3.32 In vitro antiproliferative activity

Although insoluble in aqueous cell culture medium, all of the complexes and their ligand precursors were soluble enough in DMSO not to precipitate when diluted up to 100 μM in aqueous cell medium with 1% of DMSO. Complexes **49-58** and both of the acridine ligand precursors, **L1** and **L2** were screened for their antiproliferative properties *in vitro* on a panel of human cancer cell lines, including lung adenocarcinoma cells (A549), breast adenocarcinoma (MCF-7), and promyelocytic leukaemia (HL60). The IC_{50} , (the half maximal inhibitory concentration), was then determined using a colorimetric MTS assay after 72 hours of incubation in comparison to cisplatin (as previously described in Section 2.32). The results are summarised in Table 2.

Table 2 – cytotoxic effects of complexes 49-58 and ligands L1 and L2 in comparison to cisplatin towards different human cancer cell lines after 72 h of incubation.

Complex	IC ₅₀ ± SD (μM) ^a		
	A549	MCF-7	HL60
49	43.6 ± 4.1	10.8 ± 3.5	6.0 ± 0.5
50	>100	38.7 ± 4.7	12.8 ± 0.3
51	12.7 ± 2.5	5.2 ± 1.0	2.9 ± 0.7
52	10.8 ± 2.7	3.6 ± 1.4	2.7 ± 0.4
53	22.7 ± 2.5	9.9 ± 2.1	2.5 ± 0.1
54	16.6 ± 2.8	2.7 ± 0.9	1.4 ± 0.4
55	19.9 ± 3.9	4.3 ± 0.4	1.5 ± 0.1
56	17.2 ± 4.4	6.7 ± 1.6	6.3 ± 0.1
57	15.0 ± 2.0	7.5 ± 0.6	20.7 ± 0.4
58	7.6 ± 0.6	1.5 ± 0.1	1.1 ± 0.1
L1	>100	>100	>100
L2	23.9 ± 3.5	14.4 ± 0.9	16.9 ± 0.9
Cisplatin	33.7 ± 3.7 ^b	21.2 ± 3.9 ^b	3.7 ± 0.3 ^b

^a Mean ± the standard error of at least three independent experiments. ^b Values from ref ³⁹.

Complexes **51-58** showed greater or comparable activity to cisplatin under the conditions used in this assay and were overall more cytotoxic than the gold dichloride precursors, complexes **49** and **50**. The free ligands, **L1** and **L2**, showed reduced cytotoxicity particularly **L1** which was inactive against all of the cell lines tested, with an IC₅₀ value of >100 μM against all three. **L2** also showed reduced cytotoxicity in comparison to the gold complexes therefore indicating the significance of the gold^{III} centre to the cytotoxicity of these particular acridine derivatives. However, it is not clear why **L1** was far more inactive than **L2** (IC₅₀ values of >100 μM and 14-24 μM respectively).

Overall, all of the mono-cyclometalated (C^N)-(N^X) complexes, **51-56** showed greater activity than cisplatin against both the MCF-7 and the A549 human cancer cell lines and comparable activity against the HL60 cell line. Complexes **51-56** all showed similar activities against the MCF-7 cell lines with IC₅₀ values in the 2-10 μM range. Complexes **52**, **54** and **55** showed particularly high cytotoxicity with values between 2-4 μM. IC₅₀ values for the A549

cell line were slightly higher, between 10-20 μM for all of the complexes. Here, the simpler structures, complexes **51** and **52** showed the greatest cytotoxicity.

Changing the (C^N) cyclometalating ligand between the more rigid phenyl pyridine and the more flexible 2-benzyl pyridine derivatives appeared not to significantly alter the cytotoxicity of the complexes which suggests that rigidity of the ligand was not important in this respect. For example, for the HL60 leukaemia cell line, complexes **51** and **52** have IC₅₀ values of 2.9 and 2.7 μM respectively and complexes **54** and **55** have IC₅₀ values of 1.4 and 1.5 μM respectively. This differs from results obtained by Kilpin *et al.*, where complexes containing a six-membered cyclometalating ring displayed higher cytotoxicity than those with a five-membered cyclometalating ring (discussed in Section 3.2).²⁶

In contrast, the two different types of chelating ligands, (N^O) and (N^N), appeared to have an effect on the cytotoxicity of the complexes. For all three cell lines, the (N^O) chelates appeared to be slightly more cytotoxic than the corresponding (N^N) chelates which is in contrast to the values obtained for the free acridine ligands, **L1** and **L2**. For example, for the A549 lung cancer cell line the (N^O) chelate, complex **51** has an IC₅₀ of 12.7 μM and the corresponding (N^N) chelate, **53** has an IC₅₀ of 22.7 μM . The same pattern can be seen for the acridine functionalised derivatives. Complex **54**, the (N^O) chelate is more cytotoxic than its (N^N) analogue, complex **56** against the all three cancer cell lines. Here the effect is most notable against the leukaemia HL60 cell line, (an IC₅₀ of 1.4 and 6.3 μM respectively).

Adding an acridine functionality appeared not to increase the overall cytotoxicity of the mono-cyclometalated (C^N)-(N^X) complexes. Complexes **54** and **55** were extremely cytotoxic against the MCF-7 breast cancer and the HL60 leukaemia cell lines with IC₅₀ values of between 1 and 4 μM . In comparison, complex **56** showed a slightly reduced cytotoxicity with IC₅₀ values of 6.7 and 6.3 μM for MCF-7 and HL60, respectively. Against the A549 lung cancer cells the simpler (N^O) chelates appeared to be more cytotoxic than their corresponding acridine functionalised complexes, e.g. complex **52** has the highest cytotoxicity here with an IC₅₀ of 10.8 μM . The acridine functionality appeared to reduce the cytotoxicity towards this cell line, with complexes **54-56** all displaying IC₅₀ values between 17 and 20 μM .

The (C^NN^{p2}C)Au^{III} acyclic carbene, complex **57**, showed a higher cytotoxicity than cisplatin against both the MCF-7 and the A549 cancer cell lines, (IC₅₀ values of 7.5 and 15.0 μM for each respectively), although it showed reduced activity against the HL60 cell line, (20.7 μM). These values are in good agreement with other acyclic carbene complexes discussed in

Chapter 2, particularly when considering the amino ester derivatives (e.g. GlyOEt (**44c**) – IC₅₀ values of 6.4, 13.0 and 16.7 μM for MCF-7, A549 and HL60 respectively).⁸⁶

The other (C^{N^{pz}}^C) pincer complex, **58** with the acridine functionality bound by an NHC ligand, showed the highest overall cytotoxicity with values in the low μM regions for all three cell lines. It was more than ten times more cytotoxic than cisplatin against MCF-7 cells and 3-4 times more cytotoxic against the A549 and HL60 cell lines. The higher cytotoxicity of the [(C^{N^C})Au(NHC)]⁺ complexes with respect to the [(C^{N^C})Au(ACC)]⁺ complexes is in line with previous results already discussed in Chapter 2.^{39, 86}

3.33 Cellular uptake in MCF-7 cells

The cellular uptake and the accumulation of drugs inside the cell are both major factors that influence the cytotoxicity of prospective anticancer agents.¹⁰⁸ Inductively coupled plasma-mass spectrometry, (ICP-MS) was used to quantify the amount of intracellular gold and thus measure the amount of compound taken up by the cell. ICP-MS measurements were completed by Dr Graham Chilvers.

In order to see whether the cytotoxicity of the complexes was influenced by their ability to be taken up by the cell, complexes **50**, **53**, **54** and **58** were chosen. Complexes **50** and **53** were selected because **50** showed extremely poor activity, (IC₅₀ of 38.7 μM) and **53** showed only average activity, (IC₅₀ of 9.9 μM). Complex **54** was selected as it was the best of the acridine derivatised (N^X) chelate complexes and complex **58** as it showed the best overall cytotoxicity, (IC₅₀ values of 2.7 and 1.5 μM respectively).

MCF-7 cells were incubated for 6 hours with 10 μM concentrations of each of the complexes in 1% DMSO. The results of three independent experiments are depicted in Figure **64**.

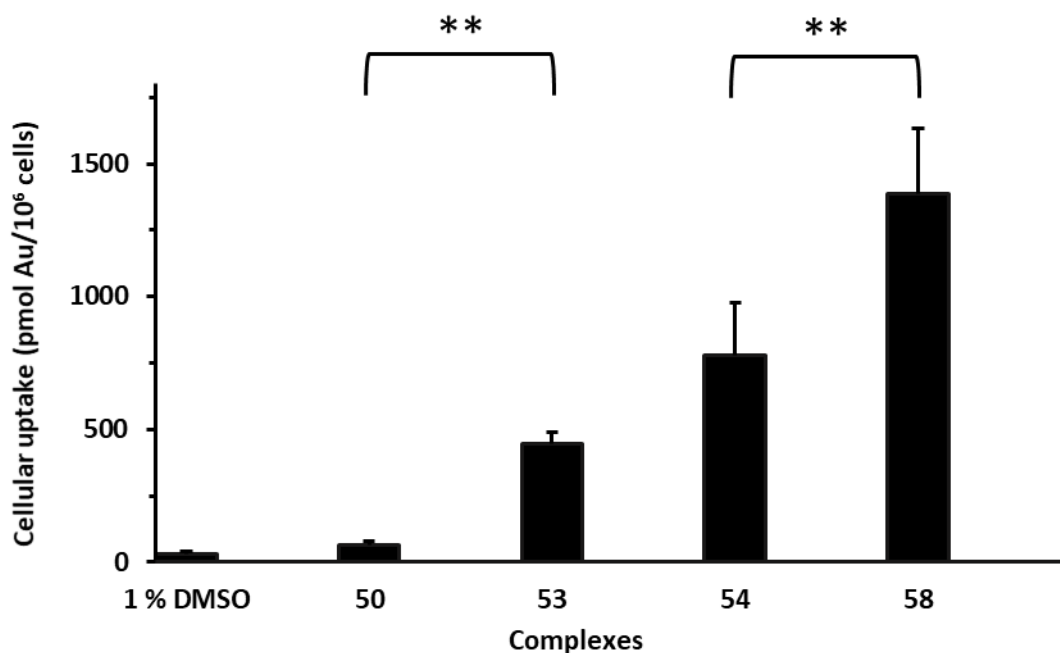


Figure 64 – cellular uptake of complexes 50, 53, 54 and 58 and a DMSO control in MCF-7 cells after 6 h of treatment at 10 μ M in 1% DMSO. The results were analysed by t-test, $P=0.05$, 50:53**, 54:58**.

There was a clear correlation between cellular uptake and the *in vitro* cytotoxicity of the complexes with the most cytotoxic complexes showing the highest levels of cell uptake (Figure 65). This suggests that the primary limitation for the poorly toxic complexes is their very low uptake into the cell.

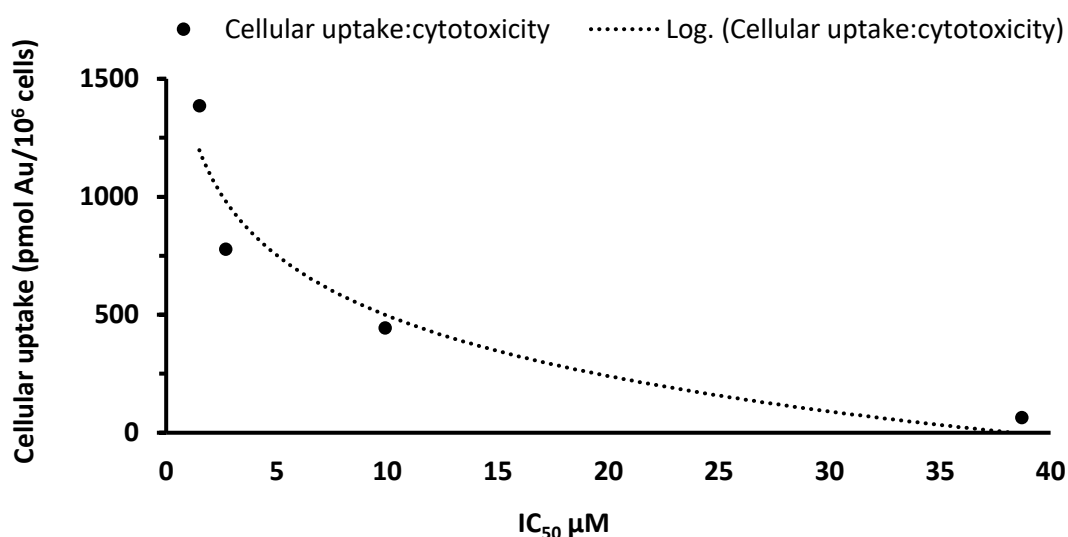


Figure 65 – the correlation between cellular uptake (pmol Au/10⁶ cells) and cytotoxicity (IC₅₀).

3.34 Quantification of reactive oxygen species

As mentioned previously (Section 2.33), the induction of reactive oxygen species (ROS) is a recognised mechanism of action for metal-based drugs.⁷⁵ The acridine derivatised complexes, **54-58**, were therefore tested for the production of ROS. The amount of intracellular ROS was measured after treatment of MCF-7 cells with 100 μM , 50 μM and 10 μM concentrations of these complexes. However, no data could be obtained due to the fluorescent properties of the acridine groups interfering with the emission spectra of the fluorescent stain used in this assay.

3.35 DNA binding assays

Acridine derivatives are known to interact with duplex DNA as well as higher order DNA structures and this can influence the cytotoxic properties of the compounds.^{100, 101, 109} DNA intercalators are of interest as probes in the study of ligand-DNA interactions and also as potential therapeutic agents.¹¹⁰ DNA intercalation is a reversible mode of DNA-ligand binding which consists of the direct insertion of planar aromatic moieties in between the base pairs of DNA which causes unwinding to the double helix. There are several examples of gold^{III} complexes acting as DNA intercalators that have already been discussed in Section 1.21. For example, both terpyridine, (**5**)¹⁷ and aminoquinoline, (**6**)¹⁸ gold^{III} derivatives have been shown to bind to intracellular DNA by intercalation of the planar gold^{III} coordination plane between the DNA base pairs.

In the presence of DNA, acridines have previously been shown to experience changes in their UV/visible absorption spectra with distinctive bathochromic shifts towards the longer wavelengths as well as hypochromic shifts indicating the decrease in absorption.¹¹¹ While this does not prove that DNA intercalation has occurred, it does indicate some sort of DNA interaction. With this in mind, the acridine derivatives complexes **54-58**, as well as their corresponding free ligand precursors, **L1** and **L2** were tested with a simple spectroscopic study for their ability to interact with duplex DNA.

No change in absorption was observed for any of the complexes when 1 mM solutions of **54-58** and **L1/L2** (in a 50:50 PBS/DMSO mix) were combined with a 1 mM solution of calf-thymus DNA (50:50, PBS/DMSO) (Figure 66). This suggests that no DNA interaction was occurring, suggesting that DNA is not the primary target for the cytotoxic effects of these complexes, possibly due to steric hindrance between the cyclometalating (C^N) or (C^N^{Pz}^A) ligands and the acridine substituent. A longer linker between the acridine functionality and the gold^{III}

centre could help to overcome this. However, the negative result in this simple study could also be due to lack of solubility in the PBS/DMSO solvents and consequently the precipitation of the complexes.

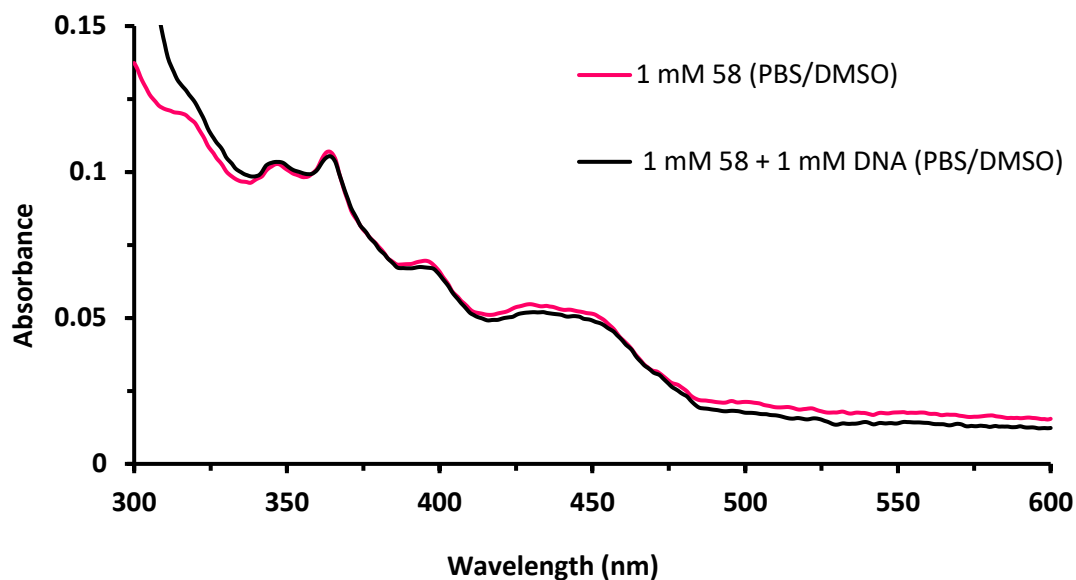


Figure 66 – UV/Vis absorbance spectra of a 1 mM solution of complex 58 in DMSO/PBS, with and without 1 mM of DNA.

Further tests were also done to determine whether or not the acridine-functionalised complexes were interacting with DNA. The Förster resonance energy transfer (FRET) DNA melting assay was used to measure the ability of complexes 51-58 and L1 and L2 to stabilise double stranded DNA. FRET is used as a tool for detecting spatial relationships between two fluorophores and involves measuring the changes in fluorescence as FRET donor and acceptor moieties are brought closer together or moved further apart as a result of DNA stabilisation or denaturation. As a result of the large differences in fluorescence between these folded and unfolded DNA structures it is possible to measure the interaction of a particular drug molecule with the DNA.^{112, 113} Results are expressed as the changes in DNA melting temperature (ΔT_m) when double stranded DNA (0.2 μ M) was dosed with 50 μ M concentrations of each drug (Figure 67).

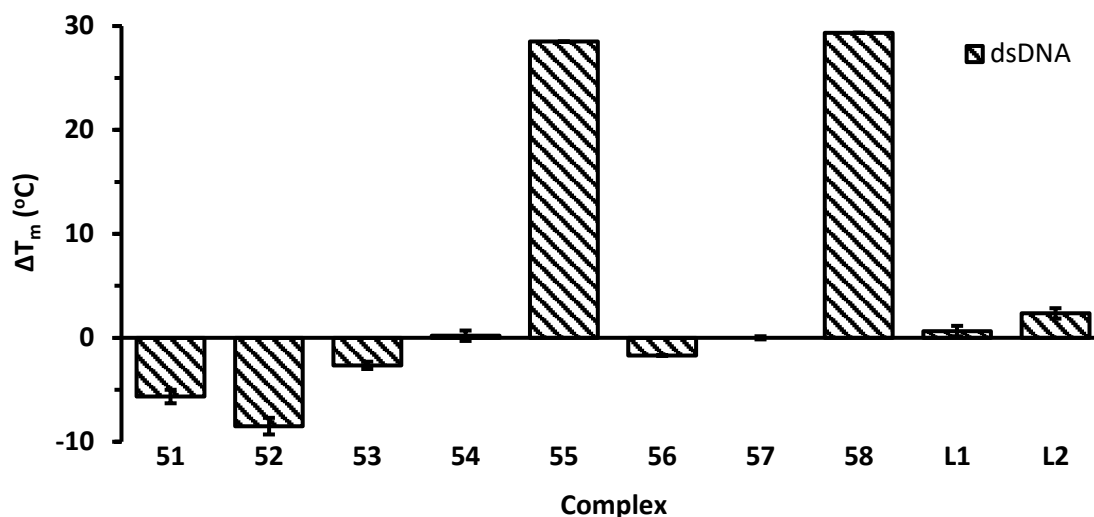


Figure 67 – stabilisation of ds DNA ($0.2 \mu\text{M}$ base pairs) by complexes **51-58** and **L1/L2** at $50 \mu\text{M}$ concentrations measured by FRET DNA melting assay. Data represents the average and standard deviation of two separate experiments.

Only two complexes showed the ability to stabilise double-stranded DNA at high temperatures. Indeed, complexes **51-53** and **56** actually appeared to destabilise ds DNA. While this can be explained for complexes **51-53**, which do not contain an acridine functionality, the result for the (N[^]N) chelated acridine functionalised derivative, complex **56** is less easy to explain. Complex **55**, the acridine functionalised 2-benzylpyridine derivative and the [(C[^]N^{pz}^C)Au(NHC)]⁺ derivative, **58** both showed high levels of DNA stabilisation which suggests that they are interacting with the DNA in some manner, possibly by intercalation of the planar aromatic rings of the acridine moiety between the base pairs of the DNA.

Our group recently discussed the DNA binding ability of another cyclometalated pyrazine-based (C[^]N^{pz}^C) gold^{III} complex with a benzimidazole-based NHC ligand, **19** (Figure 57). This complex was shown to interact with higher order DNA structures in a dose dependent manner but showed a reduced affinity towards dsDNA.³⁹ However, the acridine functionality on complex **58** appears to improve the interaction with dsDNA.

It is difficult to explain why the acridine functionalised 2-benzyl pyridine derivative, **55** should be notably better than the corresponding 2-phenyl pyridine derivatives, **54** and **56**. Hypothetically, the positive result for this complex could be due to the absence of the bulky *tert*-butyl group which is present in both of the other acridine derivatised (C[^]N)-(N[^]X) complexes which could hinder their interaction with DNA. It could also be a function of the

more flexible, 2-benzyl pyridine 6-membered cyclometalating ring enabling the release of some steric hindrance in the structure and thus allowing DNA interaction.

3.36 Reaction with Glutathione

The reduction of gold^{III} complexes by glutathione (GSH) to gold^I and gold⁰ species has been discussed in Section 1.26. The stability of complex **58** and complex **54** towards reduction by GSH was therefore explored by proton NMR. Each complex was mixed at room temperature with reduced glutathione in a 1:1 mixture of DMSO-*d*₆ and D₂O and monitored by proton NMR over time. Our group recently demonstrated the stability of a cyclometalated pyrazine-based (C[^]N^{pz}C) gold^{III} complex with a benzimidazole-based NHC ligand, **19** (Figure 57) towards reduction by GSH.³⁹ However, complex **58**, the acridine substituted [(C[^]N^{pz}C)AuNHC]⁺ complex appeared less stable and over a 24 hour period the gradual formation of oxidised glutathione (GSSG) was observed, along with the disappearance of signals for reduced GSH (Figure 68a). Although signals for the complex were extremely poorly resolved due to its poor solubility in the solvents this suggests that the complex was being gradually reduced to a gold^I active species. The same pattern was seen for the acridine substituted (C[^]N)-(N[^]O) chelate complex, **54** (Figure 68b).

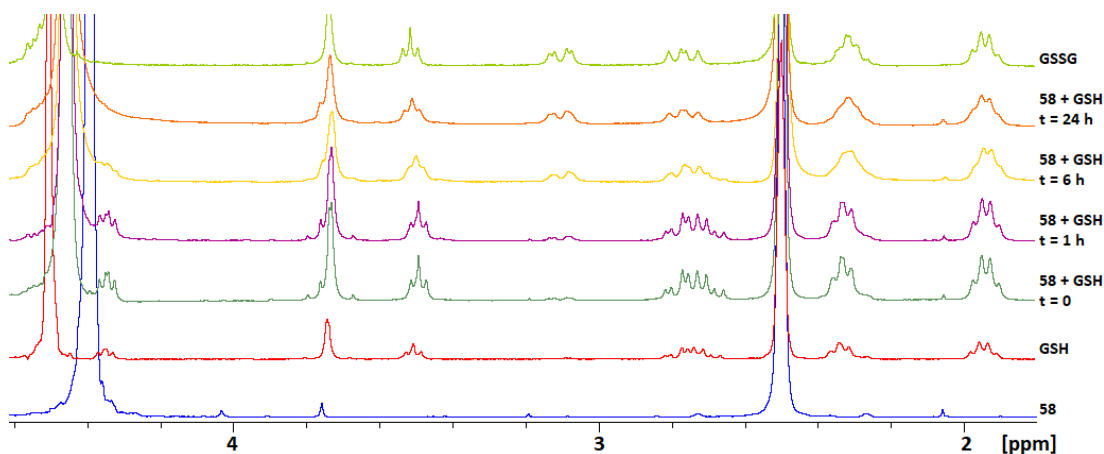


Figure 68a – ¹H NMR spectra of a 1:1 mixture of **58** with GSH at room temperature, in comparison with the starting materials, **58**, GSH and GSSG (DMSO-*d*₆/D₂O 1:1).

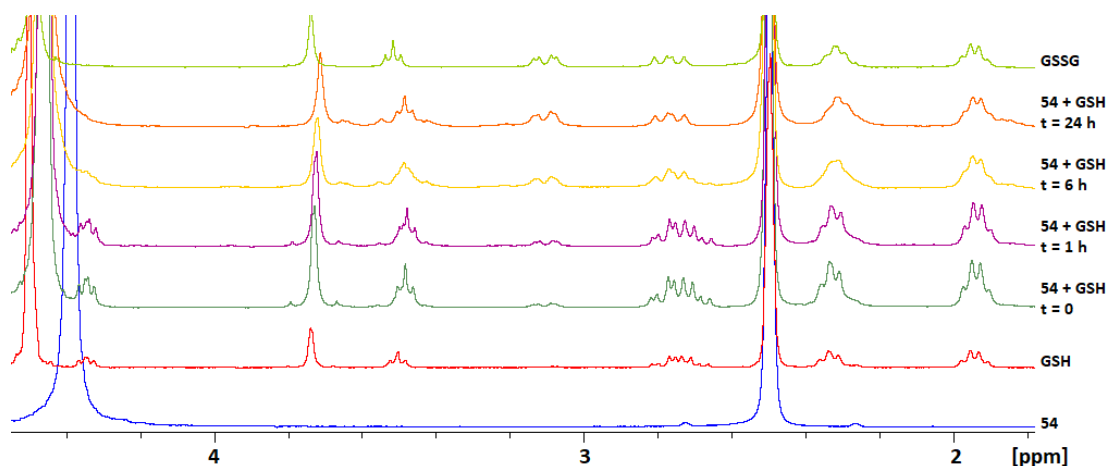


Figure 68b – ^1H NMR spectra of a 1:1 mixture of **54** with GSH at room temperature, in comparison with the starting materials, **54**, GSH and GSSG (DMSO- d_6 /D $_2$ O 1:1).

3.4 Conclusion

This chapter has described the synthesis and anticancer activity of a series of new cyclometalated gold^{III} complexes. These complexes included a series of neutral mono-cyclometalated (C[^]N)-(N[^]X)Au^{III} complexes with both simple and acridine-decorated (N[^]O) and (N[^]N) chelating ligands and two bis-cyclometalated (C[^]N^{pz}^C)Au^{III} pincer complexes where the acridine functionality is attached by either an acyclic or N-heterocyclic carbene ligand.

The complexes were tested for their cytotoxicity towards three cancer cell lines and these studies identified complex **58**, the NHC derivative as the most promising candidate, with IC₅₀ values in the low μM range for all three cell lines. However, having an acridine functionality did not appear to increase the cytotoxicity of the complexes towards the cancer cell lines.

Cell uptake studies demonstrated a clear correlation between cellular uptake and the *in vitro* cytotoxicity of the complexes with the most cytotoxic complexes showing the highest levels of cell uptake, thus indicating that cellular uptake is the primary limitation for the non-toxic complexes. Finally, DNA binding studies showed that two of the derivatives; complex **55**, the acridine functionalised 2-benzylpyridine derivative and the N-heterocyclic carbene derivative, complex **58** both showed high levels of DNA stabilisation suggestive of DNA intercalation.

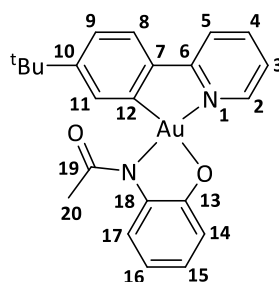
However, both the bis-cyclometalated [(C[^]N^{pz}^C)Au(NHC)]⁺ derivative, **58** and also one of the mono-cyclometalated (C[^]N)Au(N[^]X) derivatives, **54** showed reduction in the presence of glutathione which could suggest that it is reduced to a gold^I active species within a cellular

environment. Further work is required to investigate other the possible modes of action of these complexes.

3.5 Experimental

When required, manipulations were performed using standard Schlenk techniques under dry nitrogen or in a MBraun glove box. Nitrogen was purified by passing through columns of supported P_2O_5 with moisture indicator and activated 4 Å molecular sieves. Anhydrous solvents were freshly distilled from appropriate drying agents. 1H and $^{13}C[^1H]$ spectra were recorded using a Bruker Avance DPX-300 spectrometer. 1H NMR spectra (300.13 MHz) were referenced to the residual protons of the deuterated solvent used. $^{13}C[^1H]$ NMR spectra (75.47 MHz) were referenced internally to the D-coupled ^{13}C resonances of the NMR solvent. Elemental analyses were carried out at London Metropolitan University. Complexes **49**, **50** and **52** and the $(C^{\wedge}N^{Pz^{\wedge}}C)Au-Cl$ starting material, **37**, were synthesized following reported procedures.^{98, 106, 107}

3.51 Synthesis of complex **51**



A mixture of 2-(4-*t*-butyl)phenyl pyridine gold dichloride, (**49**), (0.200 g, 0.418 mmol), 2-acetamidophenol (0.100 g, 0.661 mmol) and aqueous trimethylamine (2 mL) was refluxed in methanol (30 mL) for 30 min. The reaction was then cooled and water (40 mL) was added causing an immediate orange precipitation. The flask was then placed in the freezer for two days. The orange solid was filtered and purified by dissolving in minimal dichloromethane (2 mL) and precipitating the product with an excess of light petroleum (bp. 40-60 °C) (20 mL). This was filtered and dried under vacuum (0.181 g, 0.325 mmol, 78%). Anal. Calcd. for $C_{23}H_{23}AuN_4O_2 \cdot 2H_2O$ (592.45): C, 46.63; H, 4.59; N, 4.73. Found: C, 46.23; H 4.21; N 4.76. 1H NMR (CD_2Cl_2 , 300 MHz, 298 K): 8.97 (d, $^3J_{H-H} = 5.1$ Hz, 1H, H²), 8.07 (t, $^3J_{H-H} = 8.1$ Hz, 1H, H⁴), 7.83 (d, $^3J_{H-H} = 8.1$ Hz, 1H, H⁵), 7.75 (d, $^4J_{H-H} = 1.5$ Hz, 1H, H¹¹), 7.51-7.40 (m, 2H, H³⁺⁸), 7.37 (dd, $^3J_{H-H} = 8.3$ Hz, $^4J_{H-H} = 1.5$ Hz, 1H, H⁹), 7.22 (dd, $^3J_{H-H} = 7.7$ Hz, $^4J_{H-H} = 1.3$ Hz, 1H, H^{14/17}), 6.84 (m, 1H, H^{15/16}), 6.66 (dd, $^3J_{H-H} = 7.7$ Hz, $^4J_{H-H} = 1.3$ Hz, 1H, H^{14/17}), 6.49 (m, 1H, H^{15/16}), 2.32 (s, 3H, H²⁰), 1.35 (s, 9H, ^tBu). $^{13}C[^1H]$ NMR (CD_2Cl_2 , 75 MHz): 173.7 (s, C¹⁹), 164.2 (s, C¹²), 161.3 (s,

$C^{6/7}$, 155.5 (s, $C^{6/7}$), 147.0 (s, C^2), 144.7 (s, C^{10}), 144.3 (s, $C^{13/18}$), 142.7 (s, C^4), 139.4 (s, $C^{13/18}$), 133.0 (s, C^{11}), 125.4 (s, C^3), 124.8 (s, C^8), 124.2 (s, C^9), 123.8 (s, $C^{14/17}$), 123.4 (s, $C^{14/17}$), 120.2 (s, C^5), 115.6 (s, $C^{15/16}$), 115.3 (s, $C^{15/16}$), 35.3 (s, $C(CH_3)_3$), 30.8 (s, $C(CH_3)_3$), 25.2 (s, C^{20}).

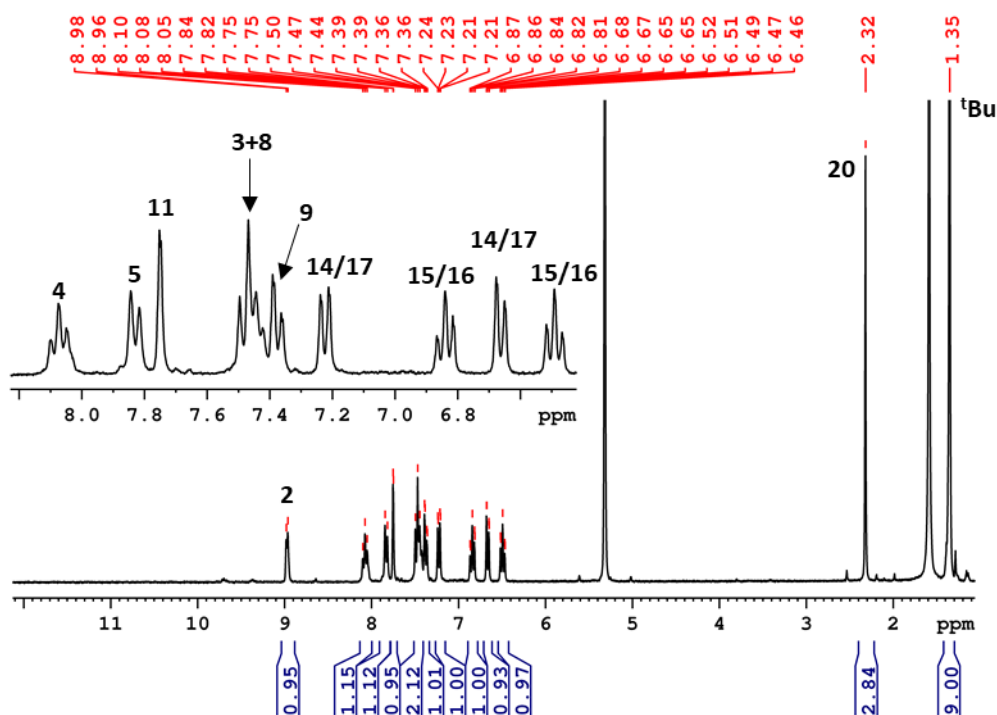


Figure 3.51a – 1H NMR of complex **51** in CD_2Cl_2 .

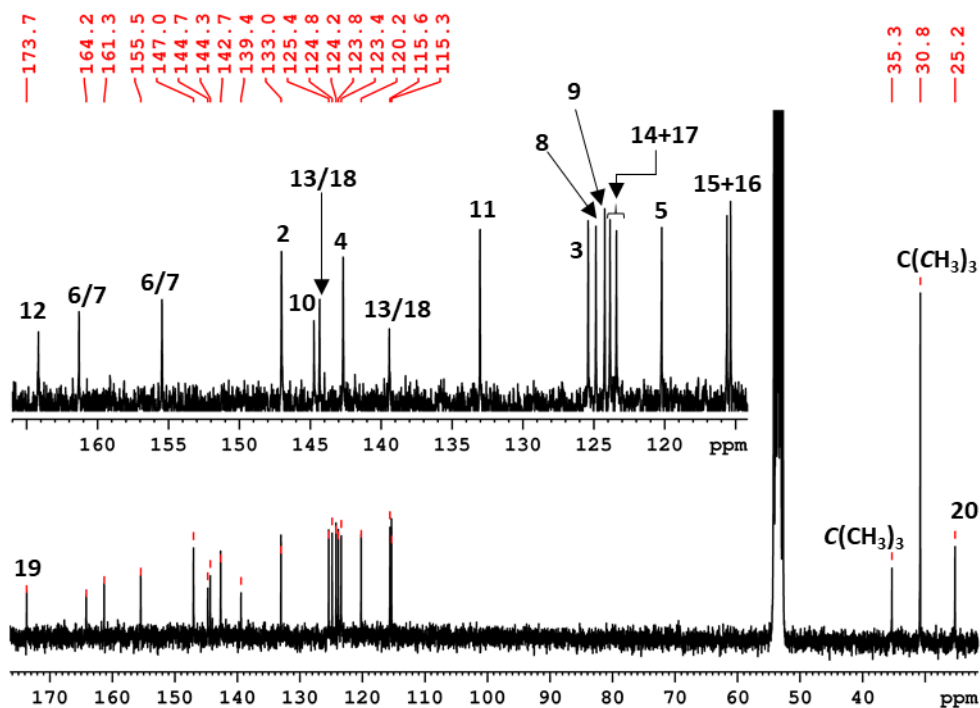
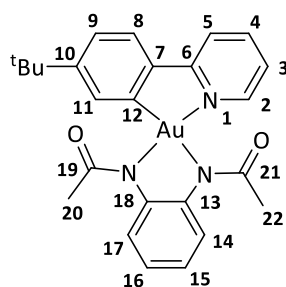


Figure 3.51b – $^{13}C[^1H]$ NMR of complex **51** in CD_2Cl_2 .

3.52 Synthesis of complex **53**

A mixture of 2-(4-*t*-butyl)phenyl pyridine gold dichloride, (**50**) (0.200 g, 0.418 mmol), 1,2-diacetamidobenzene (0.081 g, 0.421 mmol) and silver^I oxide (200 mg, 0.863 mmol) was added to dichloromethane (30 mL) and refluxed for 24 h. The mixture was then cooled, filtered through celite and the filtrate was concentrated under vacuum. A large excess of diethyl ether (20 mL) was added to precipitate the product as a pale-yellow, fluffy, solid. This was filtered and dried under vacuum (0.224 g, 0.375 mmol, 89%). Anal. Calcd. for C₂₅H₂₆AuN₃O₂ (597.47): C, 50.26; H, 4.39; N, 7.03. Found: C, 50.12; H 4.38; N 6.97. ¹H NMR (CD₂Cl₂, 300 MHz, 298 K): 9.30 (s, 1H, H²), 8.02 (t, ³J_{H-H} = 7.8 Hz, 1H, H⁴), 7.79 (d, ³J_{H-H} = 7.8 Hz, 1H, H⁵), 7.55 (d, ⁴J_{H-H} = 1.4 Hz, 1H, H¹¹), 7.48 (d, ³J_{H-H} = 8.0 Hz, 1H, H⁸), 7.41-7.28 (m, 3H, H^{9+3+14/17}), 7.09 (m, 1H, H^{14/17}), 6.99 (dt, ³J_{H-H} = 7.3 Hz, ⁴J_{H-H} = 1.4 Hz, 1H, H^{15/16}), 6.91 (dt, ³J_{H-H} = 7.3 Hz, ⁴J_{H-H} = 1.4 Hz, 1H, H^{15/16}), 2.27 (s, 3H, H^{20/22}), 2.15 (s, 3H, H^{20/22}), 1.34 (s, 9H, ^tBu). ¹³C[¹H] NMR (CD₂Cl₂, 75 MHz): 174.1 (s, C^{19/21}), 173.1 (s, C^{19/21}), 164.6 (s, C¹²), 154.8 (s, C²), 153.3 (s, C^{6/7}), 145.5 (s, C¹⁰), 142.2 (s, C⁴), 140.5 (s, C^{13/18}), 130.8 (s, C¹¹), 125.2 (s, C^{3/9}), 124.6 (s, C^{15/16}), 124.2 (s, C⁸), 124.0 (s, C^{14/17}), 123.0 (s, C^{3/9}), 122.7 (s, C^{15/16}), 119.7 (s, C⁵), 35.3 (s, C(CH₃)₃), 30.8 (s, C(CH₃)₃).

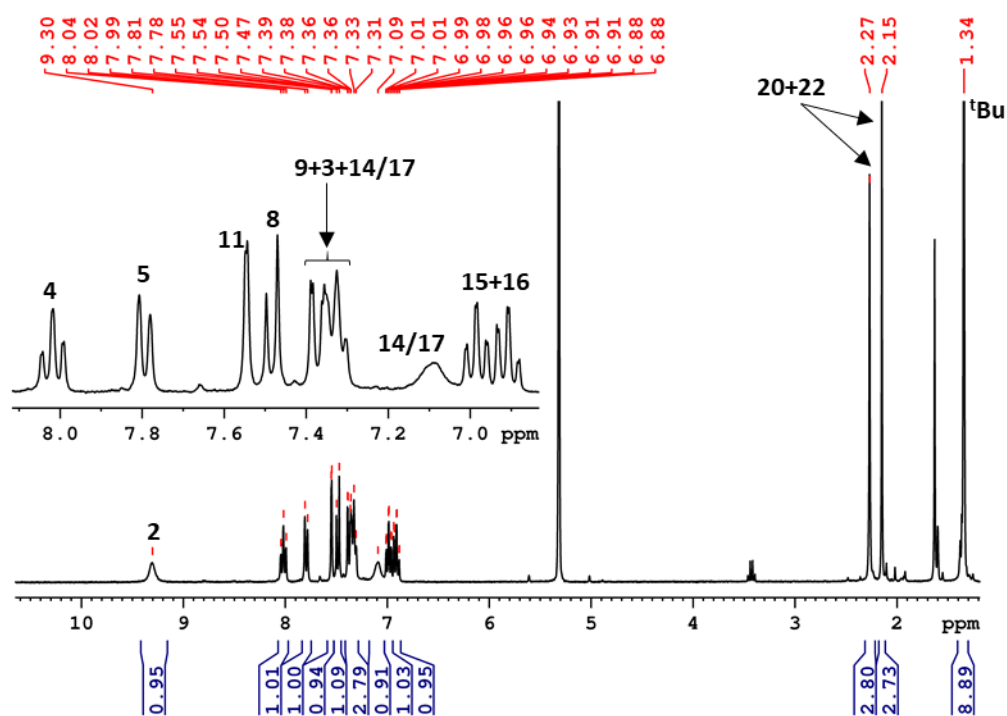


Figure 3.52a – ^1H NMR of complex **53** in CD_2Cl_2 .

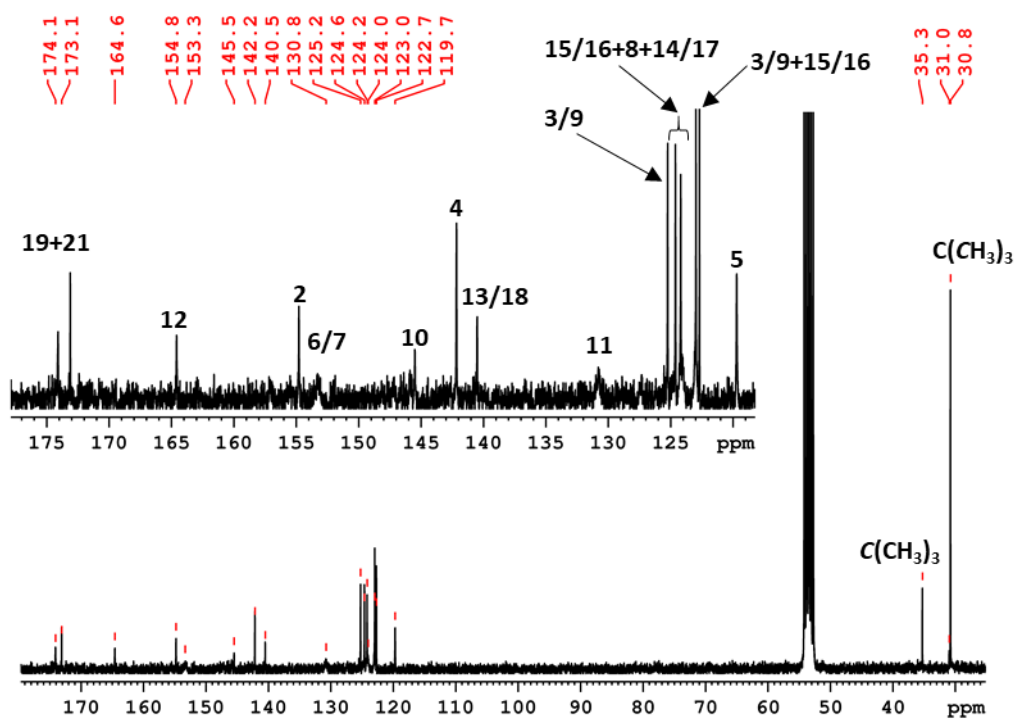


Figure 3.52b – ^{13}C NMR of complex **53** in CD_2Cl_2 .

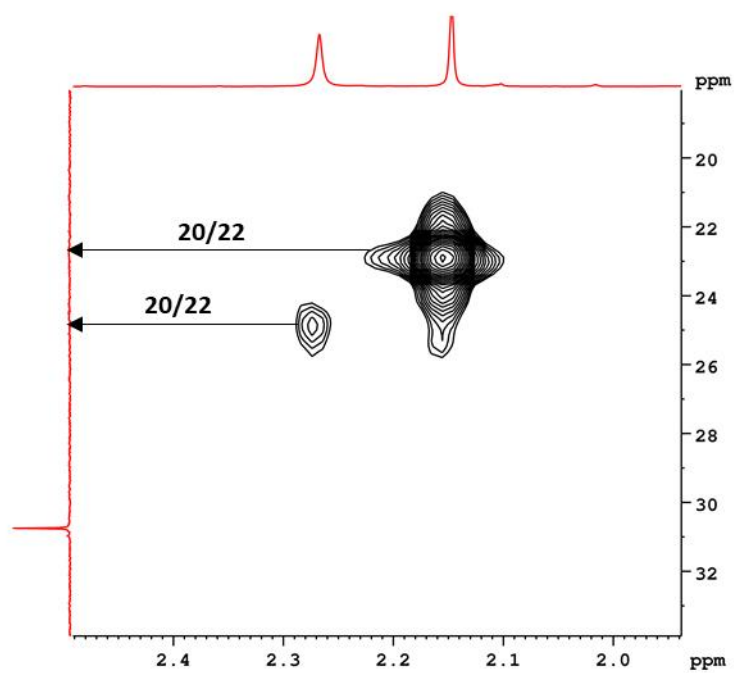
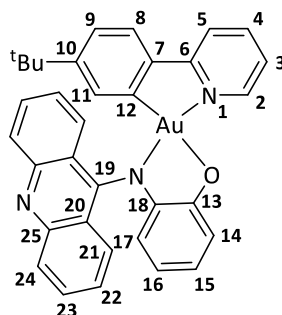


Figure 3.52c – HMQC spectrum of complex **53** in CD_2Cl_2 showing C^{20+22} .

3.53 Synthesis of complex **54**

A mixture of 2-(4-*t*-butyl)phenyl pyridine gold dichloride, (**49**), (0.235 g, 0.491 mmol), ligand **L1** (0.300 g, 1.048 mmol) and aqueous trimethylamine (2 mL) was refluxed in methanol (30 mL) for 30 min. The reaction was then cooled and water (40 mL) was added causing an immediate dark brown precipitation. The flask was placed in the freezer for two days. The brown solid was filtered off and purified by dissolving in dichloromethane (2 mL), followed by precipitation with an excess of light petroleum (bp. 40-60 °C) (20 mL). This product was filtered off and dried under vacuum (0.273 g, 0.394 mmol, 80%). Anal. Calcd. for C₃₄H₂₈AuN₃O (691.19): C, 59.05; H, 4.08; N, 6.08. Found: C, 58.84; H 4.13; N 6.02. ¹H NMR (CD₂Cl₂, 300 MHz, 298 K): 9.61 (dd, ³J_{H-H} = 5.9 Hz, ⁴J_{H-H} = 1.0 Hz, 1H, H²), 8.49 (dd, ³J_{H-H} = 8.7 Hz, ⁴J_{H-H} = 0.7 Hz, 2H, H^{21/24}), 8.30 (d, ³J_{H-H} = 8.7 Hz, 2H, H^{21/24}), 8.08 (dt, ³J_{H-H} = 8.1 Hz, ⁴J_{H-H} = 1.0 Hz, 1H, H⁴), 7.82 (d, ³J_{H-H} = 8.1 Hz, 1H, H⁵), 7.75 (m, 2H, H^{22/23}), 7.54 (m, 1H, H³), 7.48-7.36 (m, 3H, H^{8+22/23}), 7.01 (dd, ³J_{H-H} = 8.2 Hz, ⁴J_{H-H} = 1.7 Hz, 1H, H⁹), 6.85 (dd, ³J_{H-H} = 7.7 Hz, ⁴J_{H-H} = 1.2 Hz, 1H, H^{14/17}), 6.48 (dt, ³J_{H-H} = 7.7 Hz, ⁴J_{H-H} = 1.2 Hz, 1H, H^{15/16}), 6.12 (dt, ³J_{H-H} = 7.7 Hz, ⁴J_{H-H} = 1.2 Hz, 1H, H^{15/16}), 5.39 (dd, ³J_{H-H} = 7.7 Hz, ⁴J_{H-H} = 1.2 Hz, 1H, H^{14/17}), 5.23 (d, ⁴J_{H-H} = 1.7 Hz, 1H, H¹¹), 0.35 (s, 9H, ^tBu). ¹³C[¹H] NMR (CD₂Cl₂, 75 MHz): 163.3 (s, C²), 156.1 (s, C¹²), 155.2 (s, C^{6/7}), 153.3 (s, C^{6/7}), 151.0 (s, C¹⁹), 150.9 (s, C²⁰), 147.5 (s, C¹⁰), 142.5 (s, C^{13/18}), 141.9 (s, C⁴), 140.2 (s, C^{13/18}), 130.3 (s, C²¹), 130.2 (s, C²²), 127.4 (s, C⁹), 126.2 (s, C²³), 125.4 (s, C⁸), 124.5 (s, C²⁵), 124.3 (s, C²⁴), 124.0 (s, C¹¹), 123.5 (s, C³), 120.2 (s, C⁵), 118.4 (s, C^{15/16}), 117.0 (s, C^{15/16}), 115.1 (s, C^{14/17}), 113.7 (s, C^{14/17}), 34.4 (s, C(CH₃)₃), 29.9 (s, C(CH₃)₃).

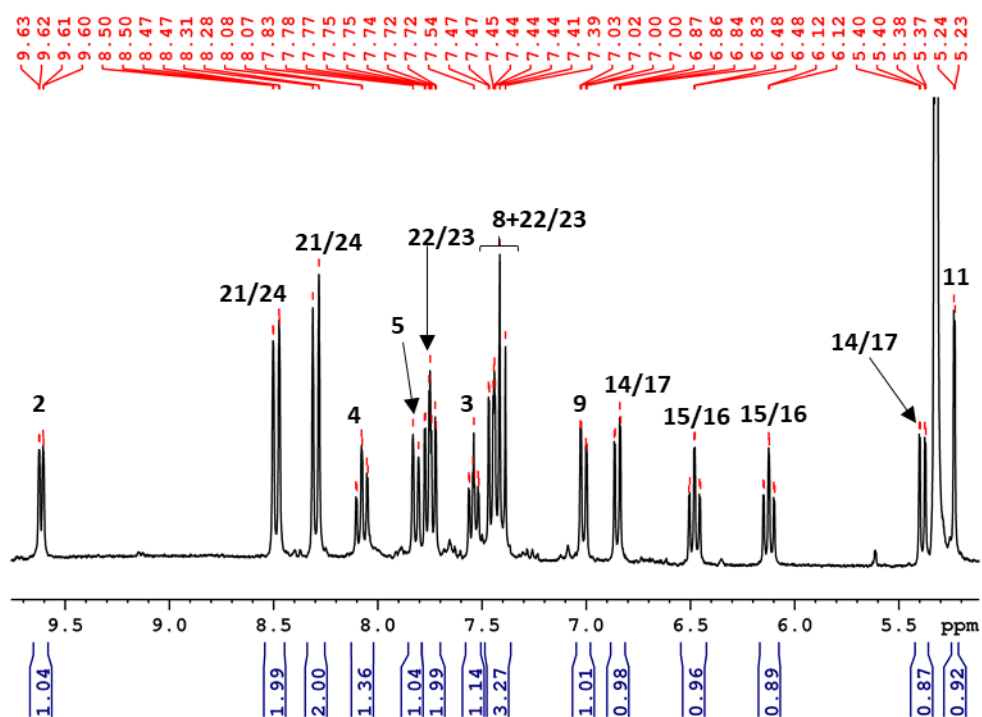


Figure 3.53a – ^1H NMR of complex **54** in CD_2Cl_2 (*tert*-Bu singlet at 0.35 ppm not shown).

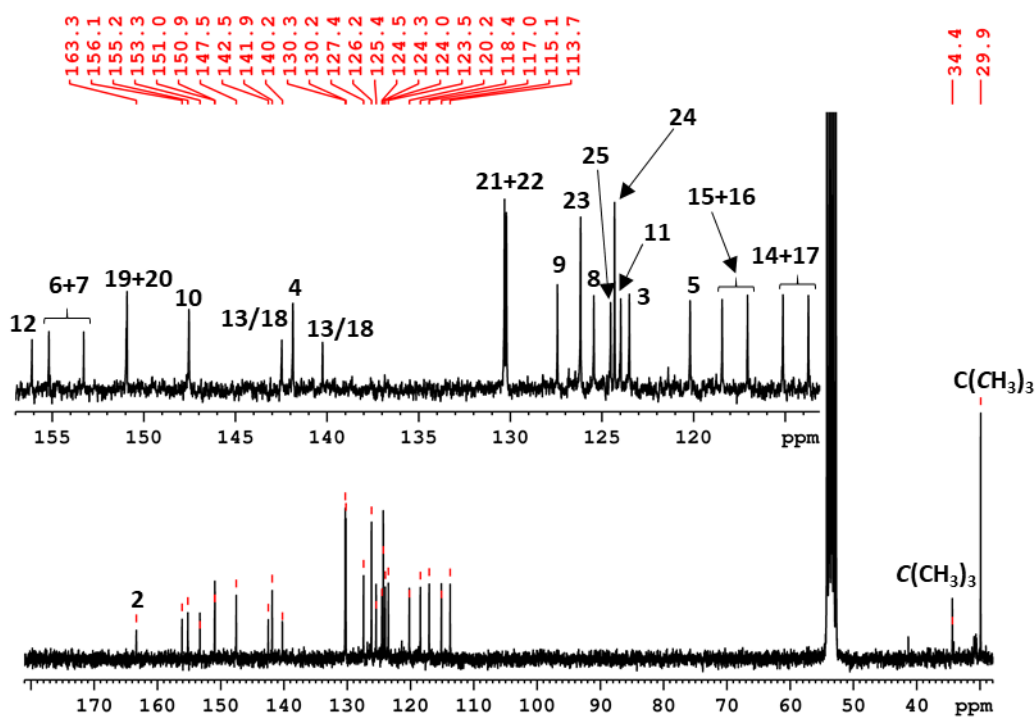
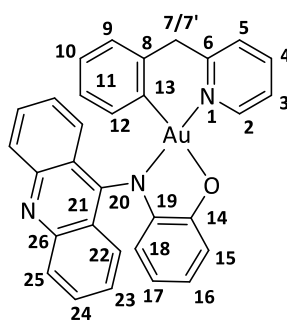


Figure 3.53b – ^{13}C [^1H] NMR of complex **54** in CD_2Cl_2 .

3.54 Synthesis of complex **55**

A mixture of 2-benzylpyridine gold dichloride, (**50**), (0.200 g, 0.459 mmol), ligand **L1** (0.178 g, 0.622 mmol) and aqueous trimethylamine (2 mL) was refluxed in methanol (30 mL) for 30 min. The reaction was then cooled and water (40 mL) was added causing an immediate dark brown precipitation. The flask was then placed in the freezer for two days. The brown solid was then filtered and purified by dissolving in minimal dichloromethane and acetone (3 mL). The product was precipitated with an excess of light petroleum (bp. 40-60 °C) (20 mL), filtered off and dried under vacuum (0.201 g, 0.309 mmol, 67%). Anal. Calcd. for $C_{31}H_{22}AuN_3O \cdot 0.5H_2O$ (739.58): C, 50.35; H, 4.36; N, 5.68. Found: C, 50.63; H 3.36; N 7.45. 1H NMR (CD_2Cl_2 , 300 MHz, 263 K): 9.23 (d, $^3J_{H-H} = 5.6$ Hz, 1H, H²), 8.51 (d, $^3J_{H-H} = 8.6$ Hz, 1H, H^{22/25}), 8.46 (d, $^3J_{H-H} = 8.6$ Hz, 1H, H^{22/25}), 8.21 (d, $^3J_{H-H} = 8.6$ Hz, 1H, H^{22/25}), 8.03 (dt, $^3J_{H-H} = 7.7$ Hz, $^4J_{H-H} = 1.4$ Hz, 1H, H⁴), 7.95 (d, $^3J_{H-H} = 8.6$ Hz, 1H, H^{22/25}), 7.80 (m, 1H, H^{23/24}), 7.67 (d, $^3J_{H-H} = 7.7$ Hz, 1H, H⁵), 7.62-7.46 (m, 3H, H^{3+23/24}), 7.25 (t, $^3J_{H-H} = 8.6$ Hz, 1H, H^{23/24}), 6.78-6.71 (m, 2H, H^{15/18+9/12}), 6.55 (t, $^3J_{H-H} = 7.4$ Hz, 1H, H^{16/17}), 6.47 (t, $^3J_{H-H} = 7.4$ Hz, 1H, H^{10/11}), 6.16 (t, $^3J_{H-H} = 7.4$ Hz, 1H, H^{16/17}), 5.99-5.84 (m, 2H, H^{9/12+10/11}), 5.69 (dd, $^3J_{H-H} = 7.4$ Hz, $^4J_{H-H} = 1.0$ Hz, 1H, H^{15/18}), 4.43 (d, $^2J_{H-H} = 15.3$ Hz, 1H, H^{7/7'}), 3.91 (d, $^2J_{H-H} = 15.3$ Hz, 1H, H^{7/7'}). ^{13}C [1H] NMR (CD_2Cl_2 , 75 MHz): 157.2 (s, C¹³), 157.1 (s, C^{6/8}), 151.7 (s, C^{6/8}), 151.5 (s, C^{14/19}), 150.7 (s, C²), 141.7 (s, C⁴), 138.5 (s, C^{14/19}), 132.3 (s, C^{20/21/26}), 130.2 (s, C^{22/25}), 130.1 (s, C^{9/12}), 129.8 (s, C^{22/25}), 129.5 (s, C^{23/24}), 126.4 (s, C^{9/12}), 126.4 (s, C^{10/11}), 126.4 (s, C^{10/11}), 126.1 (s, C⁵), 125.6 (s, C^{23/24}), 124.7 (s, C³), 118.3 (s, C^{16/17}), 116.7 (s, C^{16/17}), 115.4 (s, C^{15/18}), 113.4 (s, C^{15/18}), 47.8 (s, C^{7/7'}).

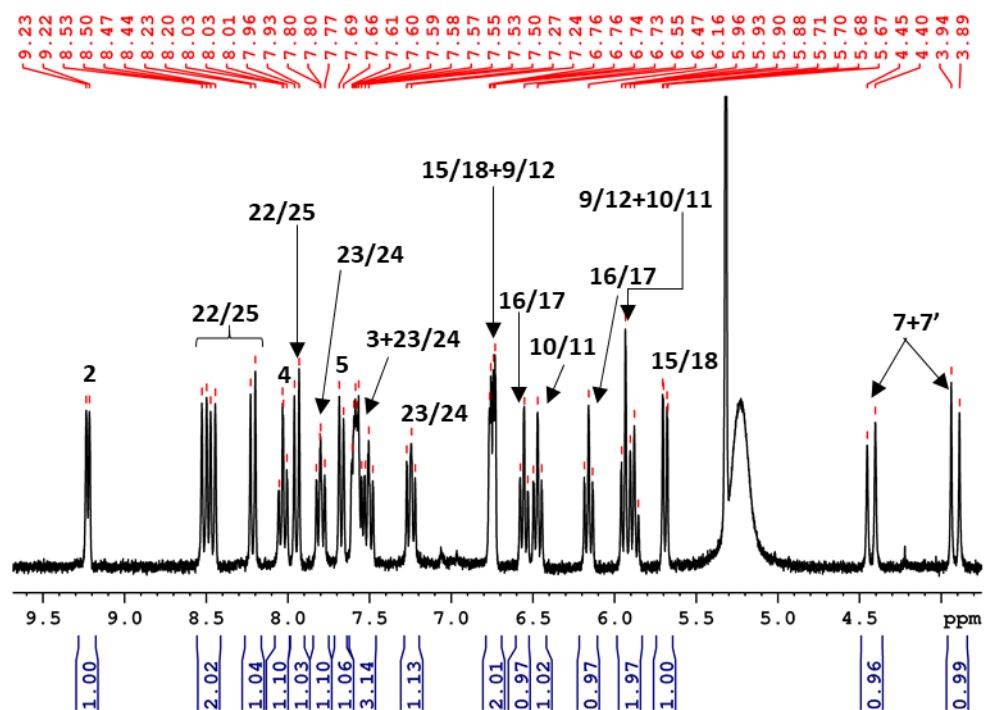


Figure 3.54a – ^1H NMR of complex **55** in CD_2Cl_2 .

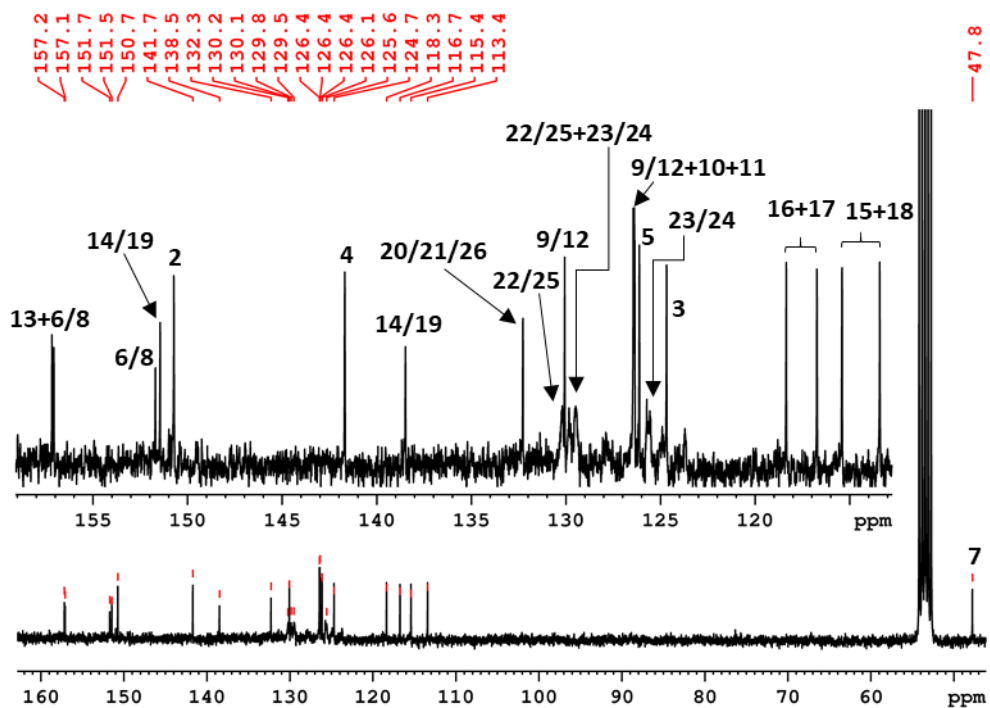
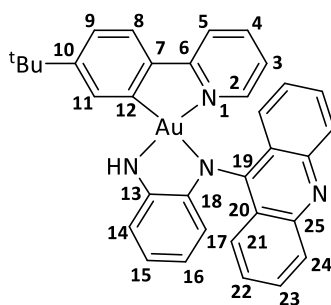


Figure 3.54b – ^{13}C [^1H] NMR of complex **55** in CD_2Cl_2 .

3.55 Synthesis of complex **56**

A mixture of 2-(4-*t*-butyl)phenyl pyridine gold dichloride, (**49**), (0.200 g, 0.418 mmol), ligand **L2** (0.177 g, 0.620 mmol) and aqueous trimethylamine (2 mL) was refluxed in methanol (30 mL) for 30 min. The reaction was then cooled and water (40 mL) was added causing an immediate light brown precipitation. The flask was then placed in the freezer for two days. The brown solid was then filtered and purified by dissolving in minimal dichloromethane (2 mL). The product was precipitated with an excess of light petroleum (bp. 40-60 °C) (20 mL), filtered off and dried under vacuum (0.214 g, 0.310 mmol, 74%). Anal. Calcd. for $C_{34}H_{29}AuN_4 \cdot 3H_2O$ (744.65): C, 54.84; H, 4.74; N, 7.52. Found: C, 54.25; H, 4.20; N, 7.41. 1H NMR (CD_2Cl_2 , 300 MHz, 298 K): 8.40 (dd, $^3J_{H-H} = 8.7$ Hz, $^4J_{H-H} = 0.7$ Hz, 2H, $H^{21/24}$), 8.24 (d, $^3J_{H-H} = 8.7$ Hz, 2H, $H^{21/24}$), 7.78-7.68 (m, 4H, $H^{22/23+2+4/5}$), 7.64-7.55 (m, 2H, $H^{3+4/5}$), 7.41 (dd, $^3J_{H-H} = 8.2$ Hz, $^4J_{H-H} = 1.7$ Hz, 1H, H^9), 7.35 (m, 2H, $H^{22/23}$), 6.97 (dd, $^3J_{H-H} = 7.7$ Hz, $^4J_{H-H} = 1.1$ Hz, 1H, $H^{14/17}$), 6.44 (t, $^3J_{H-H} = 7.7$ Hz, 1H, $H^{15/16}$), 6.36-6.18 (m, 3H, $H^{8+11+15/16}$), 5.62 (dd, $^3J_{H-H} = 7.7$ Hz, $^4J_{H-H} = 1.1$ Hz, 1H, $H^{14/17}$), 1.46 (s, 9H, tBu). $^{13}C[^1H]$ NMR (CD_2Cl_2 , 75 MHz): 164.6 (s, C^2), 155.3 (s, C^{12}), 154.5 (s, $C^{6/7}$), 150.5 (s, $C^{6/7}$), 149.6 (s, C^{19}), 148.0 (s, C^{20}), 145.6 (s, C^{10}), 145.0 (s, $C^{13/18}$), 140.4 (s, C^4), 139.7 (s, $C^{13/18}$), 130.2 (s, $C^{21/24}$), 130.0 (s, $C^{21/24}$), 126.5 (s, C^{25}), 126.0 (s, C^9), 125.5 (s, $C^{22/23}$), 124.9 (s, C^8), 124.8 (s, $C^{22/23}$), 124.6 (s, C^{11}), 122.3 (s, C^3), 120.1 (s, C^5), 118.2 (s, $C^{15/16}$), 116.3 (s, $C^{15/16}$), 113.3 (s, $C^{14/17}$), 112.6 (s, $C^{14/17}$), 35.6 (s, $C(CH_3)_3$), 31.0 (s, $C(CH_3)_3$).

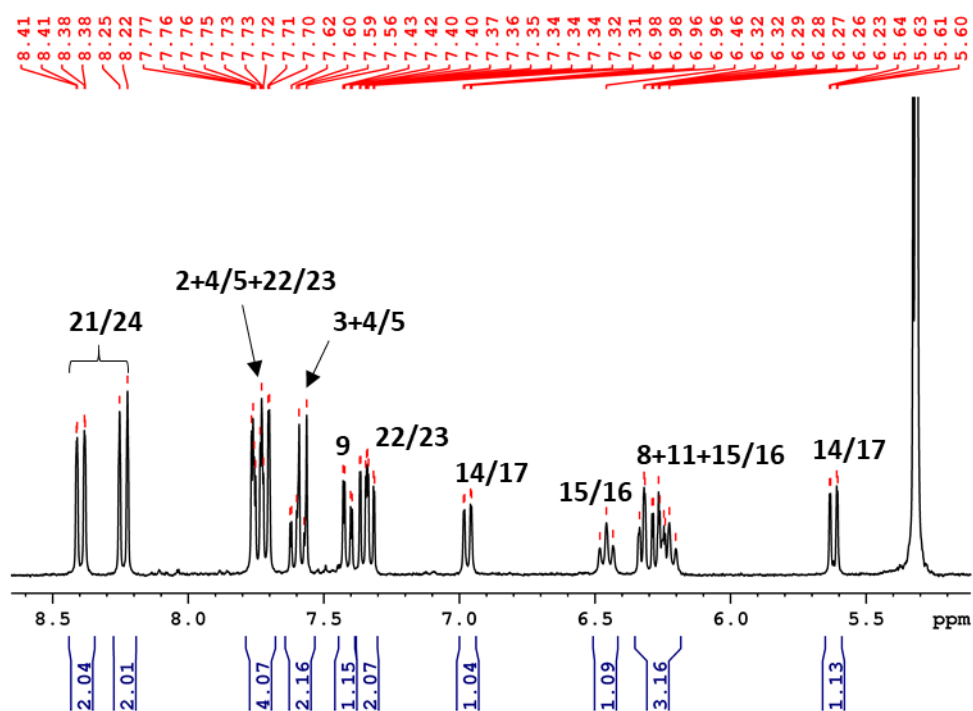


Figure 3.55a – ^1H NMR of complex **56** in CD_2Cl_2 (*tert*-Bu singlet at 1.46 ppm not shown).

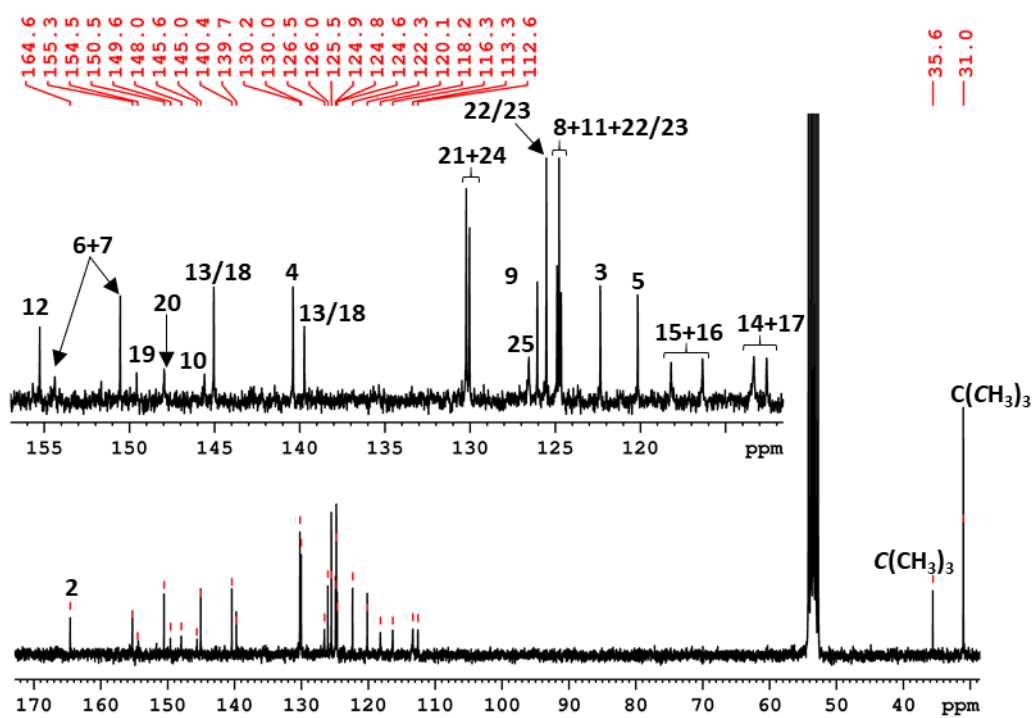
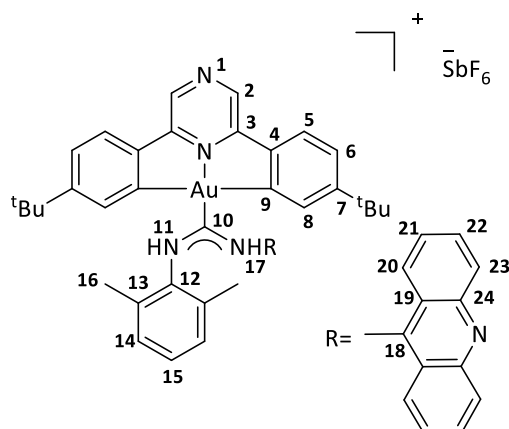


Figure 3.55b – ^{13}C [^1H] NMR of complex **56** in CD_2Cl_2 .

3.56 Synthesis of complex **57**

A mixture of $(C^{\wedge}N^{p^z\wedge}C)AuCl$, (**37**), (0.060 g, 0.104 mmol), 2,6-dimethylphenyl isocyanide (0.016 g, 0.125 mmol), $AgSbF_6$ (0.043 g, 0.125 mmol) and a few pellets of 4 Å molecular sieves were combined in a flame-dried Schlenk flask under a nitrogen atmosphere with dry dichloromethane (15 mL). The mixture was left to stir at room temperature for 4 h. A white precipitate of $AgCl$ was removed by filtration through celite, and the filtrate collected under an N_2 atmosphere. The solvent was evaporated to a minimum and the product was precipitated with an excess of light petroleum (bp. 40-60 °C). The supernatant was removed and the residue dried under vacuum to yield a yellow solid. 9-amino acridine (0.028 g, 0.146 mmol) was added to a flame-dried Schlenk flask. The solution was sonicated for 30 min and transferred to a separate flame-dried Schlenk flask containing the $[(C^{\wedge}N^{p^z\wedge}C)Au(2,6\text{-dimethylphenyl isocyanide})]SbF_6$. The reaction was then stirred for 16 h at room temperature and the precipitate removed from solution via filtration through a celite plug. Next, the solvent was removed under vacuum and the solid residue re-dissolved in dichloromethane (2 mL). The product was precipitated using a 2:1 mixture of light petroleum (bp. 40-60 °C) / diethyl ether (5 mL), and after removing the solvent, dried under vacuum to yield a dark yellow solid. Proton NMR showed a mixture of the desired product and the formamide hydrolysis product. The solid was washed twice with dry dichloromethane (40 mL) followed by petroleum ether (10 mL) and dried under vacuum (0.053 g, 0.048 mmol, 46%). Anal. Calcd. for $C_{46}H_{45}AuF_6N_5Sb$ (1100.62): C, 50.20; H, 4.12; N, 6.36. Found: C, 49.97; H 4.03; N 6.35. 1H NMR ($(CD_3)_2SO$, 300 MHz, 298 K): 10.34 (s, 1H, NH), 9.14 (s, 2H, H²), 8.26 (d, $^3J_{H-H} = 8.2$ Hz, 2H, H^{20/23}), 7.96 (d, $^4J_{H-H} = 1.5$ Hz, 2H, H⁸), 7.85 (d, $^3J_{H-H} = 8.4$ Hz, 2H, H⁵), 7.74-7.57 (m, 4H, H^{20/23+21/22}), 7.30 (dd, $^3J_{H-H} = 8.4$ Hz, $^4J_{H-H} = 1.5$ Hz, 2H, H⁶), 7.25-7.14 (m, 3H, H¹⁴⁺¹⁵), 6.96 (t, 2H, $^3J_{H-H} = 7.5$ Hz, 2H, H^{21/22}), 2.56 (s, 6H, H¹⁶), 1.20 (s, 18H, ^tBu). $^{13}C[^1H]$ NMR (CD_3CN , 75 MHz): 167.6 (s, C⁹), 156.0 (s, C⁴), 155.6 (s, C³), 144.7 (s, C⁷), 139.9 (s, C²), 139.6 (s, C¹³), 135.1 (s, C⁸),

134.0 (s, $C^{20/23}$), 128.6 (s, C^{15}), 127.7 (s, C^{14}), 127.6 (s, $C^{20/23}$), 127.6 (s, C^{12}), 127.0 (s, C^5), 124.5 (s, C^6), 123.6 (s, $C^{21/22}$), 123.5 (s, $C^{21/22}$), 117.8 (s, C^{18}), 117.8 (s, C^{19}), 117.8 (s, C^{24}), 35.7 (s, $C(CH_3)_3$), 31.4 (s, $C(CH_3)_3$), 19.3 (s, C^{16}). ν_{max} (neat)/ cm^{-1} : 3388 (NH), 3270 (NH) 2957 (tBu), 2867 (Ar), 1586 (carbene).

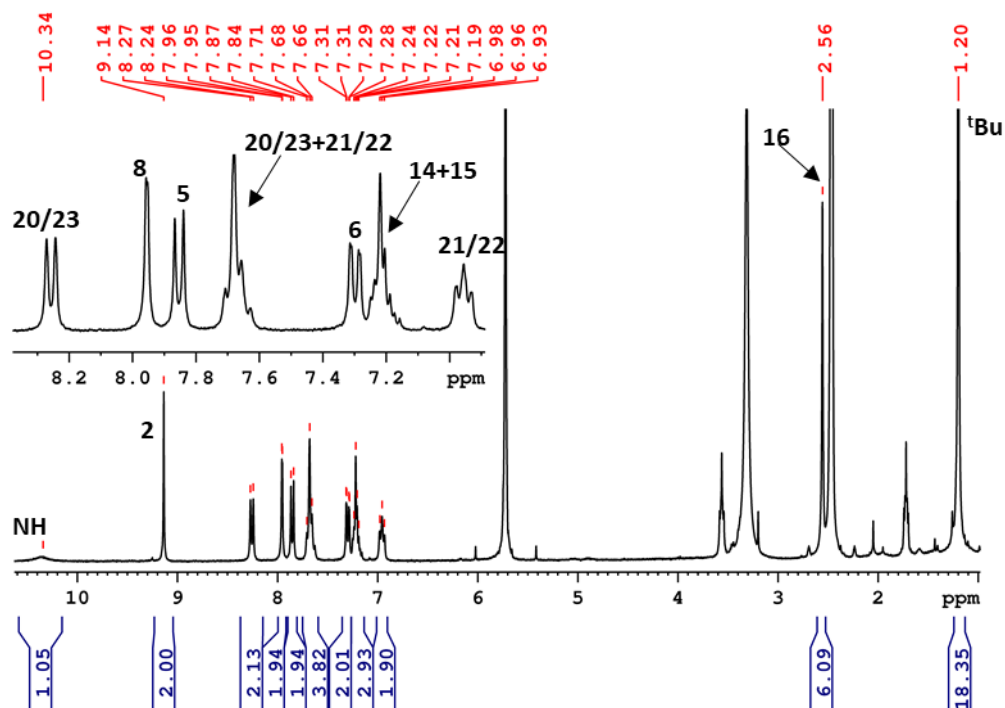


Figure 3.56a – 1H NMR of complex **57** in $(CD_3)_2SO$.

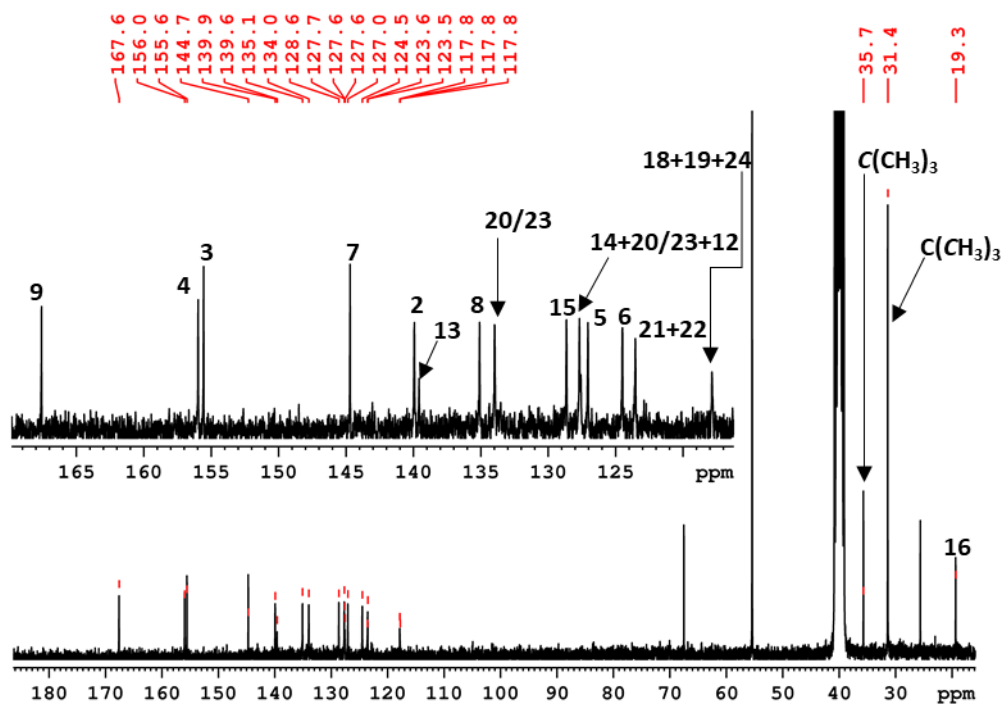
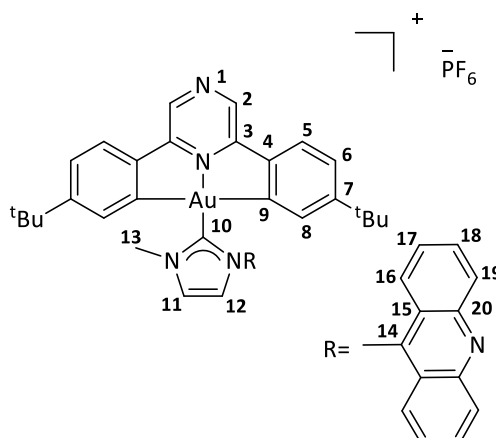


Figure 3.56b – ^{13}C NMR of complex **57** in $(CD_3)_2SO$.

3.57 Synthesis of complex **58**

[(MelmAcr)H]Cl (0.070 g, 0.232 mmol) and silver oxide (0.043 g, 0.186 mmol) and acetonitrile (15 mL) were combined in a Schlenk and stirred for 56 h. (C^NPz^C)AuCl, (**37**), (0.133 g, 0.232 mmol) and KPF₆ (0.128 g, 0.695 mmol) were then added to the flask and the reaction was stirred for a further 16 h before being filtered through a celite plug. The filtrate was concentrated under vacuum and the product was precipitated using a 2:1 mixture of light petroleum (bp. 40-60 °C) / diethyl ether (5 mL), and after removing the solvent, dried under vacuum to yield a dark yellow solid (0.170 g, 0.180 mmol, 78%). Anal. Calcd. for C₄₁H₃₉AuF₆N₅P.5MeCN (1148.99): C, 53.31; H, 4.74; N, 12.19. Found: C, 52.92; H, 5.10; N, 11.80. ¹H NMR (CD₃CN, 300 MHz, 298 K): 8.68 (s, 2H, H²), 8.12-8.02 (m, 3H, H¹¹⁺¹⁹), 7.96 (d, 1H, ³J_{H-H} = 1.9 Hz, H¹²), 7.88-7.77 (m, 4H, H¹⁶⁺¹⁸), 7.55 (d, 2H, ³J_{H-H} = 8.3 Hz, H⁵), 7.45 (t, 2H, ³J_{H-H} = 7.8 Hz, H¹⁷), 7.33 (dd, 2H, ³J_{H-H} = 8.3 Hz, ⁴J_{H-H} = 1.7 Hz, H⁶), 7.21 (d, 2H, ⁴J_{H-H} = 1.7 Hz, H⁸), 4.15 (s, 3H, H¹³), 1.30 (s, 18H, ^tBu). ¹³C[¹H] NMR (CD₃CN, 75 MHz): 166.1 (s, C⁹), 156.8 (s, C⁴), 156.3 (s, C³), 154.9 (s, C¹⁰), 146.6 (s, C²⁰), 144.6 (s, C⁷), 140.5 (s, C¹⁴), 139.3 (s, C²), 133.3 (s, C¹⁸), 133.0 (s, C⁸), 128.9 (s, C¹⁷), 127.0 (s, C¹²), 126.9 (s, C¹⁹), 126.7 (s, C⁵), 126.3 (s, C¹¹), 125.2 (s, C⁶), 123.5 (s, C¹⁶), 122.2 (s, C¹⁵), 39.1 (s, C¹³), 35.1 (s, C(CH₃)₃), 30.3 (s, C(CH₃)₃).

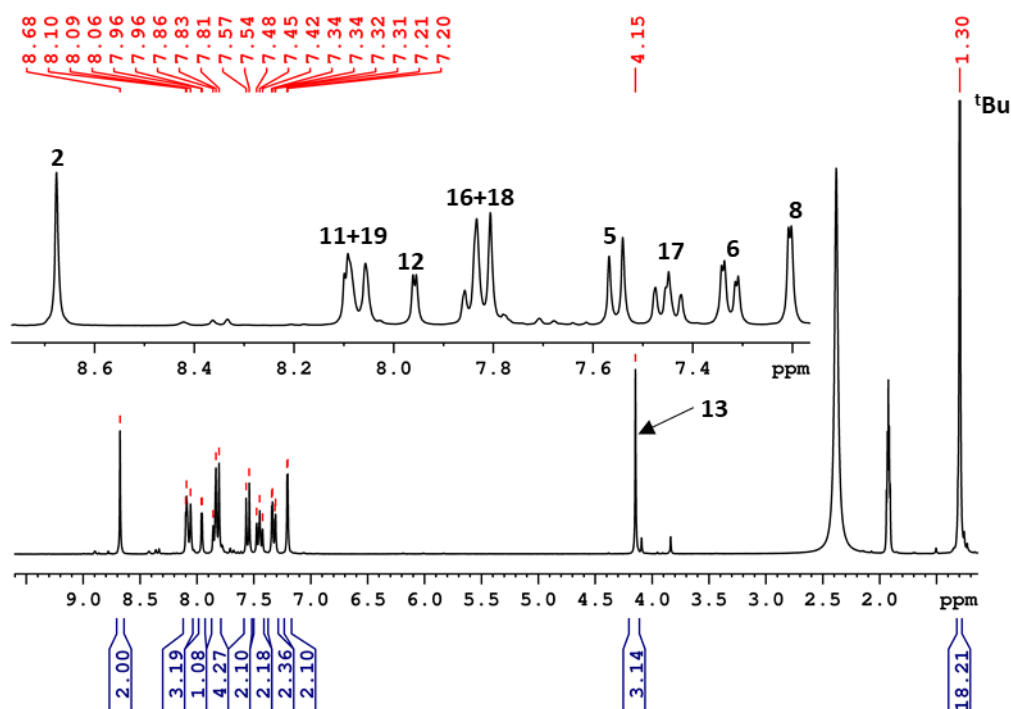


Figure 3.57a – ^1H NMR of complex **58** in CD_3CN .

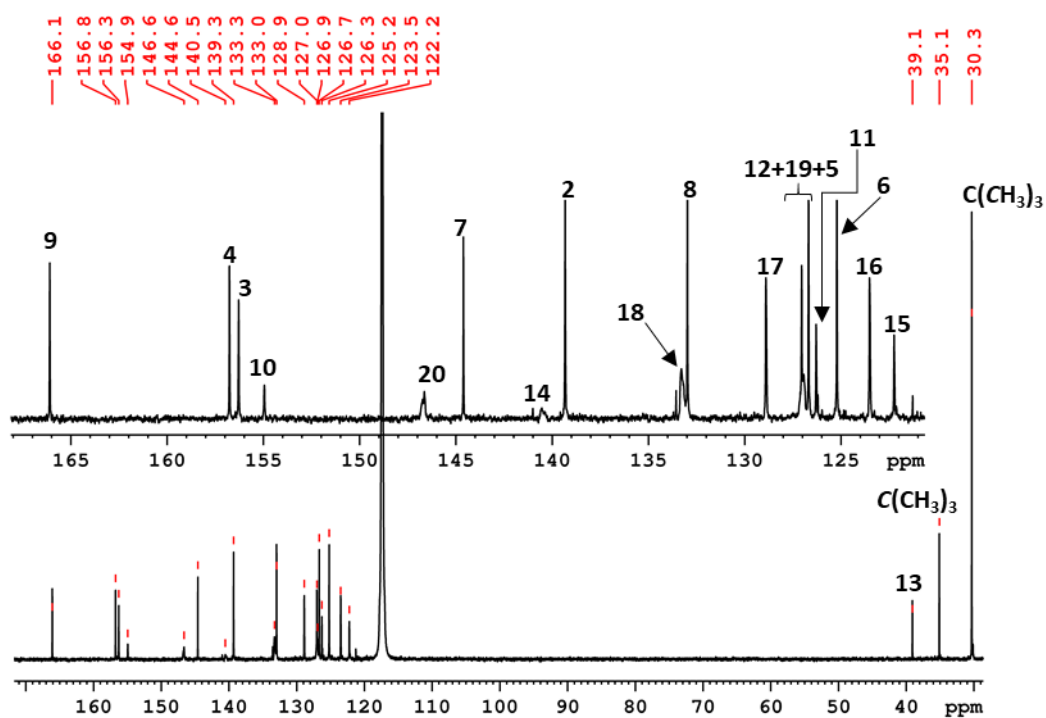
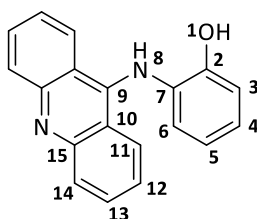


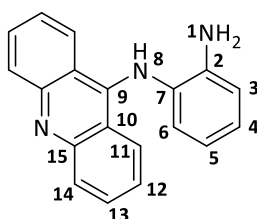
Figure 3.57b – ^{13}C NMR of complex **58** in CD_3CN .

3.58 Synthesis of L1



4-(Acridin-9-ylamino)-benzoic acid (0.600 g, 2.100 mmol) and carbonyldiimidazol (0.341 g, 2.103 mmol) were placed in a flame dried flask, fitted with a condenser and stirred in dry tetrahydrofuran (20 mL) under a nitrogen atmosphere, for 15 min. 2-amino phenol (0.301 g, 2.758 mmol) was then added and the reaction was stirred for a further 15 min before being heated to reflux overnight. After cooling to room temperature, the orange solid was filtered and washed twice with light petroleum (bp. 40-60 °C) before being dried under vacuum (0.551 g, 1.925 mmol, 92%). $^1\text{H NMR}$ ($(\text{CD}_2)_2\text{SO}$, 300 MHz, 298 K): 10.18 (s, 1H, H⁸), 8.26 (d, $^3J_{\text{H-H}} = 8.8$ Hz, 1H, H^{3/6}), 8.18 (d, $^3J_{\text{H-H}} = 7.9$ Hz, 1H, H^{3/6}), 8.08-7.88 (m, 5H, H^{4/5+11+14}) 8.28-7.50 (m, 4H, H¹²⁺¹³), 7.03 (t, $^3J_{\text{H-H}} = 7.9$ Hz, 1H, H^{4/5}). $^{13}\text{C}[^1\text{H}] \text{NMR}$ ($(\text{CD}_2)_2\text{SO}$, 75 MHz): 156.8 (s, C^{2/7/9}), 152.9 (s, C^{2/7/9}), 140.5 (s, C^{2/7/9}), 136.1 (s, C^{11/14}), 131.9 (s, C^{4/5}), 130.5 (s, C^{10/15}), 128.1 (s, C^{3/6}), 128.0 (s, C^{12/13}), 125.9 (s, C^{3/6}), 124.6 (s, C^{12/13}), 121.0 (s, C^{10/15}), 119.9 (s, C^{11/14}), 117.8 (s, C^{4/5}), 114.1 (s, C⁹).

3.59 Synthesis of L2



4-(Acridin-9-ylamino)-benzoic acid (1.500 g, 4.772 mmol) and carbonyldiimidazol (0.774 g, 4.773 mmol) were placed in a flame dried flask, fitted with a condenser, and stirred in dry tetrahydrofuran (50 mL) under a nitrogen atmosphere for 15 min. *O*-phenylenediamine (0.675 g, 6.242 mmol) was then added and the reaction was stirred for a further 15 min before being heated to reflux overnight. After cooling to room temperature, the orange solid was filtered and washed twice with light petroleum (bp. 40-60 °C) before being dried under vacuum (1.102 g, 3.862 mmol, 81%). $^1\text{H NMR}$ ($(\text{CD}_2)_2\text{SO}$, 300 MHz, 298 K): 8.24 (d, $^3J_{\text{H-H}} = 8.1$ Hz, 2H, H^{11/14}), 8.02 (d, $^3J_{\text{H-H}} = 8.1$ Hz, 2H, H^{11/14}), 7.90 (t, $^3J_{\text{H-H}} = 8.1$ Hz, 2H, H^{12/13}), 7.33 (t, $^3J_{\text{H-H}} = 8.1$ Hz, 2H, H^{12/13}), 7.18 (t, $^3J_{\text{H-H}} = 7.7$ Hz, 1H, H^{4/5}), 7.05 (d, $^3J_{\text{H-H}} = 7.7$ Hz, 1H, H^{3/6}), 6.89 (d,

$^3J_{\text{H-H}} = 7.6$ Hz, 1H, H^{3/6}), 6.60 (t, $^3J_{\text{H-H}} = 7.6$ Hz, 1H, H^{4/5}). $^{13}\text{C}[^1\text{H}]$ NMR ((CD₂)SO, 75 MHz): 156.5 (s, C^{2/7/9}), 145.1 (s, C^{2/7/9}), 140.3 (s, C^{2/7/9}), 135.3 (s, C^{12/13}), 129.9 (s, C^{4/5}), 127.2 (s, C^{3/6}), 126.2 (s, C^{11/14}), 125.0 (s, C^{10/15}), 123.7 (s, C^{12/13}), 119.2 (s, C^{11/14}), 116.9 (s, C^{4/5}), 116.3 (s, C^{3/6}), 113.6 (s, C^{10/15}).

3.510 X-ray crystallography

Crystal structures were solved by Dr Julio Fernandez-Cestau.

3.511 Antiproliferation assay

The human A549 and HL60 cancer cell lines (from ECACC) were cultured in RPMI 1640 medium with 10% foetal calf serum, 2 mM L-glutamine, 100 U mL⁻¹ penicillin and 100 µg mL⁻¹ streptomycin (Invitrogen). The cells were maintained under a humidified atmosphere at 37 °C and 5% CO₂. The human MCF-7 cancer cell line (from ECACC) was cultured in DMEM medium with 10% foetal calf serum, 2 mM L-glutamine, 100 U mL⁻¹ penicillin and 100 µg mL⁻¹ streptomycin (Invitrogen). The cells were maintained under a humidified atmosphere at 37 °C and 5% CO₂. Inhibition of cancer cell proliferation was measured by the 3-(4,5-dimethylthiazol-2-yl)-5-(3-carboxymethoxyphenyl)-2-(4-sulfophenyl)-2H-tetrazolium (MTS) assay using the CellTiter 96 Aqueous One Solution Cell Proliferation Assay (Promega) and following the manufacturer's instructions. Briefly, the cells (3 × 10⁴ per 100 µL for HL60, 8 × 10³ per 100 µL for A549 and MCF-7) were seeded in 96-well plates and left untreated or treated with 1 µL of DMSO (vehicle control) or 1 µL of complexes diluted in DMSO at different concentrations, in triplicate for 72 h at 37 °C with 5% CO₂. Following this, MTS assay reagent was added for 4 h and absorbance measured at 490 nm using a Polarstar Optima microplate reader (BMG Labtech). IC₅₀ values were calculated using GraphPad Prism Version 5.0 software.

3.512 Uptake study

MCF-7 cells were grown in 75 cm² flasks up to 70% of confluence in 10 mL of culture medium. Compounds **50**, **53**, **54** and **58** were added to the flasks (100 µL of 1 mM solution in DMSO) and incubated for 6 h at 37 °C with 5% CO₂. Negative controls were used by incubating cells with DMSO alone under the same conditions. After removal of the medium and washing of the cells with PBS pH 7.4, the cells were detached using a trypsin solution. After quenching of trypsin with fresh medium, centrifugation and removal of the supernatant, the cell pellet was resuspended into 1 mL of PBS pH 7.4 and split into twice 500 µL for metal and protein quantification. The number of cells (expressed per million cells) of each sample was determined by measuring the protein content of the treated samples using a BCA assay

(ThermoFischer Scientific) corrected by the amount of protein/ 10^6 cells determined for each cell type by measuring the protein content of an untreated sample and dividing by the corresponding number of cells measured with a hemacytometer following a reported procedure. Microwave digestion was used to solvate the samples to liquid form. Nitric acid and hydrogen peroxide were used in a Milestone Ethos 1 microwave system using SK-10 10 place carousel. The digest was ramped to 200 °C in 15 minutes holding at 200 °C for 15 min. The sample was weighed into a microwave vessel before digestion, and decanted and rinsed into a pre-weighed PFA bottle after digestion. ICP-MS samples were spiked with rhodium internal standard and run on a Thermo X series 1 ICP-MS. The isotopes selected were ^{63}Cu , ^{65}Cu , ^{107}Ag , ^{109}Ag and ^{197}Au . Certified standards and independent reference were used for accuracy. Acid blanks were run through the system and subtracted from sample measurements before corrections for dilution.

3.513 *ROS assay*

100 μL of MCF-7 cells were seeded at a density of 1×10^5 cells per mL in a 96-well black plate with a transparent bottom. The cells were incubated at 37 °C for 24 h. The medium was removed and replaced with 50 μM H_2DCFDA (from Life Technologies) solution in PBS for 40 min. H_2DCFDA was removed and replaced with fresh medium. The cells were left for recovery for 20 min at 37 °C. Basal fluorescence was measured at 485/520 nm on a POLARstar Optima. The cells were incubated with 10 μM , 50 μM , or 100 μM of compounds, 1% DMSO (negative control) and 100 μM of H_2O_2 (positive control) for 24 h. Fluorescence was read at 485/520 nm. Basal fluorescence was subtracted from the fluorescence in the treated cells to calculate the amount of fluorescence caused by the compounds.

3.514 *FRET assay.*

The initial FRET melting screen was performed using a fluorescence resonance energy transfer (FRET) DNA melting based assay. The sequence used was DS_{FRET} FAM-d(TAT-AGC-TAT-A-HEG(18)-TAT-AGC-TAT-A)-TAMRA-3'). The labelled oligonucleotide (donor fluorophore FAM is 6-carboxyfluorescein; acceptor fluorophore TAMRA is 6-carboxytetramethyl-rhodamine) were prepared as a 220 nM solution in 10 mM sodium cacodylate buffer at the indicated pH with 100 mM sodium chloride and then thermally annealed. Strip-tubes (QIAGEN) were prepared by aliquoting 20 μL of the annealed DNA, followed by 0.5 μL of the compound solutions. Control samples for each run were prepared with the same quantity of DMSO with the DNA in buffer. Fluorescence melting curves were determined in a QIAGEN Rotor-Gene Q-series PCR machine, using a total reaction volume of 20.5 μL . Measurements were made with excitation at 470 nm and detection at 510 nm. Final

analysis of the data was carried out using QIAgen Rotor-Gene Q-series software and Origin or Excel.

Chapter 4

The synthesis and anticancer activity of cyclometalated gold^{III} dithiocarbamate complexes.

4.1 Abstract

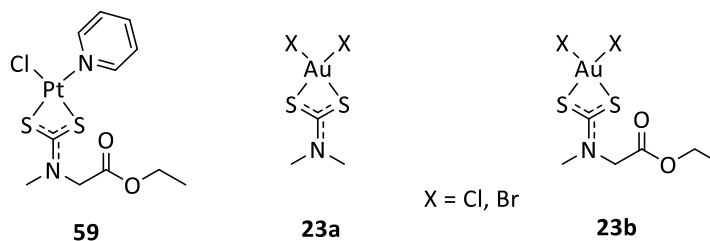
A series of cyclometalated gold^{III} dithiocarbamate complexes have been synthesised and characterised as prospective anticancer drug candidates. These included a series of cationic 2-phenyl pyridine derivatives, $[\text{Au}^{\text{III}}(\text{C}^{\wedge}\text{N})(\text{R}_2\text{NCS}_2)]^+$, where R = methyl (**61**), ethyl (**62**), sarcosine ethyl ester (**63**), pyrrolidine (**64**) and butyl (**65**). The final complex was a neutral ($\text{C}^{\wedge}\text{C}$) cyclometalated diethyldithiocarbamate derivative, $\text{Au}^{\text{III}}(\text{C}^{\wedge}\text{C})(\text{Et}_2\text{NCS}_2)$, (**66**). The complexes have been screened for their cytotoxic activity against a panel of human cancer cell lines with several of the derivatives displaying high levels of cytotoxicity with IC_{50} values dropping to sub-micromolar levels. Cell uptake studies demonstrated a clear correlation between the cellular uptake and the *in vitro* cytotoxicity of the complexes. FRET DNA binding studies towards higher order DNA structures showed a correlation between the cytotoxicity of the complexes and their ability to stabilise i-motif and G-quadruplex structures indicating these structures as a possible target of these complexes.

4.2 Introduction

Chapter 1 (Section 1.1) has already introduced cisplatin and its clinically approved derivatives carboplatin and oxaliplatin.¹ These are highly effective and successful chemotherapeutic agents and in the past forty years they have revolutionised the treatment of cancer.² However, despite their clinical success they do have some drawbacks. One of the most severe is that high dosage of platinum-based therapeutics, and the resulting accumulation of platinum within the body, causes severe side effects including severe nephrotoxicity (renal failure) and this limits the administrable dosage to patients.³

Pabla *et al.* hypothesised that one of the causes of cisplatin induced nephrotoxicity is the platinum binding to, and the resulting inactivation of thiol-containing enzymes.¹¹⁴ The high affinity of platinum towards sulfur-containing biomolecules such as glutathione, albumin, cysteine and methionine is thought to play an important role in the metabolic processes of platinum based drugs. The strong and irreversible binding of platinum towards intercellular thiolato ligands contributes towards drug deactivation, and reactions with sulphur-containing peptides and proteins can lead to conformational changes in the protein which causes changes to their biological activity.¹¹⁵ As a result, thiol and sulfur-based nucleophiles have been tested as chemoprotectants in combination with cisplatin to modulate cisplatin nephrotoxicity, and sodium diethyldithiocarbamate was shown to be particularly effective.^{116, 117} As a result of these findings, Ronconi *et al.* designed a series of metal-dithiocarbamate complexes to combine the cytotoxic activity of the metal centres with the

nephroprotective benefits of the dithiocarbamate ligand. These included platinum, **59** and gold, **23a** and **23b** derivatives (Figure 69).¹¹⁸



Complex	IC ₅₀ (μM)				
	HeLa ^a	HL60 ^b	A549 ^c	2008 ^d	C13 ^e
59	7.0	2.9	15.2	5.9	8.3
23a (X = Cl)	2.1	0.8x10 ⁻²	0.4x10 ⁻²	0.2x10 ⁻²	0.1x10 ⁻²
23b (X = Cl)	8.2	0.4	4.7	49.3	23.8
Cisplatin	15.6	25.6	35	43.2	556

Figure 69 – structures of platinum^{II} and gold^{III} dithiocarbamate derivatives and their cytotoxicity towards human cancer cell lines in comparison to cisplatin; ^a Cervical adenocarcinoma, ^b Leukaemia, ^c Lung carcinoma, ^d Cisplatin sensitive ovarian carcinoma, ^e Cisplatin resistant ovarian carcinoma. Data taken from ref¹¹⁸.

Despite the platinum dithiocarbamate variant, **59** showing very promising results both in *in vitro* and *in vivo* experiments, it was poorly soluble in aqueous medium and highly unstable under physiological conditions thus rendering it unsuitable as a drug candidate. The gold^{III} derivatives however showed better solubility properties as well as high cytotoxicities towards a panel of human cancer cell lines. The dimethyl variant, **23a** was particularly effective, displaying higher cytotoxicities than both cisplatin and the platinum dithiocarbamate derivative, **59**. The *in vivo* antitumor activity of **23a** on Ehrlich solid-tumour bearing mice resulted in 74% inhibition of tumour growth after 11 days of treatment compared to the untreated control animals – a two-fold increase compared to the activity of cisplatin under the same conditions. Chemotherapy with the gold derivative was also better tolerated than with cisplatin particularly regarding the nephrotoxic effect which was considerably reduced.^{59, 118}

The mechanism of action of the Au^{III}Cl₂(DTC) complexes remains unclear although one thing remains undisputed; that the mechanism of action of these Au^{III}-dithiocarbamate derivatives differs from that of classical platinum^{II}-based anticancer agents.^{59, 118} Section 1.21 introduces the mechanism of action of cisplatin; briefly, cisplatin forms covalent adducts between DNA

base pairs, causing distortion of the DNA double helix which inhibits DNA replication and transcription processes.⁵³ Although the Au^{III}Cl₂(DTC) complexes were proved to bind to DNA to a greater extent than cisplatin, it was thought that this was a consequence of their higher reactivity towards isolated biological molecules and therefore DNA cannot be assigned as the only target of these complexes.¹¹⁸ Indeed, Tomasello *et al.* showed that **23b** was able to suppress tumour growth by proteasome inhibition in MCF-7 cells,⁶⁹ and Milacic *et al.* also demonstrated a similar result for **23a** in MDA-MB-231 breast cancer cells.⁶⁸ Other work also showed that the complexes were able to inhibit the enzyme thioredoxin reductase (TrxR) by irreversible covalent binding to its catalytic site, leading to an increase in intracellular reactive oxygen species (ROS) (Section 1.24).^{43, 44}

Dithiocarbamate ligands can also be used to conjugate cancer targeting oligopeptides to a gold^{III} centre; **26** and **60** (Figure 70/71) (Section 1.16).⁴⁷ These ‘second generation’ gold^{III} compounds are able to maintain both high levels of anticancer activity together with an improved selectivity towards cancer cells. This is achieved by the targeting of peptide transporters which are upregulated in certain cancers, which improves the bioavailability of the complex as well as the tumour specificity.^{47, 119} One dipeptide derivative Au^{III}Br₂(DTC-Sar-AA-O^tBu), **26** (AA = Glycine) (Figure 70), synthesised by Nardon *et al.* showed high levels of cytotoxicity towards MDA-MB-231 breast cancer cell cultures *in vitro* (IC₅₀ of 13 μM) and towards MDA-MB-231 xenographs in an *in vivo* nude mice model. Remarkably, tumour growth was inhibited by more than 57% in comparison to the negative control with no observed side effects from the treatment. The proteasome was identified as the major target of the complex, both *in vitro* in purified human 20S proteasome and also in intact MDA-MB-231 cell extracts as well as in an *in vivo* nude mice model.⁴⁷

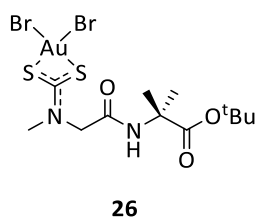
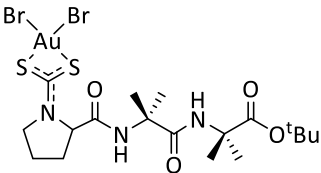


Figure 70 – gold^{III} dithiocarbamate peptide conjugate, **26**.⁴⁷

Other tripeptide derivatives by Kouodom *et al.*, Au^{III}Cl₂(DTC-Pro-(MeAla)₂-O^tBu), **60** (Figure 71) also showed high levels of *in vitro* cytotoxic activity with IC₅₀ values lower than cisplatin towards all of the tested cell lines. The complex was thought to act by inducing apoptosis and necrosis.¹¹⁹



Complex	IC ₅₀ ± SD (μM)			
	PC3 ^a	2008 ^b	C13 ^c	L540 ^d
60	3.0 ± 0.2	8.2 ± 0.7	7.8 ± 0.5	2.2 ± 0.2
Cisplatin	3.3 ± 0.3	19.4 ± 1.2	117.2 ± 9.1	2.5 ± 0.1

60

Figure 71 – structure of **60** and its cytotoxicity towards human cancer cell lines in comparison to cisplatin; ^a Prostate cancer, ^b Cisplatin sensitive ovarian cancer, ^c Cisplatin resistant ovarian cancer, ^d Hodgkin's lymphoma. Data taken from ref¹¹⁹.

There are very few examples of cyclometalated gold^{III} dithiocarbamate derivatives although one example has already been discussed in Section 1.15; derivatives of [Au^{III}(C[^]N)(R₂NCS₂)]⁺ were synthesised by Zhang *et al.* (C[^]N = 2-phenylpyridine), **25** (Figure 72). These derivatives were shown to act as potent deubiquitinase inhibitors as well as showing selective *in vitro* cytotoxicity towards MDA-MB-231 breast cancer cells over immortalised liver cells (MIHA). The cytotoxicity correlated to a high uptake of the gold complexes into the cell resulting in cell cycle arrest and apoptosis.⁴⁶

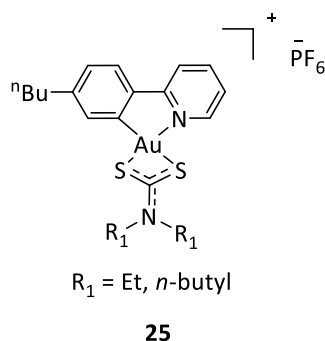


Figure 72 – structure of the cyclometalated gold^{III} dithiocarbamate derivative.⁴⁶

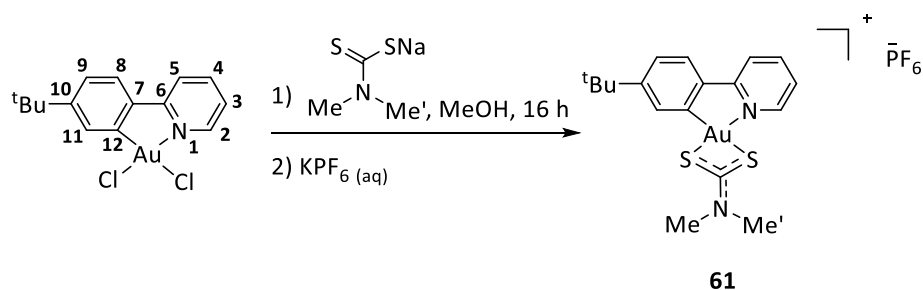
This chapter introduces the synthesis and anticancer activity of cyclometalated [Au^{III}(C[^]N)(R₂NCS₂)]⁺ complexes (C[^]N = 2-(4-*t*-butyl)phenyl pyridine). The complexes were tested for their cytotoxicity towards a panel of human cancer cells and Human Umbilical Vein Endothelial cells for comparison. Studies into the possible mode of action were also undertaken and the reactivity of the complexes towards GSH, N-acetyl cysteine, double-stranded DNA and higher order DNA structures, (*i*-motifs and G-quadruplexes), was tested.

4.3 Results and Discussion

4.3.1 Synthesis and structural characterisation

The 2-(4-*t*-butyl)phenyl pyridine) cyclometalated gold dichloride precursor was synthesised in good yield, (72%) by previously reported methods (Section 3.3.1, Scheme 13).¹⁰⁶ An overnight reaction with sodium dimethyl-dithiocarbamate hydrate in methanol followed by the addition of aqueous potassium hexafluorophosphate gave the cyclometalated dimethyl-dithiocarbamate complex, **61** in good yield (82%), as depicted in Scheme 21.

¹H NMR showed a significant downfield shift in the characteristic H² doublet from 9.71 ppm to 8.74 ppm as well as a downfield shift in the signal for H¹¹ from 8.03 to 7.03 ppm, confirming the successful formation of complex **61**. The appearance of two inequivalent methyl groups at 3.49 and 3.44 ppm also confirmed the successful coordination of the dithiocarbamate ligand. The two methyl groups are inequivalent due to the rigidity of the delocalised double bond between the NCS₂ ligand which prevents free rotation. A singlet at 193.3 ppm in the C¹³[¹H] NMR for the NCS₂ carbon was also present. The presence of the KPF₆ anion was confirmed by both fluorine and phosphorus NMR. The IR spectrum also showed a clear vibration 1579 cm⁻¹ which can be attributed to the delocalised NCS₂ system of the dithiocarbamate ligand.



Scheme 21 – synthesis of the [(C^N)Au(DMDTC)]⁺, **61** (DMDTC = *N,N*-dimethyl dithiocarbamate).

By replacing the sodium dimethyl-dithiocarbamate with the diethyl variant, complex **62** was obtained in high yield, (94%) (Figure 73). Once again, the significant downfield shift in the signals for both H² and H¹¹ in the ¹H NMR spectrum to 8.78 and 7.06 ppm respectively as well as the distinctive vibration at 1559 cm⁻¹ in the IR spectrum and a singlet at 193.3 ppm in the C¹³[¹H] NMR for the NCS₂ carbon confirmed the successful formation of complex **62**. Two multiplets also appeared at 3.87 and 1.35 ppm in the ¹H NMR for the two ethyl groups of the dithiocarbamate ligand.

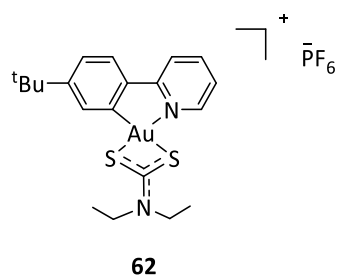


Figure 73 – structure of complex **62**, the (C^N) Au^{III} dithiocarbamate.

Slow vapour diffusion of diethyl ether into a concentrated acetonitrile solution of complex **62** gave crystals suitable for X-ray diffraction. These were characterised in the solid state by Dr David Hughes (Figure 74).

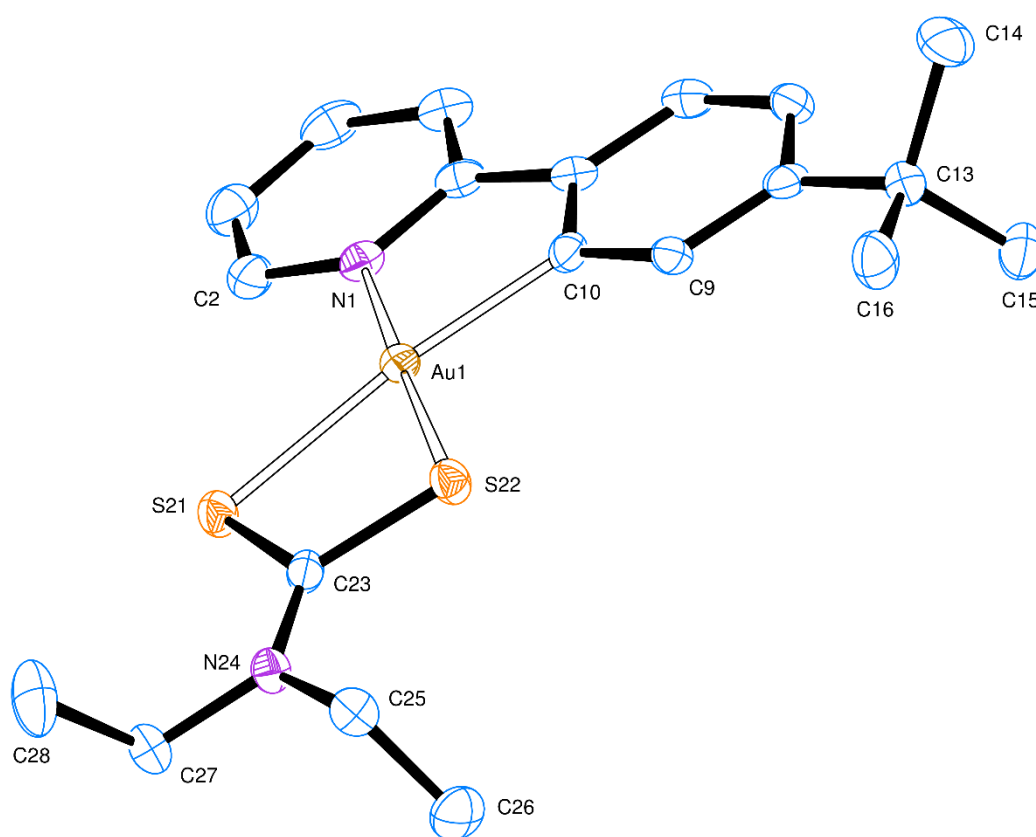


Figure 74 – structure of **62** (hydrogen atoms omitted for clarity). Ellipsoids set at 50% probability. Selected bond distances (Å) and angles (°): Au1-N1 2.061 (3), Au1-C10 2.038 (3), Au1-S21 2.984 (8), Au1-S22 2.2821 (8), C10-Au1-N1 80.64 (11), C10-Au1-S22 98.36 (9), N1-Au1-S21 105.30 (7), S22-Au1-S21 75.54 (3), N1-Au1-S22 177.22 (7), C10-Au1-S21 173.08 (9), S21-C23-S22 111.47 (19).

The crystals display the typical, slightly distorted square planar geometry to the gold^{III} centre due to the accommodation of the (C^N) cyclometalating ligand with a C10-Au1-N1 angle of 80.64 ° in the cyclometalating ligand. The coordinated dithiocarbamate ligand also contributes to the distortion due to the restricted chelate angle of 75.54 ° of the S21-Au1-S22 dithiocarbamate ligand. The Au1-S21 and Au1-S22 bond distances also differ from each other; Au1-S21 = 2.984 Å and Au1-S22 = 2.2821 Å. Both these bond distances and also the angle of the coordinated dithiocarbamate ligand are in good agreement with other crystal structures for Au^{III}Cl₂(DTC) complexes, synthesised by Altaf *et al.*⁴⁵

A reaction with sarcosine ethyl ester dithiocarbamate under the same conditions gave complex **63** in good yield (78%) (Figure 75). This time both isomers of the product were obtained in a 1:0.8 ratio and consequently all the proton signals for the cyclometalating (C^N) ligand were doubled. The presence of two doublets at 8.77 and 8.71 ppm and two singlets at 7.15 and 7.01 ppm in the ¹H NMR spectrum for H² and H¹¹ respectively confirmed the successful formation of complex **63** as two separate isomers. Two singlets also appeared at 3.54 and 3.45 ppm for the NMe protons in the sarcosine ligand along with two singlets for the NCH₂CO protons at 4.82 and 4.78 ppm and two multiplets for the ethyl group protons at 4.21 and 1.23 ppm.

The ¹³C[¹H] NMR of this complex was of poor quality due to the poor solubility of the complex in the NMR solvent. However, the presence of a broad singlet at 198.7 ppm for the delocalised dithiocarbamate NCS₂, and the presence of two separate signals at 166.3 and 166.2 ppm for the C=O (one in each isomer), also confirmed the successful formation of complex **63**. The IR spectrum for this complex also showed the distinctive NCS₂ vibration 1558 cm⁻¹ as well as a sharp C=O vibration at 1736 cm⁻¹.

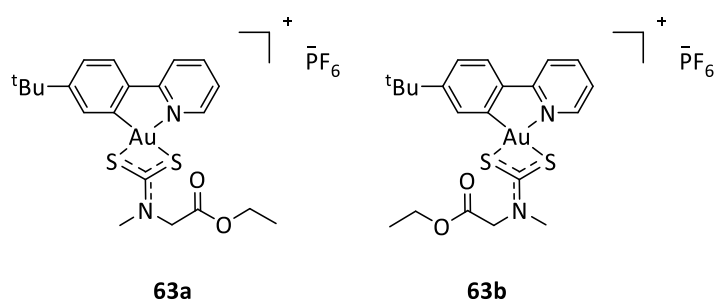


Figure 75 – isomers of complex **63**.

A reaction with sodium pyrrolidine dithiocarbamate also led to the successful formation of complex **64**, (71%) (Figure 76). The formation of this complex was once again confirmed by

the downfield shift of the signals for H² and H¹¹ to 8.48 and 7.13 ppm respectively and the appearance of two multiplets at 3.98 and 2.24 ppm for the pyrrolidine protons in the ¹H NMR spectrum. A singlet at 190.4 ppm for the delocalised dithiocarbamate NCS₂ in the C¹³[¹H] NMR and an NCS₂ vibration at 1556 cm⁻¹ in the IR spectrum also confirmed the successful formation of **64**.

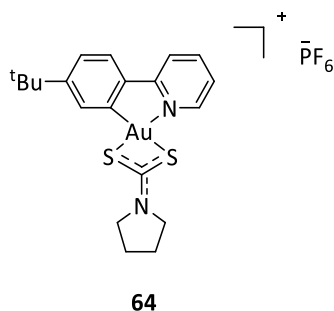
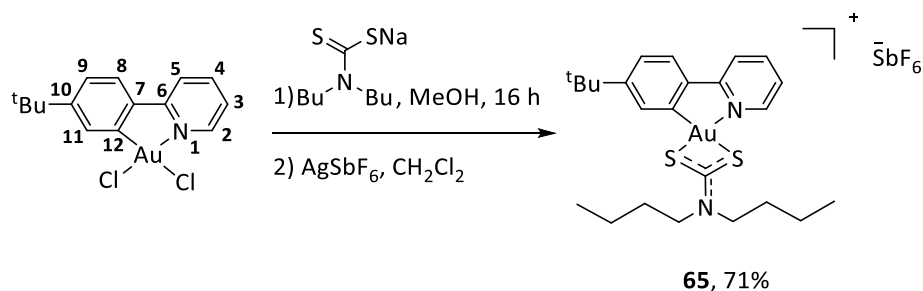


Figure 76 – structure of **64**.

Complex **65** was more difficult to obtain as the product from the first reaction step, [(C[^]N)Au^{III}(DTC)]Cl, was too insoluble to react with the aqueous potassium hexafluorophosphate in the anion exchange step. Dissolving in dichloromethane and adding an excess of silver hexafluoroantimonate gave complex **65** in good yield (71%), (Scheme 22). Once again, the formation of **5** was confirmed by the downfield shift of the signals for H² and H¹¹ to 8.40 and 7.08 ppm respectively in the ¹H NMR spectrum as well as the appearance of four multiplets at 3.77, 1.78, 1.42 and 0.98 ppm for the butyl protons. A singlet at 194.4 ppm for the delocalised dithiocarbamate NCS₂ in the C¹³[¹H] NMR and an NCS₂ vibration at 1550 cm⁻¹ in the IR spectrum also confirmed the successful formation of **65**.



Scheme 22 – synthesis of dithiocarbamate **65**.

Complex **66** was synthesised by Dr Isabel Fernandez using previous methods published by David *et al.*; by the reaction of the oligomeric (AuCl(^tBu₂Bip))_n with sodium diethyl-dithiocarbamate to form the neutral (C[^]C)Au^{III}(DTC) complex (Figure 77).⁹² Complex **66** was

included to see whether the presence of the more lipophilic (C[^]C) cyclometalated ligand and the absence of a positive charge would significantly alter the cytotoxicity of the complex.

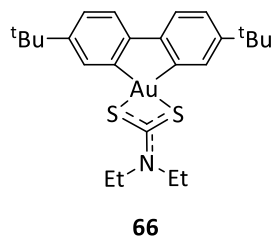


Figure 77 – structure of complex 66.⁹²

4.32 In vitro antiproliferative activity

Although the dithiocarbamate complexes **61-66** were poorly soluble in aqueous cell culture medium by themselves, they were soluble enough in DMSO not to precipitate when diluted up to 100 μ M in the aqueous culture medium with 1% DMSO. IC₅₀ values for the six complexes were then determined on a panel of human cancer cell lines. These included solid tumour cell lines; lung adenocarcinoma cells (A549), breast adenocarcinoma (MCF-7 and MDA-MB-231) and human colon cancer (HCT-116) and suspension cells; promyelocytic leukaemia (HL60) as well as healthy Human Umbilical Vein Endothelial Cells (HUVEC) for comparison. Results were determined using a colorimetric MTS assay after 72 hours of incubation in comparison to cisplatin (as previously described in Section 2.32). The results are reported in Table 3.

Table 3 – IC₅₀ values for complexes **61-66** in comparison to cisplatin against different human cancer cell lines and healthy lung fibroblast cells after 72 h of incubation.

Complex	IC ₅₀ \pm SD (μ M) ^a					
	A549	MCF-7	HL60	HCT-116	MDA-MB-231	HUVEC
61	4.6 \pm 0.7	1.4 \pm 0.3	0.2 \pm 0.05	2.5 \pm 0.3	8.6 \pm 1.0	0.8 \pm 0.04
62	2.9 \pm 0.6	1.2 \pm 0.2	0.2 \pm 0.03	2.4 \pm 0.4	1.9 \pm 0.1	0.7 \pm 0.02
63	>100	>100	17.8 \pm 2.1	>100	>100	33.9 \pm 5.4
64	10.8 \pm 0.3	1.1 \pm 0.03	1.4 \pm 0.07	6.0 \pm 0.4	3.0 \pm 0.2	0.7 \pm 0.05
65	5.3 \pm 0.3	1.7 \pm 0.04	0.8 \pm 0.01	3.5 \pm 0.3	3.1 \pm 0.1	1.2 \pm 0.2
66	>100	8.8 \pm 0.2	1.9 \pm 0.3	>100	>100	3.3 \pm 0.03
Cisplatin	33.7 \pm 3.7 ^b	21.2 \pm 3.9 ^b	3.7 \pm 0.3 ^b	5.3 \pm 0.2 ^c	28.4 \pm 0.1 ^c	>100

^a Mean \pm the standard error of at least three independent experiments. ^b Values from ref ³⁹.

^c Values from ref ⁸⁶.

Complexes **61**, **62**, **64** and **65** all showed similar cytotoxicity profiles, with high levels of cytotoxicity towards all the tested cell lines. The dimethyl-dithiocarbamate, complex **61** showed 7 times the activity of cisplatin towards the lung cancer cell line (A549) and more than 15 times the activity towards the MCF-7 breast cancer and the HL60 leukaemia cells. The complex also showed more than twice the activity of cisplatin towards the MDA-MB-231 metastatic breast cancer and the HCT-116 colon cancer cell lines.

Complex **62**, the diethyl variant, showed even higher activity with more than fifteen times the activity of cisplatin towards the A549, MCF-7, HL60 and MDA-MB-231 cell lines and IC_{50} values of between 2.9-0.2 μM . It was assumed that this was because the slight increase in lipophilicity of the complex increased its cellular uptake. However, the more lipophilic pyrrolidine and dibutyl variants, **64** and **65**, showed slightly reduced levels of cytotoxicity in comparison to **61** and **62** although they still showed extremely promising levels in comparison to cisplatin.

However, despite their promising anticancer activities, all four of the complexes showed poor selectivity towards the Human Umbilical Vein Endothelial Cells, HUVEC, although further tests on other healthy cell lines are needed for a more accurate conclusion as HUVEC are perhaps not the most reliable comparison as they typically show a reduced sensitivity towards cisplatin.

The sarcosine ethyl ester dithiocarbamate, complex **63**, showed extremely low cytotoxicity across the panel of cells with IC_{50} values of more than 100 μM for A549, MCF-7, MDA-MB-231 and HCT-116. This could be due to poor cellular uptake as the complex is extremely hydrophilic and therefore might struggle to cross the cell membrane. The complex also showed poor activity towards HL60 leukaemia cells with an IC_{50} of 17.8 μM . However, this complex also showed the best selectivity profile of the new dithiocarbamates towards this cell line (selectivity factor $S_{\text{HL60}/\text{HUVEC}} = 1.9$).

The (C⁺) variant, complex **66**, also showed reduced cytotoxicity, particularly towards the HCT-116, MDA-MB-231 and A549 cells although it showed a reasonable activity towards MCF-7 breast cancer and HL60 leukaemia cells, (IC_{50} of 8.8 and 1.9 μM respectively). Once again, the reduced activity could be due to a reduced cellular uptake as the (C⁺) cyclometalated ligand and the absence of the positive charge makes this complex extremely lipophilic and this could affect its ability to cross the cell membrane.

4.33 Cellular uptake in MCF-7 cells

As mentioned previously (Section 3.33), the cellular uptake of drugs can have a significant influence on the cytotoxicity of prospective chemotherapeutic agents.¹⁰⁸ ICP-MS was used to quantify the amount of intracellular gold and determine whether the cellular uptake of the dithiocarbamate complexes was affecting their cytotoxicity. ICP-MS measurements were completed by Dr Graham Chilvers. Complexes **61** and **65** (the dimethyl and dibutyl variants) were selected as these represented the smallest and largest alkyl group respectively in the $[\text{Au}^{\text{III}}(\text{C}^{\wedge}\text{N})(\text{R}_2\text{NCS}_2)]^+$ series of complexes. Complex **63**, the sarcosine ethyl ester variant, was selected because it showed extremely poor cytotoxicity towards all the cell lines tested and **66**, the (C^C) diethyl dithiocarbamate, as it was the only complex with a (C^C) cyclometalating ligand and the absence of a positive charge. MCF-7 cells were incubated for 6 hours with 10 μM concentrations of each of the complexes in 1% DMSO. The results of three independent experiments are depicted in Figure 78.

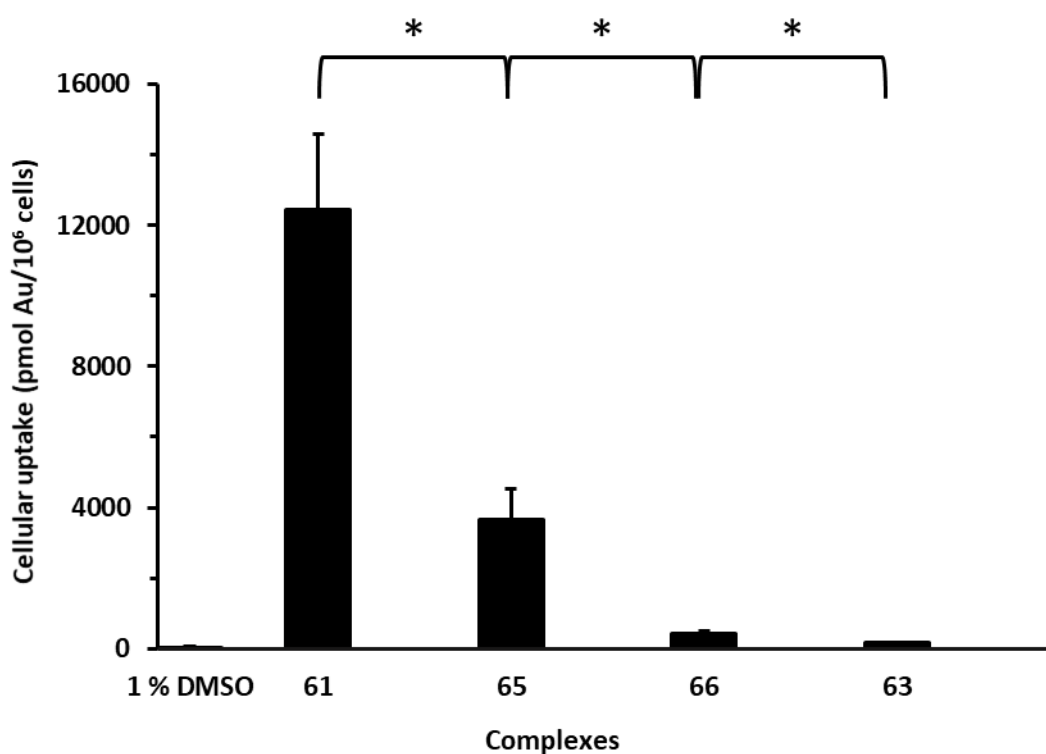


Figure 78 – cellular uptake of complexes **61**, **65**, **66** and **63** and a DMSO control in MCF-7 cells after 6 h of treatment at 10 μM in 1% DMSO. The results were analysed by t-test, $P=0.05$, **61:65***, **65:66***, **66:63***.

There was a clear correlation between the cellular uptake and the *in vitro* cytotoxicity of the complexes. The most cytotoxic complexes, **61** and **65**, which have IC_{50} values of 1.4 and 1.7

μM respectively both show high levels of uptake, particularly the dimethyl variant, **61** which displays more than three times the cellular uptake of complex **65**. Complex **66**, the neutral ($\text{C}^{\wedge}\text{C}$) dithiocarbamate, displays moderate cytotoxicity towards MCF-7 cells with an IC_{50} of $8.8 \mu\text{M}$ and also displays moderate cellular uptake. Both **61** and **65** display significantly higher levels of cellular uptake than **66** (twenty-eight and eight times respectively). This could be a factor of the increased lipophilicity of this complex due to the lack of positive charge which makes it poorly soluble in aqueous medium. Complex **63**, the most hydrophilic sarcosine ethyl ester variant, displays both extremely poor *in vitro* cytotoxicity (IC_{50} value of $>100 \mu\text{M}$) and also poor cellular uptake. This could be a factor of the increased hydrophilicity of the complex hindering its ability to cross the phospholipid bilayer.

4.34 Quantification of reactive oxygen species

As previously mentioned in Section 2.33, the induction of reactive oxygen species (ROS) is a recognised mechanism of action for metal-based drugs, including Au^{I} -NHC complexes.⁷⁵ All six of the cyclometalated dithiocarbamate complexes were therefore tested for the production of ROS. The amount of intracellular ROS was measured after treatment of MCF-7 cells with $100 \mu\text{M}$, $50 \mu\text{M}$ and $10 \mu\text{M}$ concentrations of each complex. The results are summarised in Figure 79. None of the complexes tested appeared to increase the production of ROS and therefore this mode of action can be ruled out for these cyclometalated dithiocarbamate complexes.

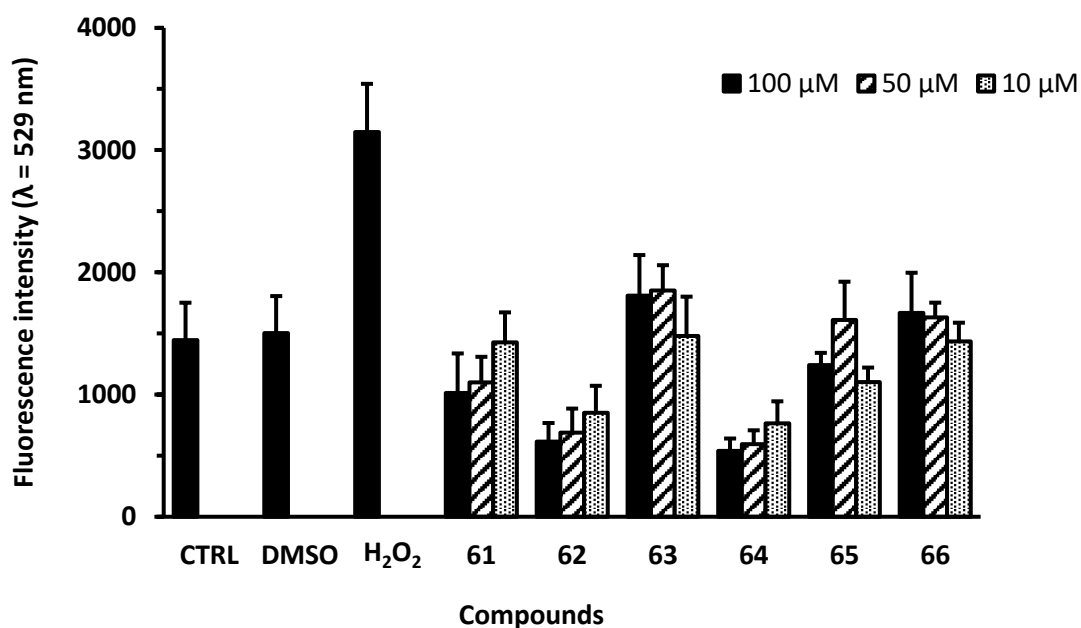


Figure 79 – ROS measurements in MCF-7 cells after 24 h incubation with complexes 61-66.

4.35 Reaction with Glutathione and N-Acetyl Cysteine

Cytotoxic gold compounds have shown high reactivity towards model proteins and consequently gold-protein interactions are generally thought to be responsible for the cytotoxic effects of these complexes and proteins are generally regarded as their primary targets.^{5, 6, 120} Metal-protein binding sites generally involve the side chain residues of amino acids such as the thioether and thiolate sulphur atoms in *L*-methionine and *L*-cysteine respectively.⁵⁰ Complex **61** was selected to act as the representative $[\text{Au}^{\text{III}}(\text{C}^{\wedge}\text{N})(\text{DTC})]^+$ and was reacted with glutathione and N-acetyl cysteine, which were selected to act as reliable models of target biomolecules (Figure **80**).

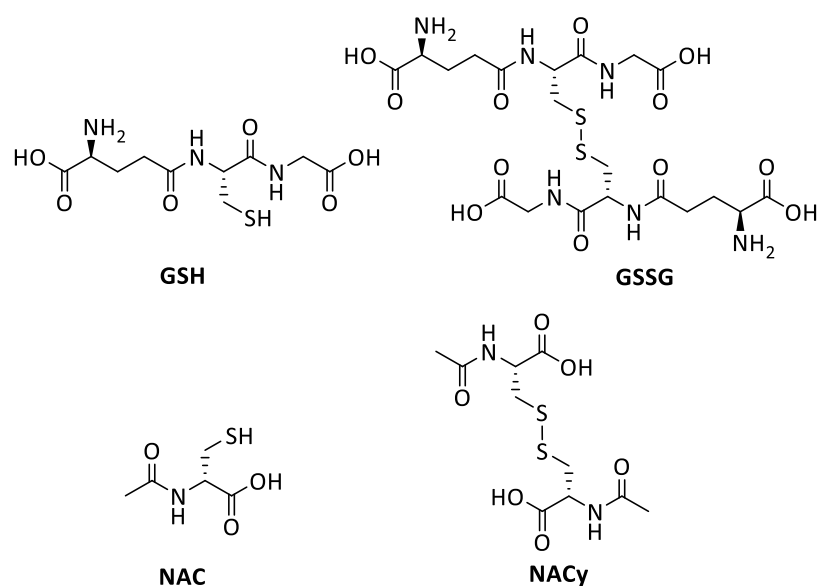


Figure **80** – structures of reduced glutathione (GSH), oxidised glutathione (GSSG), reduced N-acetyl cysteine (NAC) and oxidised N-acetyl cysteine (NACy).

When complex **61** was mixed at room temperature with reduced glutathione in a 1:1 mixture of $\text{DMSO-}d_6$ and D_2O , ^1H NMR spectroscopy showed the immediate formation of oxidised glutathione (GSSG) (Figure **81**). Although no signals for the complex could be seen due to its poor solubility in the solvents, the formation of a pale-yellow product was observed thus suggesting that an immediate reduction to a gold^I species was occurring. The gold^I species can be attributed to $(\text{CH}^{\wedge}\text{N})\text{Au}^{\text{I}}(\text{S}_2\text{CNR}_2)$.

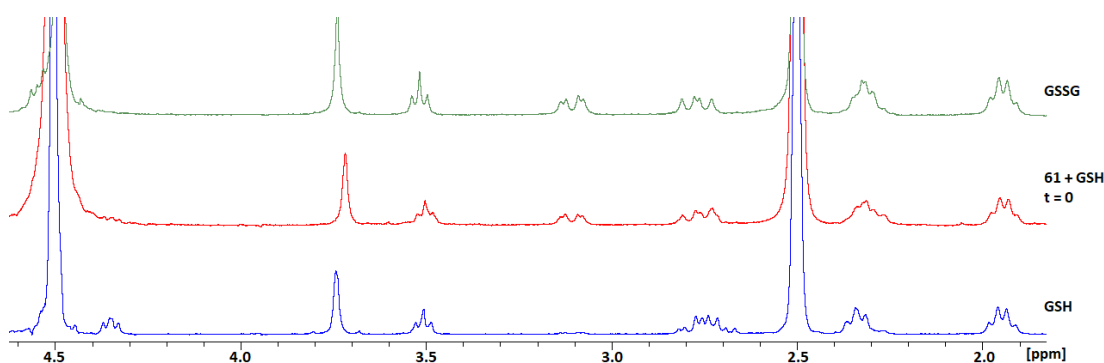


Figure 81 – ^1H NMR spectra of a 1:1 mixture of **61** with GSH at room temperature, in comparison with the starting materials, GSH and GSSG (DMSO- d_6 /D $_2$ O 1:1).

The reduction of complex **61** by GSH to a gold^I species could be followed by UV/Vis spectroscopy. Upon mixing a 1 mM solution of the complex in DMSO with 1 mM of reduced glutathione in H $_2$ O, the characteristic ligand-to-metal-charge-transfer (LMCT) band at 350 nm completely disappeared, confirming that an immediate reduction was occurring. The presence of a pale-yellow product also suggested that a gold^I species was being formed. Casini *et al.* demonstrated a very similar result using gold^{III} complexes with bipyridyl ligands.¹²¹ The appearance of a low but broad band at 400-450 nm could also be tentatively attributed to a gold^I species.⁵⁹ The same features could be seen when all of the dithiocarbamate derivatives were reacted with GSH. The UV-Vis spectra of **61** are depicted in Figure 82.

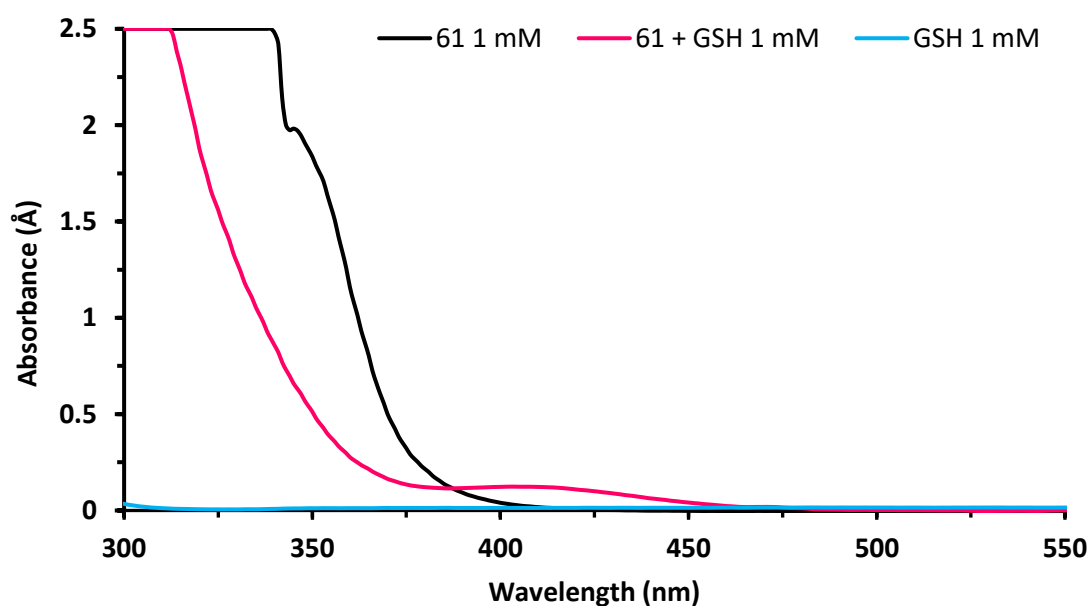


Figure 82 – UV/Vis spectrum of complex **61** (1 mM), GSH (1 mM) and a mixture of complex **61** and GSH (1 mM), (DMSO-H $_2$ O 1:1).

The interaction of **61** and **62** with N-acetyl cysteine (NAC) was also investigated, using NAC as a model for thiol containing biomolecules. Boscutti *et al.* showed that Au^{III}Br₂(DTC) complexes underwent a rapid multi-step reduction in the presence of NAC during which the NAC was oxidised to NACy and the gold^{III} was reduced to a gold^I species, possibly AuBr with the release of the dithiocarbamate ligand.¹²² Both **61** and **62** were mixed at room temperature with NAC in CD₃CN and ¹H NMR spectroscopy was used to follow the reaction over a 48 h period (Figure **83a** and **83b**). No reaction was observed for either complex during this time and it was concluded that the presence of the (C^N) cyclometalating ligand gave the system stability towards reduction by NAC.

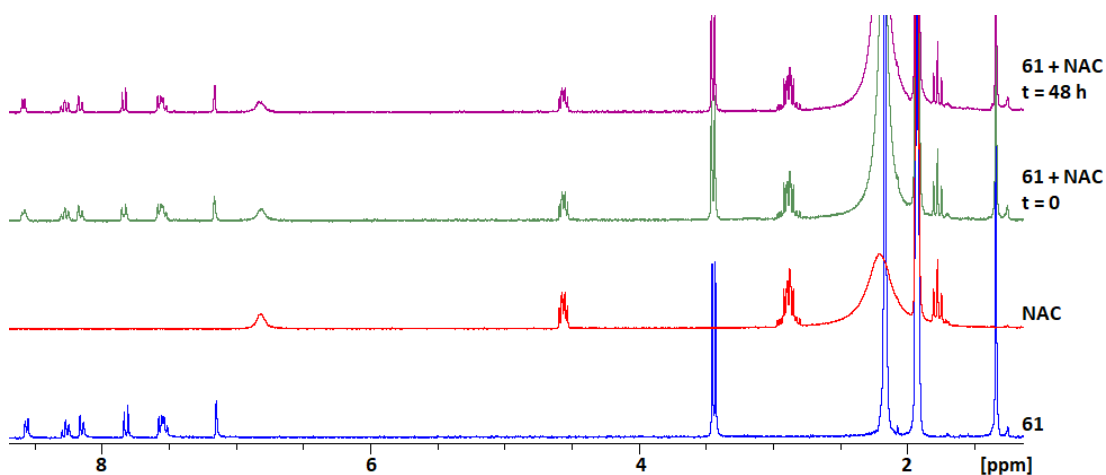


Figure **83a** – ¹H NMR spectra of a 1:1 mixture of **61** with NAC at different reaction times at room temperature, in comparison with the starting materials **61** and NAC (CD₃CN).

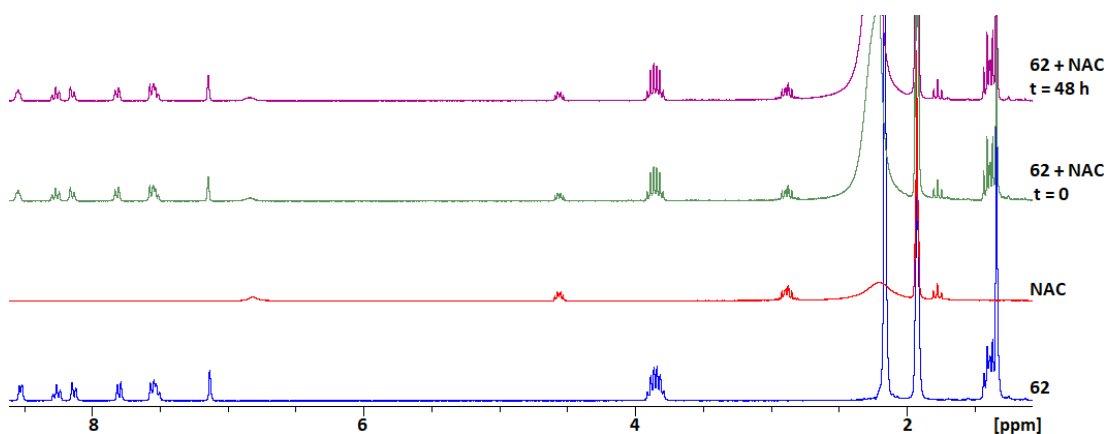


Figure **83b** – ¹H NMR spectra of a 1:1 mixture of **62** with NAC at different reaction times at room temperature, in comparison with the starting materials **62** and NAC (CD₃CN).

4.36 DNA-binding properties

As previously discussed in Section 1.22, higher order DNA structures like G-quadruplexes and i-motifs are emerging as promising targets for the development of new anticancer agents.⁶¹⁻⁶⁴ G-quadruplexes are four-stranded DNA secondary structures that form in guanine-rich DNA sequences. They are formed by the stacking of tetrads of guanine residues linked via hydrogen-bonding and stabilized by the presence of typically monovalent cations in the centre of the tetrad.¹²³ The selective stabilization of G-quadruplex structures has been investigated as a method of controlling key cellular events such as telomerase activity or oncogene expression. These structures are gaining interest as potential anticancer targets, particularly because they are found both in the telomers and in the over-expressed gene promoter regions of cancer genes.^{61, 62} Recently, there have been several examples of potential chemotherapeutic gold^{III} and gold^I complexes that target G-quadruplexes.^{33, 66} Bazzicalupi *et al.* co-crystallised a caffeine-based gold^I bis NHC cation with a G-quadruplex, showing that DNA-ligand interaction occurred via π -stacking on the accessible tetrads.¹²⁴ Gratteri *et al.* also showed that dioxobridged gold^{III} complexes and cyclometalated oxo-compounds were able to bind strongly and selectively to DNA G-quadruplexes whereas double stranded DNA was not affected at all.⁶⁶

i-Motifs are also emerging as potential targets for anticancer agents. These are higher order DNA structures that form in cytosine-rich DNA sequences via hydrogen bonding between hemiprotonated pairs of cytosines. As i-motifs require cytosine-rich sequences, they are likely to form in the complementary strands opposing G-quadruplexes in the genome.⁶³ Stabilisation of i-motif structures has been shown to alter gene expression of the oncogene bcl-2 and disrupt telomerase activity and therefore compounds that stabilise these structures also have potential as anticancer drugs.⁶⁴ Our group recently showed that a gold^{III} benzimidazole-based NHC complex could selectively stabilise both G-quadruplex and i-motif structures over double stranded DNA.³⁹

The established Förster resonance energy transfer (FRET) DNA melting assay was used to give a broad indication of the DNA binding capabilities of the dithiocarbamate complexes **61-66** towards different DNA targets.¹²⁵ These included a G-quadruplex forming sequence from the human telomere (hTeloG), the human telomeric i-motif sequence (hTeloC), an i-motif forming sequence from the promoter region of the oncogene (hif-1- α), a promoter i-motif forming sequence (c-MycC), as well as double stranded DNA. The human telomeric i-motif forming sequence, TeloC is only stable up to pH 5.5. The binding capabilities of the complexes

were therefore assessed at a transitional pH of 6.0 (the pH where the structure is 50% folded).¹²⁶ The c-MYC i-motif is also only stable up to pH 6.5 and has a transitional pH of 6.6.⁶⁴ The remaining sequences were all tested at the transitional pH of hif-1-alpha, pH 7.2.¹²⁷

As mentioned previously in Section 3.34, FRET measures the changes in fluorescence as the spatial distance between two fluorophores is changed as they are brought closer together or moved further apart as a result of DNA stabilisation or denaturation.^{112, 113} Results are expressed as the changes in DNA melting temperature (ΔT_m) when double stranded DNA (0.2 μ M) was dosed with 50 μ M concentrations of each drug. A higher ΔT_m suggests an increased level of DNA stabilisation and thus a compound-DNA interaction (Figure 84).

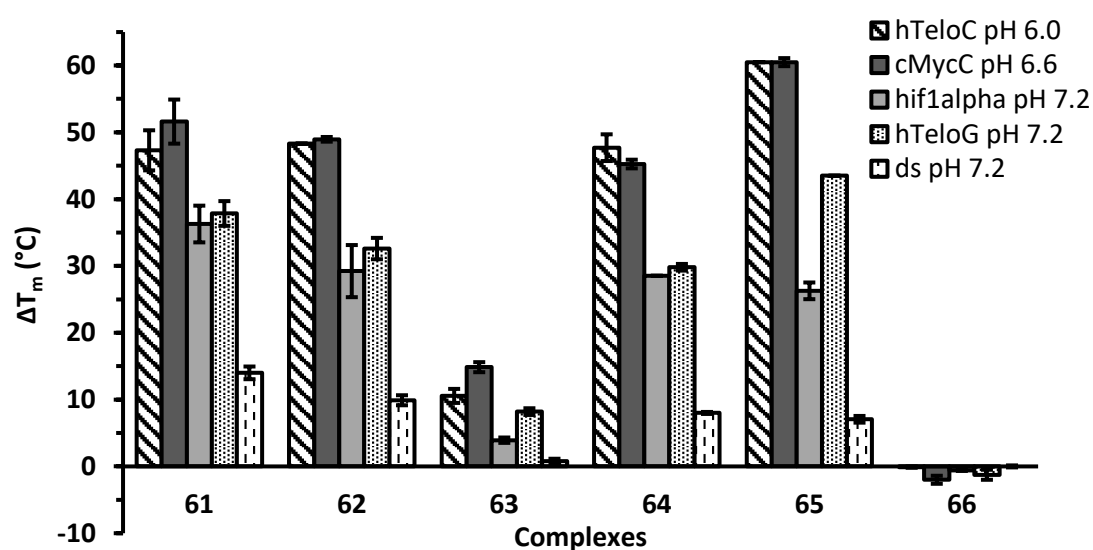


Figure 84 – stabilisation of different DNA structures (0.2 μ M) when dosed with 50 μ M concentrations of dithiocarbamate complexes 61-66. Data represents the average and standard deviations of two experiments.

Complexes 61, 62, 64 and 65 appeared to show high levels of DNA stabilisation towards all of the DNA structures tested. These four complexes showed particularly high levels of stabilisation towards two of the i-motif forming sequences; the human telomeric i-motif sequence, (hTeloC) and the promoter i-motif forming sequence, (c-MycC). For these two sequences, ΔT_m values were between 47-51 $^{\circ}$ C for complexes 61, 62 and 64 and >60 $^{\circ}$ C for complex 65. For the G-quadruplex forming sequence, (hTeloG), and the i-motif forming sequence, (hif-1- α), ΔT_m values were somewhat lower, between 26-37 $^{\circ}$ C for all four complexes, indicating lower levels of complex-DNA stabilisation and thus weaker DNA binding.

In good agreement with the cytotoxicity data, both **63**, the least cytotoxic of the $[(C^N)Au(DTC)]^+$ complexes, and **66**, the neutral $(C^C)Au(DTC)$ showed extremely poor levels of DNA interaction towards all of the tested structures. For both of these complexes, ΔT_m values were below 10 °C for all of the DNA structures tested. Indeed, complex **66** appeared to destabilise all three of the i-motif forming sequences; hTeloC, hif1- α and c-MycC, ($\Delta T_m = <0$ °C). These values could be a product of the lack of a cationic charge as this is consistent with our previous work which highlights the importance of a cationic charge on the ability of gold complexes to interact with higher order nucleic acid structures.³⁹ However, the data is generally in good agreement with the cytotoxicity data, with the most cytotoxic complexes displaying the highest levels of stabilisation towards the higher order DNA structures. This suggests that the stabilisation of G-quadruplex and i-motif structures is a possible mechanism of action for these complexes. Higher order nucleic acid structures could therefore be a possible intracellular target of these gold^{III} dithiocarbamate complexes.

4.4 Conclusion

This chapter has introduced the synthesis and anticancer activity of a series of gold^{III} dithiocarbamate complexes. These included a series of cationic $[Au^{III}(C^N)(R_2NCS_2)]^+$ complexes with methyl (**61**), ethyl (**62**), sarcosine ethyl ester (**63**), pyrrolidine (**64**) and butyl (**65**) groups and also one $Au^{III}(C^C)(Et_2NCS)$ complex, (**66**) to act as a comparison between the cationic and neutral complexes.

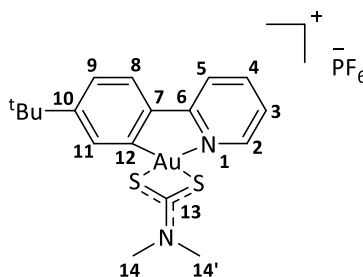
The complexes were tested for their *in vitro* cytotoxicity towards a panel of human cancer cell lines including lung adenocarcinoma cells (A549), breast adenocarcinoma (MCF-7 and MDA-MB-231), human colon cancer (HCT-116) and promyelocytic leukaemia (HL60) as well as healthy Human Umbilical Vein Endothelial Cells (HUVEC) for comparison. Complexes **61**, **62**, **64** and **65** showed the highest levels of cytotoxicity with IC_{50} values dropping to sub-micromolar levels. The most hydrophilic complex, **63**, the sarcosine ethyl ester derivative, was non-toxic across all of the cell lines, and the most lipophilic complex, the (C^C) derivative, **66**, also showed extremely poor cytotoxicity.

Cellular uptake studies in MCF-7 breast cancer cells indicated that there was a clear correlation between the *in vitro* cytotoxicity of the complexes and their ability to enter the cell. Complex **61** and **65** both showed high levels of cellular uptake in comparison to **63** and **66**. This suggests that low cellular uptake is one of the limitations of the non-toxic complexes.

The antiproliferative mode of action of these complexes is so far unknown although FRET DNA binding studies towards higher order DNA structures suggested that there was a correlation between the cytotoxicity of the complexes and their ability to stabilise i-motif and G-quadruplex structures. Complex **61** was also rapidly reduced in the presence of GSH which could indicate that these particular dithiocarbamate complexes are reduced to a gold^I active species under physiological conditions. However, neither **61** nor **62** showed any reaction with N-acetyl cysteine, which was used as a model for other thiol containing biomolecules. Other mechanisms of action have also been ruled out and we established that these complexes did not increase the formation of reactive oxygen species. Further studies are currently underway to see if any of these new dithiocarbamate complexes act as Thioredoxin reductase inhibitors.

4.5 Experimental

When required, manipulations were performed using standard Schlenk techniques under dry nitrogen or in a MBraun glove box. Nitrogen was purified by passing through columns of supported P₂O₅ with moisture indicator and activated 4 Å molecular sieves. Anhydrous solvents were freshly distilled from appropriate drying agents. ¹H and ¹³C[¹H] spectra were recorded using a Bruker Avance DPX-300 spectrometer. ¹H NMR spectra (300.13 MHz) were referenced to the residual protons of the deuterated solvent used. ¹³C[¹H] NMR spectra (75.47 MHz) were referenced internally to the D-coupled ¹³C resonances of the NMR solvent. Elemental analyses were carried out at London Metropolitan University. The (C^N)Au-Cl starting material, **49** and complex **66** were synthesized following reported procedures.^{92, 106}

4.51 Synthesis of complex **61**

Sodium dimethyldithiocarbamate hydrate (0.020 g, 0.140 mmol) in methanol (10 mL) was added drop by drop to a suspension of 2-(4-*t*-butyl)phenyl pyridine gold dichloride (0.060 g, 0.125 mmol) in methanol (15 mL) and stirred at room temperature overnight. A colour change from white to pale yellow was observed during the addition. Excess saturated KPF₆ (aqueous solution) was then added causing an immediate fluffy white precipitation. The solid was filtered and purified by dissolving in minimal acetonitrile (2 mL) and precipitating the product with an excess of diethyl ether (20 mL). This was filtered and dried under vacuum (0.069 g, 0.103 mmol, 82%). Anal. Calcd. For C₁₈H₂₂AuF₆N₂PS₂·5H₂O (762.51): C, 28.35; H, 4.23; N, 3.67. Found C, 28.15; H, 3.98; N, 3.69. ¹H NMR ((CD₃)₂SO, 300 MHz, 298 K): 8.74 (d, ³J_{H-H} = 6.0 Hz, 1H, H²), 8.43-8.30 (m, 2H, H⁴⁺⁵), 7.99 (d, ³J_{H-H} = 8.2 Hz, 1H, H⁸), 7.60 (t, ³J_{H-H} = 6.0 Hz, 1H, H³), 7.53 (d, ³J_{H-H} = 8.2 Hz, 1H, H⁹), 7.03 (s, 1H, H¹¹), 3.49 (s, 3H, H^{14/14'}), 3.44 (s, 3H, H^{14/14'}), 1.28 (s, 9H, ^tBu). ¹³C[¹H] NMR ((CD₃)₂SO, 75 MHz): 193.3 (s, C¹³), 163.7 (s, C¹²), 155.8 (s, C^{6/7}), 151.6 (s, C^{6/7}), 150.1 (s, C²), 144.1 (s, C⁴), 141.8 (s, C¹⁰), 127.5 (s, C⁸), 126.7 (s, C⁹), 126.2 (s, C³), 124.7 (s, C¹¹), 122.6 (s, C⁵), 42.5 (s, C¹⁴), 41.2 (s, C^{14'}), 35.9 (s, C(CH₃)₃), 31.2 (s, C(CH₃)₃). IR: ν_{max} (neat)/cm⁻¹: 2960 (^tBu), 2868 (Ar), 1579 (Dithiocarbamate).

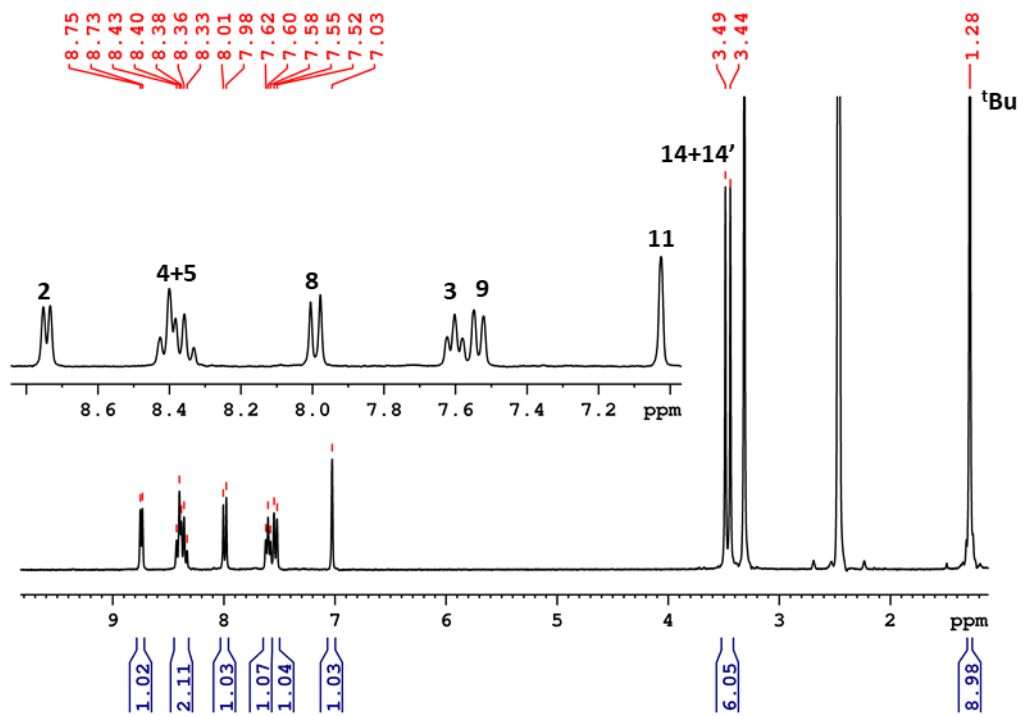


Figure 4.51a – ^1H NMR of **61** in $(\text{CD}_3)_2\text{SO}$.

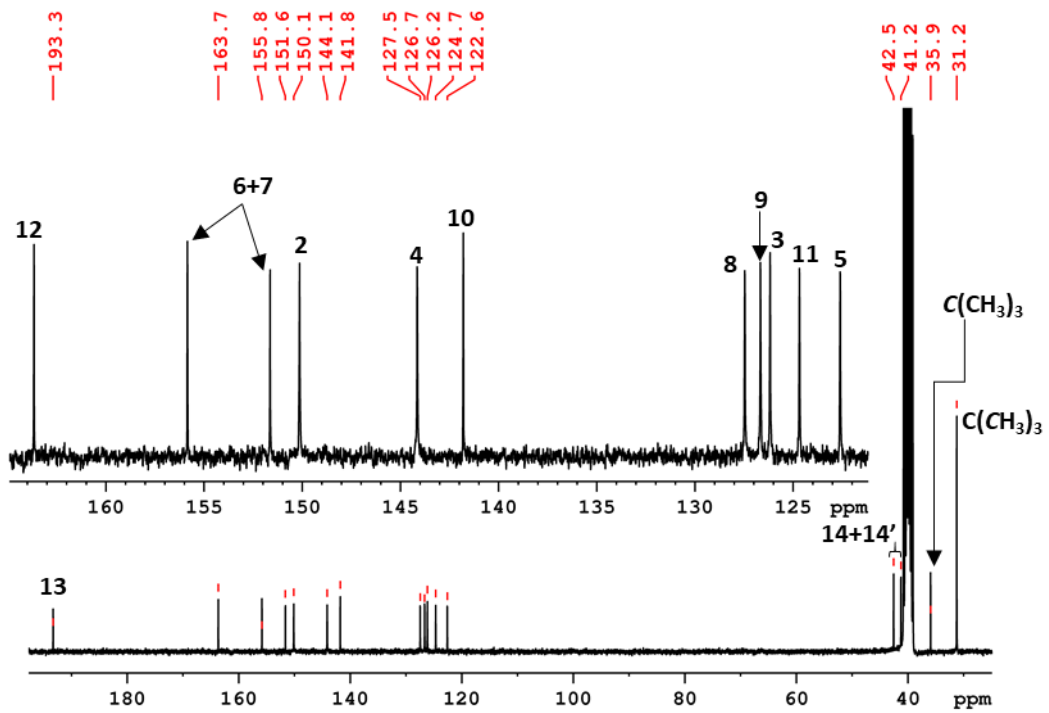
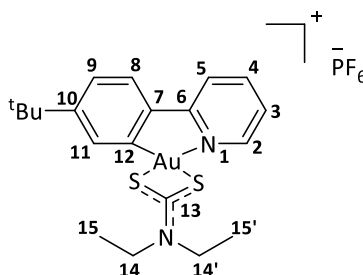


Figure 4.51b – $^{13}\text{C}[^1\text{H}]$ NMR of **61** in $(\text{CD}_3)_2\text{SO}$.

4.52 Synthesis of complex **62**

Sodium diethyldithiocarbamate hydrate (0.028 g, 0.125 mmol) in methanol (10 mL) was added drop by drop to a suspension of 2-(4-*t*-butyl)phenyl pyridine gold dichloride (0.060 g, 0.125 mmol) in methanol (15 mL) and stirred at room temperature overnight. A colour change from white to pale yellow was observed during the addition. Excess saturated KPF₆ (aqueous solution) was then added causing an immediate fluffy white precipitation. The solid was filtered and purified by dissolving in minimal acetonitrile (2 mL) and precipitating the product with an excess of diethyl ether (20 mL). This was filtered and dried under vacuum (0.083 g, 0.118 mmol, 94%). Anal. Calcd. For C₂₀H₂₆AuF₆N₂PS₂·6H₂O (808.58): C, 29.71; H, 4.74; N, 3.46. Found C, 29.46; H, 4.52; N, 3.55. ¹H NMR ((CD₃)₂SO, 300 MHz, 298 K): 8.78 (d, ³J_{H-H} = 5.4 Hz, 1H, H²), 8.45-8.31 (m, 2H, H⁴⁺⁵), 8.00 (d, ³J_{H-H} = 8.2 Hz, 1H, H⁸), 7.60 (t, ³J_{H-H} = 5.4 Hz, 1H, H³), 7.54 (dd, ³J_{H-H} = 8.2 Hz, ⁴J_{H-H} = 1.2 Hz, 1H, H⁹), 7.06 (d, ⁴J_{H-H} = 1.2 Hz, 1H, H¹¹), 3.87 (m, 4H, H^{14+14'}), 1.35 (m, 6H, H^{15+15'}), 1.29 (s, 9H, ^tBu). ¹³C[¹H] NMR ((CD₃)₂SO, 75 MHz): 193.3 (s, C¹³), 163.6 (s, C¹²), 155.9 (s, C^{6/7}), 151.7 (s, C^{6/7}), 150.1 (s, C²), 144.2 (s, C⁴), 141.8 (s, C¹⁰), 127.5 (s, C⁸), 126.6 (s, C⁹), 126.1 (s, C³), 124.8 (s, C¹¹), 122.6 (s, C⁵), 48.8 (s, C¹⁴), 47.3 (s, C^{14'}), 35.9 (s, C(CH₃)₃), 31.2 (s, C(CH₃)₃), 13.0 (s, C¹⁵), 12.5 (s, C^{15'}). IR: ν_{max} (neat)/cm⁻¹: 2948 (^tBu), 2866 (Ar), 1559 (Dithiocarbamate).

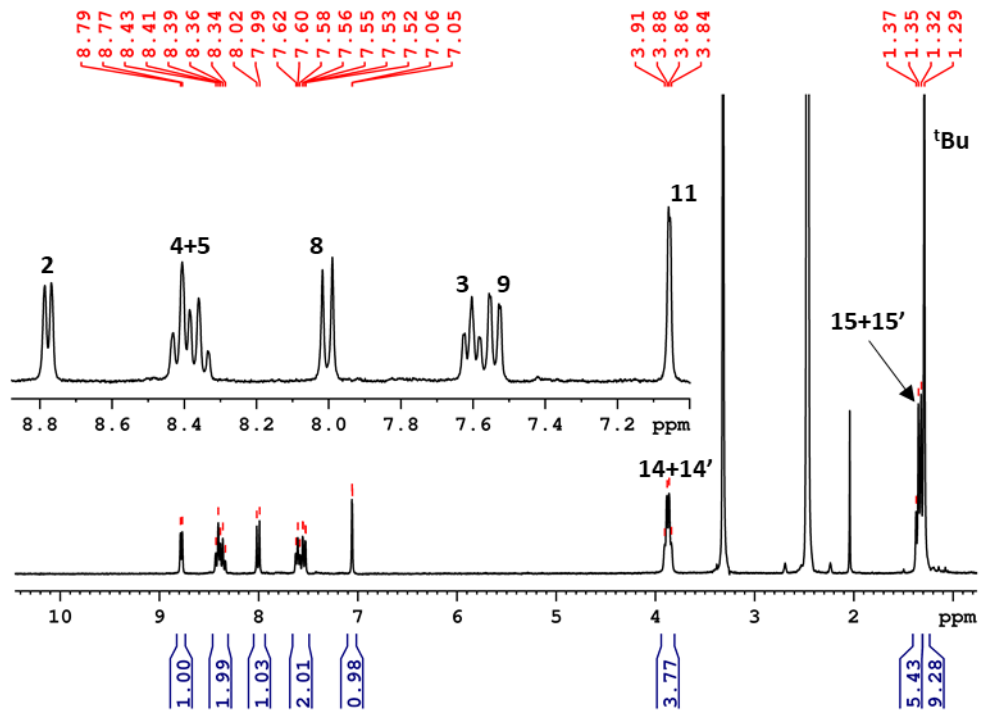


Figure 4.52a – ^1H NMR of **62** in $(\text{CD}_3)_2\text{SO}$.

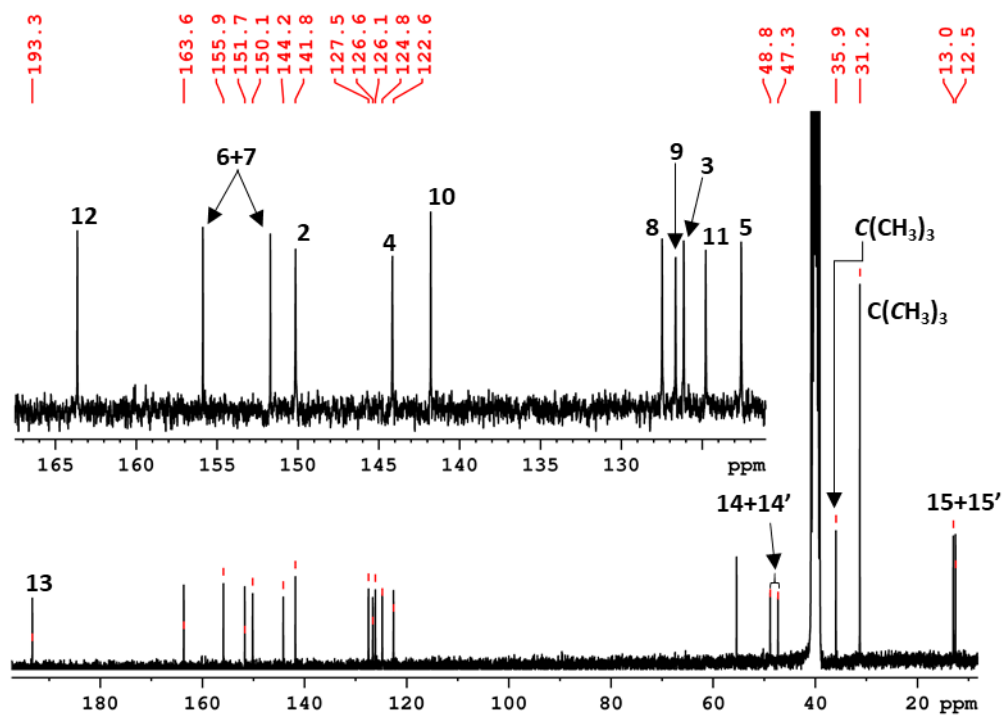
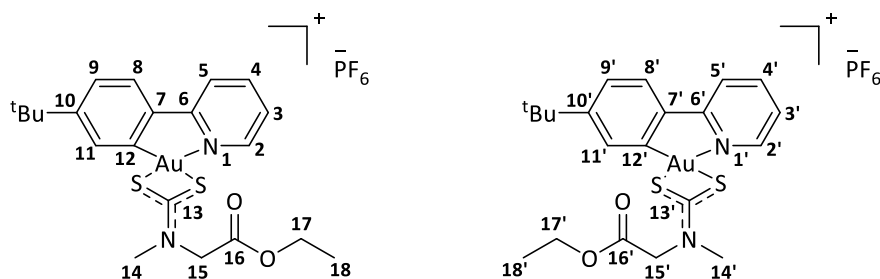


Figure 4.52b – ^{13}C [^1H] NMR of **62** in $(\text{CD}_3)_2\text{SO}$.

4.53 Synthesis of complex **63**

Sarcosine ethyl ester dithiocarbamate hydrate (0.100 g, 0.517 mmol) in methanol (10 mL) was added drop by drop to a suspension of 2-(4-*t*-butyl)phenyl pyridine gold dichloride (0.060 g, 0.125 mmol) in methanol (15 mL) and stirred at room temperature overnight. A colour change from white to pale yellow was observed during the addition. Excess saturated KPF₆ (aqueous solution) was then added causing an immediate fluffy white precipitation. The solid was filtered and purified by dissolving in minimal acetonitrile (2 mL) and precipitating the product with an excess of diethyl ether (20 mL). This was filtered and dried under vacuum (0.073 g, 0.098 mmol, 78%). Anal. Calcd. For C₂₁H₂₆AuF₆N₂PS₂·8H₂O (906.64): C, 27.82; H, 4.89; N, 3.09. Found C, 27.34; H, 4.42; N, 3.29. ¹H NMR ((CD₃)₂SO, 300 MHz, 298 K): 8.77 (d, ³J_{H-H} = 5.6 Hz, 0.8H, H^{2'}), 8.71 (d, ³J_{H-H} = 5.6 Hz, 1H, H²), 8.40-8.27 (m, 3.6H, H^{4'+4'+5'+5'}), 7.94 (m, 1.8H, H^{9+9'}), 7.63-7.49 (m, 3.6H, H^{3+3'+8+8'}), 7.15 (d, ⁴J_{H-H} = 1.4 Hz, 1H, H¹¹), 7.01 (d, ⁴J_{H-H} = 1.4 Hz, 0.8H, H^{11'}), 4.82 (s, 1.6H, H^{15'}), 4.78 (s, 2H, H¹⁵), 4.21 (m, 3.6H, H^{17+17'}), 3.54 (s, 3H, H¹⁴), 3.45 (s, 2.4H, H^{14'}), 1.29 (s, 9H, ^tBu), 1.27 (s, 7.2H, ^tBu'), 1.23 (m, 5.4H, H^{18+18'}). ¹³C[¹H] NMR ((CD₃)₂SO, 75 MHz): 198.7 (s, C¹³), 166.3 (s, C^{16'}), 166.2 (s, C¹⁶), 163.5 (s, C^{12'}), 163.3 (s, C¹²), 156.0 (s, C^{6'/7'}), 156.0 (s, C^{6/7}), 151.5 (s, C^{6'/7'}), 151.2 (s, C^{6/7}), 150.1 (s, C^{2'}), 150.0 (s, C²), 144.1 (s, C^{4'}), 144.1 (s, C⁴), 141.6 (s, C^{10'}), 141.4 (s, C¹⁰), 127.4 (s, C^{8'}), 127.4 (s, C⁸), 126.8 (s, C^{9'}), 126.7 (s, C⁹), 126.1 (s, C³), 126.0 (s, C^{3'}), 124.8 (s, C^{11'}), 124.7 (s, C¹¹), 122.5 (s, C⁵), 122.5 (s, C⁵), 62.6 (s, C^{14'}), 62.6 (s, C¹⁴), 55.3 (s, C^{15'}), 54.1 (s, C¹⁵), 35.9 (s, C(CH₃)₃), 31.4 (s, C^{17'}), 31.1 (s, C(CH₃)₃), 31.0 (s, C¹⁷), 14.3 (s, C¹⁸), 14.3 (s, C^{18'}). IR: ν_{max} (neat)/cm⁻¹: 2961 (^tBu), 2867 (Ar), 1736 (C=O), 1558 (Dithiocarbamate).

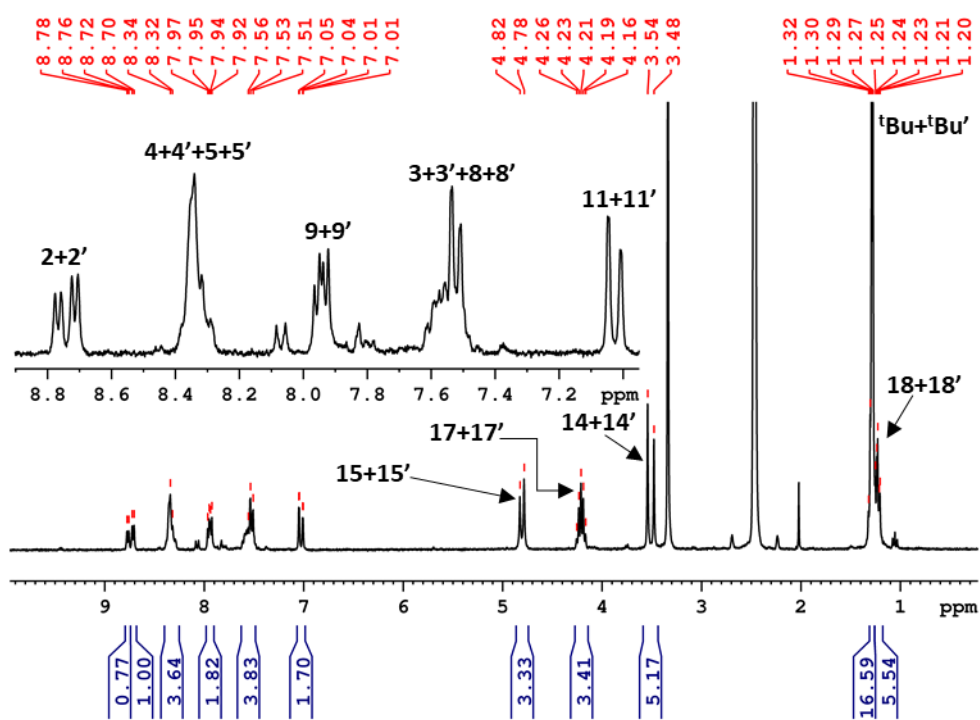


Figure 4.53a – ^1H NMR of **63** in $(\text{CD}_3)_2\text{SO}$.

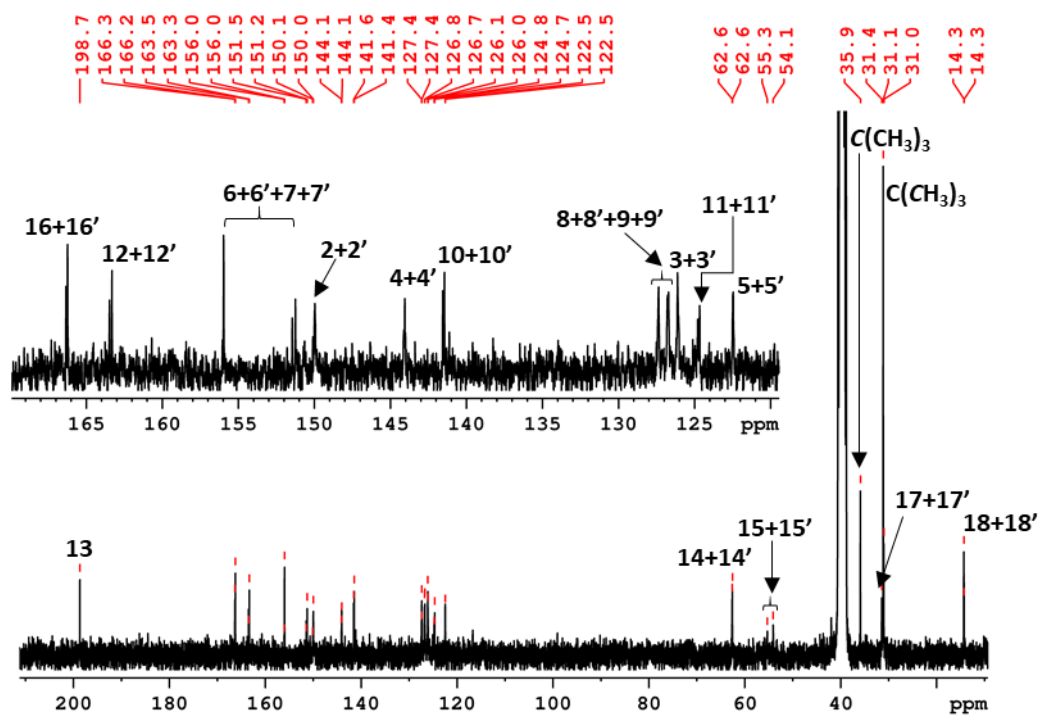
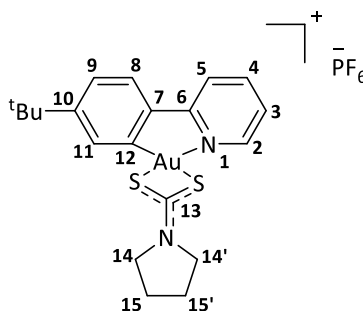


Figure 4.53b – ^{13}C NMR of **63** in $(\text{CD}_3)_2\text{SO}$.

4.54 Synthesis of complex **64**

Sodium pyrrolidinedithiocarbamate hydrate (0.085 g, 0.502 mmol) in methanol (10 mL) was added drop by drop to a suspension of 2-(4-*t*-butyl)phenyl pyridine gold dichloride (0.060 g, 0.125 mmol) in methanol (15 mL) and stirred at room temperature overnight. A colour change from white to pale yellow was observed during the addition. Excess saturated KPF₆ (aqueous solution) was then added causing an immediate fluffy white precipitation. The solid was filtered and purified by dissolving in minimal acetonitrile (2 mL) and precipitating the product with an excess of diethyl ether (20 mL). This was filtered and dried under vacuum (0.062 g, 0.089 mmol, 71%). Anal. Calcd. For C₂₀H₂₄AuF₆N₂PS₂·4H₂O (770.54): C, 31.18; H, 4.19; N, 3.64. Found C, 30.85; H, 3.78; N, 3.25. ¹H NMR (CD₂Cl₂, 300 MHz, 298 K): 8.48 (d, ³J_{H-H} = 5.6 Hz, 1H, H²), 8.26 (dt, ³J_{H-H} = 8.1 Hz, ⁴J_{H-H} = 1.5 Hz, 1H, H⁴), 8.07 (d, ³J_{H-H} = 8.1 Hz, 1H, H⁵), 7.72 (d, ³J_{H-H} = 8.3 Hz, 1H, H⁸), 7.59-7.50 (m, 2H, H³⁺⁹), 7.13 (d, ⁴J_{H-H} = 1.6 Hz, 1H, H¹¹), 3.98 (t, ³J_{H-H} = 6.6 Hz, 4H, H^{14+14'}), 2.24 (m, 4H, H^{15+15'}), 1.36 (s, 9H, ^tBu). ¹³C[¹H] NMR (CD₂Cl₂, 75 MHz): 190.4 (s, C¹³), 164.4 (s, C¹²), 157.1 (s, C^{6/7}), 151.8 (s, C^{6/7}), 148.4 (s, C²), 143.6 (s, C⁴), 140.5 (s, C¹⁰), 126.6 (s, C⁸), 126.5 (s, C⁹), 125.3 (s, C³), 125.3 (s, C¹¹), 122.0 (s, C⁵), 52.0 (s, C^{14/14'}), 35.8 (s, C(CH₃)₃), 30.7 (s, C(CH₃)₃), 24.6 (s, C^{15/15'}), 24.2 (s, C^{15/15'}). IR: ν_{max} (neat)/cm⁻¹: 2961 (^tBu), 2863 (Ar), 1556 (Dithiocarbamate).

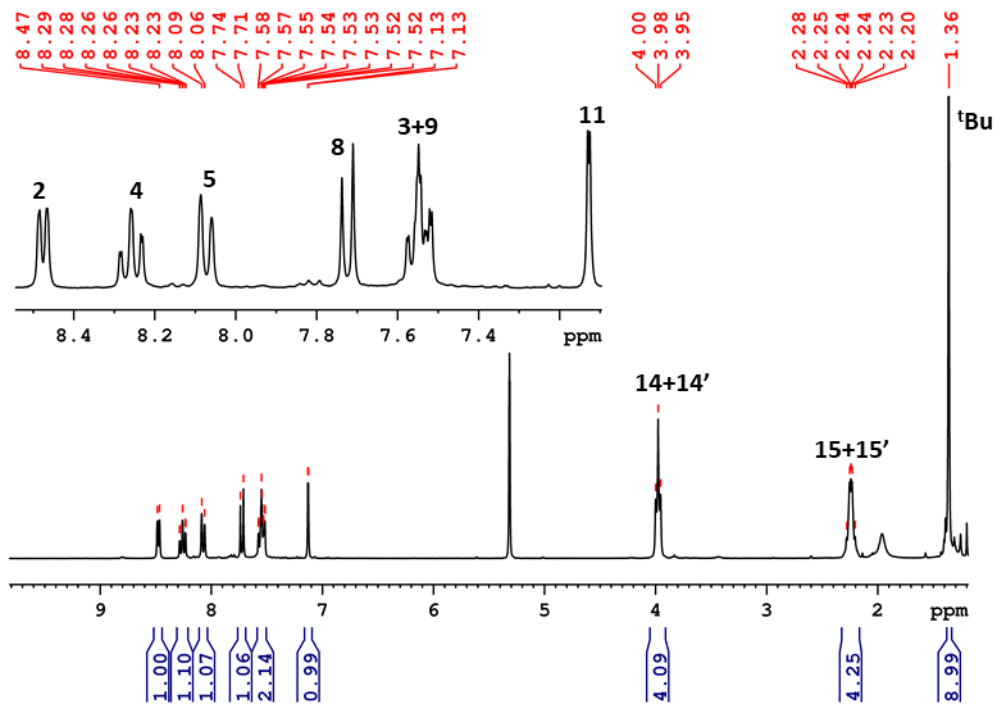


Figure 4.54a – ^1H NMR of **64** in CD_2Cl_2 .

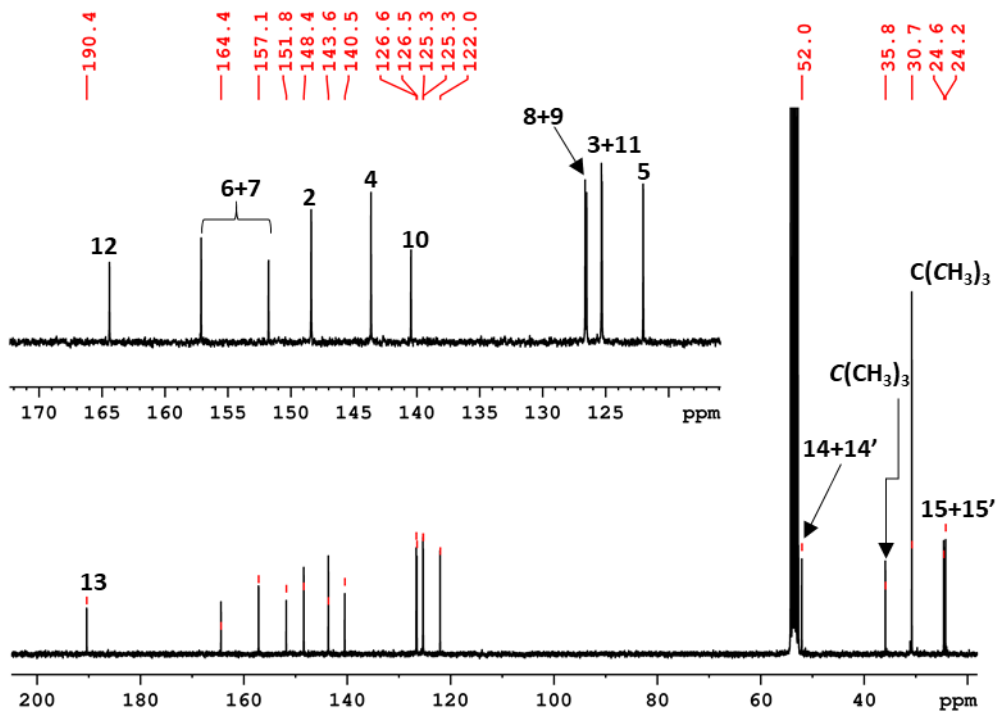
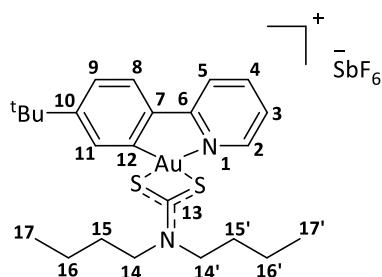


Figure 4.54b – ^{13}C [^1H] NMR of **64** in CD_2Cl_2 .

4.55 Synthesis of complex **65**

Sodium dibutyldithiocarbamate (0.105 g, 0.379 mmol) in methanol (10 mL) was added drop by drop to a suspension of 2-(4-*t*-butyl)phenyl pyridine gold dichloride (0.060 g, 0.125 mmol) in methanol (15 mL) and stirred at room temperature overnight. A colour change from white to pale yellow was observed during the addition. The solvent was removed under vacuum and the dark yellow residue was dissolved in dichloromethane (15 mL). Excess AgSbF_6 in dichloromethane (5 mL) was then added and the solvent was removed under vacuum. The solid was purified by dissolving in minimal acetonitrile (2 mL) and precipitating the product with an excess of diethyl ether (20 mL). This was filtered and dried under vacuum (0.073 g, 0.086 mmol, 71%). Anal. Calcd. For $\text{C}_{24}\text{H}_{34}\text{AuF}_6\text{N}_2\text{S}_2\text{Sb}\cdot 2\text{MeCN}$ (929.49): C, 36.18; H, 4.34; N, 6.03. Found C, 35.70; H, 3.96; N, 6.09. ^1H NMR (CD_3CN , 300 MHz, 298 K): 8.40 (d, $^3J_{\text{H-H}} = 5.6$ Hz, 1H, H²), 8.23 (dt, $^3J_{\text{H-H}} = 8.1$ Hz, $^4J_{\text{H-H}} = 1.4$ Hz, 1H, H⁴), 8.06 (d, $^3J_{\text{H-H}} = 8.1$ Hz, 1H, H⁵), 7.71 (d, $^3J_{\text{H-H}} = 8.1$ Hz, 1H, H⁸), 7.55-7.44 (m, 2H, H³⁺⁹), 7.08 (d, $^4J_{\text{H-H}} = 1.7$ Hz, 1H, H¹¹), 3.77 (m, 4H, H^{14+14'}), 1.78 (m, 4H, H^{15+15'}), 1.42 (m, 4H, H^{16+16'}), 1.33 (s, 9H, ^{*t*}Bu), 0.98 (m, 6H, H^{17+17'}). ^{13}C [^1H] NMR (CD_3CN , 75 MHz): 194.4 (s, C¹³), 163.8 (s, C¹²), 156.4 (s, C^{6/7}), 151.6 (s, C^{6/7}), 148.9 (s, C²), 143.6 (s, C⁴), 141.1 (s, C¹⁰), 126.7 (s, C⁸), 126.5 (s, C⁹), 125.5 (s, C³), 125.0 (s, C¹¹), 122.1 (s, C⁵), 53.6 (s, C^{14/14'}), 52.0 (s, C^{14/14'}), 35.5 (s, C(CH₃)₃), 30.2 (s, C(CH₃)₃), 28.9 (s, C^{15/15'}), 28.6 (s, C^{15/15'}), 19.6 (s, C^{16/16'}), 12.9 (s, C^{17/17'}). IR: ν_{max} (neat)/ cm^{-1} : 2962 (^{*t*}Bu), 2873 (Ar), 1550 (Dithiocarbamate).

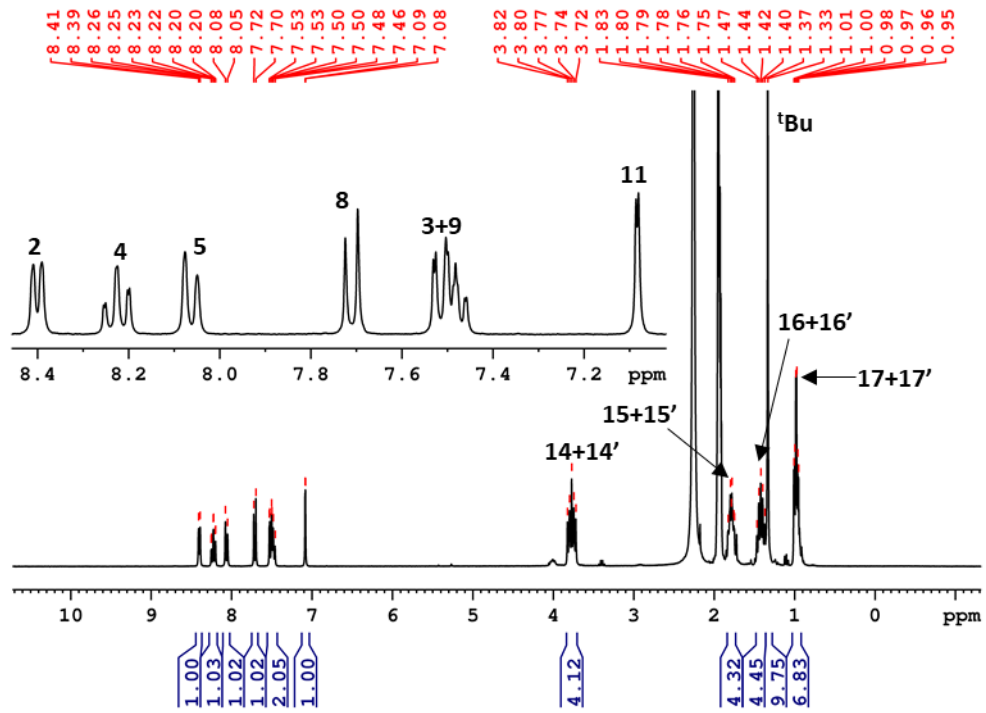


Figure 4.55a – ^1H NMR of **65** in CD_3CN .

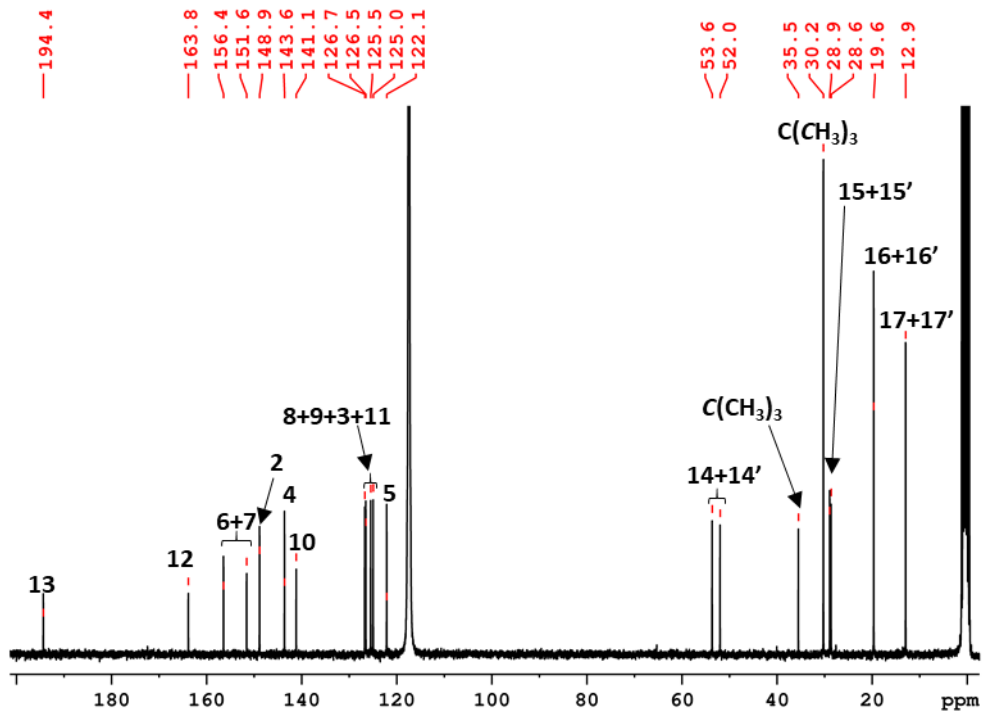


Figure 4.55b – ^{13}C [^1H] NMR of **65** in CD_3CN .

4.56 *X-ray crystallography*

Crystal structures were solved by Dr David Hughes.

4.57 *Antiproliferation assay*

The human A549 and HL60 cancer cell lines (from ECACC) were cultured in RPMI 1640 medium with 10% foetal calf serum, 2 mM L-glutamine, 100 U mL⁻¹ penicillin and 100 µg mL⁻¹ streptomycin (Invitrogen). The cells were maintained under a humidified atmosphere at 37 °C and 5% CO₂. The human MCF-7, HCT116 and MDA-MB-231 cancer cell lines (from ECACC) were cultured in DMEM medium with 10% foetal calf serum, 2 mM L-glutamine, 100 U mL⁻¹ penicillin and 100 µg mL⁻¹ streptomycin (Invitrogen). The HUVEC cells were cultured in Endothelial Cell Growth Medium with growth and antibiotic supplement. The cells were maintained under a humidified atmosphere at 37 °C and 5% CO₂. Inhibition of cancer cell proliferation was measured by the 3-(4,5-dimethylthiazol-2-yl)-5-(3-carboxymethoxyphenyl)-2-(4-sulfophenyl)-2H-tetrazolium (MTS) assay using the CellTiter 96 Aqueous One Solution Cell Proliferation Assay (Promega) and following the manufacturer's instructions. Briefly, the cells (3 × 10⁴ per 100 µL for HL60, 8 × 10³ per 100 µL for A549, MCF-7, HCT116, MDA-MB-231 and HUVEC) were seeded in 96-well plates and left untreated or treated with 1 µL of DMSO (vehicle control) or 1 µL of complexes diluted in DMSO at different concentrations, in triplicate for 72 h at 37 °C with 5% CO₂. Following this, MTS assay reagent was added for 4 h and absorbance measured at 490 nm using a Polarstar Optima microplate reader (BMG Labtech). IC₅₀ values were calculated using GraphPad Prism Version 5.0 software.

4.58 *Uptake study*

MCF-7 cells were grown in 75 cm² flasks up to 70% of confluence in 10 mL of culture medium. Compounds **61**, **63**, **65** and **66** were added to the flasks (100 µL of 1 mM solution in DMSO) and incubated for 6 h at 37 °C with 5% CO₂. Negative controls were used by incubating cells with DMSO alone under the same conditions. After removal of the medium and washing of the cells with PBS pH 7.4, the cells were detached using a trypsin solution. After quenching of trypsin with fresh medium, centrifugation and removal of the supernatant, the cell pellet was resuspended into 1 mL of PBS pH 7.4 and split into twice 500 µL for metal and protein quantification. The number of cells (expressed per million cells) of each sample was determined by measuring the protein content of the treated samples using a BCA assay (ThermoFischer Scientific) corrected by the amount of protein/10⁶ cells determined for each cell type by measuring the protein content of an untreated sample and dividing by the corresponding number of cells measured with a hemacytometer following a reported

procedure. Microwave digestion was used to solvate the samples to liquid form. Nitric acid and hydrogen peroxide were used in a Milestone Ethos 1 microwave system using SK-10 10 place carousel. The digest was ramped to 200 °C in 15 minutes holding at 200 °C for 15 min. The sample was weighed into a microwave vessel before digestion, and decanted and rinsed into a pre- weighed PFA bottle after digestion. ICP-MS samples were spiked with rhodium internal standard and run on a Thermo X series 1 ICP-MS. The isotopes selected were ^{63}Cu , ^{65}Cu , ^{107}Ag , ^{109}Ag and ^{197}Au . Certified standards and independent reference were used for accuracy. Acid blanks were run through the system and subtracted from sample measurements before corrections for dilution.

4.59 *ROS assay*

100 μL of MCF-7 cells were seeded at a density of 1×10^5 cells per mL in a 96-well black plate with a transparent bottom. The cells were incubated at 37 °C for 24 h. The medium was removed, and replaced with 50 μM H_2DCFDA (from Life Technologies) solution in PBS for 40 min. H_2DCFDA was removed and replaced with fresh medium. The cells were left for recovery for 20 min at 37 °C. Basal fluorescence was measured at 485/520 nm on a POLARstar Optima. The cells were incubated with 10 μM , 50 μM , or 100 μM of compounds, 1% DMSO (negative control) and 100 μM of H_2O_2 (positive control) for 24 h. Fluorescence was read at 485/520 nm. Basal fluorescence was subtracted from the fluorescence in the treated cells to calculate the amount of fluorescence caused by the compounds.

4.510 *FRET assay.*

The initial FRET melting screen was performed using a fluorescence resonance energy transfer (FRET) DNA melting based assay. The sequences used were hTeloC_{FRET} (5'-FAM-d[TAA-CCC-TAA-CCC-TAA-CCC-TAA-CCC]-TAMRA-3'); hif-1- α _{FRET} (5'-d[CGC-GCT-CCC-GCC-CCC-TCT-CCC-CTC-CCC-GCG-C]-TAMRA-3'), hTeloG_{FRET} (5'-FAM-d[GGG-TTA-GGG-TTA-GGG-TTA-GGG]-TAMRA-3'), cMycC_{FRET} (5'-FAM-d[CCC-CAC-CTT-CCC-CAC-CCT-CCC-CAC-CCT-CCC-C]-TAMRA-3') and DS_{FRET} FAM-d(TAT-AGC-TAT-A-HEG(18)-TAT-AGC-TAT-A)-TAMRA-3'). The labelled oligonucleotides (donor fluorophore FAM is 6-carboxyfluorescein; acceptor fluorophore TAMRA is 6-carboxytetramethyl-rhodamine) were prepared as a 220 nM solution in 10 mM sodium cacodylate buffer at the indicated pH with 100 mM sodium chloride and then thermally annealed. Strip-tubes (QIAGEN) were prepared by aliquoting 20 μL of the annealed DNA, followed by 0.5 μL of the compound solutions. Control samples for each run were prepared with the same quantity of DMSO with the DNA in buffer. Fluorescence melting curves were determined in a QIAGEN Rotor-Gene Q-series PCR machine, using a total reaction volume of 20 μL . Measurements were made with excitation

at 470 nm and detection at 510 nm. Final analysis of the data was carried out using QIAgen Rotor-Gene Q-series software and Origin or Excel.

References

1. B. Rosenberg, L. Vancamp and T. Krigas, *Nature*, **1965**, *205*, 698.
2. T. W. Hambley, *J. Chem. Soc. Dalton Trans.*, **2001**, 2711-2718.
3. K. R. Barnes and S. J. Lippard, *Metal Ions in Biological Systems*, **2004**, *42*, 143-177.
4. C. A. Rabik and M. E. Dolan, *Cancer Treatment Reviews*, **2007**, *33*, 9-23.
5. B. Bertrand and A. Casini, *Dalton Trans.*, **2014**, *43*, 4209-4219.
6. I. Ott, *Coord. Chem. Rev.*, **2009**, *253*, 1670-1681.
7. T. T. Zou, C. T. Lum, C. N. Lok, W. P. To, K. H. Low and C. M. Che, *Angew. Chem. Int. Ed.*, **2014**, *53*, 5810-5814.
8. S. J. Berners-Price and A. Filipovska, *Metallomics*, **2011**, *3*, 863-873.
9. H. Z. Zhao and Y. T. Ning, *Gold Bull.*, **2001**, *34*, 24-29.
10. W. F. Kean, L. Hart and W. W. Buchman, *Br. J. Rheumatol.*, **1997**, *36*, 560-572.
11. B. M. Sutton, *Gold Bull.*, **1986**, *19*, 15-16.
12. C. K. Mirabelli, R. K. Johnson, C. M. Sung, L. Faucette, K. Muirhead and S. T. Crooke, *Cancer Research*, **1985**, *45*, 32-39.
13. A. A. Isab, M. N. Shaikh, M. Monim-ul-Mehboob, B. A. Al-Maythalony, M. I. M. Wazeer and S. Altuwaijri, *Spectrochim. Acta Pt. A-Molec. Biomolec. Spectr.*, **2011**, *79*, 1196-1201.
14. G. Marcon, S. Carotti, M. Coronello, L. Messori, E. Mini, P. Orioli, T. Mazzei, M. A. Cinellu and G. Minghetti, *J. Med. Chem.*, **2002**, *45*, 1672-1677.
15. V. Amani, A. Abedi, S. Ghabeshi, H. R. Khayasi, S. M. Hosseini and N. Safari, *Polyhedron*, **2014**, *79*, 104-115.
16. P. Shi, Q. Jiang, J. Lin, Y. Zhao, L. Lin and Z. Guo, *J. Inorg. Biochem.*, **2006**, *100*, 939-945.
17. P. F. Shi, Q. Jiang, Y. M. Zhao, Y. M. Zhang, J. Lin, L. P. Lin, J. Ding and Z. J. Guo, *J. Biol. Inorg. Chem.*, **2006**, *11*, 745-752.

18. T. Yang, C. Tu, J. Y. Zhang, L. P. Lin, X. M. Zhang, Q. Liu, J. Ding, Q. Xu and Z. J. Guo, *Dalton Trans.*, **2003**, 3419-3424.
19. C. Gabbiani, M. A. Cinellu, L. Maiore, L. Massai, F. Scaletti and L. Messori, *Inorg. Chim. Acta*, **2012**, *393*, 115-124.
20. R. V. Parish, B. P. Howe, J. P. Wright, J. Mack, R. G. Pritchard, R. G. Buckley, A. M. Elsome and S. P. Fricker, *Inorg. Chem.*, **1996**, *35*, 1659-1666.
21. D. M. Fan, C. T. Yang, J. D. Ranford, P. F. Lee and J. J. Vittal, *Dalton Trans.*, **2003**, 2680-2685.
22. L. Engman, M. McNaughton, M. Gajewska, S. Kumar, A. Birmingham and G. Powis, *Anti-Cancer Drugs*, **2006**, *17*, 539-544.
23. D. M. Fan, C. T. Yang, J. D. Ranford, J. J. Vittal and P. F. Lee, *Dalton Trans.*, **2003**, 3376-3381.
24. J. J. Zhang, R. W. Y. Sun and C. M. Che, *Chem. Commun.*, **2012**, *48*, 3388-3390.
25. R. Rubbiani, T. N. Zehnder, C. Mari, O. Blacque, K. Venkatesan and G. Gasser, *ChemMedChem*, **2014**, *9*, 2781-2790.
26. K. J. Kilpin, W. Henderson and B. K. Nicholson, *Polyhedron*, **2007**, *26*, 434-447.
27. M. Coronello, E. Mini, B. Caciagli, M. A. Cinellu, A. Bindoli, C. Gabbiani and L. Messori, *J. Med. Chem.*, **2005**, *48*, 6761-6765.
28. C. Gabbiani, A. Casini, G. Kelter, F. Cocco, M. A. Cinellu, H. H. Fiebig and L. Messori, *Metallomics*, **2011**, *3*, 1318-1323.
29. J. J. Zhang, W. Lu, R. W. Y. Sun and C. M. Che, *Angew. Chem. Int. Ed.*, **2012**, *51*, 4882-4886.
30. M. P. Rigobello, L. Messori, G. Marcon, M. A. Cinellu, M. Bragadin, A. Folda, G. Scutari and A. Bindoli, *J. Inorg. Biochem.*, **2004**, *98*, 1634-1641.
31. C. K. L. Li, R. W. Y. Sun, S. C. F. Kui, N. Y. Zhu and C. M. Che, *Chem. Eur. J.*, **2006**, *12*, 5253-5266.
32. R. W. Y. Sun, C. N. Lok, T. T. H. Fong, C. K. L. Li, Z. F. Yang, T. T. Zou, A. F. M. Siu and C. M. Che, *Chem. Sci.*, **2013**, *4*, 1979-1988.

33. B. Bertrand, L. Stefan, M. Pirrotta, D. Monchaud, E. Bodio, P. Richard, P. Le Gendre, E. Warmerdam, M. H. de Jager, G. M. M. Groothuis, M. Picquet and A. Casini, *Inorg. Chem.*, **2014**, *53*, 2296-2303.
34. R. Rubbiani, S. Can, I. Kitanovic, H. Alborzina, M. Stefanopoulou, M. Kokoschka, S. Monchgesang, W. S. Sheldrick, S. Wolfli and I. Ott, *J. Med. Chem.*, **2011**, *54*, 8646-8657.
35. W. K. Liu, K. Bendsdorf, M. Proetto, U. Abram, A. Hagenbach and R. Gust, *J. Med. Chem.*, **2011**, *54*, 8605-8615.
36. L. Messori, L. Marchetti, L. Massai, F. Scaletti, A. Guerri, I. Landini, S. Nobili, G. Perrone, E. Mini, P. Leoni, M. Pasquali and C. Gabbiani, *Inorg. Chem.*, **2014**, *53*, 2396-2403.
37. J. J. Yan, A. L. F. Chow, C. H. Leung, R. W. Y. Sun, D. L. Ma and C. M. Che, *Chem. Commun.*, **2010**, *46*, 3893-3895.
38. S. K. Fung, T. T. Zou, B. Cao, P. Y. Lee, Y. M. E. Fung, D. Hu, C. N. Lok and C. M. Che, *Angew. Chem. Int. Ed.*, **2017**, *56*, 3892-3896.
39. B. Bertrand, J. Fernandez-Cestau, J. Angulo, M. M. D. Cominetti, Z. A. E. Waller, M. Searcey, M. A. O'Connell and M. Bochmann, *Inorg. Chem.*, **2017**, *56*, 5728-5740.
40. T. T. Zou, C. T. Lum, S. S. Y. Chui and C. M. Che, *Angew. Chem. Int. Ed.*, **2013**, *52*, 2930-2933.
41. B. K. Rana, A. Nandy, V. Bertolasi, C. W. Bielawski, K. Das Saha and J. Dinda, *Organometallics*, **2014**, *33*, 2544-2548.
42. H. Sivararn, J. Tan and H. V. Huynh, *Organometallics*, **2012**, *31*, 5875-5883.
43. L. Cattaruzza, D. Fregona, M. Mongiat, L. Ronconi, A. Fassina, A. Colombatti and D. Aldinucci, *Int. J. Cancer*, **2011**, *128*, 206-215.
44. D. Saggiaro, M. P. Rigobello, L. Paloschi, A. Folda, S. A. Moggach, S. Parsons, L. Ronconi, D. Fregona and A. Bindoli, *Chem. Biol.*, **2007**, *14*, 1128-1139.
45. M. Altaf, A. A. Isab, J. Vanco, Z. Dvorak, Z. Travnicek and H. Stoeckli-Evans, *RSC Adv.*, **2015**, *5*, 81599-81607.
46. J. J. Zhang, K. M. Ng, C. N. Lok, R. W. Y. Sun and C. M. Che, *Chem. Commun.*, **2013**, *49*, 5153-5155.

47. C. Nardon, S. M. Schmitt, H. J. Yang, J. Zuo, D. Fregona and Q. P. Dou, *PLoS One*, **2014**, *9*, 10.
48. W. Henderson, B. K. Nicholson, S. J. Faville, D. Fan and J. D. Ranford, *J. Organomet. Chem.*, **2001**, *631*, 41-46.
49. C. M. Che, R. W. Y. Sun, W. Y. Yu, C. B. Ko, N. Y. Zhu and H. Z. Sun, *Chem. Commun.*, **2003**, 1718-1719.
50. B. D. Glisic, Z. D. Stanic, S. Rajkovic, V. Kojic, G. Bogdanovic and M. I. Djuran, *J. Serb. Chem. Soc.*, **2013**, *78*, 1911-1924.
51. J. Lemke, A. Pinto, P. Niehoff, V. Vasylyeva and N. Metzler-Nolte, *Dalton Trans.*, **2009**, 7063-7070.
52. L. Ortego, M. Meireles, C. Kasper, A. Laguna, M. D. Villacampa and M. C. Gimeno, *J. Inorg. Biochem.*, **2016**, *156*, 133-144.
53. P. Pil, S. J. Lippard, S. J. L. P. Pil and J.R Bertino, *Encyclopedia of Cancer, Vol. 1*, Academic Press, San Diego **1997**, *1*, 392-410.
54. S. Gomez-Ruiz, D. Maksimovic-Ivanic, S. Mijatovic and G. N. Kaluderovic, *Bioinorg. Chem. Appl.*, **2012**.
55. Y. Wang, Q. Y. He, R. W. Y. Sun, C. M. Che and J. F. Chiu, *Eur. J. Pharmacol.*, **2007**, *554*, 113-122.
56. Y. Wang, Q. Y. He, R. W. Y. Sun, C. M. Che and J. F. Chiu, *Cancer research*, **2005**, *65*, 11553-11564.
57. C. T. Lum, X. Liu, R. W. Y. Sun, X. P. Li, Y. Peng, M. L. He, H. F. Kung, C. M. Che and M. C. M. Lin, *Cancer Lett.*, **2010**, *294*, 159-166.
58. R. W. Y. Sun, C. K. L. Li, D. L. Ma, J. J. Yan, C. N. Lok, C. H. Leung, N. Y. Zhu and C. M. Che, *Chem. Eur. J.*, **2010**, *16*, 3097-3113.
59. L. Ronconi, C. Marzano, P. Zanello, M. Corsini, G. Miolo, C. Macca, A. Trevisan and D. Fregona, *J. Med. Chem.*, **2006**, *49*, 1648-1657.
60. Y. H. Hsiang and L. F. Liu, *Cancer research*, **1988**, *48*, 1722-1726.

61. S. Balasubramanian, L. H. Hurley and S. Neidle, *Nat. Rev. Drug Discov.*, **2011**, *10*, 261-275.
62. S. Neidle, *J. Med. Chem.*, **2016**, *59*, 5987-6011.
63. K. Gehring, J. L. Leroy and M. Gueron, *Nature*, **1993**, *363*, 561-565.
64. H. A. Day, P. Pavlou and Z. A. E. Waller, *Bioorg. Med. Chem.*, **2014**, *22*, 4407-4418.
65. V. Tjong, L. Tang, S. Zauscher and A. Chilkoti, *Chem. Soc. Rev.*, **2014**, *43*, 1612-1626.
66. P. Gratteri, L. Massai, E. Michelucci, R. Rigo, L. Messori, M. A. Cinellu, C. Musetti, C. Sissi and C. Bazzicalupi, *Dalton Trans.*, **2015**, *44*, 3633-3639.
67. J. B. Almond and G. M. Cohen, *Leukemia*, **2002**, *16*, 433-443.
68. V. Milacic and Q. P. Dou, *Coord. Chem. Rev.*, **2009**, *253*, 1649-1660.
69. M. F. Tomasello, C. Nardon, V. Lanza, G. Di Natale, N. Pettenuzzo, S. Salmaso, D. Milardi, P. Caliceti, G. Pappalardo and D. Fregona, *Eur. J. Med. Chem.*, **2017**, *138*, 115-127.
70. H. Ostrowska, *Cell. Mol. Biol. Lett.*, **2008**, *13*, 353-365.
71. K. Becker, S. Gromer, R. H. Schirmer and S. Muller, *Eur. J. Biochem.*, **2000**, *267*, 6118-6125.
72. L. W. Zhong, E. S. J. Arner and A. Holmgren, *Proc. Natl. Acad. Sci. U. S. A.*, **2000**, *97*, 5854-5859.
73. S. Gromer, L. D. Arscott, C. H. Williams, R. H. Schirmer and K. Becker, *J. Biol. Chem.*, **1998**, *273*, 20096-20101.
74. K. P. Bhabak, B. J. Bhuyan and G. Mugesh, *Dalton Trans.*, **2011**, *40*, 2099-2111.
75. R. Rubbiani, E. Schuh, A. Meyer, J. Lemke, J. Wimberg, N. Metzler-Nolte, F. Meyer, F. Mohr and I. Ott, *MedChemComm*, **2013**, *4*, 942-948.
76. E. Vergara, A. Casini, F. Sorrentino, O. Zava, E. Cerrada, M. P. Rigobello, A. Bindoli, M. Laguna and P. J. Dyson, *ChemMedChem*, **2010**, *5*, 96-102.
77. M. Selenius, M. Hedman, D. Brodin, V. Gandin, M. P. Rigobello, J. Flygare, C. Marzano, A. Bindoli, O. Brodin, M. Bjornstedt and A. P. Fernandes, *J. Cell. Mol. Med.*, **2012**, *16*, 1593-1605.

78. G. H. Hwang, J. M. Ryu, Y. J. Jeon, J. Choi, H. J. Han, Y. M. Lee, S. Lee, J. S. Bae, J. W. Jung, W. Chang, L. K. Kim, J. G. Jee and M. Y. Lee, *Eur. J. Pharmacol.*, **2015**, *765*, 384-393.
79. X. Saelens, N. Festjens, L. Vande Walle, M. van Gurp, G. van Loo and P. Vandenabeele, *Oncogene*, **2004**, *23*, 2861-2874.
80. S. J. Park and I. S. Kim, *Br. J. Pharmacol.*, **2005**, *146*, 506-513.
81. N. Traverso, R. Ricciarelli, M. Nitti, B. Marengo, A. L. Furfaro, M. A. Pronzato, U. M. Marinari and C. Domenicotti, *Oxidative medicine and cellular longevity*, **2013**, 972913.
82. H. H. W. Chen and M. T. Kuo, *Metal-based drugs*, **2010**.
83. M. Wade, Y. C. Li and G. M. Wahl, *Nat. Rev. Cancer*, **2013**, *13*, 83-96.
84. D. Hu, Y. G. Liu, Y. T. Lai, K. C. Tong, Y. M. Fung, C. N. Lok and C. M. Che, *Angew. Chem. Int. Ed.*, **2016**, *55*, 1387-1391.
85. J. C. Ghosh, T. Dohi, B. H. Kang and D. C. Altieri, *J. Biol. Chem.*, **2008**, *283*, 5188-5194.
86. M. Williams, A. I. Green, J. Fernandez-Cestau, D. L. Hughes, M. A. O'Connell, M. Searcey, B. Bertrand and M. Bochmann, *Dalton Trans.*, **2017**, *46*, 13397-13408.
87. J. E. Parks and A. L. Balch, *J. Organomet. Chem.*, **1974**, *71*, 453-463.
88. G. Minghetti, F. Bonati and G. Banditelli, *Inorg. Chem.*, **1976**, *15*, 1718-1720.
89. R. Uson, A. Laguna and M. D. Villacampa, *Inorg. Chim. Acta*, **1984**, *81*, 25-31.
90. O. Crespo, M. C. Gimeno, A. Laguna, S. Montanel-Perez and M. D. Villacampa, *Organometallics*, **2012**, *31*, 5520-5526.
91. S. Montanel-Perez, R. P. Herrera, A. Laguna, M. D. Villacampa and M. C. Gimeno, *Dalton Trans.*, **2015**, *44*, 9052-9062.
92. B. David, U. Monkowius, J. Rust, C. W. Lehmann, L. Hyzak and F. Mohr, *Dalton Trans.*, **2014**, *43*, 11059-11066.
93. N. Metzler-Nolte, in *Medicinal Organometallic Chemistry*, G. Jaouen and N. Metzler-Nolte, Springer-Verlag Berlin, Berlin, **2010**, *32*, 195-217.
94. B. Albada and N. Metzler-Nolte, *Chem. Rev.*, **2016**, *116*, 11797-11839.

95. S. D. Koster, H. Alborzinia, S. Z. Can, I. Kitanovic, S. Wolf, R. Rubbiani, I. Ott, P. Riesterer, A. Prokop, K. Merz and N. Metzler-Nolte, *Chem. Sci.*, **2012**, *3*, 2062-2072.
96. J. Fernandez-Cestau, B. Bertrand, M. Blaya, G. A. Jones, T. J. Penfold and M. Bochmann, *Chem. Commun.*, **2015**, *51*, 16629-16632.
97. D. A. Rosca, J. Fernandez-Cestau, A. S. Romanov and M. Bochmann, *J. Organomet. Chem.*, **2015**, *792*, 117-122.
98. C. H. A. Goss, W. Henderson, A. L. Wilkins and C. Evans, *J. Organomet. Chem.*, **2003**, *679*, 194-201.
99. J. Janockova, J. Plsikova, J. Kasparikova, V. Brabec, R. Jendzelovsky, J. Mikes, J. Koval, S. Hamulakova, P. Fedorocko, K. Kuca and M. Kozurkova, *Eur. J. Pharm. Sci.*, **2015**, *76*, 192-202.
100. L. A. Howell, R. Gulam, A. Mueller, M. A. O'Connell and M. Searcey, *Bioorg. Med. Chem. Lett.*, **2010**, *20*, 6956-6959.
101. L. A. Howell, R. A. Bowater, M. A. O'Connell, A. P. Reszka, S. Neidle and M. Searcey, *ChemMedChem*, **2012**, *7*, 792-804.
102. C. L. Smyre, G. Saluta, T. E. Kute, G. L. Kucera and U. Bierbach, *ACS Med. Chem. Lett.*, **2011**, *2*, 870-874.
103. A. C. Matsheku, M. Y. H. Chen, S. Jordaan, S. Prince, G. S. Smith and B. C. E. Makhubela, *Appl. Organomet.*, **2017**, *31*, 3852.
104. L. C. Eiter, N. W. Hall, C. S. Day, G. Saluta, G. L. Kucera and U. Bierbach, *J. Med. Chem.*, **2009**, *52*, 6519-6522.
105. S. A. Perez, C. de Haro, C. Vicente, A. Donaire, A. Zamora, J. Zajac, H. Kostrhunova, V. Brabec, D. Bautista and J. Ruiz, *ACS Chem. Biol.*, **2017**, *12*, 1524-1537.
106. E. C. Constable and T. A. Leese, *J. Organomet. Chem.*, **1989**, *363*, 419-424.
107. M. A. Cinellu, A. Zucca, S. Stoccoro, G. Minghetti, M. Manassero and M. Sansoni, *J. Chem. Soc. Dalton Trans.*, **1995**, 2865-2872.
108. S. Spreckelmeyer, C. Orvig and A. Casini, *Molecules*, **2014**, *19*, 15584-15610.

109. S. Imoto, T. Hirohama and F. Nagatsugi, *Bioorg. Med. Chem. Lett.*, **2008**, *18*, 5660-5663.
110. M. Searcey, P. N. Martin, N. M. Howarth, B. Madden and L. P. G. Wakelin, *Bioorg. Med. Chem. Lett.*, **1996**, *6*, 1831-1836.
111. L. P. G. Wakelin, P. Chetcuti and W. A. Denny, *J. Med. Chem.*, **1990**, *33*, 2039-2044.
112. W. M. Howell, M. Jobs and A. J. Brookes, *Genome Res.*, **2002**, *12*, 1401-1407.
113. V. V. Didenko, *Biotechniques*, **2001**, *31*, 1106.
114. N. Pabla and Z. Dong, *Kidney Int.*, **2008**, *73*, 994-1007.
115. X. Y. Wang and Z. J. Guo, *Anti-Cancer Agents Med. Chem.*, **2007**, *7*, 19-34.
116. R. Dorr, *Platinum and Other Metal Coordination Compounds in Cancer Chemotherapy* Plenum Press, New York, 2 edn., **1996**.
117. R. Borch, P. Dedon, A. Gringeri and T. Montine, *Platinum and Other Metal Compounds in Cancer Chemotherapy*, Martinus Nijhoff Publishing, Boston, **1988**.
118. L. Ronconi and D. Fregona, *Dalton Trans.*, **2009**, 10670-10680.
119. M. N. Kouodom, G. Boscutti, M. Celegato, M. Crisma, S. Sitran, D. Aldinucci, F. Formaggio, L. Ronconi and D. Fregona, *J. Inorg. Biochem.*, **2012**, *117*, 248-260.
120. C. M. Che and R. W. Y. Sun, *Chem. Commun.*, **2011**, *47*, 9554-9560.
121. A. Casini, M. A. Cinellu, G. Minghetti, C. Gabbiani, M. Coronello, E. Mini and L. Messori, *J. Med. Chem.*, **2006**, *49*, 5524-5531.
122. G. Boscutti, L. Marchio, L. Ronconi and D. Fregona, *Chem. Eur. J.*, **2013**, *19*, 13428-13436.
123. D. Monchaud and M. P. Teulade-Fichou, *Org. Biomol. Chem.*, **2008**, *6*, 627-636.
124. C. Bazzicalupi, M. Ferraroni, F. Papi, L. Massai, B. Bertrand, L. Messori, P. Gratteri, A. Casini, *Angew. Chem. Int. Ed.* **2016**, *55*, 4256-4259.
125. A. De Cian, L. Guittat, M. Kaiser, B. Sacca, S. Amrane, A. Bourdoncle, P. Alberti, M. P. Teulade-Fichou, L. Lacroix and J. L. Mergny, *Methods*, **2007**, *42*, 183-195.

126. A. T. Phan and J. L. Mergny, *Nucleic Acids Res.*, **2002**, *30*, 4618-4625.
127. J. A. Brazier, A. Shah and G. D. Brown, *Chem. Commun.*, **2012**, *48*, 10739-10741.